

THE OCTOBER 1983
VOL. 62, NO. 8, PART 1
BELL SYSTEM
TECHNICAL JOURNAL



High-Power Lasers and Optical Waveguides for Robotic Material- Processing Applications	2479
Chinlon Lin, G. Beni, S. Hackwood, and T. J. Bridges	
Estimates of Path Loss and Radiated Power for UHF Mobile- Satellite Systems	2493
D. O. Reudink	
Coding of Two-Level Pictures by Pattern Matching and Substitution	2513
O. Johnsen, J. Segen, and G. L. Cash	
Data-Transport Performance Analysis of Fasnet	2547
D. P. Heyman	
Forecasting With Adaptive Gradient Exponential Smoothing	2561
A. Feuer	
Application of the Minimum-Weight Spanning-Tree Algorithm to Assignment of Communication Facilities	2581
N. A. Strakhov	
Note on the Properties of a Vector Quantizer for LPC Coefficients	2603
L. R. Rabiner, M. M. Sondhi, and S. E. Levinson	
Upper Bounds on the Minimum Distance of Trellis Codes	2617
A. R. Calderbank, J. E. Mazo, and H. M. Shapiro	
 PAPERS BY BELL LABORATORIES AUTHORS	 2647
CONTENTS, NOVEMBER 1983	2661

THE BELL SYSTEM TECHNICAL JOURNAL

ADVISORY BOARD

D. E. PROCKNOW, *President*

I. M. ROSS, *President*

W. M. ELLINGHAUS, *President*

Western Electric Company

Bell Telephone Laboratories, Incorporated

American Telephone and Telegraph Company

EDITORIAL COMMITTEE

A. A. PENZIAS, *Committee Chairman, Bell Laboratories*

M. M. BUCHNER, JR., *Bell Laboratories*

R. P. CLAGETT, *Western Electric*

T. H. CROWLEY, *Bell Laboratories*

B. R. DARNALL, *Bell Laboratories*

B. P. DONOHUE, III, *AT&T Information Systems*

I. DORROS, *AT&T*

R. A. KELLEY, *Bell Laboratories*

R. W. LUCKY, *Bell Laboratories*

R. L. MARTIN, *Bell Laboratories*

J. S. NOWAK, *Bell Laboratories*

L. SCHENKER, *Bell Laboratories*

G. SPIRO, *Western Electric*

J. W. TIMKO, *AT&T Information Systems*

EDITORIAL STAFF

B. G. KING, *Editor*

PIERCE WHEELER, *Managing Editor*

LOUISE S. GOLLER, *Assistant Editor*

H. M. PURVIANCE, *Art Editor*

B. G. GRUBER, *Circulation*

THE BELL SYSTEM TECHNICAL JOURNAL (ISSN0005-8580) is published by the American Telephone and Telegraph Company, 195 Broadway, N. Y., N. Y. 10007; C. L. Brown, Chairman and Chief Executive Officer; W. M. Ellinghaus, President; V. A. Dwyer, Vice President and Treasurer; T. O. Davis, Secretary.

The Journal is published in three parts. Part 1, general subjects, is published ten times each year. Part 2, Computing Science and Systems, and Part 3, single-subject issues, are published with Part 1 as the papers become available.

The subscription price includes all three parts. Subscriptions: United States—1 year \$35; 2 years \$63; 3 years \$84; foreign—1 year \$45; 2 years \$73; 3 years \$94. Subscriptions to Part 2 only are \$10 (\$12 foreign). Single copies of the Journal are available at \$5 (\$6 foreign). Payment for foreign subscriptions or single copies must be made in United States funds, or by check drawn on a United States bank and made payable to The Bell System Technical Journal and sent to Bell Laboratories, Circulation Dept., Room 1E-335, 101 J. F. Kennedy Parkway, Short Hills, N. J. 07078.

Single copies of material from this issue of The Bell System Technical Journal may be reproduced for personal, noncommercial use. Permission to make multiple copies must be obtained from the editor.

Comments on the technical content of any article or brief are welcome. These and other editorial inquiries should be addressed to the Editor, The Bell System Technical Journal, Bell Laboratories, Room 1J-319, 101 J. F. Kennedy Parkway, Short Hills, N. J. 07078. Comments and inquiries, whether or not published, shall not be regarded as confidential or otherwise restricted in use and will become the property of the American Telephone and Telegraph Company. Comments selected for publication may be edited for brevity, subject to author approval.

Printed in U.S.A. Second-class postage paid at Short Hills, N. J. 07078 and additional mailing offices. Postmaster: Send address changes to The Bell System Technical Journal, Room 1E-335, 101 J. F. Kennedy Parkway, Short Hills, N. J. 07078.

© 1983 American Telephone and Telegraph Company.

THE BELL SYSTEM TECHNICAL JOURNAL

DEVOTED TO THE SCIENTIFIC AND ENGINEERING
ASPECTS OF ELECTRICAL COMMUNICATION

Volume 62

October 1983

Number 8, Part 1

High-Power Lasers and Optical Waveguides for Robotic Material-Processing Applications

By CHINLON LIN,* G. BENI,* S. HACKWOOD,* and
T. J. BRIDGES*

(Manuscript received April 4, 1983)

For various material-processing applications with robots we propose the use of high-power continuous wave and pulsed lasers (Nd³⁺:YAG, Argon ion, CO₂, excimer, etc.) and optical waveguides for delivering high powers in the ultraviolet (UV), the visible, and the infrared (IR) regions. We discuss the use of low-loss silica glass fiber waveguides for delivering high-power laser beam in the UV to near-IR spectral region (0.3 to 2 μm), and the use of a waveguiding articulating arm for delivering high-power laser beam in the long IR (2 to 10 μm). We also describe a design for fitting a CO₂ laser waveguiding arm to the robotic arm, as well as the advantages of using optical waveguides for high-power laser delivery to robots for material processing.

I. INTRODUCTION

Optical waveguides are known to be useful for optical signal transmission in which low-power, modulated semiconductor injection laser

* Bell Laboratories.

©Copyright 1983, American Telephone & Telegraph Company. Photo reproduction for noncommercial use is permitted without payment of royalty provided that each reproduction is done without alteration and that the Journal reference and copyright notice are included on the first page. The title and abstract, but no other portions, of this paper may be copied or distributed royalty free by computer-based and other information-service systems without further permission. Permission to reproduce or republish any other portion of this paper must be obtained from the Editor.

light is used for lightwave communication applications.¹ The advent of low-loss optical fiber waveguides, for example, has made possible long-distance, high-bandwidth lightwave communication systems for transmitting audio, data, and video signals. This paper discusses the use of optical waveguides for a different application: *high-power laser transmission* for robotic material-processing applications. Using high-power continuous wave (cw) and pulsed lasers and appropriate optical waveguides for the ultraviolet (UV), the visible, the near infrared (IR), and the longer IR, a robot can manipulate the output beam of a variety of high-power lasers for various processing functions. In Section II we discuss the available flexible waveguides for high-power laser transmission. In Section III we describe a manually operated CO₂ laser waveguiding articulating arm, and in Section IV a design for fitting the waveguiding articulating CO₂ laser arm to a robot arm.

At present, automation of material processing using high-power lasers requires costly, dedicated, large-size equipment. We believe that an inexpensive, small-size robot controlling a high-power laser beam with the help of optical waveguides will make possible many new applications in material processing.

II. HIGH-POWER LASER TRANSMISSION IN OPTICAL FIBER WAVEGUIDES

While the use of high-power lasers for material processing is well known,^{2,3} the use of low-loss optical waveguides for high-optical-power transmission is not widely practiced.⁴ For robotic applications (applications requiring the unique dexterity and versatility of robots), it is essential that the combination of high-power laser technology and robotics does not reduce the dexterity or flexibility of the robots. The essential element here for providing the flexible link between the high-power lasers (usually heavy and bulky) and the robots is the optical waveguide.

Figure 1 illustrates the basic system schematic for using high-power lasers and optical waveguides in robotic material-processing applications. Depending on the type of high-power lasers, different optical waveguides can be used. For example, in the near-infrared region of 1 to 2 μm , e.g., for high-power Nd:YAG lasers at 1.06 μm , silica glass fibers have excellent transmission characteristics (see Fig. 2). As a result of advances in lightwave communications technology, the loss in a silica fiber waveguide can be very low (~ 1 dB/km, or 0.01 dB/10 m at 1.06 μm). In this case the loss due to coupling into and out of the fiber waveguide is much larger than the transmission loss for even a 1-km-long optical fiber. Losses in silica glass fibers also can be low enough (for 10 to 100m lengths) for guiding blue-green and red lasers; thus such silica fibers are useful for transmission of high-power Argon

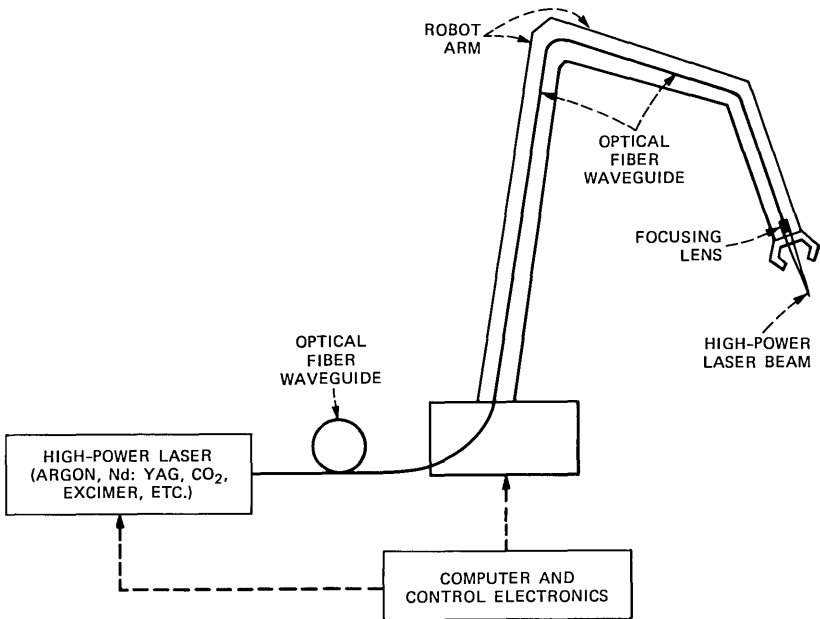


Fig. 1—Schematic of a system using flexible optical fiber waveguides for delivering high-power laser radiation to the robotic arm/hand for various material-processing applications.

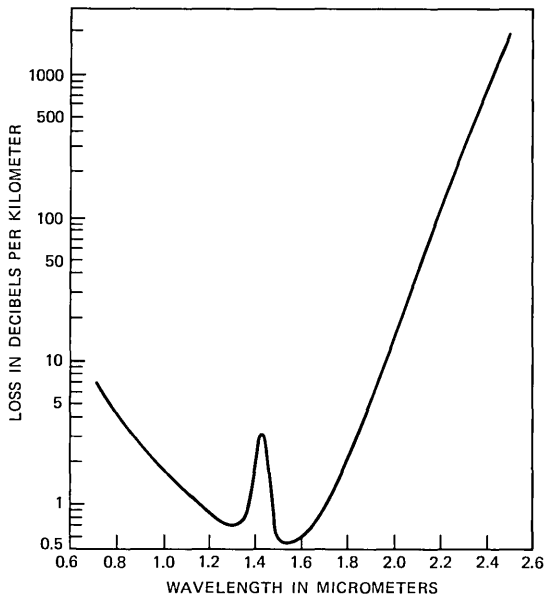


Fig. 2—Loss spectra of a typical low-loss silica glass fiber waveguide. For practical robotic material-processing applications, fiber loss of 1 dB/10 m (or 100 dB/km) could be considered low loss.

ion and Krypton ion lasers, as well as high-power ruby and alexandrite lasers. Recently available special UV silica glass fibers* may also be used for the ultraviolet wavelength region (0.3 to 0.4 μm). The loss is about 1 to 2 dB for every 10m, which is still low. Such fibers are useful for transmitting UV lasers (e.g., He-Cd lasers and excimer lasers) in, for example, photochemical applications.

Thus we have available appropriate optical fiber waveguides for transmitting high-power laser radiation in the spectral region from UV to near IR through at least 5 ~ 10 meters. This allows the bulky high-power laser head and its high-energy power supply (and cooling system, if any) to be separated from the robot, while allowing the powerful laser beam to be delivered to the robot arm or fingertip. As we saw in Fig. 1 a high-power Nd:YAG laser and silica glass fiberguide could be used for guiding the laser radiation to the robot hand (gripper). The silica glass fiber can be routed inside the robotic arm assembly, or mounted externally but attached to the side of the arm, depending on the situation or work requirement. The output fiber end can have a microlens (such as a half-pitch graded-index-rod lens) or a small conventional lens attached for output beam focusing.

For transmitting Nd:YAG lasers, ruby lasers, Argon ion lasers (in the visible and the near-infrared spectral region), the silica glass fibers are typically very small in dimension: outer diameters are on the order of a few hundred micrometers to a few millimeters, including the protecting jacket or cable. For high-laser-power output with well-defined spatial distribution (e.g., for maximum brightness, or best focusing), single-mode fibers with appropriate refractive index difference Δn and core diameter $2a$ can be designed (with normalized frequency $V \leq 2.4$ at the laser wavelength) for use in these different wavelength regions. If maximum overall energy transmission without concern for the spatial quality of the laser beam output is desired, a large-core, high numerical aperture (N.A.) silica glass fiber can be used for high-energy delivery to the robot. For the propagation properties and design considerations in single-mode and multimode silica glass fibers, appropriate references¹ should be consulted.

For transmitting high-power, longer infrared (2 to 10 μm) lasers such as CO₂ lasers, a configuration similar to that shown in Fig. 1 can be used, if a truly flexible CO₂ laser fiberguide is available. Presently, various glass and crystal fibers are being developed for this spectral region.⁵ Notably among them are the polycrystalline KRS-5 fibers⁶ and the single-crystal AgBr fibers⁷ for CO₂ lasers transmission. However, presently available long infrared fibers tend to be very lossy and

* UV fibers with losses in the 150 dB/km range for $\lambda \sim 310$ nm range have been reported by, for example, Quartz and Silice, France.

fragile. Thus the mechanical and optical properties are not yet truly satisfactory. Therefore, at present, bulky conventional articulating arms (consisting of aligned mirrors) are used for most applications requiring some flexibility in CO₂ laser delivery. To improve the flexibility and stability, Bridges and Strnad have developed a novel "waveguiding" articulating arm for transmitting high-power CO₂ laser radiation.⁸ The arm, shown in Fig. 3, has been designed for manual control. It is compact and relatively articulate. In the future, truly

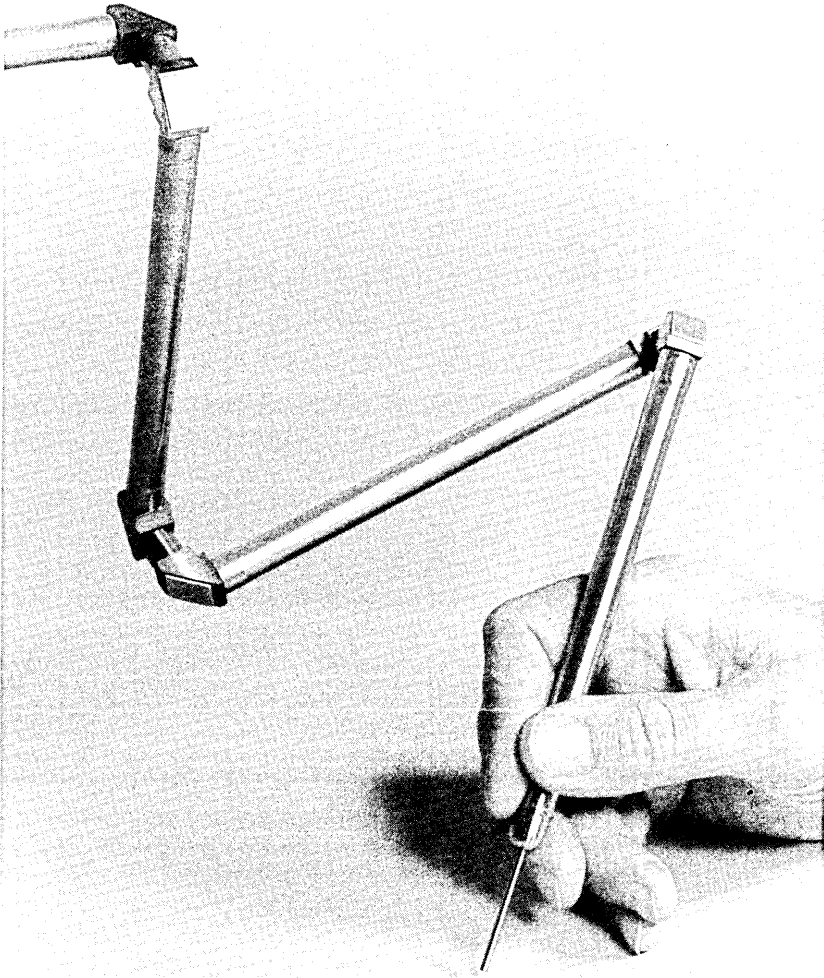


Fig. 3—The Bridges/Strnad waveguiding articulating arm for high-power CO₂ laser delivery.

flexible long-wavelength fibers are expected to have lower loss and higher strength than those presently available. Until then, the Bridges/Strnad waveguiding articulating arm would be the choice for CO₂ laser delivery to the robot. In Section III we discuss in more detail the design of this CO₂ laser arm; in Section IV we describe designing this laser arm to fit onto a robot arm for material processing.

III. BRIDGES/STRNAD WAVEGUIDING ARTICULATING ARM FOR LONG-IR LASER RADIATION

Figure 4 shows the design details of the Bridges/Strnad arm used for manual operation (see Fig. 3). This articulating arm uses the principles of waveguiding in hollow dielectric tubes. This new arm has

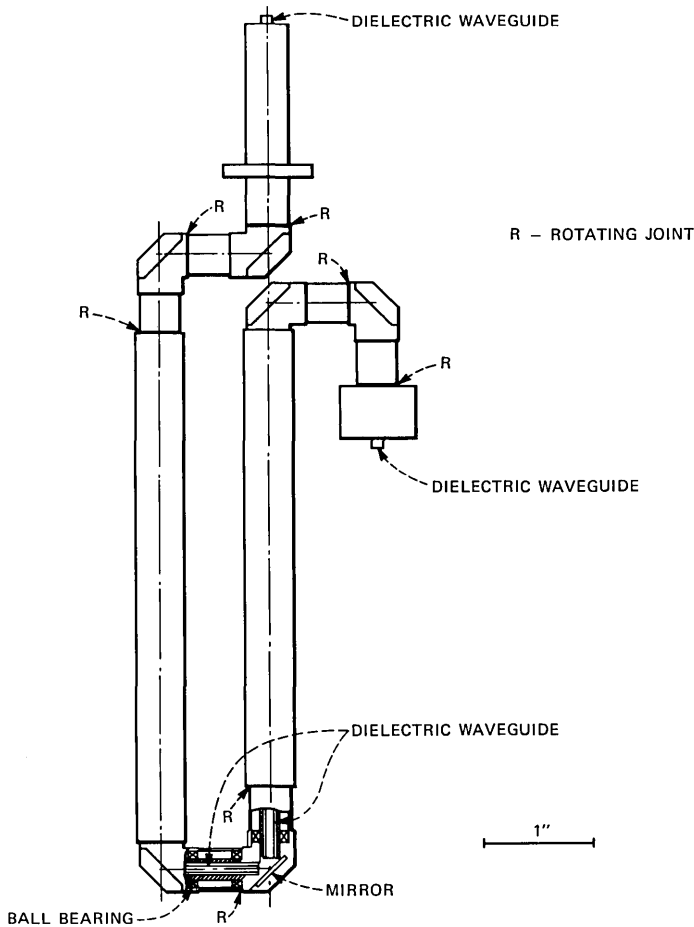


Fig. 4—The design of the Bridges/Strnad waveguiding articulating laser arm for flexible delivery of high-power, long-IR (e.g., CO₂ laser at 10.6 μm) optical radiation.

a number of advantages over previous articulating arms, including compactness and better pointing accuracy when compared with conventional articulating arms.⁹ Flexible waveguides such as metal waveguides¹⁰ and presently available infrared fibers are problematic because of the multimode nature of the guide. Single-mode radiation from the laser is rapidly degraded into a multiple-mode pattern that changes in form as the guide is moved. The degradation reduces considerably the maximum intensity that can be obtained by focusing the output radiation. In the case of articulating arms of conventional design the single mode is preserved, but unless the input beam is launched precisely on axis and the mechanism of the arm is precisely correct, the output beam will wander in a complicated manner as the arm is manipulated. Such arms are also characteristically large and cumbersome. The Bridges/Strnad arm design avoids this problem by propagating the radiation in straight, hollow, dielectric waveguides of the Marcatili-Schmeltzer type.¹¹ A single mode can be maintained in the guide, while the pointing accuracy is far less affected by initial launch conditions and accuracy of construction. (Pointing accuracy is determined by how closely the direction of the output beam conforms to the mechanical axis of the arm.) A further advantage is the compact design resulting from the elimination of diffraction spreading of the beam, by the guiding action of the waveguide.

The Marcatili-Schmeltzer waveguide carries radiation in the hollow circular bore of a dielectric tube. The dielectric need not be transparent to the radiation being guided. The mechanism of guiding can be thought of as a continual-glancing-angle Fresnel reflection from the dielectric walls. This reflection is not total, but close to 100 percent for very shallow incident angles to the walls. The modes of propagation have been calculated by Marcatili and Schmeltzer,¹¹ and they find that the lowest loss mode is the EH_{11} mode. An appropriate waveguide size is 50 to 200 wavelengths in diameter. This size is large enough to give low loss, but still retain adequate guiding so that straightness of the tube is not an important factor, although curvature of the tube axis introduces extra loss by an amount that increases with tube diameter.

Since the dielectric need not be transparent to the radiation, glass or quartz tubing which is readily obtainable in precision bore form can be used to transport 10.6- μm radiation. Single-mode laser radiation is conveniently launched into the waveguide by means of a lens (Fig. 5). The focal length of the lens is chosen to closely match the input Gaussian beam to the guided beam with small loss.¹² Short gaps in the tube can be tolerated with small loss so that mirrors which turn the beam through a 90-degree angle and are basic to the operation of the infrared articulating arm can be used in a simple arrangement (see Fig. 4).

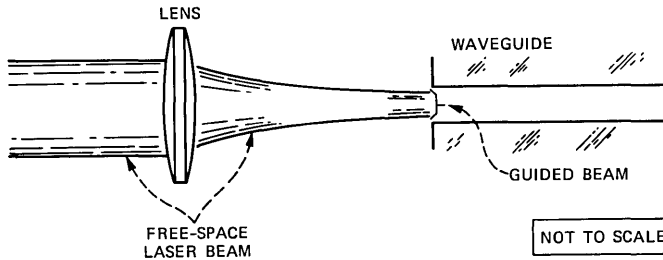


Fig. 5—Launching a free-space Gaussian beam into waveguide by means of a lens.

As a secondary feature, the glass or other visibly transparent waveguide tube can act as a light pipe to carry visible light through the arm. This light can be used for illuminating the work area, or for aiming the output beam. For this application the mirrors should be highly reflective in the visible as well as the infrared range. A suitable material is evaporated silver.

With the above concept in mind, various components of a possible waveguide articulating arm were tested in the laboratory, using a 10- μm CO_2 laser as a source. A 13.9-cm length of fused quartz tubing with 1.55-mm bore was tested. When a 30-cm focal length lens was used to focus the radiation into the guide, a transmission of 93 percent was found. To test the effect of small misalignments, the tube was pivoted off axis around the input point by one-half of one degree, and the transmission dropped by only 2 percent. Finally, a mock-up of a corner elbow (see Fig. 4) was made on the bench and a transmission of 95 percent was measured. This information demonstrated the feasibility of the idea and a complete arm was designed and fabricated (see Fig. 3). The arm contains three sections of waveguide that are 13 cm long and three more that are 2 cm long. The six corner mirrors used were commercially obtained. They were made from silicon 1 mm thick and were coated with silver and a transparent protective layer. The corners swivel on precision ball bearings. With a total length of 40 cm the arm can access any point in a 80-cm-diameter sphere. The completed arm was tested and found to have a transmission of 80 percent. Power up to 5W cw was transmitted with no damage. The 1.55-mm diameter beam from the output tube was substantially single mode and could be focused to a near-diffraction limited spot. As we expected, there was no wander of the output beam relative to the output tube as the arm was moved. The small size and light weight made it very easy to manipulate the arm and to place the output beam in any desired position.

IV. A ROBOTIC ARM FITTED WITH THE WAVEGUIDING ARTICULATING CO₂ LASER ARM

The simplistic approach to using the Bridges/Strnad waveguiding CO₂ laser arm is to make the robot gripper hold and maneuver the tip of the articulating laser waveguide. This approach, however, has a major drawback. Reorientation of the laser-beam output requires, in general, rotations of all five revolute joints of the articulated waveguide. In many cases, this complex reconfiguration of the articulated waveguide prevents a continuous rotation of the laser-output tip and requires the robot to follow a complicated path.

In addition, a force and torque sensor on the gripper would be essential to ensure that the articulated waveguide is not damaged by the robot in the attempt of imposing a particular five-link configuration. This is still beyond state of the art robotics, since even the turning of a simple two-link crank by a robot arm is a complex compliance problem not yet satisfactorily solved.

A second approach is to fit the waveguide within or beside the robot. Because of the required 90-degree revolute joint articulations, this is not a trivial task. In fact, many existing robots have prismatic joints and/or unsuitable dimensions.

We now propose a new robot system consisting of two arms: master and slave. The master arm is positioned by motors, whereas the slave arm only carries the waveguide. The slave arm is the Bridges-Strnad-type five-link waveguiding laser arm with 90-degree rotational joints. Unlike the original Bridges-Strnad arm shown in Fig. 2, it now has nine (rather than six) mirrors and a different link geometry as described below. The master arm is, for example, a Microbot Alpha* whose hand gripper and side casing have been removed. The robot has a repeatability of $\sim 250 \mu\text{m}$ and a positioning speed of 50 cm/s. The two arms are connected "in parallel" as follows.

Figure 6 shows schematically the connection between the master and the slave arms. The mirrors of the slave arm are labeled 'b' to 'j'. Laser input and output are at 'a' and 'k', respectively. Five mirrors are rigid and four ('b', 'e', 'g', and 'h') are movable. The axes of rotation of the master arm are indicated by rotation angles θ_1 to θ_5 . Except for axis 5, the axes of rotation of the slave arm coincide with the corresponding axes of rotation of the master arm. For example, a rotation θ_3 of the master arm corresponds to an equal angle rotation of the slave arm about the direction 'f'-'g'. The slave arm direction 'i'-'j' does not coincide with, but is parallel to, θ_5 of the master arm. The connection between these two axes is through a pair of identical gears, as shown in Fig. 7. The connection between the two arms at the other

* New industrial-quality product of Microbot, Inc.

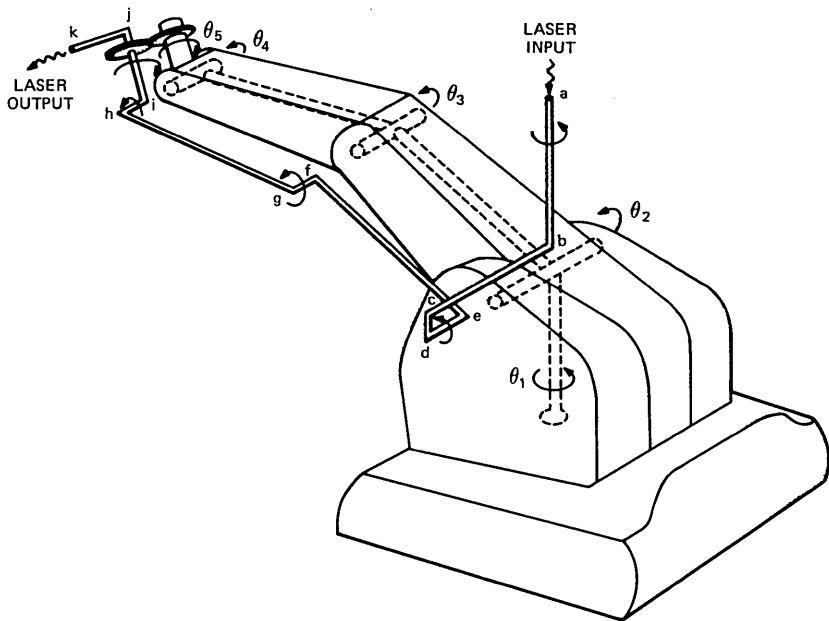


Fig. 6—Schematic diagram showing the master slave configuration of the CO₂ laser beam positioning robot.

four axes of rotation is via rigid mounts (not shown in Fig. 6) except for axis 3, where a moderately compliant plastic mount is used for attaching the two arms. This connection compensates for possible slight misalignments between the first four pairs of axes and thus prevents damage to the slave arm.

A precise description of the two-arm assembly is conveniently done using Denavit-Hartenberg¹³ notation, which is standard for robots. The five links of the slave arm are defined as follows. The origin is at the intersection between axes θ_1 and θ_2 . Link 1 is segment 'bcde'; Link 2 is segment 'defg'; Link 3 is segment 'fghi'; Link 4 is segment 'hij'; and Link 5 is segment 'ijk'. The exact geometry is given in Table I, where α_i is the twist angle, a_i is the i th link length, and d_i is the (i-1) to i th link distance. These definitions correspond to the conditions: 1) $a_2 = a_3 = 'hg' = 'ef'$; 2) $'hi' = 'gf' = 'de' = 2d_4$; 3) $'ab' 'cd', 'ij', 'jk'$ have arbitrary length.

The transmitted power efficiency should remain high. Extrapolating from the 6-mirror configuration, approximately 70-percent efficiency is expected. The resolution is determined by the master arm. In our case it is approximately 250 μ m. Note that the slave arm is detachable so that the robot can be used for other tasks.

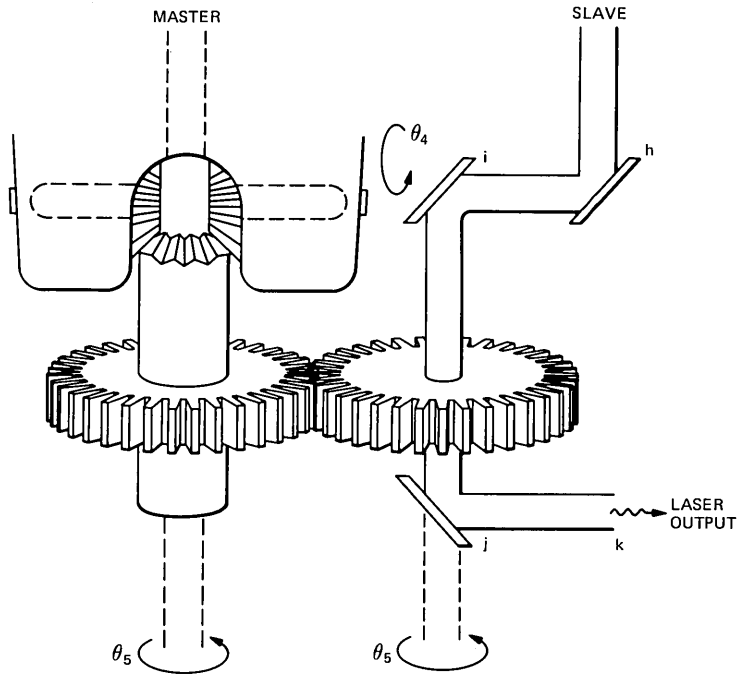


Fig. 7—Detail of the gear-connection of the 4th and 5th revolute axes of the master arm with the 'h-i' and 'i-j' revolute axes of the slave arm.

Table I—Denavit-Hartenberg manipulator parameters for the two-arm robot system

Link	Master			Slave		
	Twist Angle, α_i , in degrees	Link Length, a_i , in cm	Link Distance, d_i , in cm	Twist Angle, α_i , in degrees	Link Length, a_i , in cm	Link Distance, d_i , in cm
1	-90	0	0	-90	0	10.0
2	0	17.78	0	0	17.78	0
3	0	17.78	0	0	17.78	0
4	+90	0	0	+90	0	1.27
5	0	0	0	0	0	0

V. ROBOTIC MATERIAL PROCESSING

The use of high-power Nd:YAG lasers and CO₂ lasers for material processing such as welding, cutting, drilling, scribing, trimming, heat treating, annealing, etc., are well-documented.² Thermally and photochemically induced reactions are also well known. The advantages of robot-laser-processing of materials are dexterity in robotic-laser-beam maneuvering, processing of complex-shaped materials, and versatility in adapting the changing environments and changing material-

processing functions. Existing nonrobotic, dedicated laser material processing apparatus^{2,3} is much more restricted and expensive to modify should work requirement change. The combination of robots and high-power lasers is a natural technological direction to pursue for more versatile material handling and processing. The various forms of optical waveguides we describe here provide the important, and maybe indispensable, flexible links between robots and high-power lasers.

The use of these flexible, lightweight optical fiber waveguides (assuming they will also be available at long IR in the near future) for delivering high-power laser radiation to robots for material processing has several distinct advantages:

1. The bulky, heavy laser system could be remotely located so that any high electromagnetic interference (noise interfering with computer signal control of the robot and data transmission) could be eliminated.
2. The use of lightweight flexible optical fiber waveguides on the robot arm (or body) allows laser-material processing in mobile robots without undue constraints on their mobility.
3. Since the work space is not crowded by the use of high-power lasers, multiple robots can work together simultaneously in a complicated laser-material-processing task.
4. The use of several different kinds of high-power lasers at different wavelengths in a single robot can be achieved easily by routing multiple waveguides of different types through the robot, with appropriate shutters to control the switching of laser beams.

Our preliminary experimental results show that we can transmit (deliver) 5W of cw Nd:YAG laser power to the silica glass fiber output suitable for laser soldering. With high-power Nd:YAG lasers and more effort in fiber design and coupling, we expect to be able to deliver more than 10W (cw) through single-mode fibers and more than 25W (cw) through multimode, large-core silica glass fibers. Since the damage threshold for silica glass fibers is in the GW/cm² range, pulsed laser of high peak power also can be transmitted. With such lightweight optical fibers giving out such high-output laser power at the fingertip (gripper) of a robot, even a small inexpensive robot can perform many complicated material-processing or microprocessing functions.

With long IR lasers such as CO₂ lasers and the Bridges/Strnad type waveguiding articulating arm, 5W of power has been transmitted. Much higher-power (20 to 100W) transmission is expected before mirror damage occurs. With future advances in low-loss long IR fibers, truly flexible CO₂ laser transmission at 20- to 40W levels⁶ can be expected.

The positioning resolution and repeatability in robotic laser material processing depend on the specific robot design. High positioning

precision (10- μ m repeatability) and high positioning speed (1.6-m/s) robots¹⁴ are fast becoming available. The use of lightweight flexible waveguides for high-power laser delivery to robot arm ensures that such high positioning accuracy and speed will not be compromised. This is another distinct, significant advantage.

In summary, the use of appropriate optical waveguides for transmitting and delivering high-power laser radiation to a robot arm will make possible complex robotic-laser-processing of materials. Medical and biological applications of robotic microprocessing with fiber-guided lasers can also be envisioned. These could be considered a special case of robotic material processing. The combination of technology of high-power lasers, optical waveguides, and robotics will certainly open up a new era of laser material processing.

REFERENCES

1. See, for example, the review papers in Proc. IEEE (October 1980), special issue on Lightwave Communication Technology, and their references.
2. S. S. Charschan, *Lasers in Industry*, Western Electric Series, New York: Van Nostrand Reinhold, 1972.
3. J. F. Ready, *Industrial Applications of Lasers*, New York: John Wiley, 1980.
4. G. Nath, "Hand-held laser welding of metals using fiber optics," *Optics and Laser Technology*, 6, No. 5 (October 1974), pp. 233-5.
5. T. Miyashita and T. Manabe, "Infrared optical fibers," *IEEE Trans. Microwave Theory and Tech.*, *MTT-30*, No. 10 (October 1982), pp. 1420-38.
6. S. Sakuragi, "Polycrystalline KRS-5 infrared fibers for power transmission," in *Advances in IR Fibers*, Tech. Digest, SPIE, Los Angeles, CA., January 26-28, 1982, paper 320-02.
7. T. J. Bridges, J. S. Hasiak, and A. R. Strnad, "Single crystal AgBr infrared optical fibers," *Opt. Lett.*, 5, No. 3 (March 1980), pp. 85-6.
8. T. J. Bridges and A. R. Strnad, "Waveguiding Articulating Arm for Laser Radiation," *Tech. Digest, 1st International Congress on Applications of Lasers and Electro-Optics*, Boston, Massachusetts, September 20-23, 1982, paper 1C-3, p. 25.
9. D. R. Herriott, "Application of Laser Light," *Scientific American*, 219 (September 1968), pp. 141-56.
10. E. Garmire et al., "Low loss propagation and polarization rotation in twisted infrared metal waveguides," *Appl. Phys. Letters*, 34, No. 1 (January 1979), pp. 35-7.
11. E. A. J. Marcatili and R. A. Schmelzter, "Hollow Metallic and Dielectric Waveguides for Long Distance Optical Transmission and Lasers," *B.S.T.J.* 43 (July 1964), pp. 1783-809. U. S. Patent #3,386,043, "Dielectric waveguide, maser amplifier and oscillator," E. A. J. Marcatili and R. A. Schmelzter; assigners to Bell Telephone Laboratories.
12. P. W. Smith, "A waveguide gas laser," *Appl. Phys. Letters*, 19, No. 5 (September 1971), pp. 132-4.
13. See, for example, R. P. Paul, *Robot Manipulators: Mathematics, Programming and Control*, Boston: MIT Press, 1981.
14. See, for example, *Robotics Today*, 5, No. 1 (February 1983).

AUTHORS

Chinlon Lin, B.S.E.E., 1967, National Taiwan University; M.S., 1970, University of Illinois; Ph.D., 1973, University of California at Berkeley; Bell Laboratories, 1974—. Mr. Lin has worked on tunable dye lasers, short-pulse generation, nonlinear optics in fibers for frequency conversion, single-mode fiber dispersion and bandwidth studies, picosecond-injection-laser pulse generation, and high-speed optoelectronics. At Berkeley, he received an IBM

Fellowship and a Lankersheim Scholarship. He is currently in the Laser Science Research Department. Mr. Lin received an IEE (London) Electronics Letters Premium Paper Award in 1980 for a paper on zero-dispersion-wave-length tailoring in single-mode fibers. Senior Member, IEEE, Topical Advisor for Fiber and Integrated Optics for the Optical Society of America since 1982.

Gerado Beni, Laurea (Physics), 1970, University of Florence (Italy); Ph.D. (Physics), 1974, University of California, Los Angeles; Bell Laboratories, 1974—. Mr. Beni has been involved in research with Bell Labs, first at Murray Hill as a Resident Physicist in the Scattering & Low Energy Physics Department (1974–76), and as MTS in the Theoretical Physics Department (1976); at Holmdel he was a member of the Solid State Device Physics Department (1977–82), and currently is in the Robotics Systems Research Department. His expertise includes four major fields: theoretics, electrochemistry, displays, and robotics. In these fields he has contributed approximately 80 papers and 8 patents. Fellow, American Physics Society; Member, New York Academy of Science, the Electrochemical Society, SID, and Robotics International.

Susan Hackwood, Ph.D., 1979 (Solid State Electrochemistry), Leicester Polytechnic, United Kingdom; Bell Laboratories, 1980—. Ms. Hackwood has conducted research in catalysis, display technology, physical electrochemistry, sensors, and device robotics. Currently in the Electronics Research laboratory, she is involved with device robotics research for semiconductor fabrication. She has contributed approximately 40 technical papers and holds eight patents in the fields of physical electrochemistry, displays, and robotics. She is on the steering committee for Display Technology (ECS), which now includes robot sensors, and is the robotics representative of the Electronic Materials Committee of the Metallurgical Society of AIME. Member, American Physical Society, The Electrochemical Society, SID, and Robotics International.

Thomas J. Bridges, B.Sc. (Engineering), 1943, London University; Royal Naval Scientific Service (U. K.), 1944–1956, 1959–1963; Bell Laboratories, 1956–1958, 1963—; Massachusetts Institute of Technology, 1967–1968. At MIT Mr. Bridges was a Visiting Professor of Electrical Engineering. At Bell Laboratories he has worked on millimeter waves, microwaves, infrared lasers, and optically pumped far-infrared lasers. He currently supervises a group working on vapor phase epitaxy of semiconductor compounds.

Estimates of Path Loss and Radiated Power for UHF Mobile-Satellite Systems

By D. O. REUDINK*

(Manuscript received March 29, 1982)

This paper examines the satellite power requirements for land-mobile satellite systems, taking into account both shadow and multipath fading. Depending upon reliability objectives, present-day satellite capabilities will permit from 20 to 200 "(Advanced Mobile Phone Service) AMPS-like" circuits. Since satellite systems cost hundreds of millions of dollars, mobile-satellite telephony in a conventional sense would be expensive. Techniques are examined that in the far-term may permit a factor of 10 increase in capacity while still using moderate-size satellites.

I. INTRODUCTION

For the next decade or more the new 900-MHz land-mobile systems using cellular concepts will be introduced only in large cities. Any kind of nationwide service with full coverage will take many years. However, there are many nonurban applications where telephone service would be highly desirable, including service to vehicles along the nation's interstate highways, to rural residences currently without means of obtaining wire-line service, and to aircraft.¹⁻³ Communication from a satellite to small, portable terminals has been achieved, primarily demonstrating technical feasibility.^{4,5} Other studies examined system costs assuming satellite payloads much larger than current capability, and paying little attention to propagation effects.⁶⁻⁸ Although the monetary costs looked rather favorable, no such satellites or launch

* Bell Laboratories.

©Copyright 1983, American Telephone & Telegraph Company. Photo reproduction for noncommercial use is permitted without payment of royalty provided that each reproduction is done without alteration and that the Journal reference and copyright notice are included on the first page. The title and abstract, but no other portions, of this paper may be copied or distributed royalty free by computer-based and other information-service systems without further permission. Permission to reproduce or republish any other portion of this paper must be obtained from the Editor.

capabilities are expected in the near future. Here, the capacity-performance trade-offs are examined on realistic assumptions of near-term satellite capabilities, considering propagation conditions in some detail.

The issue of cost is not addressed except to mention that a modern, one-of-a-kind* satellite, in orbit, might be expected to cost well over 100 million dollars. At the same time the circuit capacity compared to a satellite system with large, fixed ground antennas will be smaller.

The procedure for the remainder of this paper is first to calculate an optimistic link budget based upon the assumption that there is a line-of-sight path between the satellite and the mobile system. Following this, estimates are made for the additional losses on the path due to obstructions near the mobile system; then an attempt is made to determine whether it is feasible to obtain sufficient radiated power in the satellite to make up these losses; finally, more spectrum- and power-efficient options are examined.

II. LINE-OF-SIGHT LINK BUDGET

The radiated power requirements on the satellite resources will be determined by working backwards from the mobile system. Assume for now frequency-division multiple access with a minimum carrier-to-noise ratio (CNR) of 10 dB in a 20-kHz bandwidth. These numbers are roughly consistent with the FM threshold and bandwidth requirements for present-day cellular mobile systems and would correspond to something that might be feasible in terms of a digital system in the future. These numbers imply $10 \log C/kT = 53 \text{ dBW/K/Hz}$.

Since the mobile system can be driven in any direction, it is necessary that the antenna be omnidirectional in the azimuthal plane; however, since the satellite is never directly overhead, it is possible to form a conical beam in the elevation plane, and obtain a gain of about 6 dB. Assume a system noise temperature of 400 degrees for the mobile system. Although lower-noise receivers certainly could be built, limitations of man-made noise will prevent the effective use of lower-noise receivers; furthermore, the additional cost of ultra-low-noise receivers in mobile systems may be prohibitive. These two assumptions imply a $G/T = -20$. With these numbers the required illumination on the earth is -134 dBW/m^2 . The path loss from the satellite to the mobile system calculates to 184 dB. As shown in Table I, the required Effective Isotropic Radiated Power (EIRP) per channel is 28 dBW at the satellite.

* Multiple-satellite operation with frequency reuse would be practically impossible to achieve because the mobile antennas radiate essentially in an omnidirectional pattern, so there is no way to discriminate one satellite from another.

Table I—Link budget for a single mobile-satellite channel

Minimum CNR at mobile	10 dB
Noise bandwidth	20 kHz
Mobile receiver noise temperature	400°K
Antenna gain	6 dB
G/T	-20
Path loss	184 dB
Required satellite EIRP	28 dBW

It is possible to have an antenna with nearly a 15-foot diameter within the Space Shuttle. At 900 MHz such an antenna would provide an on-axis gain of 31 dB, while the gain at the edge of the country would be about 29 dB. We assume on the average that 30 dB of antenna gain is available, which implies a required radiated power per channel of -2 dBW for Continental United States (CONUS) coverage. The average RF power consistent with moderate-size satellites in the 1980s time frame is about 200W (+23 dBW), which implies 316 satellite-mobile channels.

III. ADDITIONAL PATH LOSSES

Excess path losses on land-mobile paths have been measured at numerous frequencies over a variety of paths worldwide. A great amount of data exists in the 800- to 900-MHz frequency band for land-mobile paths, but little data have been published on the losses over satellite-to-mobile paths. To estimate what losses might be expected, Fig. 1 shows a plot of the median path loss in excess of the free space path loss as measured for various base-station antenna heights,⁹ plotted in terms of the elevation angle between the mobile and the base station. For distances of both 1 and 2 km from the base station, the points lie nearly on a straight line on semilog paper.

A recently published paper indicates that satellite path losses in the Denver area (elevation angle 32 degrees) range from 3 to 20 dB over line-of-sight.¹⁰ The author's statistical description for excess path loss, corresponding to 50-percent large-scale coverage, estimates 9.8-dB excess path loss for a suburban environment with an elevation angle of 30 degrees. This value is in good agreement with the curve depicting a suburban environment plotted in Fig. 1. For more rural locations, satellite measurements would predict 5.3-dB excess path loss,³ which tends to agree with the straight-line projection of the two data points taken 10 km distant from the high-elevation base stations. In all cases, due to the more favorable elevation angles, excess path losses are less severe on satellite-mobile paths compared to typical land-mobile paths, as long as the satellite is located at a longitude such that the slant range is not excessive.

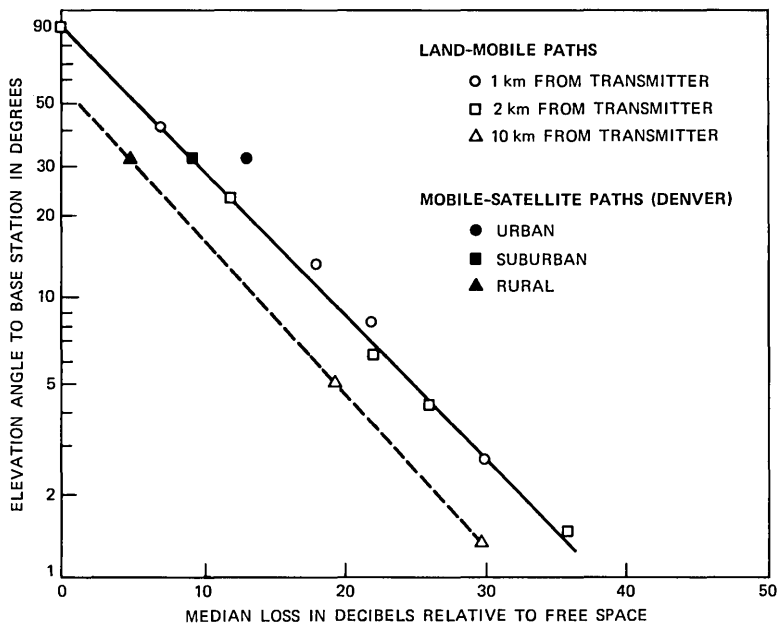


Fig. 1—Excess attenuation vs elevation angle at 900 MHz.

For a favorable satellite longitude and for most locations in the United States, the elevation angle to the satellite generally will be greater than 30 degrees and less than 60 degrees, indicating that it is reasonable to expect the median losses over free space to range from 3 to 10 dB, except possibly in urban areas where greater losses would be expected.

Data reported on land-mobile paths indicate that the distribution of the signal about the median is log normal with standard deviations ranging from 5 to 10 dB.⁹ The log-normal distribution found in the land-mobile case arises from large-scale obstructions such as tall buildings and hills, which shadow the line-of-sight path. Intuitively, one might expect the variation of signal strength to be less severe on a satellite-mobile path, since typical elevation angles for a satellite are 30 degrees or more, where usual land-mobile paths have elevation angles more on the order of a degree or so. Based on the satellite data of Ref. 10, the variance of the log normal appears to be somewhat less for satellite paths than for land-mobile paths, but not dramatically so.

Figure 2 is a plot of what might be called the expected range of additional losses relative to free space based on available measured data.¹⁰ It can be seen that high margins are required to provide service to approximately 99 percent of the regions of the country. Even assuming most regions of service interest are rural, margins in excess

of 10 dB are often required. Furthermore, this would assume the propagation characteristics of the entire country are similar to those in the Denver area. A far safer approach (and perhaps more accurate) is to employ the suburban model to represent the small cities and towns where the bulk of the demand may be expected. In this case, to cover 90 percent of locations would require a signal approximately 16 dB above the line-of-sight value, and the value would increase to 21 dB for 99-percent coverage.

IV. MULTIPATH FADING

Another factor crucial to system performance is the effect of multipath fading. A line-of-sight component can be expected frequently on the satellite path. This component plus signal components, which scatter into the mobile antenna from nearby objects, produce a Rician signal distribution with significantly less fading than occurs with a Rayleigh distributed signal. Data on satellite paths confirm Rician-like signal statistics.¹⁰ For example, level crossing rates can be an

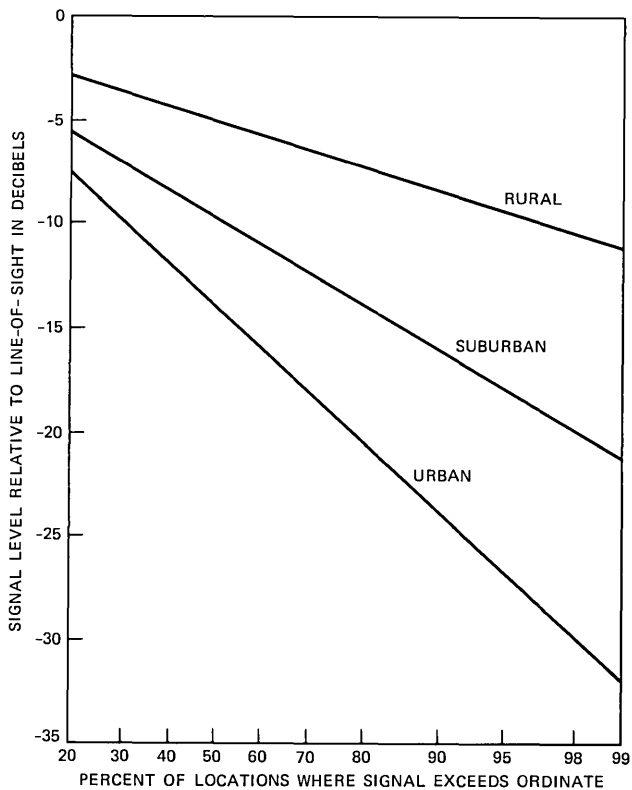


Fig. 2—Estimates of signal strength distribution on satellite-mobile paths.

order of magnitude or more lower compared to Rayleigh fading. Unfortunately, fading will be worst just at the wrong time—when the line-of-sight component is obscured and the received signal strength is low. Under these conditions the received signal can be assumed Rayleigh, and expected performance has been calculated.¹¹ In white Gaussian noise, a 10^{-3} Bit Error Rate (BER) is attained with an average energy per bit (E_b) 6.9 dB above the noise density (N_0) for biphase coherent phase shift keyed signals, while in the presence of Rayleigh fading an average E_b/N_0 of 24 dB is required. Spatially separated antennas whose signals are combined in phase can significantly reduce bit error rates. Figure 3 is a plot of BER vs E_b/N_0 for various numbers of diversity elements. For a 10^{-3} BER with three elements, E_b/N_0 per element drops to 7 dB, and with eight diversity elements it drops to 0 dB E_b/N_0 . This somewhat surprising result is readily understood if one considers the eight elements as an antenna array, whose effective gain is 9 dB higher than a single element.

Space diversity works well on mobile systems, even with closely spaced elements ($< \lambda$) that have highly correlated (0.5) signals.⁹ However, space diversity cannot be achieved at the satellite because the arriving signal is essentially a plane wave, and extremely large separation of the satellite antennas would be required. A technique

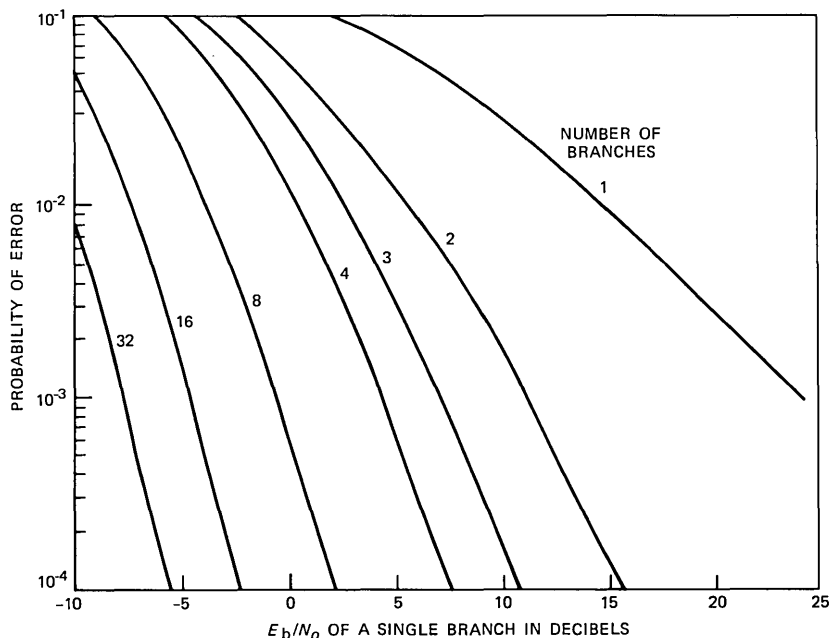


Fig. 3—Error probability of Two Coherent Phase Shift Keying (CPSK) with Rayleigh fading and diversity.

called retransmission diversity has been suggested for both analog⁹ and digital transmission.¹² The idea is to transmit the conjugate phase of the received carrier on the same or a closely spaced carrier. By doing so, the signals from all mobile diversity branches will automatically arrive in phase at the satellite. In the original thinking for land-mobile system use, retransmissions would occur at the base stations, thereby simplifying the mobile system. In this instance, the only workable method is to place the retransmission apparatus at the mobile system. The analog scheme mentioned above would be very difficult to build, since the transmit and receive frequencies are closely spaced (<100 kHz), and the two signals differ in power by many tens of decibels. The digital techniques employ packet transmissions, and any hope for compatibility with cellular systems would be lost.

If the system were not constrained in bandwidth, then similar results could be obtained by employing frequency diversity channels. Beyond its obvious inefficiency, another drawback with frequency diversity is that the satellite must transmit the same signal on multiple channels, which requires more equipment and power. Another approach that achieves diversity advantage is to employ frequency hopping or spread-spectrum techniques.¹³ This would eliminate the retransmission problem of space diversity but with possible reduction in capacity. An interesting possibility would be to combine space diversity with spread spectrum, using space-diversity mobile reception (because satellite power is at a premium) and spread-spectrum mobile transmission to combat Rayleigh fading.

Table II summarizes the per-channel power margins required for the various conditions of shadow and multipath fading, as discussed previously. We assume that a threshold of 10^{-3} BER is achieved with a calculated signal-to-noise ratio (s/n) = 10 dB. This allows 3.1 dB of implementation margin for filter and transmission line losses, antenna pointing errors, and nonideal detection equipment. The first observation from this table is that, without diversity, satellite-mobile com-

Table II—Power margin in excess of free space propagation, required to overcome shadow fading, and attain $BER \leq 10^{-3}$ in Rayleigh fading

Per- cent Cover- age	Margin Above Line-of-Sight (dB)								
	Urban Environment			Suburban Environment			Rural Environment		
	No Di- versity	2 Di- versity	8 Di- versity	No Di- versity	2 Di- versity	8 Di- versity	No Di- versity	2 Di- versity	8 Di- versity
50%	31	18	13	27	14	9	22	9	4
90%	41	28	23	33	20	15	25.5	12.5	7.5
99%	49	36	31	38	25	20	28	15	10

munications in dense urban areas is unachievable for the majority of locations. However, it is expected that cellular mobile systems will handle this traffic anyway. A margin of 15 dB with two-branch diversity would provide service to 99 percent of the rural locations, 60 percent of suburban locations, but only 25 percent of the urban locations.

Using Figs. 2 and 3, together with the link budget calculated in Table I, we can estimate quality of service for a given satellite EIRP. Table III gives the percentage of rural or suburban locations where performance exceeds the given BER for the indicated per-channel satellite transmitter power and for mobile systems with three diversity branches. Having only two diversity branches would increase power requirements by 3 to 5 dB, while having four diversity branches would lower the transmitter requirement by 2 to 3 dB, depending on the chosen threshold.

It is clear that typical satellite configurations are severely power limited when it comes to providing mobile services. Previously we saw that 316 circuits were available when all mobiles are line-of-sight. Permitting 15 dB of margin on each circuit reduces the capacity to only 10 circuits. Thus, ways of obtaining more EIRP must be found.

V. ADDITIONAL SATELLITE EIRP

It appears obvious that an approximate 10-dB signal-strength margin will be required for any reasonable satellite-mobile system. In Section II, calculations showed that 200W of RF power were required for 316 channels based on line-of-sight propagation. If only 32 channels were used, then an additional 10 dB of radiated power per channel would be available. However, cost estimates in this paper's introduction indicate that this would be almost certainly a cost-ineffective approach. On the other hand, the state-of-the-art cannot provide 2 kW of RF power in a satellite today; thus, we look to other means of effecting higher EIRP or its equivalent.

The question of efficient multiple-channel satellite transmission is

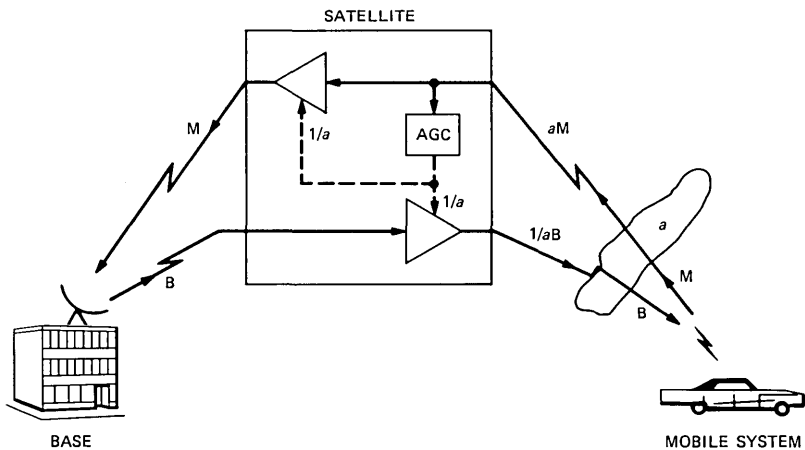
Table III—System performance for mobiles with three diversity branches

Percentage of Locations With BER Less Than Value	Satellite EIRP/Channel					
	33 dBW		38 dBW		43 dBW	
	Rural	Suburban	Rural	Suburban	Rural	Suburban
10^{-1}	>99.9	85	>99.9	92	>99.9	98
10^{-2}	96	45	>99.9	82	>99.9	91
10^{-3}	50	18	97	50	>99.9	78
10^{-4}	12	6	82	35	99.7	65

very complex. Given a total payload mass for power amplifiers and solar cells and batteries, what techniques best satisfy the system requirements? When there are only a few channels, a single-amplifier-per-channel operation is usually the simplest. For a large number of channels, the hardware complexity of a multitude of amplifiers and of multiplexing these RF signals onto an antenna feed necessitates another approach. Multicarrier operation (for analog or digital signals) simplifies the satellite tremendously but at a cost of power efficiency and potential intermodulation distortion. Transmitting digitally multiplexed signals from the satellite eliminates intermodulation and allows efficient high-power class C amplification, but requires that all signals be of the same power and that mobiles have high-speed Time-Division Multiple Access (TDMA) receivers. These issues as well as other transmission-efficient techniques are addressed in the following subsections.

5.1 Power control

We note that it is wasteful to provide all vehicles with the 10 dB or so margin to ensure that most of the vehicles have a signal above threshold. After all, some vehicles will be line-of-sight to the satellite and require substantially less power than those behind a mountain. Ideally, just enough power should be made available to ensure that each vehicle has a signal above threshold. This can be accomplished by using the technique illustrated in Fig. 4. The automatic gain-control signal is applied to a second transmitter carrying the message from the ground to the satellite. For illustration, the circuit is shown in the



AGC – AUTOMATIC GAIN CONTROL

Fig. 4—A technique to reduce shadow fading on mobile-satellite paths.

satellite, but it could be located at the earth station just as well if the satellite amplifier is linear. Because of the path delays, it could take a half-second or so to make a power adjustment. Therefore, the technique can be applied against slowly varying shadowing such as hills or large terrain features but not against multipath fading.

Recent work of Yeh and Schwarz allows us to calculate the total power expected from the sum of any number of log-normally distributed carriers.¹⁴ Figure 5 contains plots that show the mean decibel value of a log-normal distribution that is derived from the sum of a number of log normals with the same mean (0 dB) and standard deviations ($\sigma = 2.5, 5, 7.5$ and 10 dB); these σ 's correspond roughly to rural, suburban, urban, and dense urban environments. For example, the resultant of summing 100 carriers whose standard deviations are 5 dB is (approximately) a log normal whose mean is 22.5 dB. This means that providing a total peak RF power that is 22.5 dB above that of a single carrier would satisfy the power demand 50 percent of

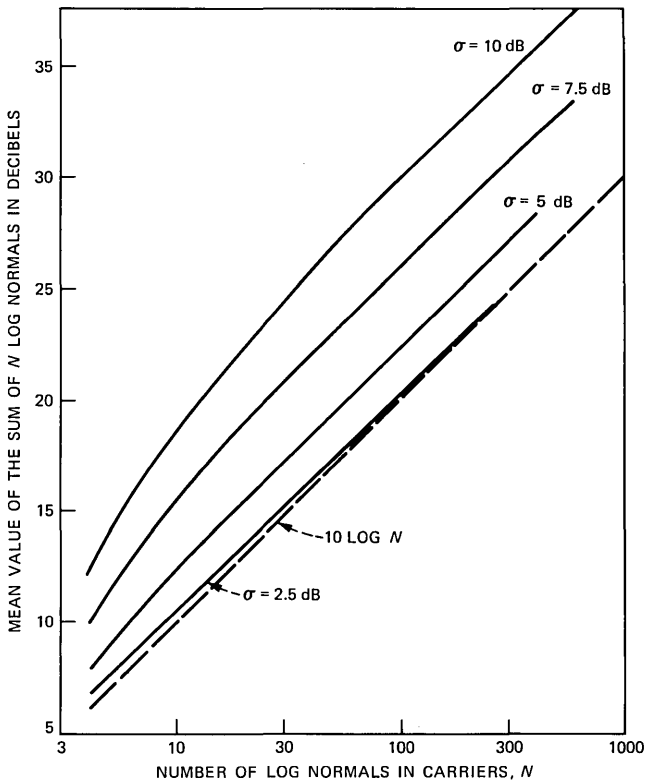


Fig. 5—Mean decibel values of log-normal distribution derived from log normals with same mean and standard deviations.

the time when 100 log-normal carriers are individually transmitted. Figure 6, similar to Fig. 5, is a plot of the mean plus twice the standard deviation of the resultant log normals when a number of identically distributed carriers are summed. Permitting an average power of the value shown in Fig. 6 reduces to 4.3 percent the time fraction that power is not available to meet demand. Compared with the previous example of 100 individually transmitted carriers with $\sigma = 5$ dB, the peak power must now be 24.5 dB above that for a single carrier, about a 2-dB increase.

To ensure 95.7-percent coverage assuming a standard deviation of 5 dB for a single log-normal carrier, requires a margin 10 dB (2σ) above its mean. Thus, it appears that transmitting each carrier with power just sufficient to overcome the path attenuation results in a power savings of about 5.5 dB compared to transmitting all signals with power 10 dB above the mean.

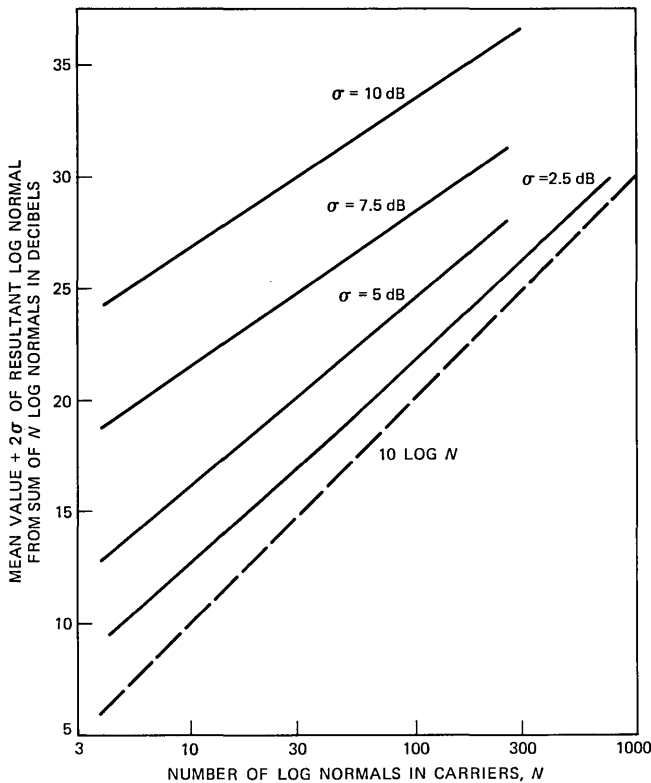


Fig. 6—Plot of mean plus twice the standard deviation of resultant log normals when identically distributed carriers are summed.

5.2 Multicarrier considerations

The calculations above imply that each carrier is transmitted separately. Usually it is far more efficient from the point-of-view of spacecraft hardware and complexity to combine signals and transmit them from a single high-power amplifier rather than employ many (hundreds) of low-power amplifiers. Since the signals add in voltage, the peak power requirement will be considerably above the average; and since amplifiers are not ideal, intermodulation results. Calculations of intermodulation distortion for the case of equal-amplitude but randomly phased signals for both ideal and typical power amplifiers have been made by Saleh.¹⁵ Typical results are shown in Fig. 7. To achieve the minimum acceptable $C/(I + N)$ of 10 dB requires that the average power of an ideal amplifier be "backed off" 3 dB from its peak power and that any realistic amplifier be backed off 3.5 dB from its peak power point. For more typical operating conditions, $C/(I + N) > 15$ dB, back-offs would be 5 to 7 dB, depending on the amplifier and compensation used. This implies that, even for a power amplifier which is 50 percent efficient at saturation when operated in the linear region, the dc-to-RF efficiency can only be about 12 percent. Still there can be an overall weight savings in the satellite compared to using individual amplifiers, but quantitative calculations are beyond the scope of these considerations.

The power back-off numbers cited are calculated for equal-amplitude carriers with random phases. For the mobile-satellite case with power control, the carriers have independent randomly distributed phases, but the amplitudes are log-normally distributed. Greenstein has reasoned that similar results should be expected for this case; however, the calculations remain to be done.*

5.3 Resource sharing and coding

Resource sharing has been suggested for TDMA systems as a means to increase a link margin by nearly 10 dB. The idea is to assign the user in a shadow fade a longer time slot, and encode the signal. For digital mobile-satellite service, this technique could be considered, but for analog modulation its implementation is less obvious. For resource sharing to be effective, it is necessary that the majority of mobiles not require the use of the additional resource of a coded signal. For a given system bandwidth, the cost of resource sharing is a reduction in

* Simulations of L. Greenstein and A. Saleh have shown that for sample cases with as few as 100 log-normal carriers with random phases, the resultant envelope tends to be Rayleigh distributed. Thus, at least over time periods where the amplitudes of the carriers, and thus the average power, can be considered fixed, the calculated results based on equal amplitude carriers should be usable.

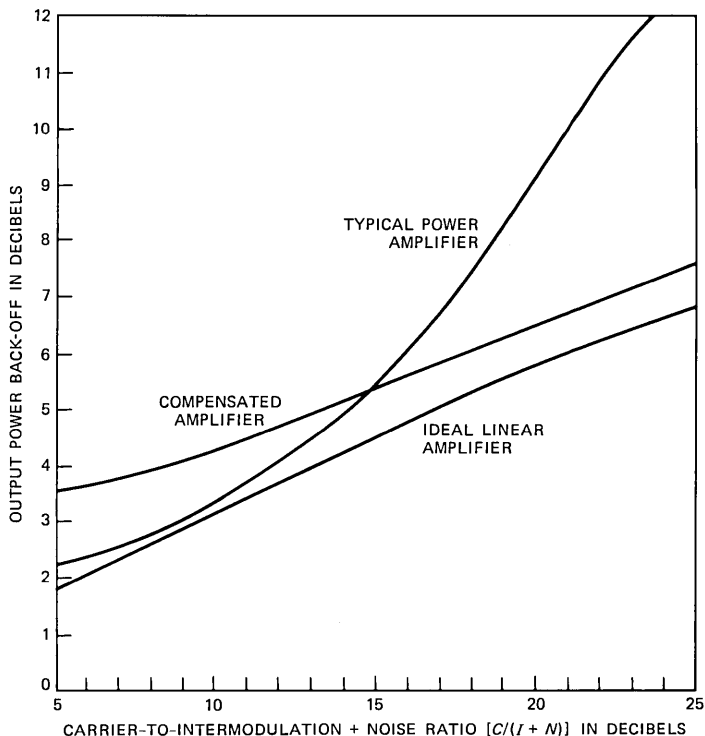


Fig. 7—Back-off required to achieve a given $C/(I + N)$.

transmission rate, but at an increase in margin. For 12/14 GHz fixed-satellite systems, the intent is to apply resource sharing only to those stations experiencing rain fading. Even using a rate 1/3 code (i.e., three transmitted bits per information bit) for these users, it was estimated that the loss in throughput is only a few percent, since very few users need resource sharing simultaneously.¹⁶ As shown in Fig. 8, the throughput drops dramatically when the fraction of simultaneous users of resource sharing becomes significant. The curve in Fig. 8 assumes a fixed total system bandwidth and a rate 1/3 code for users of resource sharing. For example, when 10 percent of the users need resource sharing, the total number of users decreases by 17 percent while, if 50 percent of the users need resource sharing, the system capacity drops to 50 percent of the original value. To ensure that at any one time only a small percentage of the mobiles require resource sharing implies that the system normally operates with a margin somewhat above the median excess path loss. From Fig. 2 we see that (depending upon the degree of optimism), providing somewhere between 6 and 12 dB extra power over free space propagation would

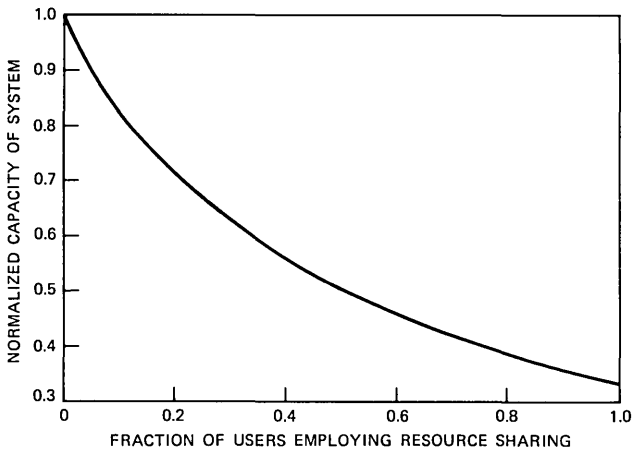


Fig. 8—Capacity loss with resource sharing using rate one-third code.

ensure that fewer than one third of the mobiles would require resource sharing at any given time. The additional margin obtainable from resource sharing then can extend the range of coverage from approximately two thirds of all locations to more than 90 percent. As in the case of power control, resource sharing cannot be applied instantaneously because of the time delays involved from the time measurement to the application of coding. Thus, the application is only for cases of slowly varying changes in signal strength.

The original resource sharing concept assumed that all users shared a single wideband channel. Implementation in a frequency-channelized system is less straightforward. However, if the system is not bandwidth limited, then all channels could use, say, a rate 1/3 code, thereby gaining an advantage of roughly 4 dB, plus or minus a decibel, depending upon the constraint length of the code and the particular implementation of the decoder.¹⁷ Since the channel bandwidth is now three times wider, the mobile receiver is degraded by 5 dB, thus the large apparent gains of resource sharing cannot be realized.

5.4 Trade-offs between radiated power and antenna gain

There are two ways to increase effective radiated power from a satellite. The first is simply to increase the transmitter power. The second is to increase the antenna gain. Although the techniques are equivalent in terms of the radiation to a point on earth, each implementation has different ramifications. Increasing radiated power is relatively straightforward in that the coverage area remains the same, and the burden on the satellite is to obtain more dc power through the use of more solar cells and to provide more battery power for eclipse

operation. Note that the eclipses only occur at night when, presumably, usage and power requirements would be greatly reduced.

Normally the satellite-mobile service would not be a broadcast mode, that is, it would not be necessary to talk to more than one mobile system over a single channel; therefore, the information to that mobile system can be confined to a small antenna beam. Thus, having a large number of high-gain beams covering the entire country becomes power efficient, since the power is only radiated in the beam intended for that mobile.^{1,2,5} An additional benefit of spot beams is the possibility that the channels can be reused between areas that are spatially separated by a few beamwidths. In the case of conventional point-to-point telephony, demand is spatially nonuniform and highly peaked. If such is the case here, the advantages of reuse cannot be fully realized.

In a recent note it is proved for idealized constraints that maximum EIRP is obtained when the communications payload of the satellite is divided equally between the RF power subsystem and the antenna subsystem.¹⁸ Sample calculations indicate that at frequencies above 1 GHz, multibeam antennas are more effective in increasing EIRP compared to using United States coverage antennas and high-power amplifiers. Earlier it was stated that a satellite providing 53-dBW EIRP (30-dB antenna gain, 200W RF power) could be achieved fairly conveniently. With battery backup either reduced or eliminated, 55 dBW should be attainable in an advanced state-of-the-art satellite using a United States coverage antenna.

Plotted in Fig. 9 are two curves that show EIRP as a function of payload mass. The lower curve is for a satellite with a United States coverage antenna where EIRP is increased only through increased transmitter power. The upper curve is the case where EIRP is maximized by dividing the payload equally between the antenna and the transmitter subsystems. At the point where a satellite with a United States coverage antenna provides 55 dBW, the maximum EIRP available is 58.2 dBW, assuming gain is achieved at 50 times isotropic per kg, and RF power is produced at 2.5 W/kg.* Under these conditions the antenna would weigh 73 kg and have a gain of 35.5 dB, implying three or four zone beam coverage of the United States, and a total RF power of approximately 180W would be transmitted.

Use of spot beams for EIRPs near 55 dB can generate an EIRP increase of about 3 dB. At 900 MHz the antenna diameter is already

* The units here are somewhat unusual, but for a given frequency, antenna gain is proportional to the antenna surface area that weighs so many kg/m². Likewise, power is derived from solar cells producing so many watts/kg. Thus, both antenna gain and RF power can be expressed as functions of mass.

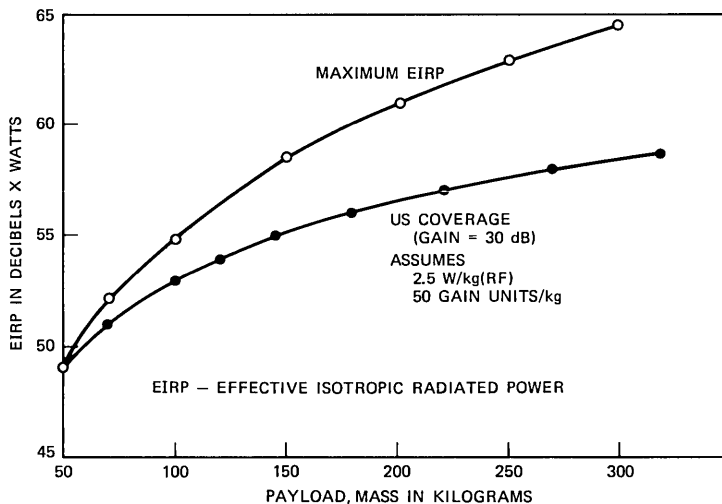


Fig. 9—Effective radiated power as a function of payload mass.

around 8m to provide a gain of 35.5 dB. For large payload satellites with EIRPs of 65 dBW, over 3 kW of RF power would have to be transmitted if United States coverage antennas were used, while use of a spot beam antenna with maximized EIRP permits 65 dBW of radiated power with one quarter the payload mass. Still, the required payload mass is 300 kg, twice the size of most current-day satellites.

5.5 Source coding and narrowband modulation

Although obvious, it should be mentioned that employing narrower band channels improves the predetection CNR. Although modulations such as companded Single-Sideband (SSB) have been demonstrated, their performance in multipath environments will be degraded. Likewise, low-bit-rate voice coders (10 kb/s) may provide reasonable voice quality, but such coders are complex, and whether acceptable performance can be achieved with channel errors is not known. However, since the prospects for compatibility of satellite transmission with present-day land-mobile radio look dismal, the possibility of using other techniques to gain perhaps as much as 6 dB in link budget compared to analog FM need to be investigated further.

5.6 Summary of possible improvements in link budget

Since it is envisioned that much more than a thousand channels are necessary for any practical system, the single-amplifier-per-channel approach is not feasible. The next most straightforward technique is to use multiple carriers on a single (or few) wideband channel. This

does not rule out compatibility with FM cellular systems, but major system problems remain.

Multicarrier operation should result in increased payload, and thus higher potential EIRP, but actual increases are difficult to calculate. Back-off can be eliminated if the downlink signals are digital and multiplexed onto a single carrier; however, downlink power control cannot be achieved under this condition. Mobiles would require TDMA receivers, and for bandwidths greater than 1 MHz, reception may be impaired by multipath propagation.

Table IV lists techniques that can potentially increase or decrease effective radiated power. For cellular-like service using a present-day satellite, techniques D, E, F, and G can be applied, yielding possible increases in EIRP from 0 to 8 dB. With SSB an additional 6 dB advantage may be possible (Item C). With digital modulation Item A is added and B replaces C, for a link-budget gain of 3 to 15 dB. With digital multiplexing, D and E are eliminated and H can replace A, for possible link-budget increases of 11 to 19 dB. Finally, using more diversity elements (Item I) helps the link budget significantly, especially at low BER.

VI. CAPACITY CALCULATIONS

Satellite design is very complex, and no claim is made that actual satellites can be designed with the calculated capacities. Rather, the purpose here is to determine the effect in a general sense to some of the many options available. To that end, we make the simplifying assumption that changes in capacity are proportional to changes in effective radiated power. Thus when bandwidth is not a constraining factor, the number of circuits is determined by the simple relationship,

$$C = C_{\beta} 10^{\left(\frac{G_L - M}{10}\right)},$$

where C_{β} is the baseline capacity calculated in on a line-of-sight basis

Table IV—Possible improvements in link budget

Technique	dB Increase
A Channel coding (Sec. 5.3)	2 to 4
B Source coding (Sec 5.5)	1 to 3
C Modulation (receiver bandwidth) (Sec 5.5)	3 to 6
D Power control on each channel (Sec. 5.1)	3 to 5
E Back-off loss (Sec. 5.2)	-7 to -4
F Maximize EIRP (Sec. 5.4)	2 to 4
G Reduced battery for eclipse (Sec. 5.4)	2 to 3
H Resource sharing (Sec. 5.3)	6 to 9
I Diversity elements (3 to 8) (compared to 2) (Sec. 4.0)	5 to 8
J Double-size payload (Sec. 5.4)	3 to 6
K Four-times payload (Sec. 5.4)	6 to 12

in Section II, G_L are the gains in the link budget discussed in Section V, and M is the margin determined in Section III for a given grade of service and terrain type.

For example, assume a rather low grade of service with only a 7-dB margin. Combine this with the most optimistic link-budget gain of 19 dB. Then the possible number of circuits is $316 \times 10^{1.2} = 5008$, and a 300-MHz spectrum allocation would be required. More realistically, a 10-dB improvement in the link budget might be obtained for a specially designed satellite system not compatible with current cellular systems. On the other hand a 10-dB margin is almost essential for good service. Taken together the 10-dB improvement is offset by a 10-dB margin and the capacity calculates to the baseline value of about 300 circuits.

VII. DISCUSSION AND CONCLUSIONS

It should be noted that use of diversity and tolerance of more bit errors can lower margin requirements significantly. For example, from Fig. 3 we see that, at 10^{-3} BER, going from two to four diversity elements reduces the margin requirement by 7 dB. Also, using two-branch diversity, but setting the system threshold at 10^{-2} BER instead of 10^{-3} BER, reduces the system margin by over 5 dB. The combination of the four-branch diversity at 10^{-2} BER threshold permits a 9-dB reduction in satellite EIRP compared to two-branch diversity and a 10^{-3} BER threshold. If this power savings could be directly traded for capacity, then eight times the number of circuits could be achieved. Downsizing the baseline calculations for low-bandwidth applications such as paging or emergency telephony is also possible.

As noted in Table IV, there is the potential of economy of scale. Satellite costs tend to run nearly linearly with weight¹⁹, but EIRP can increase with the square of satellite mass;¹⁸ and provided there are no bandwidth constraints, channel capacity can increase in direct proportion to EIRP. Thus, for satellites of twice the size (and at least twice the cost) four times as many circuits are obtained. In-orbit satellite mass as high as 5,000 kg are envisioned using the shuttle/Centaur. This represents a factor of 5 to 10 compared to present-day technology and suggests that future land-mobile service via satellite could become attractive. Trading power for capacity comes at the expense of bandwidth, a very precious commodity. On the other hand, terrestrial cellular systems will reuse frequencies hundreds of times nationwide. Making satellite-mobile systems spectrally efficient through the use of multibeam satellite antennas that can reuse frequencies is a tremendous technical challenge. Mile-diameter antennas are needed to get cell sizes comparable to terrestrial radio systems.

For service to aircraft, a 6-dB antenna gain for an aircraft in level flight seems reasonable, thus, line-of-sight capacity numbers apply

directly. For service to residences, an antenna gain of 16 dB is readily obtainable using a 1-m dish. Assuming there is a line-of-sight path and that there is sufficient bandwidth available, about 3000 circuits should be obtainable with present-day satellite capabilities, before power limitations become constraining.

Finally, it is safe to conclude that (1) cellular-compatible satellite-mobile systems are highly unlikely to be developed in the near future, (2) systems with modest-coverage objectives using enhanced-capability satellites and high-performance mobile sets look marginally attractive, and (3) very large satellites offer a possibility for mobile systems, in the long-term.

VIII. ACKNOWLEDGMENT

The author wishes to thank Y. S. Yeh and S. Schwarz for providing guidance on log-normal distributions; to A. Saleh for many helpful discussions and information on power amplifier performance; and to L. J. Greenstein for critically reading this manuscript and providing his helpful insights on this problem.

REFERENCES

1. G. H. Knouse and P. A. Castruccio, "The Concept of an Integrated Terrestrial/Land Mobile Satellite System," ICC 1980 Int. Conf. Commun. (June 1980), pp. 35.1.1-5.
2. G. H. Knouse, "Terrestrial/Land Mobile Satellite Considerations, NASA Plans, and Critical Issues," IEEE Trans. Veh. Technol., VT-29, No. 4 (November 1980), pp. 370-4.
3. M. W. Cardullo and C. Dorian, "Mobile Communications via Satellite," Telecommun. J. 36, (September 1969), pp. 426-36.
4. I. J. Jones et al., "A Study and Experiment Plan for Digital Mobile Communication Via Satellite," NASA Contract NASZ-9936, Report Number N81-1964.
5. R. E. Anderson et al., "Satellite-Aided Mobile Communications, Experiments, Applications and Prospects," IEEE Trans. Veh. Technol., VT-30, No. 2 (May 1981), pp. 54-61.
6. T. Iida, "Satellite Systems for Land Mobile Communications," J. Radio Res. Lab., 27, Nos. 122/123, March-July 1980, pp. 97-115.
7. D. L. Wright and J. D. Kiesling, "Communication Satellite Services for Special Purpose Users," Proc. First Int. Telecommun. Exposition, Atlanta, 1, (October 1977), pp. 200-8.
8. J. A. Weiss, "Low Cost Satellite Land Mobile Service for Nationwide Applications," 28th IEEE-VT Conf., Denver, CO, March 22-24, 1978, pp. 428-37.
9. W. C. Jakes, Jr., Ed., *Microwave Mobile Communications*, N. Y.: John Wiley, 1974.
10. G. C. Hess, "Land-Mobile Satellite Excess Path Loss Measurements," IEEE Trans. on VT, VT-29, No. 2 (May 1980), pp. 290-7.
11. M. Schwartz, W. A. Bennett, and S. Stein, "Communication Systems and Techniques," New York: McGraw Hill, 1966, Chapter 7.
12. B. Glance and P. S. Henry, "A New Approach to High-Capacity Digital Mobile Radio," B.S.T.J., 60, No. 8 (Oct. 1981), pp. 1891-904.
13. D. J. Goodman, P. S. Henry, and V. K. Prabhu, "Frequency Hopped-Multilevel FSK for Mobile Radio," B.S.T.J., 59, No. 7 (September 1980), pp. 1257-75.
14. Y. S. Yeh and S. Schwarz, "On the Distribution Function and Moments of Power Sums with Log-Normal Components," B.S.T.J., 61, No. 7 (September 1982) 1441-62.
15. A. A. M. Saleh, "Intermodulation Analysis of FDMA Satellite Systems Employing Compensated and Uncompensated TWT's," IEEE Trans. Commun. COM-30, No. 5 (May 1982), pp. 1233-42.

16. A. S. Acampora, "Rain Margin Improvement Using Resource Sharing in 12 GHz Satellite Downlink," *B.S.T.J.* 60, No. 2 (February 1981), pp. 167-92.
17. I. M. Jacobs, "Practical Applications of Coding," *IEEE Trans. on I.T., IT-20*, No. 3 (May 1974), pp. 305-10.
18. D. O. Reudink, "Maximum Power Transmission in Mass-Limited Radio Systems," *IEEE COM SOC*, February 1982.
19. D. H. Staelin and R. L. Harvey, "Future Large Broadband Switched Satellite Communication Networks," NASA Report NAS-5-25091, December 1979.

AUTHOR

Douglas O. Reudink, B. A. (Physics), 1961, Linfield College; Ph.D. (Mathematics), 1965, Oregon State University; Bell Laboratories, 1965—. Mr. Reudink was initially involved in studies related to mobile telephony. He has headed the Satellite Systems Research Department and holds nearly two dozen patents in satellite and mobile communications, and mathematics. Mr. Reudink is currently Director of Radio Research at Crawford Hill Laboratory, Holmdel, New Jersey. Member, American Institute of Aeronautics and Astronautics (AIAA), Commission C of the U. S. National Committee for the International Union of Radio Science (URSI), USIA/Voice of America Radio Engineering Advisory Committee. Fellow, Institute for Electronic and Electrical Engineers (IEEE).

Coding of Two-Level Pictures by Pattern Matching and Substitution

By O. JOHNSEN,* J. SEGEN,* and G. L. CASH*

(Manuscript received September 28, 1982)

A pattern matching approach is proposed for coding of two-level pictures. Patterns, which are either symbols such as characters, or fractions of black regions, such as line segments, are extracted from the facsimile. They are compared and matched to already transmitted patterns, called library patterns. If a correct match is detected, only the position of the pattern and the identification of the matching library pattern are transmitted. If a pattern does not match any library pattern, it is added to the library and its binary description is transmitted. Compared to conventional two-dimensional codes, the compression is often doubled and is sometimes 4.5 times higher. Compared to a symbol-matching coding technique,² the compression has increased by 20 to 80 percent, depending upon the document.

I. INTRODUCTION

Conventional two-level picture coding techniques are based on the statistical dependence between neighboring picture elements (pels).¹ The calculation of entropies, according to a local source model, gives the maximum achievable bit rates. Run length or predictive coding techniques or a combination of them takes advantage of the statistical dependence between neighboring pels and leads to bit rates close to the entropy. Each exploits what can be called the microscopic (pel) properties of a facsimile.

Pattern-recognition coding techniques exploit macroscopic proper-

* Bell Laboratories.

©Copyright 1983, American Telephone & Telegraph Company. Photo reproduction for noncommercial use is permitted without payment of royalty provided that each reproduction is done without alteration and that the Journal reference and copyright notice are included on the first page. The title and abstract, but no other portions, of this paper may be copied or distributed royalty free by computer-based and other information-service systems without further permission. Permission to reproduce or republish any other portion of this paper must be obtained from the Editor.

ties of the facsimiles. The image source is a source of patterns such as characters, lines, and black spaces. We can code the facsimile more efficiently, since the description is closer to the perceptual level. We can consider two kinds of pattern-recognition coding techniques. The first technique is pattern (or image) understanding. It recognizes a certain pattern, for example a letter, that possibly includes some font information. The second technique is pattern matching. Here, a pattern is not recognized, but is simply matched with already transmitted patterns, and if a correct match is detected, it is replaced by the matching pattern. It does not use the image-understanding level. The image-understanding approach has the potential advantage of a very high compression, but the often important aesthetic details of the documents can be lost, and there is a risk of errors at the present level of such techniques. The matching approach yields lower compression, but keeps more of the original pictorial information. There are also lower risks of errors, since matching allows only slight modifications in the pattern shapes. Naturally, neither of the pattern-recognition techniques is lossless, since they modify the picture content.

Ascher and Nagy³ and Pratt et al.² have already proposed facsimile coding techniques using matching techniques. In the system presented here, not only the symbols, as in Pratt's case, but also graphical elements such as line segments and black regions are matched. The patterns are efficiently coded and updated, leading to significantly higher compressions.

II. SYSTEM DESCRIPTION

Figure 1 shows the block diagram of the system. The pattern locator examines the facsimile line by line. When it locates a black pel, the pattern isolator picks up a pattern. The pattern is either a symbol (defined as a set of black pels completely surrounded by white pels) or, when no symbol can be extracted, a fraction of the black region. Therefore, contrary to Ref. 2, there is no residue to be coded, since all black pels belong to a pattern.

The matcher makes a template matching of the incoming pattern, with existing library patterns to determine whether the incoming pattern is similar to an already transmitted pattern. The system screens the library patterns to reduce the time-consuming template matching. Thus, we consider only the patterns that might match the incoming pattern. We screen by comparing features of the library patterns with those of the incoming pattern. We apply a very efficient and simple two-pass screening. If a correct match is detected, the matcher sends the information about the position of the pattern and its library identification to the coder. If no match has occurred, the incoming pattern is added to the pattern library. The pattern library

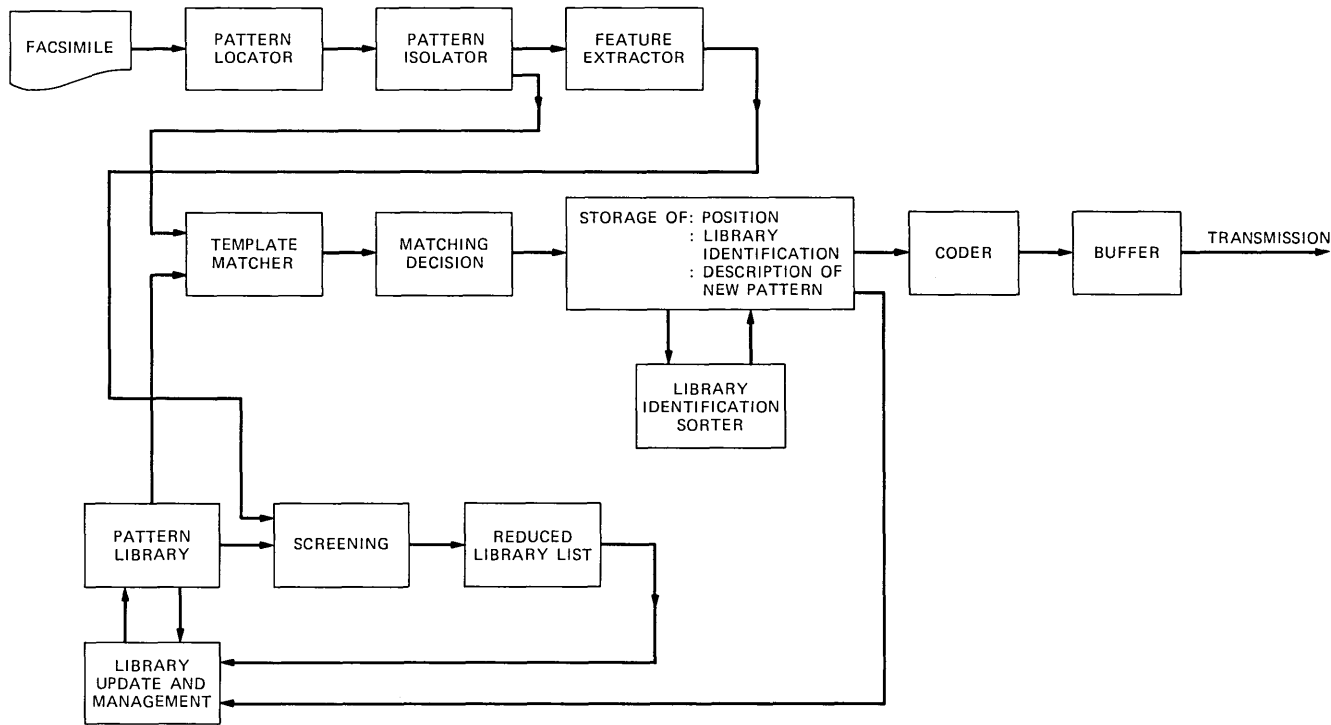


Fig. 1—Block diagram of facsimile coder by pattern matching.

is empty at the beginning of the coding and is gradually built up by the incoming library patterns. The matcher then also sends the information about the position and description of the new library patterns to the coder.

A library update and management unit takes care of the addition and deletion of library patterns and organizes them for the quickest possible match and most efficient coding. All the patterns isolated along one line are stored in the coder. When the end of the line is reached, we sort the patterns, which allows a more efficient coding.

III. LOCATION AND ISOLATION OF PATTERNS

Patterns, in the present context, are the primitive elements of the coding process. They are isolated, and sent to the matching block sequentially, in a raster order. We distinguish two classes of patterns, relative to a square window of a predetermined size, W .

1. A symbol is defined as a connected region consisting of black pels and completely surrounded by white pels, such that it can completely fit into the window.

2. A nonsymbol is defined as a windowed portion of a black connected region that is larger than the window.

Usually, characters and small graphics elements can be represented as symbols, while lines and larger figures can be decomposed into nonsymbols. The decomposed figures can be later reconstructed by taking the union of the nonsymbols. The nonsymbols do not have to be disjoint, and a better compression may sometimes result from a decomposition into overlapping symbols.

Decomposing large figures into nonsymbols allows us to use matching techniques to compress graphical information, as well as text. A figure can be decomposed in many ways, and the compression that results from grouping similar nonsymbols usually depends on the decomposition. The final compression, or the number of different classes of nonsymbols, can be used as a measure of quality of the decomposition, and one may try to find the best decomposition in respect to such measures. Finding the optimal decomposition, however, may be computationally quite complex (we do not know of any related study) and it would certainly require many passes through a figure. At present, we use a one-pass isolation procedure, which allows us to keep the computation within reasonable bounds.

The isolation procedure repeatedly isolates and removes the upper-left portion of a black region, up to a maximum size allowed by the window. If the isolated pattern has no black pel extensions, then it is a symbol; otherwise it is a nonsymbol.

The isolation algorithm operates on a two-dimensional one-bit array containing the original picture. The picture memory is scanned line

by line from the upper-left element. When a black pel is found, the procedure attempts to trace the boundary of a black region, clockwise. The tracing algorithm is a standard one; however, we describe it here for further reference. Let us call the first black pel (x_1, y_1) . The neighbors (adjacent pels in eight directions of (x_1, y_1)) are being examined, beginning at (x_1+1, y_1) and searching clockwise around (x_1, y_1) up to (x_1-1, y_1+1) . If a black pel is found, it becomes the second pel of the contour — (x_2, y_2) ; otherwise (x_1, y_1) is erased from the picture memory (single pels are neglected) and the scan continues. Each subsequent pel of the contour is found by searching around the current pel (x_i, y_i) , beginning two steps clockwise from the previous pel (x_{i-1}, y_{i-1}) (Fig. 2). The contour trace ends when it returns to the first pel in such a way that the next pel would be (x_2, y_2) . The tracing algorithm checks for the limits of the picture array and it maintains a window. Pels beyond the limits of the picture array and those outside of the current window are always treated as white (0 valued). The purpose of the window is to restrict the maximal size of isolated pattern to $W \times W$. The window is initially set to a size $2W \times W$, and positioned in such a way that (x_1, y_1) is in the center of its upper edge. When the traced part of the boundary reaches a width of W , the window is reset to a size $W \times W$, and it is placed over the boundary part that has been traced, such that (x_1, y_1) is still at the upper edge of the window (Fig. 3).

The tracing of the boundary is recorded in a two-dimensional one-bit array S in the following way. When the search around the current boundary pel (x_i, y_i) goes past the pel (x_i+1, y_i) , a 1 is put in $S(x_i+1, y_i)$. If the search goes past the element (x_i-1, y_i) then a 1 is put in $S(x_i-1, y_i)$. All the elements of S are initially set to 0. The information in S (Fig. 4), after the trace termination, completely represents the boundary (it is a form of run-length code). The pattern now can be isolated by copying and erasing the portion of the picture that is enclosed by the boundary (including the boundary). This is accomplished using the

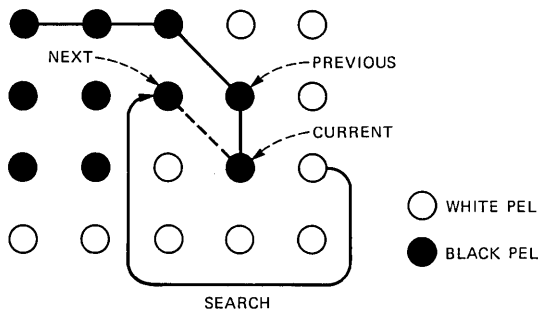


Fig. 2—Contour tracing.

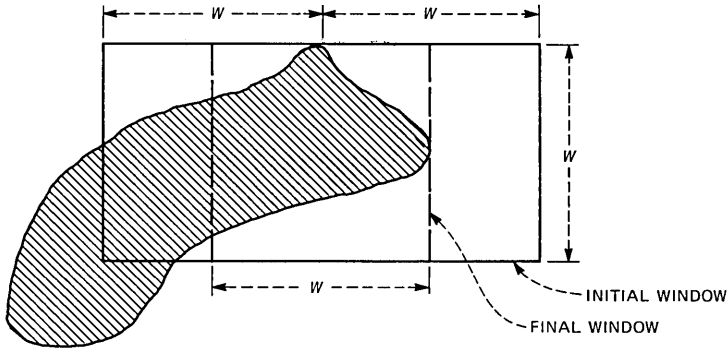


Fig. 3—Window positioning for isolation.

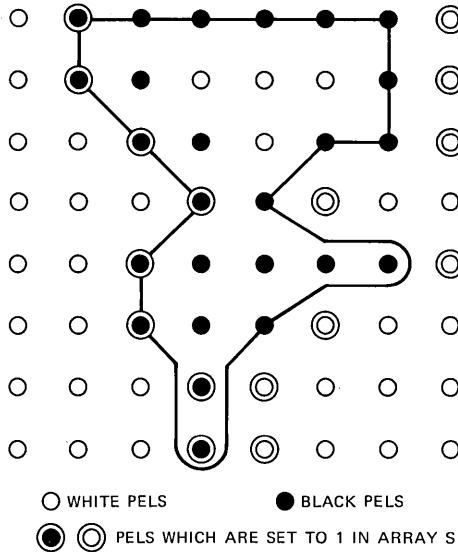


Fig. 4—Contour encoding in array S.

information in the array S. For any row of S, let $S_1, S_2 \dots S_n$ be the position (x-coordinates) of 1-valued elements in a row. The number n is always even, which is a property of the boundary encoding that we use. For every row of S, the pixels of a corresponding row of the picture memory between S_1 and S_2, S_3 and S_4 , etc., are copied to another array, and set to 0 in the picture memory, including $S_1, S_3 \dots$ and excluding S_2, S_4, \dots . The pattern is now isolated and erased from the picture memory. While the isolation algorithm described above always works correctly, i.e., it isolates symbols and completely decomposes large

figures into nonsymbols, it does not attempt in any way to optimize the decomposition, so the results are not always pleasing.

To improve the decomposition in cases commonly occurring in graphics, we have added two extensions to the basic isolation scheme:

1. L-pattern suppression

L-pattern suppression improves the segmentation of large blobs that otherwise may generate many dissimilar nonsymbols (Fig. 5). This extension is implemented in the tracing phase of the isolation algorithm as follows: If the beginning part of the traced boundary goes straight down from either first or second pel over more than k (currently $k = 10$) pels, then an attempt to turn immediately to the right resets the lower edge of the window to the last pel before the right turn, so the boundary is forced to turn left (see Fig. 6).

2. Cross decomposition

If the isolated pattern can be represented as an intersection of a horizontal and a vertical line segment (a cross), then each segment becomes a separate pattern. This is implemented by comparing each isolated pattern (with the matching technique described in Section 4) to a cross formed by secting this pattern with vertical and horizontal lines one pel from the edges of the final window (Fig. 7). If a sufficiently close match is found, then one of the line segments from the cross is

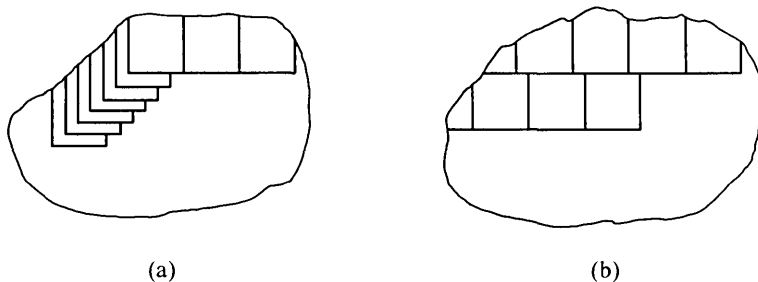


Fig. 5—Improvement in segmentation due to L-pattern suppression. (a) Before suppression. (b) After suppression.

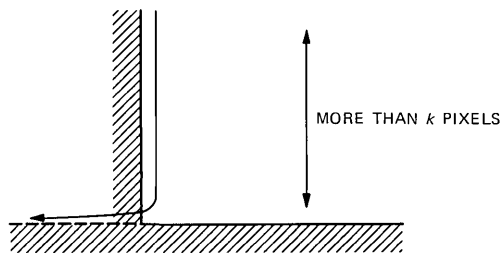


Fig. 6—L-pattern suppression. When tracing reaches the corner, it is forced to follow the dashed line.

returned to the picture memory, while the other replaces the isolated pattern. This extension reduces the number of patterns generated by line crossings in grids and tables (Fig. 8).

The basic isolation algorithm is similar to the region extraction method of Dudani⁴, but in contrast to the latter it does not need to store and process a list of boundary points, and it extracts regions containing holes in one pass. This algorithm can be shown to work correctly in every case and it is well suitable for a hardware implementation. The extensions of the basic algorithm are heuristic in nature, but they improve considerably the decomposition of large regions. Examples of such improvements are shown in Fig. 5 and 8. Additional improvements may be possible at some increase of the computational cost.

IV. MATCHING

The matching includes all the processes necessary to know whether an incoming pattern matches any of the library patterns. In this system, we divide the matching into three parts.

1. The screening unit makes a selection of the library patterns, and

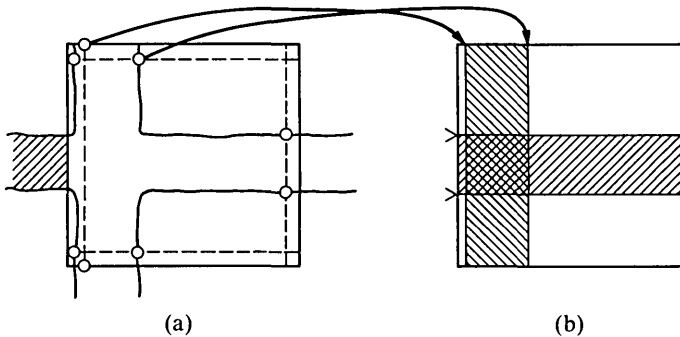


Fig. 7—Forming an intersection pattern.

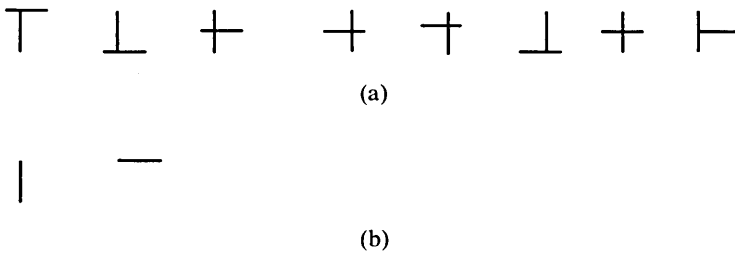


Fig. 8—Patterns resulting from grid segmentation. (a) Before cross decomposition. (b) After cross decomposition.

directs for template matching only those library patterns that might match.

2. The template matcher creates a new binary picture called error picture, containing black pels or 1's in the locations where the two template-matched patterns are dissimilar.

3. The matching decision process uses the error pictures and other information to decide whether a correct match has occurred.

4.1 Screening

The purpose of the screening is to reduce the time-consuming task of the matcher. It should direct to the template matcher only the library patterns that might match the incoming (unknown) pattern. The screening is obtained by measuring some characteristics of the patterns, called features, and comparing them. The features must be easy to compute and compare, and also must form an easily classifiable space. The digitization of a facsimile adds much noise to a pattern. To get an efficient screening, the features must also be relatively noise independent. Four features were chosen for the screening. Two of them are obvious: the pattern length and the pattern height. The two others are the number of horizontal and the number of vertical white runs enclosed in the pattern. They are characteristics of the inside of a pattern, separating, for example, c from e or o. The chosen features are shown in Fig. 9. The straightforward feature "number of black pels" was found to be of little use because of its high variability and dependency upon the other features.

The screening process also must decide in which order to send the library patterns to the matcher. The most probable match should be sent first, to reduce the number of matches. The probability of a match between patterns depends not only on the similarity of their features, but also on the probability of occurrence of a library pattern. For example, an incoming pattern having the same feature distance to an O and a Q is much more likely to match the O than the Q since O is much more frequent than Q. The screening takes into account both the feature similarity and the probability of occurrence of a library pattern. We consider the probability of occurrence by sorting the library patterns according to the number of times they have matched (see Section 5.2.1). We take the feature distance into account by allowing for each feature only a fixed margin between the two patterns. The margin must be wide enough not to preclude any correct match and tight enough to reduce the number of template matches. A two-pass screening was found very efficient. In the first screening, only library patterns with features very similar to those of the incoming patterns are sent to the template matcher. A second, much looser, screening is applied only in the few cases where no match occurred.

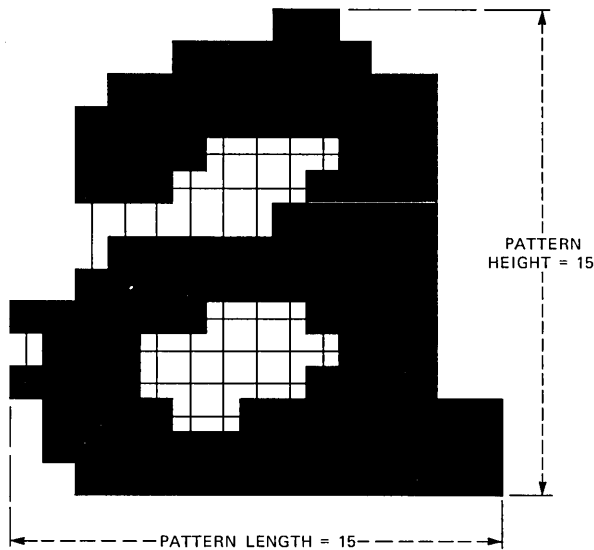


Fig. 9—Features chosen for screening. Horizontal lines indicate which runs are included in count of horizontal runs. Vertical lines indicate which runs are included in count of vertical runs. Horizontal run count is six and vertical run count 15.

The screening and the sorting are very efficient in reducing the number of matches. For example, for a typewritten document, the average number of matches per incoming pattern is reduced to 2.5, compared to 25 without screening and sorting.

4.2 Template matching

The template matcher creates a new picture called error picture, which contains 1's in the locations where the two patterns are different. The error picture is obtained simply by superimposing the two patterns and making "exclusive or" of the corresponding pels. Figure 10 is an example of matching two patterns of the same character, while Fig. 11 shows the matching of two unlike patterns. Two patterns are always matched nine times, allowing the displacement of one pattern compared to the other by ± 1 in both the horizontal and vertical directions.

4.3 Matching decision

The matching decision unit must process the error picture to detect whether there is a correct match, and to decide which relative position of the library pattern gives the best match.

The straightforward approach is to count the number of errors (or 1's) in the error picture and to threshold it to make the decision. Such

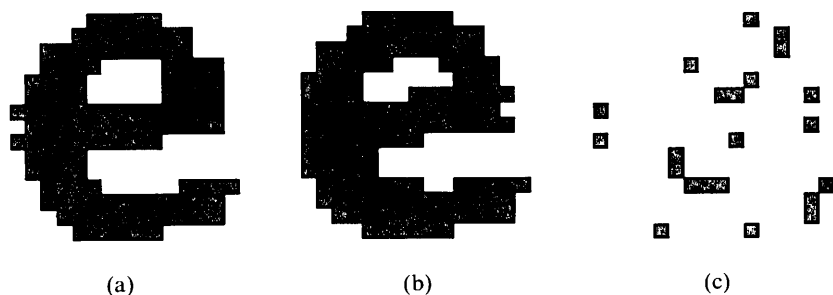


Fig. 10—Template matching of two similar patterns, with (a) and (b) original patterns and (c) error picture.

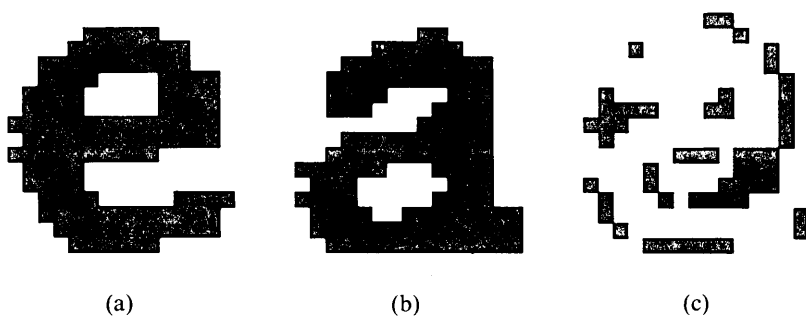


Fig. 11—Template matching of two different patterns, with (a) and (b) original pattern and (c) error picture.

a technique would lead to many mismatches or many undetected matches, since, as shown in Ref. 2, the error count for two patterns corresponding to the same character is sometimes higher than the count for two patterns corresponding to different characters. This is caused by the digitization noise. Figure 10 shows that the template matching of two patterns of the same character gives relatively randomly distributed errors. Figure 11 shows that in the case of patterns of different characters, a cluster of errors appears where there are morphological differences between patterns.

As Ref. 2 shows, we could apply a weighted error count where the weight of an error is equal to the number of error pels among its eight neighbors. Single errors are erased and the maximum weight is eight. Figure 12 gives the weighted error pictures from the error pictures of Figs. 10 and 11. The weighted error count is not sufficient for the matching decision, as shown by Fig. 13. We must look at local error patterns to make the decision. The reason is that it is the local characteristics of the pattern that indicate whether two patterns are the same. Therefore, any decision made upon a count or integration

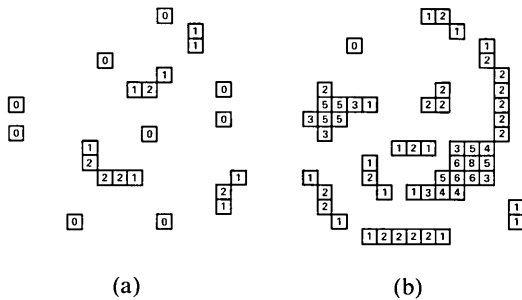


Fig. 12—Weighted error pictures. (a) Weighted error count is 18 in Fig. 10 and (b) 144 in Fig. 11.

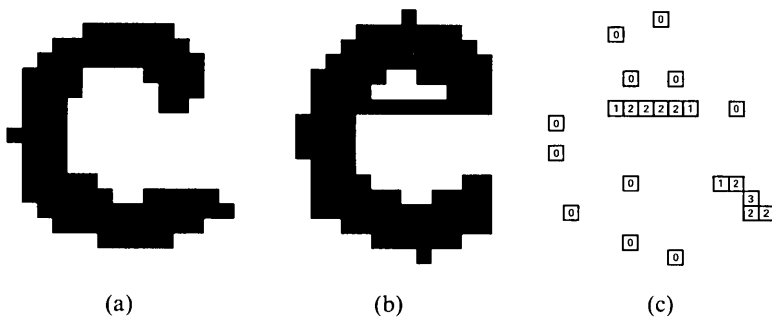


Fig. 13—A weighted error count matching criterion leads to a mismatch, with (a) and (b) original patterns, and (c) weighted error picture.

may be incorrect. The matching decision described below uses only local measures and is also made locally with the simple rule that the match is considered correct if no local rejections are detected during a template matching.

The following rule of decision is made. A match is rejected if:

Condition 1: An error pel has a weight of 4 or more, or

Condition 2: (a) an error pel has a weight of 2 or more, (b) at least two of its neighboring error pels are not connected, and (c) one of the two pels from the patterns used to obtain the error pel has a weight of 0 or 8 (corresponding to 0 or 8 surrounding black pels).

Most mismatches are detected by Condition 1, but Condition 2 is necessary in order to reject, for example, the possible match of an e and a c shown in Fig. 13. It is easy to see that Condition 2a is not necessary since it is included in 2b, but Condition 2a reduces the computation.

With these matching criterion, no visible mismatches have been detected, except slight distortion in line drawings. It is important to notice that a rejection can often be detected after processing a small

fraction of the error picture. A matching decision made at the same time as the template matching would lead to an early abortion of template matchings and thus reduce the computation.

When a correct match is detected, several relative positions sometimes give a correct match. The chosen relative position will be the one with the lowest error count. The best relative position will decide where the library pattern will be put to replace the incoming pattern.

V. CODING

Contrary to many conventional facsimile coding techniques, we must code several different kinds of events and design several separate code books. The code for a pattern includes the position and the description of the pattern. The description is usually its library identification, or in the case of a new pattern, its complete description. The coding procedure is described here for the size of the International Telegraph and Telephone Consultative Committee (CCITT) test facsimiles having 1728 pels per line and 2376 lines, but it can easily be modified for other cases.

5.1 Coding of the position of the pattern

To obtain a good-quality reproduction with pattern matching, we must position the patterns accurately. Considering the CCITT test documents, 23 bits are necessary for an absolute fixed length coding (11 bits horizontally, 12 bits vertically). We choose to transmit the horizontal position uncoded (11 bits) because variable-length run-length coding would lead only to slightly smaller coding length (typically 1 to 1.5 less bits/pattern) since the horizontal distance between patterns is large. Also since the absolute horizontal position is coded, the patterns can be transmitted in a nonsequential order, which, as shown later, leads to a significant decrease in the average coding length for the library identification code words. It should be noted that with 1728 pels/line and an 11-bit code word, the code words starting with 111 are not used and therefore can be used as special code words.

We code the vertical position of the patterns in the following way:

1. A mode bit is sent at the beginning of each line to indicate whether there are any patterns starting on that line.

2. If there are no patterns on the line, operation 1 is repeated on next line.

3. If there are patterns on a line, they are all coded. The special horizontal code word 111 indicates that there are no more patterns on the line and that the next line can be considered.

4. When a pattern is replaced by a library pattern, the position of the library pattern might be moved up or down by one line. Therefore,

after the library identification has been coded, the code words 10 and 11 are used to position the library pattern up or down, while code word 0 is used to indicate no vertical displacement. No vertical displacement code word is sent with a new library pattern, since there are no changes in vertical position.

Figure 14 shows examples of the message format for the pattern positioning.

5.2 Coding of the pattern identification

The coder must send a pattern identification word with each pattern. We can transmit the pattern number uncoded. It requires, for example, seven bits in the case of a library size of 128 and nine bits in the case of a library size of 512. The coding procedure used here will lead to an average coding length of the pattern identification of fewer than five bits/pattern. It will be obtained by a continuous library updating and by variable-length coding.

5.2.1 Library updating and management

The library management and updating is done for the following purposes:

1. Accept new library patterns, and if necessary, delete a seldom used library pattern to make room for the new one.
2. Organize the library for the fastest match, taking into account the screening and matching procedures.
3. Organize the library for minimum average library identification coding length.

All three require the same processing: to keep track of the number of times each library pattern is used. By ordering the library pattern in order of decreasing usage, the correct match will be obtained rapidly,

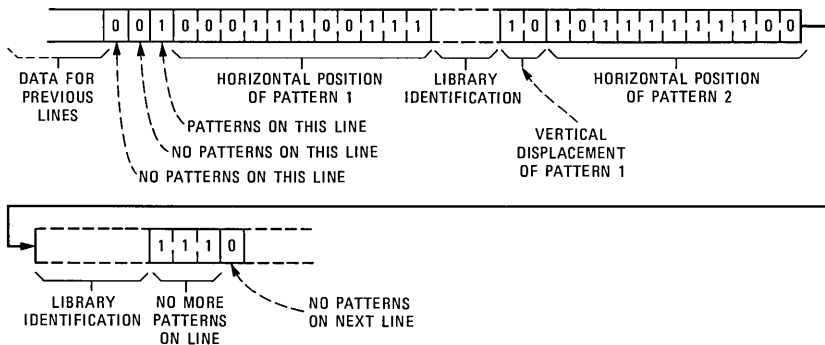


Fig. 14—Coding of positions of patterns. Two lines have no patterns, then a line has three patterns; the first on position 231 is replaced by a library pattern, the second on position 1532 is a new library pattern, There are no patterns on next line.

since the most used library patterns will be accessed first. An efficient coding of the patterns' identification is obtained by giving short code words to the first patterns in the list. The last pattern in the list, which is one of the least used patterns, can be deleted to make room for a new one.

The updating must be deterministic and use no future information, since the receiver must make the same updating to decode correctly.

The updating rule of the patterns in the library is as follows:

1. When a pattern matches a library pattern number K , that library pattern is moved to number $K/2$ and all the pattern numbers from $K/2$ to $K-1$ are increased by 1.

2. When a new pattern is added to the library, it gets number $N/2$ where N is the total number of library patterns. The patterns with numbers from $N/2$ to N will be increased by 1, and if N is equal to the maximum number of library patterns M , the library pattern with number $N + 1$ is dropped.

This updating procedure was found to efficiently give low identification numbers to often used patterns and high numbers to seldom used patterns. If M is the maximum number of library patterns, it guarantees that a new library pattern will stay in library for at least $M/2$ matches, but generally for many more.

5.2.2 Pattern identification coding table

The pattern identification coding table includes two special code words: "new pattern" and "same pattern." They are added to increase the coding efficiency. The "new pattern" code word is chosen because it is not necessary for a new library pattern to send an identification number, since the decoder uses the same rule as the coder to assign the identification number to the new pattern. The "same pattern" code word indicates that the transmitted pattern is the same as the previously transmitted pattern. It is useful particularly for typewritten text where the line-by-line search for a pattern often detects the same pattern (character).

The coding table for the pattern identification is given in Table I for a pattern library with a maximum of 512 patterns.

This code leads to an average library identification length of fewer than seven, compared to nine with a fixed-length code. The next section shows a more efficient coding procedure.

5.2.3 Pattern identification coding by sorting

Since an absolute code gives the horizontal position of a pattern, it is possible to transmit the patterns detected along a line in any order. The only condition is that the library updating be done at the end of the line. The average coding length of the library identification is

Table I—Coding table for identification of library patterns

Symbol	Code Word	Code Word Length
Same pattern	000	3
Library pattern 1-16	1XXXX	5
New pattern	00100	5
Library pattern 17-32	010XXXX	7
Library pattern 33-64	0011XXXXX	9
Library pattern 65-128	00101XXXXXX	11
Library pattern 129-512	011XXXXXXXXXX	12

reduced to fewer than five bits, by sorting the patterns on a line according to their library number. That is because:

1. Many of the patterns are the same.
2. The library pattern identification number is run-length coded (only the increase compared to the previous identification number is coded).
3. The new library patterns are sent at the end of the line; therefore, the new pattern code word is sent only once, since any more patterns are automatically new patterns.

This can be illustrated by an example. Let a line have the following pattern: pattern 23, new pattern; pattern 28, same; pattern 23, new pattern. By looking at Table I, the coding length is $7 + 5 + 7 + 3 + 7 + 5 = 34$ bits. With sorting, the patterns become: pattern 23, same; pattern 28, same; new pattern; new pattern. The coding length is $7 + 3 + 5 + 3 + 5 + 0 = 23$ bits. It should be noted in this example that pattern 28 is coded as pattern 5 since only the increase in identification number compared to the previous pattern is coded.

The library updating is done at the end of each line. This creates problems when accepting new library patterns. They must be added immediately to the top of the library, since the position of the other patterns should not be changed. It is also not possible to delete patterns to make room for the new ones. For that reason, before scanning a line, enough library patterns should be deleted to avoid an overflow of the pattern library.

5.3 Coding of the library pattern description

The size of a pattern is limited to 32×32 bits. The description starts with a 5-bit word, which indicates the height, H , of a pattern in binary. The length of a pattern is extended to 32 pels by filling the right end with 0's. Therefore, there are $32 \times H$ pels to code. For coding efficiency, one white pel (0) is added at the beginning. A coding line is made of the $32 \times H + 1$ pels considered in the raster scan order. The reference line is similar to the coded line except that all the pels are shifted to the right by 32 pels (one line). Therefore, a line is coded

using the previous line as the reference. The line is then coded by the CCITT two-dimensional code,⁵ with the only modification that the first code word, which is always the horizontal mode code word, is deleted, since it doesn't give any information. For coding efficiency, it is chosen to allow switching between two modes for the coding of the library pattern description. The first mode is as described above and called "horizontal coding." The other is called "vertical coding" and is the same as above except that the pattern is coded column after column from top to bottom. Therefore, in the vertical mode the description starts with a 5-bit word indicating the length of a pattern. A header bit indicates which mode is chosen, with a 0 for horizontal mode and a 1 for vertical mode. We could also code the pattern description using a code better matched to the source. This would reduce the coding length, but at the expense of requiring a specific code in place of a standard code.

5.4 Coding summary

The coding procedure can be summarized in the following way:

1. All the patterns isolated along a scan line are matched.
2. At the end of the line, the matched patterns are sorted in order of increasing pattern identification number. The new library patterns are added at the end in sequential order.
3. The patterns are coded and transmitted with the information sent in the following order:
 - a. Horizontal position of pattern.
 - b. Pattern identification. If it is a new pattern, the identification is sent only for the first new pattern on the line.
 - c. A 1- or 2-bit code word to specify the vertical shift of a pattern, except if it is a new library pattern.
 - d. For a new library pattern the following bits are sent: (1) a header bit indicating whether the horizontal or vertical coding mode is chosen, (2) a 5-bit word indicating the number of lines of the pattern to be coded, and (3) the CCITT two-dimensional coding of the pattern (see 5.2).
 - e. After all patterns on a line have been sent, the special horizontal code word 111 indicates the end of the line.
 - f. The library update is made according to 5.2.3. The patterns are updated in order to increasing identification number. After updating, all patterns with a number greater than 480 are deleted, thus allowing for at least 32 new library patterns to be added on the next line.

Figure 15 is an example of message transmission. The different code words are summarized in Table II.

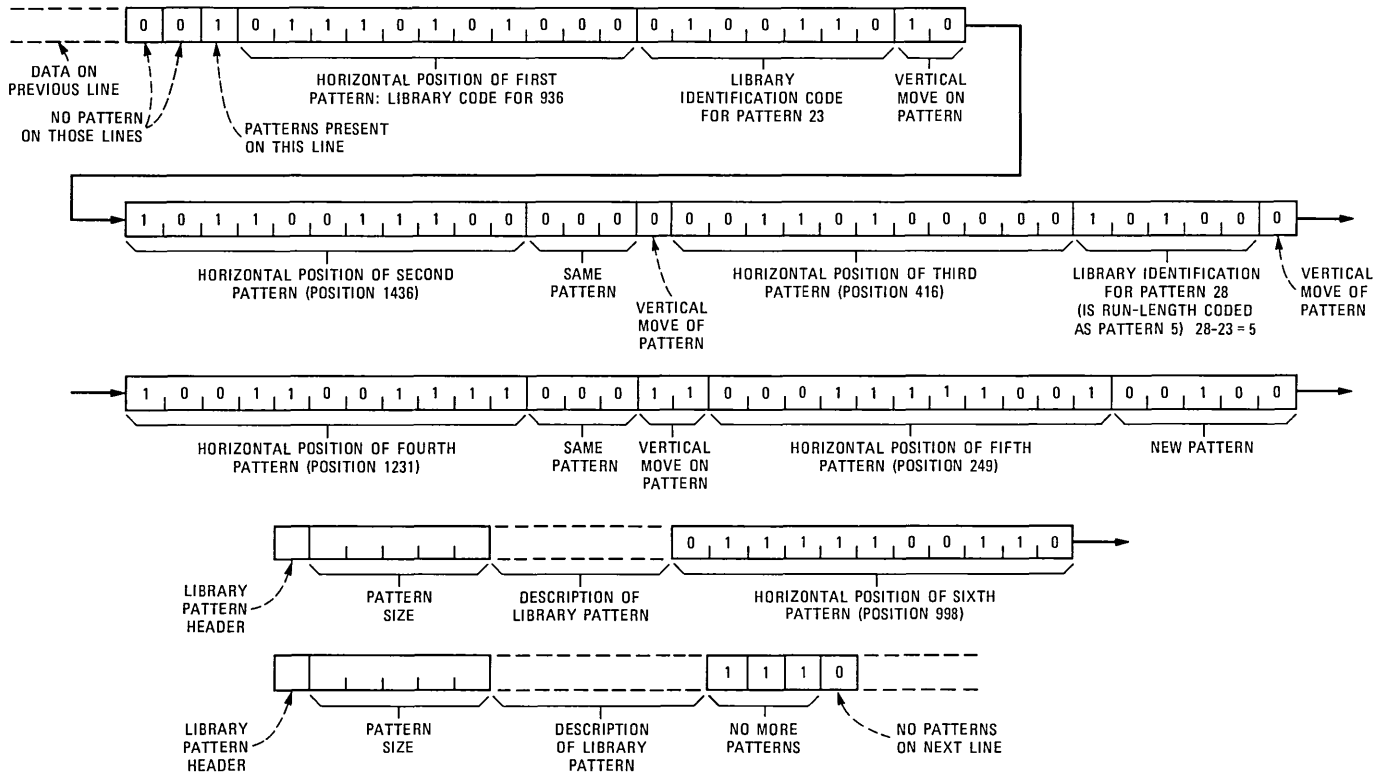


Fig. 15—Message transmission. There are two lines without patterns, next pattern 23 is in position 936, same pattern is in position 1436, pattern 28 is in position 416, same pattern is in position 1231; two new patterns are in position 249 and 998, and there are no patterns on next line.

Table II—Description of the code words for pattern matching coding

Code Definition	Word Size	Description
Mode bit	1	Indicates whether there are any patterns on the line.
Horizontal position	11	Gives in binary the absolute position of a pattern.
No more pattern	3	Indicates that there are no more patterns on the line (this code word: 111 is a special horizontal position code word).
Vertical move of pattern	1 or 2	Indicates whether the pattern must be moved up or down by one line or is not moved.
Library identification code	Variable	Defines which library pattern is transmitted.
Library pattern description header	1	Indicates whether the library pattern is coded in horizontal or vertical mode.
Library pattern size	5	
Library pattern description	Variable	Slightly modified CCITT two-dimensional code.

VI. SIMULATION RESULTS

The important criteria are the compression and the quality of the received documents. For that purpose, the set of eight CCITT facsimile documents are used. Their resolution is 7.7 pels/mm (200 pels/in.) in both the horizontal and vertical directions. They have 1728 pels/line and 2876 lines. Documents one, two, four and five are shown in Fig. 16. All eight documents are shown in Ref. 5. For accurate comparison with the matching technique by Pratt et al.,² the simulations were also made with an older nonofficial version of the CCITT documents, which is similar except each document has 1728 pels/line and 2128 lines.

6.1 Facsimile quality

In order to improve the quality of the decoded picture, a local filtering using a 3×3 window is applied. In addition, large library patterns are slightly expanded on their borders. This operation erases artifacts in large black regions.

The encoding scheme modifies the binary picture. We must therefore verify that the alterations are not visible or at least not annoying. We can consider three picture alterations: wrong matches, matches with a slightly distorted pattern, and wrong positioning. In the case of a wrong match, a pattern is replaced by a different pattern. The only detected wrong matches are such as between 0 and O, dot and comma, I and 1, which even people cannot recognize correctly without using the context. Therefore, it can be considered that the system has practically no wrong matches. A match with a slightly distorted pattern can occur with characters. A character might match a same character of a different font. Or a character might match a same but thinned or

THE SLEREXE COMPANY LIMITED

SAPORS LANE - BOOLE - DORSET - BH25 8ER
TELEPHONE BOOLE (945 13) 51617 - TELEX 123456

Our Ref. 350/PJC/EAC

18th January, 1972.

Dr. P.N. Cundall,
Mining Surveys Ltd.,
Holroyd Road,
Reading,
Berks.

Dear Pete,

Permit me to introduce you to the facility of facsimile transmission.

In facsimile a photocell is caused to perform a raster scan over the subject copy. The variations of print density on the document cause the photocell to generate an analogous electrical video signal. This signal is used to modulate a carrier, which is transmitted to a remote destination over a radio or cable communications link.

At the remote terminal, demodulation reconstructs the video signal, which is used to modulate the density of print produced by a printing device. This device is scanning in a raster scan synchronised with that at the transmitting terminal. As a result, a facsimile copy of the subject document is produced.

Probably you have uses for this facility in your organisation.

Yours sincerely,

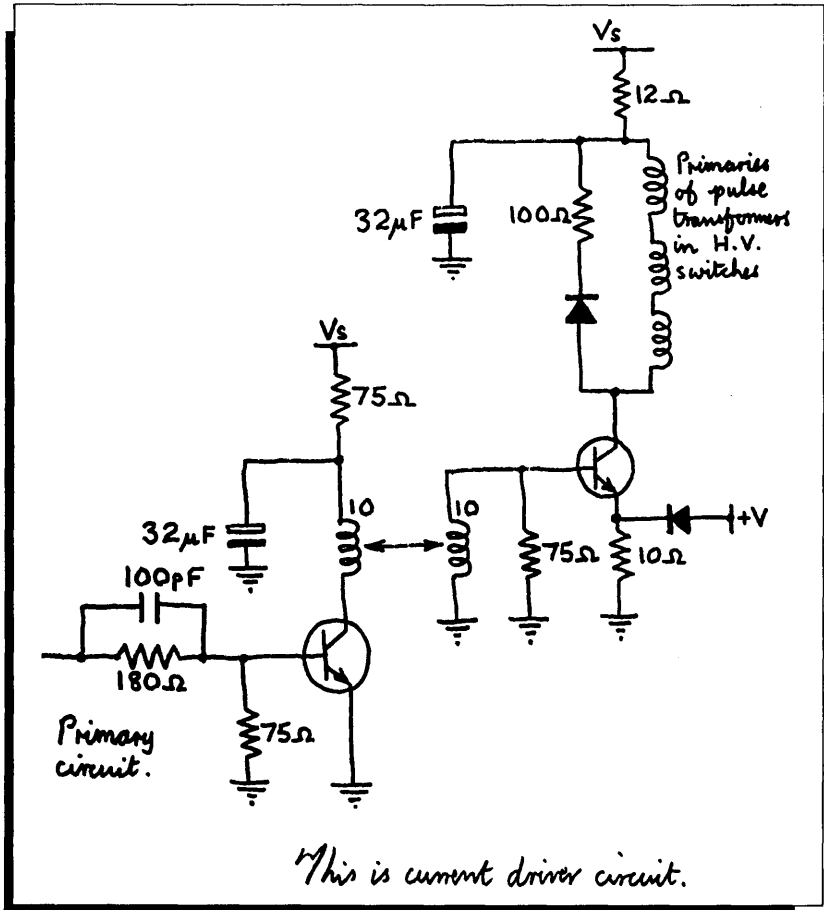
Phil.

P.J. CROSS
Group Leader - Facsimile Research

(a)

Fig. 16(a)—Original CCITT document one (first 2000 lines).

thickened character. Such matches, contrary to wrong matches, are tolerable if they don't appear too often. Such distorted matches appear when two slightly different fonts are used on a same page or when characters of a page come from a low-quality typewriter or scanner. The wrong positioning of a pattern decreases the quality of the received facsimile. No noticeable wrong positioning for patterns such as characters or other symbols is observed. Some visible wrong positionings are observed for nonsymbol patterns such as line segments, where the



(b)

Fig. 16(b)—Original CCITT document two (first 2000 lines).

successive patterns make the lines slightly jagged. Figure 17 shows the same CCITT facsimiles as Fig. 16, but after transmission by pattern matching. It can be seen that there are no significant degradations. There are some slight irregularities in line drawings, as for example in Fig. 17d. A few distorted matches appear on CCITT document one (Fig. 17a).

6.2 Compression

To make an accurate comparison with both the symbol matching and two-dimensional coding techniques, the coding simulations have been made with both the official set of CCITT facsimile documents

L'ordre de lancement et de réalisation des applications fait l'objet de décisions au plus haut niveau de la Direction Générale des Télécommunications. Il n'est certes pas question de construire ce système intégré "en bloc" mais bien au contraire de procéder par étapes, par paliers successifs. Certaines applications, dont la rentabilité ne pourra être assurée, ne seront pas entreprises. Actuellement, sur trente applications qui ont pu être globalement définies, six en sont au stade de l'exploitation, six autres se sont vu donner la priorité pour leur réalisation.

Chaque application est confiée à un "chef de projet", responsable successivement de sa conception, de son analyse-programmation et de sa mise en oeuvre dans une région-pilote. La généralisation ultérieure de l'application réalisée dans cette région-pilote dépend des résultats obtenus et fait l'objet d'une décision de la Direction Générale. Néanmoins, le chef de projet doit dès le départ considérer que son activité a une vocation nationale donc refuser tout particularisme régional. Il est aidé d'une équipe d'analystes-programmeurs et entouré d'un "groupe de conception" chargé de rédiger le document de "définition des objectifs globaux" puis le "cahier des charges" de l'application, qui sont adressés pour avis à tous les services utilisateurs potentiels et aux chefs de projet des autres applications. Le groupe de conception comprend 6 à 10 personnes représentant les services les plus divers concernés par le projet, et comporte obligatoirement un bon analyste attaché à l'application.

II - L'IMPLANTATION GEOGRAPHIQUE D'UN RESEAU INFORMATIQUE PERFORMANT

L'organisation de l'entreprise française des télécommunications repose sur l'existence de 20 régions. Des calculateurs ont été implantés dans le passé au moins dans toutes les plus importantes. On trouve ainsi des machines Bull Gamma 30 à Lyon et Marseille, des GE 425 à Lille, Bordeaux, Toulouse et Montpellier, un GE 437 à Massy, enfin quelques machines Bull 300 TI à programmes câblés étaient récemment ou sont encore en service dans les régions de Nancy, Nantes, Limoges, Poitiers et Rouen ; ce parc est essentiellement utilisé pour la comptabilité téléphonique.

À l'avenir, si la plupart des fichiers nécessaires aux applications décrites plus haut peuvent être gérés en temps différé, un certain nombre d'entre eux devront nécessairement être accessibles, voire mis à jour en temps réel : parmi ces derniers le fichier commercial des abonnés, le fichier des renseignements, le fichier des circuits, le fichier technique des abonnés contiendront des quantités considérables d'informations.

Le volume total de caractères à gérer en phase finale sur un ordinateur ayant en charge quelques 500 000 abonnés a été estimé à un milliard de caractères au moins. Au moins les tiers des données seront concernées par des traitements en temps réel.

Aucun des calculateurs énumérés plus haut ne permettait d'envisager de tels traitements.

L'intégration progressive de toutes les applications suppose la création d'un support commun pour toutes les informations, une véritable "Banque de données", répartie sur des moyens de traitement nationaux et régionaux, et qui devra rester alimentée, mise à jour en permanence, à partir de la base de l'entreprise, c'est-à-dire les chantiers, les magasins, les guichets des services d'abonnement, les services de personnel etc.

L'étude des différents fichiers à constituer a donc permis de définir les principales caractéristiques du réseau d'ordinateurs nouveaux à mettre en place pour aborder la réalisation du système informatif. L'obligation de faire appel à des ordinateurs de troisième génération, très puissants et dotés de volumineuses mémoires de masse, a conduit à en réduire substantiellement le nombre.

L'implantation de sept centres de calcul interrégionaux constituera un compromis entre : d'une part le désir de réduire le coût économique de l'ensemble, de faciliter la coordination des équipes d'informaticiens ; et d'autre part le refus de créer des centres trop importants difficiles à gérer et à diriger, et posant des problèmes délicats de sécurité. Le regroupement des traitements relatifs à plusieurs régions sur chacun de ces sept centres permettra ce leur donner une taille relativement homogène. Chaque centre "gèrera" environ un mil-

(c)

Fig. 16(c)—Original CCITT document four (first 2000 lines).

and a former nonofficial version often used for facsimile compression comparisons. Table III gives the coding lengths for the CCITT documents for the official and nonofficial set of CCITT documents, respectively. They include the code length for the different codes necessary for the pattern matching coding. Table IV gives the compression ratio for the same CCITT documents and compares them with the

Cela est d'autant plus valable que $T\Delta f$ est plus grand. A cet égard la figure 2 représente la vraie courbe donnant $|\phi(f)|$ en fonction de f pour les valeurs numériques indiquées page précédente.

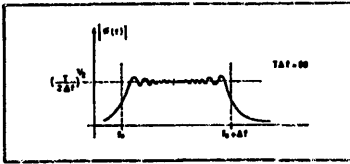


FIG. 2

Dans ce cas, le filtre adapté pourra être constitué, conformément à la figure 3, par la cascade :

— d'un filtre passe-bande de transfert unité pour $f_0 \leq f \leq f_0 + \Delta f$ et de transfert quasi nul pour $f < f_0$ et $f > f_0 + \Delta f$, filtre ne modifiant pas la phase des composants le traversant ;

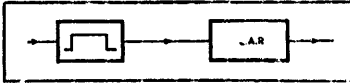
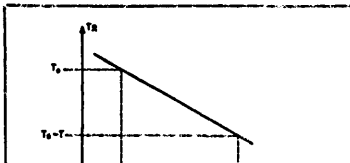


FIG. 3

— filtre suivi d'une ligne à retard (L.A.R.) dispersive ayant un temps de propagation de groupe T_R décroissant linéairement avec la fréquence f suivant l'expression :

$$T_R = T_0 + (f_0 - f) \frac{T}{\Delta f} \quad (\text{avec } T_0 > T)$$

(voir fig. 4),



telle ligne à retard est donnée par :

$$\phi = -2\pi \int_0^f T_R df$$

$$\phi = -2\pi \left[T_0 + \frac{f_0 T}{\Delta f} \right] f + \pi \frac{T}{\Delta f} f^2$$

Et cette phase est bien l'opposé de $|\phi(f)|$, à un déphasage constant près (sans importance) et à un retard T_0 près (inévitabile).

Un signal utile $S(t)$ traversant un tel filtre adapté donne à la sortie (à un retard T_0 près et à un déphasage près de la porteuse) un signal dont la transformée de Fourier est réelle, constante entre f_0 et $f_0 + \Delta f$, et nulle de part et d'autre de f_0 et de $f_0 + \Delta f$, c'est-à-dire un signal de fréquence porteuse $f_0 + \Delta f/2$ et dont l'enveloppe a la forme indiquée à la figure 5, où l'on a représenté simultanément le signal $S(t)$ et le signal $S_1(t)$ correspondant obtenu à la sortie du filtre adapté. On comprend le nom de récepteur à compression d'impulsion donné à ce genre de filtre adapté : la « largeur » (à 3 dB) du signal comprimé étant égale à $1/\Delta f$, le rapport de compression est de $\frac{T}{1/\Delta f} = T\Delta f$

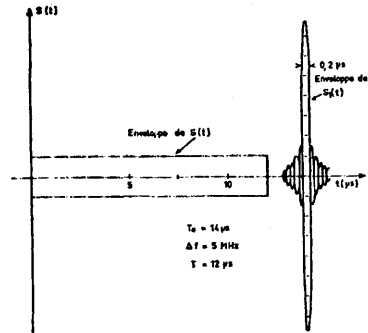


FIG. 5

On saisit physiquement le phénomène de compression en réalisant que lorsque le signal $S(t)$ entre dans la ligne à retard (L.A.R.) la fréquence qui entre la première à l'instant 0 est la fréquence basse f_0 ,

(d)

Fig. 16(d)—Original CCITT document five (first 2000 lines).

symbol-matching technique of Pratt et al.² and the two-dimensional CCITT code. The results are without any synchronization or stuffing bits, which is natural since pattern matching coding would be intended for future facsimile networks such as group four facsimile machines with fewer overhead bits. Therefore, the compressions of the two-dimensional CCITT code and symbol matching have been corrected by deleting the synchronization and stuffing bits and are different from their values given in Refs. 2 and 5.

THE SLEREXE COMPANY LIMITED

SAPORS LANE · BOOLE · DORSET · BH25 8ER

TELEPHONE BOOLE (945 13) 51617 · TELEX 123456

Our Ref. 350/PJC/EAC

18th January, 1972.

Dr. P.N. Cundall,
Mining Surveys Ltd.,
Bolroyd Road,
Reading,
Berks.

Dear Pete,

Permit me to introduce you to the facility of facsimile transmission.

In facsimile a photocell is caused to perform a raster scan over the subject copy. The variations of print density on the document cause the photocell to generate an analogous electrical video signal. This signal is used to modulate a carrier, which is transmitted to a remote destination over a radio or cable communications link.

At the remote terminal, demodulation reconstructs the video signal, which is used to modulate the density of print produced by a printing device. This device is scanning in a raster scan synchronised with that at the transmitting terminal. As a result, a facsimile copy of the subject document is produced.

Probably you have uses for this facility in your organisation.

Yours sincerely,

Phil.

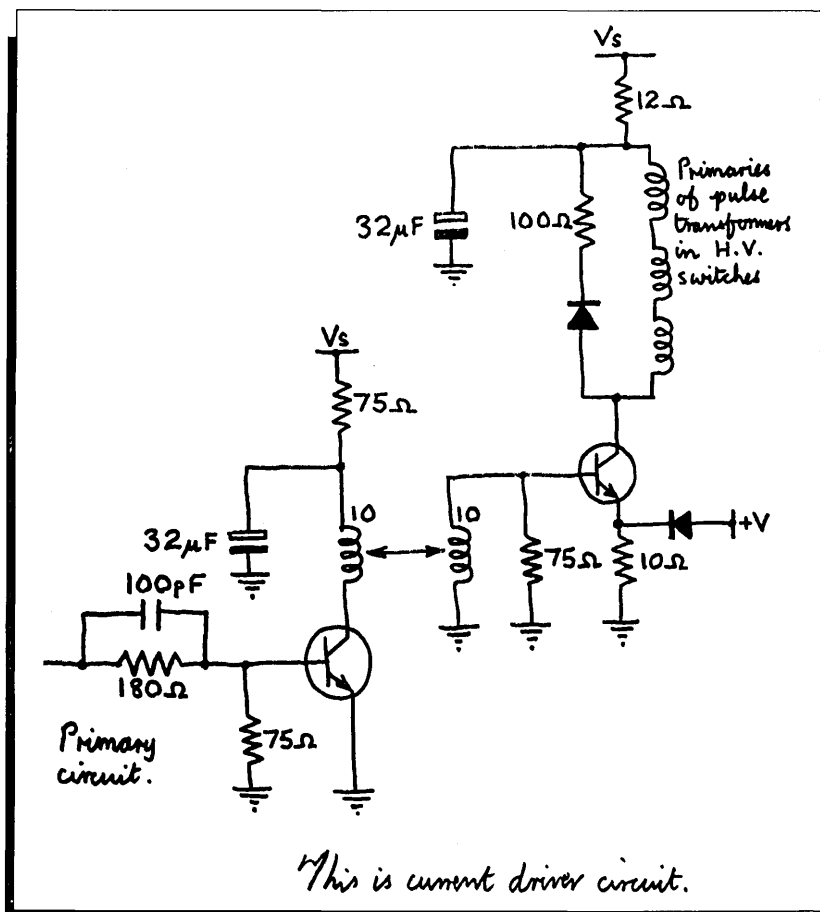
P.J. CROSS
Group Leader - Facsimile Research

(a)

Fig. 17(a)—Document on (first 2000 lines) after pattern matching (first 2000 lines).

Very high compressions are obtained—up to 80. The compression has often doubled compared to that of the two-dimensional CCITT code and is sometimes 4.8 times higher. The compression is, depending upon the documents, 20 to 80 percent higher than the compression derived from the symbol matching technique by Pratt et al.² More detailed comparisons and observations are useful when considering the performances of facsimile coding by pattern matching:

1. An astonishing fact is the difference in compression observed



(b)

Fig. 17(b)—Document two (first 2000 lines) after pattern matching.

between the old and the official version of the CCITT documents. For documents three and five the compressions are nearly twice as high for the old version than for the official version. Significant discrepancies are also observed for documents one and eight. This is in spite of the fact that old and official documents are the same except that they were scanned differently. It can also be noted that for the two-dimensional CCITT code, the difference in compression is smaller than five percent except for document eight, where the difference is about 20 percent. It must therefore be concluded that the performances of the pattern matching coding techniques are much more dependent upon the scanning and binary thresholding. Observing both versions of documents three and five, the main difference is that in the official

L'ordre de lancement et de réalisation des applications fait l'objet de décisions au plus haut niveau de la Direction Générale des Télécommunications. Il n'est certes pas question de construire ce système intégré "en bloc" mais bien au contraire de procéder par étapes, par paliers successifs. Certaines applications, dont la rentabilité ne pourra être assurée, ne seront pas entreprises. Actuellement, sur trente applications qui ont pu être globalement définies, six en sont au stade de l'exploitation, six autres se sont vu donner la priorité pour leur réalisation.

Chaque application est confiée à un "chef de projet", responsable successivement de sa conception, de son analyse-programmation et de sa mise en oeuvre dans une région-pilote. La généralisation ultérieure de l'application réalisée dans cette région-pilote dépend des résultats obtenus et fait l'objet d'une décision de la Direction Générale. Néanmoins, le chef de projet doit dès le départ considérer que son activité a une vocation nationale donc refuser tout particularisme régional. Il est aidé d'une équipe d'analyses-programmeurs et entouré d'un "groupe de conception" chargé de rédiger le document de "définition des objectifs globaux" puis le "cahier des charges" de l'application, qui sont adressés pour avis à tous les services utilisateurs potentiels et aux chefs de projet des autres applications. Le groupe de conception comprend 6 à 10 personnes représentant les services les plus divers concernés par le projet, et comporte obligatoirement un bon analyste attaché à l'application.

II - L'IMPLANTATION GEOGRAPHIQUE D'UN RESEAU INFORMATIQUE PERFORMANT

L'organisation de l'entreprise française des télécommunications repose sur l'existence de 20 régions. Des calculateurs ont été implantés dans le passé au moins dans toutes les plus importantes. On trouve ainsi des machines Bull Gamma 30 à Lyon et Marseille, des GE 425 à Lille, Bordeaux, Toulouse et Montpellier, un GE 437 à Massy, enfin quelques machines Bull 300 TI à programmes câblés étaient récemment ou sont encore en service dans les régions de Nancy, Nantes, Limoges, Poitiers et Rouen ; ce parc est essentiellement utilisé pour la comptabilité téléphonique.

A l'avenir, si la plupart des fichiers nécessaires aux applications décrites plus haut peuvent être gérés en temps différé, un certain nombre d'entre eux devront nécessairement être accessibles, voire mis à jour en temps réel : parmi ces derniers le fichier commercial des abonnés, le fichier des renseignements, le fichier des circuits, le fichier technique des abonnés contiendront des quantités considérables d'informations.

Le volume total de caractères à gérer en phase finale sur un ordinateur ayant en charge quelques 500 000 abonnés a été estimé à un milliard de caractères au moins. Au moins le tiers des données seront concernées par des traitements en temps réel.

Aucun des calculateurs énumérés plus haut ne permettait d'envisager de tels traitements. L'intégration progressive de toutes les applications suppose la création d'un support commun pour toutes les informations, une véritable "Banque de données", répartie sur des moyens de traitement nationaux et régionaux, et qui devra rester alimentée, mise à jour en permanence, à partir de la base de l'entreprise, c'est-à-dire les chantiers, les magasins, les guichets des services d'abonnement, les services de personnel etc.

L'étude des différents fichiers à constituer a donc permis de définir les principales caractéristiques du réseau d'ordinateurs nouveaux à mettre en place pour aborder la réalisation du système informatif. L'obligation de faire appel à des ordinateurs de troisième génération, très puissants et dotés de volumineuses mémoires de masse, a conduit à en réduire substantiellement le nombre.

L'implantation de sept centres de calcul interrégionaux constituera un compromis entre : d'une part le désir de réduire le coût économique de l'ensemble, de faciliter la coordination des équipes d'informaticiens ; et d'autre part le refus de créer des centres trop importants difficiles à gérer et à diriger, et posant des problèmes délicats de sécurité. Le regroupement des traitements relatifs à plusieurs régions sur chacun de ces sept centres permettra de leur donner une taille relativement homogène. Chaque centre "gèrera" environ un mil-

(c)

Fig. 17(c)—Document four (first 2000 lines) after pattern matching.

version, characters are often clustered together, which leads to incorrectly (or rather "nonconveniently") isolated characters (as shown in Fig. 18a), while for the old version, the characters are rarely clustered together. However, sometimes a character in the old version is isolated into several patterns because not all its pels are connected (as shown in Fig. 18b). The old version of documents three and five should have

Cela est d'autant plus valable que $T\Delta f$ est plus grand. A cet égard la figure 2 représente la vraie courbe donnant $|\phi(f)|$ en fonction de f pour les valeurs numériques indiquées page précédente.

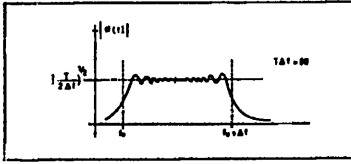


FIG. 2

Dans ce cas, le filtre adapté pourra être constitué, conformément à la figure 3, par la cascade :

— d'un filtre passe-bande de transfert unité pour $f_0 \leq f \leq f_0 + \Delta f$ et de transfert quasi nul pour $f < f_0$ et $f > f_0 + \Delta f$, filtre ne modifiant pas la phase des composants le traversant ;

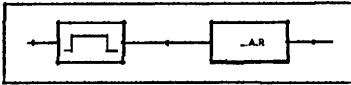
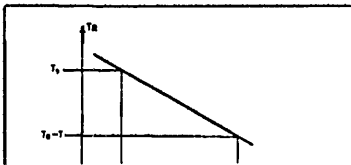


FIG. 3

— filtre suivi d'une ligne à retard (L.A.R.) dispersive ayant un temps de propagation de groupe T_R décroissant linéairement avec la fréquence f suivant l'expression :

$$T_R = T_0 + (f_0 - f) \frac{T}{\Delta f} \quad (\text{avec } T_0 > T)$$

(voir fig. 4).



telle ligne à retard est donnée par :

$$\varphi = -2\pi \int_0^f T_R df$$

$$\varphi = -2\pi \left[T_0 + \frac{f_0 T}{\Delta f} \right] f + \pi \frac{T}{\Delta f} f^2$$

Et cette phase est bien l'opposé de $|\phi(f)|$, à un déphasage constant près (sans importance) et à un retard T_0 près (inévitabile).

Un signal utile $S(t)$ traversant un tel filtre adapté donne à la sortie (à un retard T_0 près et à un déphasage près de la porteuse) un signal dont la transformée de Fourier est réelle, constante entre f_0 et $f_0 + \Delta f$, et nulle de part et d'autre de f_0 et de $f_0 + \Delta f$, c'est-à-dire un signal de fréquence porteuse $f_0 + \Delta f/2$ et dont l'enveloppe a la forme indiquée à la figure 5, où l'on a représenté simultanément le signal $S(t)$ et le signal $S_1(t)$ correspondant obtenu à la sortie du filtre adapté. On comprend le nom de récepteur à compression d'impulsion donné à ce genre de filtre adapté : la « largeur » (à 3 dB) du signal comprimé étant égale à $1/\Delta f$, le rapport de compression est de $\frac{T}{1/\Delta f} = T\Delta f$

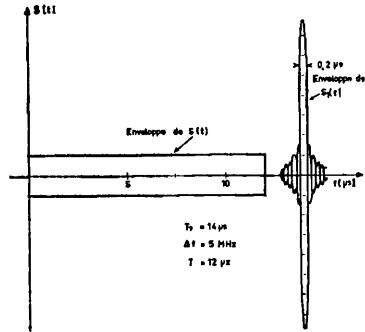


FIG. 5

On saisit physiquement le phénomène de compression en réalisant que lorsque le signal $S(t)$ entre dans la ligne à retard (L.A.R.) la fréquence qui entre la première à l'instant 0 est la fréquence basse f_0 ,

(d)

Fig. 17(d)—Document five (first 2000 lines) after pattern matching.

more patterns than the official but fewer library patterns. In fact, old CCITT document three has 2199 patterns and 225 library patterns, while the official version has 1945 patterns and 551 library patterns. The coding length of a library pattern is much greater (by a factor of about 10) than that of a nonlibrary pattern, which explains the difference in compression ratios. It can be concluded that pattern matching is much more dependent on the scanning quality and the thresholding than two-dimensional facsimile codes.

Table III—Coding length in bits with pattern matching coding

(a) CCITT documents (2376 lines, 1728 pels/line)								
	CCITT1	CCITT2	CCITT3	CCITT4	CCITT5	CCITT6	CCITT7	CCITT8
Mode bit	2376	2376	2376	2376	2376	2376	2376	2376
Horizontal position	11847	8096	21395	46464	23551	15356	36828	31240
No more pattern	888	1587	2193	1854	2235	1929	3165	3231
Vertical move of pattern	1114	411	1921	5724	2242	1347	3427	3642
Library identification code	4895	3749	9458	18584	10848	6426	19289	13085
Library pattern description	<u>43983</u>	<u>71427</u>	<u>120749</u>	<u>41138</u>	<u>94923</u>	<u>71959</u>	<u>204113</u>	<u>115415</u>
Total	65103	87646	158092	116140	136175	99393	269198	168989
(b) Older CCITT documents (same as documents used in Ref. 1) (2128 lines, 1728 pels/line)								
	CCITT1	CCITT2	CCITT3	CCITT4	CCITT5	CCITT6	CCITT7	CCITT8
Mode bit	2128	2128	2128	2128	2128	2128	2128	2128
Horizontal position	12342	7733	24189	49610	27511	16049	38566	30635
No more pattern	846	1533	2103	2574	2091	2007	3942	3168
Vertical move of pattern	1155	463	2448	5726	3028	1411	3812	2441
Library identification code	4958	3599	11078	21385	11940	6927	21842	12773
Library pattern description	<u>23254</u>	<u>62825</u>	<u>29368</u>	<u>26700</u>	<u>22441</u>	<u>55077</u>	<u>155681</u>	<u>122986</u>
Total	44683	78281	71314	108123	69139	83599	225971	174131

Table IV—Comparison of compression ratios

(a) Official CCITT documents (2376 × 1728 pels)			
Picture	Pattern Matching	Two-Dimensional CCITT Code	Increase Versus Two-Dimensional CCITT Code
CCITT1	63.1	28.3	122%
CCITT2	46.8	47.5	-1%
CCITT3	26.0	17.9	46%
CCITT4	35.4	7.4	378%
CCITT5	30.2	15.9	90%
CCITT6	41.3	30.8	34%
CCITT7	15.3	7.4	106%
CCITT8	24.3	26.9	-8%

(b) Nonofficial CCITT document (2128 × 1728 pels)					
Picture	Pattern Matching	Symbol Matching	Two-Dimensional CCITT Code	Increase Versus Symbol Matching	Increase Versus Two-Dimensional CCITT Code
CCITT1	82.3	63.1	28.6	30%	188%
CCITT2	47.0	38.1	45.4	23%	3%
CCITT3	51.6	32.4	18.5	59%	179%
CCITT4	34.0	25.6	7.5	33%	353%
CCITT5	53.2	33.6	16.5	58%	222%
CCITT6	44.0	29.5	30.2	49%	46%
CCITT7	16.3	9.0	7.1	81%	130%
CCITT8	21.1	17.8	22.1	19%	-5%

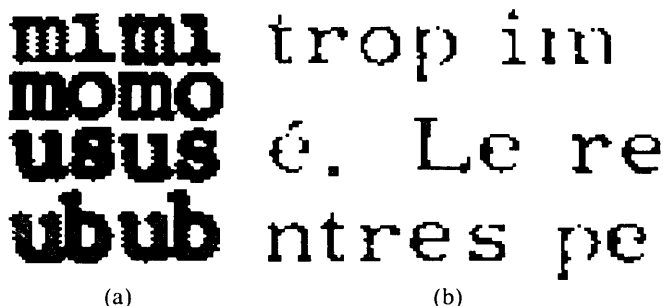


Fig. 18—Characters isolated in an unwanted way. (a) Characters clustered together. (b) Text containing characters isolated into several symbols.

2. The increase in compression ratio compared to the two-dimensional run-length code is quite variable. For documents containing mostly handwritten drawings and text, such as documents two and eight, there is sometimes a slight decrease in the compression ratio. That is because there are few matching patterns. For example, for document two, there are 736 patterns, but 448 of them are library patterns. For documents containing mostly text, such as document four, the compression ratio increases by a factor of about 4.5. For documents containing a mixture of text and drawings, the increase varies between 35 and 220 percent, depending on the content and

thresholding. It should be noted that for document seven, which contains printed ideograms, the increase in compression ratio is smaller than for regular printed text because there are more ideograms than letters, but the compression ratio still doubled.

3. The increase in compression ratio by pattern matching is 20 to 80 percent compared to the symbol matching of Ref. 2. The increase has been obtained by a combination of several factors. The most important are (a) isolation of nonsymbols (lead to significant improvement for documents three, four, five, and six, but has a slight negative effect on documents two and eight), (b) better matching, leading to fewer library patterns, and (c) improved coding efficiency obtained by sorting the patterns and by other coding modifications.

By looking at the coding length necessary for the different kinds of code words, in Table III, it is clear that the predominant part of the code is used for the description of the library patterns, accounting generally for more than 60 percent of the total coding length. Therefore, improving it can bring the highest reward. The improvement can be obtained by reducing the number of library patterns or by coding the pattern description more efficiently. The next most bit-consuming part is the coding of the horizontal position; it uses about 20 percent of the total coding length.

6.3 Complexity

The pattern-matching coding has the disadvantage of being complex and time-consuming—the price to pay for an efficient coding. The most time-consuming parts are: the isolation, the template matching, and the matching decision. The isolation is both complex and time-consuming, and therefore the most difficult part, but by using fast logic, it is possible to isolate all the patterns in about one second. The template matching is a simple operation, but it takes a long time. It is therefore less of a challenge, since it is easily done in parallel and with simple hardware. The most time-consuming part of the matching decision uses local operators on, for example, 3×3 windows and can therefore also be realized without much complication. Most of the high-level operations are much slower and can be done by microprocessors. This system should not be more complicated than in Ref. 2.

An important factor is that the decoding is much easier and faster than the coding, since there is no isolation or matching. Such a technique is therefore particularly suited for transmission with one sender and several receivers.

An experimental pattern matcher has been built to show that the same kind of compression can be obtained when scanning real documents. By using a mixture of custom logic and programmed logic, transmission has reached speeds at rates up to 64 kb/s. A document is then usually sent in one to two seconds.

VII. EXTENSIONS

Several improvements or different applications of a pattern matcher can be considered. Some of them will be described here.

7.1 Multipage document and prestored libraries

When transmitting several pages of a document, the library from one page can be used for next page, thus reducing the number of library patterns for each page. In such cases, compressions up to eight times higher than with conventional coding techniques can be achieved. If a few fonts are prestored in the coder and decoder, the compression can be increased significantly.

7.2 Very high-quality transmission

It is possible to use a tighter matching algorithm when even slight distortions are not tolerated. Such a mode can easily be implemented. It reduces the compression by an average of 15 percent. In that case, most of the postprocessing can be deleted.

7.3 Standardization

The CCITT is looking into standardizing facsimile coding techniques for future facsimile machines communicating over digital links (Group four facsimile apparatus). The modified READ code (also called two-dimensional CCITT code) has been standardized. The pattern matching coding technique has been proposed by AT&T to the CCITT as an optional coding technique yielding much higher compression. The only difference in the proposal compared to this paper is that no cross decomposition is applied. The compression is therefore slightly lower.

7.4 High-resolution graphics

Future scanners and coders will probably include resolutions higher than 200 pels/in. They will probably use 300 and 400 pels/in. The pattern matching technique can easily be modified for such resolution. The maximum size of the patterns should be increased to keep the coding efficient. In addition, the codes for the positioning of patterns must be slightly changed. The matching algorithm would stay unchanged. Compared to conventional techniques, the improvement in the compression will be as high and often even higher at such resolutions.

VIII. CONCLUSION

A system for coding of facsimiles using pattern matching has been described. It allows an important increase in the compression ratio compared with a symbol matching system² and gives a compression

ratio that is up to 4.8 times that of conventional facsimile coding techniques. The improvement is naturally greater for printed text than for handwritten text. It is felt that further significant improvements are possible by better matching and coding. An important observation is that pattern matching coding is very dependent on the digitization and thresholding. Therefore, the combination of the thresholding and the isolation could lead to significant improvements in compressions. Another consequence is that if a bad quality scanner is used, the pattern matching will hardly lead to higher compressions than conventional facsimile codes. With modern electronics components, a pattern matcher can be realized by hardware and would lead to an important reduction in the transmission costs of high-volume facsimiles.

IX. ACKNOWLEDGMENT

The authors would like to thank A. N. Netravali for the numerous and fruitful discussions, E. F. Brown and E. S. Joseph for their contribution to the experimental unit, and S. M. Rubin for providing useful software.

REFERENCES

1. R. B. Arps, "Binary image compression," in *Image Transmission Techniques*, W. K. Pratt, ed., New York: Academic Press, 1979.
2. W. K. Pratt, et al., "Combined Symbol Matching Data Compression System," *Proc. IEEE*, 68, No. 7 (July 1980), pp. 786-96.
3. R. N. Ascher and G. Nagy, "A means for achieving a high degree of compaction on scan-digitized text," *IEEE Trans. Comput.*, C-23 (November 1974) pp. 1174-9.
4. S. A. Dudani, "Region extraction using boundary following," in *Pattern Recognition and Artificial Intelligence*, C. H. Chen, ed., New York: Academic Press, pp. 216-32.
5. R. Hunger and A. H. Robinson, "International Digital Facsimile Coding Standards," *Proc. IEEE*, 68, No. 7 (July 1980), pp. 854-67.

AUTHORS

Glenn L. Cash, B.S.E.E., 1981, Monmouth College; Bell Laboratories, 1981—. Mr. Cash has worked on the design and implementation of a real-time pattern matching facsimile coder. His research interests include image processing, artificial intelligence, and computer system design. Member, Eta Kappa Nu, Sigma Pi Sigma.

Ottar Johnsen, E.E., 1974, Ph.D., 1979, Ecole Polytechnique Federale de Lausanne, Switzerland; Ecole Polytechnique Federale de Lausanne, 1974-1979; Bell Laboratories, 1979—. Mr. Johnsen was assistant at the Signal Processing Laboratory of the Ecole Polytechnique Federale de Lausanne, working in the field of picture coding. At Bell Laboratories, as a member of the Visual Communications Research Department, he is involved in research in picture processing and coding, and in communication systems.

Jakub Segen, M.S.E.E., 1971, Technical University of Wroclaw, Poland; Ph.D., 1980, Carnegie-Mellon University; Bell Laboratories, 1980—. Mr. Segen worked as a computer engineer at ZETO, Woclaw, and New York University. Recently, he has been involved with signal and image analysis, and his main research interests are machine perception and learning. He is a member of Robotics Systems Research Department, working on aspects of computer vision.

Data-Transport Performance Analysis of Fasnet

By D. P. HEYMAN*

(Manuscript received February 25, 1983)

This paper presents a queueing model to assess the performance of Fasnet, a recently invented local-area network. Fasnet is intended for high-speed lines capable of carrying a wide mix of traffic. We confine our attention to data traffic only. An approximate formula for the expected delay of a packet is obtained; the approximate formula compares favorably to simulations of Fasnet.

I. INTRODUCTION

Fasnet is an implicit token-passing local-area network.¹ It is intended for high-speed lines capable of carrying a wide mix of traffic (data, voice, video, and facsimile). In this paper, we present a queueing model to assess the performance of Fasnet with data traffic only. An approximation for the expected delay of a packet is obtained; the approximate solution compares favorably with measurements taken from a simulation of Fasnet. Our numerical results yield a mean delay that is less than 1 ms for a 1-kb packet when the line speed is 100 Mb/s and the occupancy of the line is 0.9.

Section II consists of a brief description of Fasnet. Section III describes our model and its approximate solution and Section IV presents comparisons with simulations. The effects of bursty traffic are given in Section V and our conclusions are stated in Section VI.

II. A BRIEF DESCRIPTION OF FASNET

We will now give a description of Fasnet that will enable the reader to appreciate the model in Section III. A complete description is given in Ref. 1.

* Bell Laboratories.

©Copyright 1983, American Telephone & Telegraph Company. Photo reproduction for noncommercial use is permitted without payment of royalty provided that each reproduction is done without alteration and that the Journal reference and copyright notice are included on the first page. The title and abstract, but no other portions, of this paper may be copied or distributed royalty free by computer-based and other information-service systems without further permission. Permission to reproduce or republish any other portion of this paper must be obtained from the Editor.

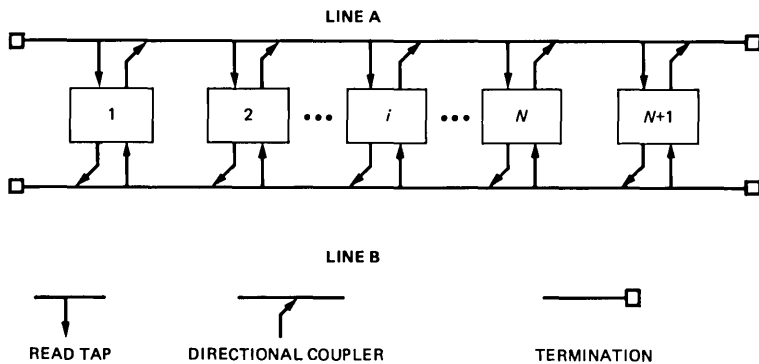


Fig. 1—Physical configuration of a Faset link.

The basic link as shown in Fig. 1 consists of two lines. One line carries traffic in one direction and the other line carries traffic in the reverse direction. For line A (which carries traffic from station 1 towards station N), station 1 is called the *head* station and station $N + 1$ is called the *end* station. For line B, the roles are reversed. Each station makes two connections to each line. A read tap precedes a passive directional coupler used for writing. The signal read from the read tap will be unaffected by the signal being written simultaneously on the line via the directional coupler. Except for specific fields of the header, the protocol ensures that only one station at a time writes on the line. Thus, once a message is written on a line, it is not removed or changed by any station.

The access control is similar for lines A and B. For line A, the head station (station 1) will initiate a *cycle*, which operates in the following way. One time each cycle, each station with packets destined toward the end station is allowed to access the line for a single time interval, during which at most p_{\max} packets can be sent. A station knows when to place its packets on the line by reading a particular bit (called the busy bit) in the access control field. This bit is added to the message packet by the network layer of the protocol. Thus, in each cycle, station 1 has the first opportunity to send packets, station 2 has the second opportunity, and station N has the N th and last* opportunity. Each station has exactly one opportunity per cycle to send packets. When station $N + 1$ receives a packet in which the busy bit indicates that the packet has not been used, it sends a message to station 1 (using line B) to start a new cycle. There may be synchronization delays at each end of the transmission of this message. The operation on line B is identical to the operation of line A, with station $N + 1$ as the head station and all flows reversed accordingly.

* We assume that station $N + 1$ will not send messages to itself.

III. THE MODEL

Fasnet behaves as an implicit token-passing protocol because control passes from station to station as if a token were sent from station 1 to station 2, \dots , to station $N + 1$ to station 1, and so forth. This suggests that a queueing model of queues served in cyclic order would be appropriate. In this type of model, there is a single server that visits $N + 1$ different queues in the cyclic order described above. For Fasnet, the server is conceptual: it is the opportunity to place packets on the line. The service time is the length of time to write a packet. The queues correspond to the buffers at each station.

Several papers have been written about queues served in cyclic order. In most of these papers, it is assumed that there is *exhaustive service* at each station. This means that the server processes all customers waiting at the station at the epoch that the server reaches the station. The most general model of exhaustive service is in Eisenberg,² where each queue is of the M/G/1 type and the times to travel between adjacent stations may depend on the pair of stations involved. The solution of this model is in terms of transforms that are not given in closed form; however, the equations can be solved numerically. A special case of the model in Ref. 2 is treated in Konheim and Meister.³ Here, all service times are the constant Δ , and all travel times between adjacent stations have the same distribution, which is concentrated on $\Delta, 2\Delta, \dots$. Konheim and Meister are able to obtain closed-form solutions for steady-state performance measures in this case. Their results will be used in our analysis. The only paper where service is not exhaustive is Ref. 4 by Eisenberg. That paper contains two M/M/1 type queues, and the server can process at most one customer during a visit to a server. The solution to this model requires extensive calculations, and the restriction to two stations is unrealistic for Fasnet.

We have chosen to seek approximate solutions where each station is of the M/D/1 type and service is either exhaustive or one-at-a-time (as in Ref. 4). These correspond to $p_{\max} = \infty$ and $p_{\max} = 1$, respectively. When the system is not heavily loaded, each station will have a small load so $p_{\max} = \infty$ should not behave much differently from $p_{\max} = 1$. This behavior is exhibited by our approximate solution and by simulations.

We will analyze our models by embedding them in a server-vacation model. In an M/G/1/FIFO queue, assume that at the end of each busy period the server takes a vacation. The vacations are iid random variables generically denoted by T . The expected delay of a customer, in the steady state, is given by

$$E(D^*) = E(D) + \frac{E(T^2)}{2E(T)}. \quad (1)$$

Here $E(D)$ is the Pollaczek-Khintchine formula for the expected delay in an M/G/1 queue: $E(D) = ab_2/2(1 - ab_1)$, where a is the arrival rate and b_1 and b_2 are the first and second moments of the service times. A derivation of eq. (1) can be found in Levy and Yechiali.⁵ Our first step is to describe the vacations.

3.1 Assumptions and notation

The notation used in this paper and some self-explanatory symbols are given below.

N = number of potential transmitting stations.

λ_i = packet arrival rate at station i .

Δ = constant service time/packet.

$\rho_i = \lambda_i \Delta$ = load due to station i .

$R = \sum_1^N \rho_i$ = load on the line.

$\Lambda = \sum_1^N \lambda_i$ = total arrival rate.

τ = one-way propagation delay.

$\gamma = 2\tau + \Delta$ = average overhead/cycle.

Lines A and B shown in Fig. 1 are the same except for direction, so it is sufficient to model only line A. Notice that station $N + 1$ does not send messages on line A and that station 1 does not send messages on line B. We assume that packets to be transmitted appear at station i according to a homogeneous Poisson process with rate λ_i , $i = 1, 2, \dots, N$. The arrivals at station i and j are independent when $i \neq j$. We assume that all the packets contain the same number of bits. The amount of time that a line spends taking a packet from a station is the time required to read the bits of the packet. Therefore, the service time of each packet is a constant, Δ , say, where Δ is the number of bits/packet divided by the line speed in b/s. The time for a bit to travel between adjacent read taps is called the *walk time*; the average walk time between stations is denoted by w .

Let τ be the time to send a bit from station 1 to station $N + 1$ (and from $N + 1$ to 1). Then 2τ is expended in each cycle to send a message indicating that the busy bit must be reset. An average of one-half of a packet processing time is lost in synchronization at each end station, so $\gamma = 2\tau + \Delta$ is the average overhead per cycle. Notice that τ is the time to walk from station 1 to station $N + 1$.

3.2 Analysis of the exhaustive service model

In this subsection, we assume that the packet arrival rates are the same at each station. We let λ denote the common arrival rate and ρ denote the common load on a station. The load on the line is $R = N\rho$. We also assume that stations 1, 2, \dots , $N + 1$ are evenly spaced along the line.

Let T represent the amount of time between a departure from

station 1 and the beginning of the next visit to station 1. Then T is the length of a vacation from station 1. By symmetry, T is the length of a vacation between successive visits to any station. Thus, when a station gains access to the line, an average of $\lambda E(T)$ packets are present. With exhaustive service, the expected time to clear a station is $\lambda E(T)\Delta/(1 - \rho)$. Since a vacation from station 1 consists of reading packets at stations 2 through N and overhead,

$$E(T) = \gamma + (N - 1) \frac{\lambda E(T)\Delta}{1 - \rho},$$

so

$$E(T) = \frac{\gamma(1 - \rho)}{1 - R}, \quad R < 1. \quad (2)$$

Equation (2) is a special case of eq. (54) in Ref. 2.

Let X denote the number of packets at station 1 at the end of a vacation. Then

$$E(X) = \lambda E(T), \quad (3a)$$

and

$$\text{Var}(X) = \lambda^2 \text{Var}(T). \quad (3b)$$

Theorem 4.7 in Ref. 3 asserts that

$$\text{Var}(X) = \frac{\lambda \rho^2 [1 - (N + 1)\rho + (2N - 1)\rho^2]}{(1 - R)^2}. \quad (4)$$

From eqs. (2), (3), and (4) we obtain

$$\frac{E(T^2)}{E(T)} = \frac{\rho(N - 1)\Delta + \gamma(1 - \rho)^2}{(1 - \rho)(1 - R)}. \quad (5)$$

Equation (5) is exact when the walk times between any pair of stations are concentrated on $\Delta, 2\Delta, \dots$. In Fasnet, we expect that the walk times are much less than Δ because the packets travel between stations at the speed of light and the read times are controlled by the speed of the line. Thus, we should regard eq. (5) as an approximation.

From eqs. (1) and (5),

$$\begin{aligned} E(D^*) &= \frac{\rho\Delta}{2(1 - \rho)} + \frac{\rho(N - 1)\Delta}{2(1 - \rho)(1 - R)} + \frac{\gamma(1 - \rho)}{2(1 - R)} \\ &= \frac{R\Delta}{2(1 - R)} + \frac{\gamma(1 - \rho)}{2(1 - R)}, \quad R < 1. \end{aligned} \quad (6)$$

By symmetry, eq. (6) gives the expected delay of a packet at any station. The expected number of packets in a buffer, $E(Q)$, say, is obtained from eq. (6) and Little's theorem:

$$E(Q) = \lambda E(D^*) = \frac{R\rho}{2(1-R)} + \frac{\gamma\lambda(1-\rho)}{2(1-R)}. \quad (7)$$

Consequently, the expected number of customers in buffers 1 through N is

$$NE(Q) = \frac{R^2}{2(1-R)} + \frac{\gamma\lambda(1-\rho)}{2(1-R)}. \quad (8)$$

Equation (7) is compared to simulation experiments in Section IV.

An intuitive understanding of eq. (6) may be gained by considering what happens for light loads. When ρ is small, the vacations are almost of constant length because (mostly) no customers are served during a vacation. Then $E(T^2)$ is about $[E(T)]^2$. Now merge all the customers to obtain an M/D/1 queue with mean delay $R\Delta/[2(1-R)]$. Then eqs. (1) and (2) yield

$$E(D^*) = \frac{R\Delta}{2(1-R)} + \frac{\gamma(1-\rho)}{2(1-R)},$$

which is eq. (6). It is surprising that this heuristic light traffic argument produces the exact (modulo our other approximations) result for any $R < 1$.

3.3 Analysis of the one-at-a-time service model

In this subsection we will obtain an approximate solution to a model where $p_{\max} = 1$. The approximation is based on an idea used in Lehoczky, Sha, and Jensen⁶ for a similar model. We do not assume that the arrival rates are the same at each station (as we did in Section 3.2).

A central notion in the approximation is the *completion time* of a station. The completion time of a station is the duration of the interval that starts when that station begins processing a packet, and ends at the first epoch that another packet may begin (does begin, provided it is present) its processing at the station. The purpose of the approximate solution is to estimate the mean and variance of the completion time, use these moments in the Pollaczek-Khintchine formula, and apply eq. (1) to an appropriate server-vacation model.

Let V_i denote a generic completion time at station i , in the steady state. Then

$V_i =$ cycle overhead + $\Delta(1 +$ number of other stations sending a packet in this cycle).

Let p_i be the asymptotic proportion of time that packets are present at station i . For T very large, the number of packets served at station i by time T is

$$\frac{\rho_i T}{\mathbf{E}(V_i)} + o(T),$$

where $o(T)$ is some function such that $o(T)/T \rightarrow 0$ as $T \rightarrow \infty$. The arrival rate at station i is λ_i . Equating the arrival and departure rates yields

$$\rho_i = \lambda_i \mathbf{E}(V_i). \quad (9)$$

Now we make our first approximation.

Approximation 1: In each cycle, the probability that station i transmits a packet is $b_i \triangleq \lambda_i \mathbf{E}(V_i)$.

The effect of approximation 1 is to use the long-run proportion ρ_i as a probability for each cycle. Thus, the expected number of other stations sending a packet during a completion time of station i is $\sum_{j \neq i} b_j$, so

$$\mathbf{E}(V_i) = \Delta \left(1 + \sum_{j \neq i} b_j \right) + \gamma. \quad (10)$$

Hence,

$$b_i \triangleq \lambda_i \mathbf{E}(V_i) = \rho_i \left(1 + \sum_{j \neq i} b_j \right) + \lambda_i \gamma, \quad i = 1, 2, \dots, N. \quad (11)$$

The solution of eq. (11) is

$$b_i = \frac{\rho_i}{1 + \rho_i} \frac{1 + \gamma/\Delta}{1 - \alpha}, \quad \alpha = \sum_1^N \frac{\rho_i}{1 + \rho_i}, \quad i = 1, 2, \dots, N, \quad (12)$$

which can be verified by substitution into eq. (11). When $\rho_i \equiv \rho$ and $\gamma = 0$, eq. (12) becomes

$$b_i = \frac{\rho}{1 - (N-1)\rho} = \frac{R/N}{1 - \frac{N-1}{N}R} \quad \text{for all } i,$$

which is the approximation given in Lehoczky et al.⁶

Since b_i must be no larger than one (because it is a probability), eq. (12) constrains the feasible values of $\{\rho_i\}$. When all the arrival rates have the common value λ , $\alpha = N\rho/(1 + \rho) = R/(1 + \rho)$, so

$$b_i < 1 \Leftrightarrow N > \frac{R\gamma/\Delta}{1 - R}. \quad (13)$$

Equation (13) shows that for a given total load, R , stability is achieved only when the load is shared by a sufficiently large number of stations. For Fasnet, $\gamma/\Delta = 3$ is a typical value. Then eq. (13) asserts that for $R = 0.9$, $N > 27$ is required for stability; for $R = 0.8$,

$N > 12$ is required for stability; and for $R = 0.5$, $N \geq 8$ is required for stability.

Here is why N cannot be too small. When N is small, the overhead per cycle (γ) will be spread over a few customers, which has the effect of decreasing the capacity of the line. To see this more precisely, let c be the expected number of packets processed in a cycle. Then use eq. (11) to obtain

$$c = \sum_1^N b_i = \frac{1 + \gamma/\Delta}{1 - \alpha} \sum_1^N \frac{\rho_i}{1 + \rho_i} = \frac{(1 + \gamma/\Delta)\alpha}{1 - \alpha}. \quad (14)$$

When all the arrival rates have the common value λ , eq. (14) yields

$$c = \frac{R(1 + \gamma/\Delta)}{1 + \rho - R}, \quad (15)$$

where $\rho = \lambda\Delta$. From eq. (15) we compute the average amount of overhead expended per packet per cycle* γ/c :

$$\frac{\gamma}{c} = \frac{1 - R + R/N}{R(1 + \gamma/\Delta)} \gamma = \frac{\gamma}{1 + \gamma/\Delta} \left(\frac{1 - R}{R} + \frac{1}{N} \right). \quad (16)$$

Eq. (16) shows that the average overhead per packet is a decreasing function of N , so if N were small, the overhead per packet might cause the line to be overloaded.

It is interesting to note that this consideration does not arise in Section 3.2. When $p_{\max} < \infty$, from time to time a station will stop transmitting packets because its quota for the cycle has been filled. This is the effect that is shown in eq. (16). We conjecture that when all other parameters are fixed, γ/c is a decreasing function of p_{\max} .

Now we turn to an approximation for the mean delay. This will be done by proposing a suitable server-vacation model and applying eq. (1). The service-time moments in the Pollaczek-Khintchine formula correspond to completion-time moments here. When a packet arrives at station i , and no other packets are waiting to be transmitted at station j , that packet cannot be transmitted until station i gains access to the line. The length of time that station i does not have access to the line is the length of time to process the other stations in a cycle plus the overhead time, which is the completion time less one service time. Thus, $T_i = V_i - \Delta$, so

$$E(T_i) = E(V_i) - \Delta, \quad (17)$$

* The fact that γ/c is the right quantity to compute may not be obvious. A rigorous proof could use ergodic theory for regenerative processes (see, e.g., Section 6-4 of Heyman and Sobel,⁷ particularly Theorem 6-8).

and

$$\text{Var}(T_i) = \text{Var}(V_i). \quad (18)$$

From eqs. (10), (12), and (17) we can obtain $E(T_i)$. From eqs. (1) and (18) we see that only $\text{Var}(V_i)$ remains to be obtained. To get it, we make our second approximation.

Approximation 2: In each cycle, the event that station i transmits a packet is independent of the event that station j transmits a packet for every $j \neq i$.

The effect of approximation 2 is that the variance of the number of packets served at station i is $b_i(1 - b_i)$ and the variance of the number of packets served in a cycle is $\sum_{i=1}^N b_i(1 - b_i)$. This yields the approximation

$$\text{Var}(V_i) = \Delta^2 \sum_{j \neq i} b_j(1 - b_j). \quad (19)$$

Using eqs. (10), (12), (17), (18), and (19) in eq. (1) produces our approximation for the expected delay at station i , $i = 1, 2, \dots, N$. The resulting formula does not appear to provide any insight and is omitted.

As a partial check on the efficacy of our approximation for the mean delay, we consider the limiting case of no overhead and identical stations. In this situation, the total content of the output buffers at stations $1, 2, \dots, N$ fluctuates as the queue length in an M/D/1 queue with arrival rate λ and service time Δ . From the Pollaczek-Khintchine formula, the expected queue length in the steady state, $E(Q_0)$, say, is

$$E(Q_0) = \frac{R^2}{2(1 - R)}, \quad R < 1.$$

Our approximations produce (after some algebra)

$$E(\hat{Q}_0) = \frac{R^2}{2(1 - R + \rho)} \frac{\rho[R + (1 - R)(R - \rho)] + 1 - R}{1 - R}, \quad R < 1.$$

Now let $N \rightarrow \infty$ and $\rho \downarrow 0$ with $R = N\rho$ held fixed. This represents a system with many lightly loaded stations. Then

$$E(\hat{Q}_0) \rightarrow \frac{R}{2(1 - R)} \quad \text{as } \rho \downarrow 0.$$

In this limiting case, $E(\hat{Q}_0)$ overestimates $E(Q_0)$ by $R/2$ and, the relative error is $(1 - R)/R$. Thus, the absolute error increases with R and is less than one-half, and the relative error decreases as the absolute error increases.

IV. COMPARISONS WITH SIMULATIONS

A computer simulation of Fasnets has been constructed. There are $N = 50$ sending stations equally spaced along the line. The propagation time (τ) equals the packet processing time at each station (Δ). We have chosen to consider 1000-bit packets and a line speed of 100 Mb/s, which is representative of the operating region. Then $\Delta = 10 \mu\text{s}$, and $\lambda = (R/50) \times 10^5$ packets/s.

The measure of performance is the average queue length at the stations. Specifically, the simulation estimates the steady-state distribution of the queue length at station i and then computes the mean, $E(Q_i)$, say. The average queue length is $\sum_{i=1}^{50} E(Q_i)/50 \triangleq E(Q)$. The corresponding quantity from our formulas is called $E(\hat{Q})$. From the queueing formula $E(Q) = \lambda E(D)$ we use $E(\hat{Q})$ to estimate the average delay of a packet, $E(\hat{D})$.

Table I shows the results.

The analytic approximation adequately replicates the simulation results. Table I and Fig. 2 demonstrate that for R as large as 0.8, $p_{\max} = 1$ and $p_{\max} = \infty$ produce nearly the same average queue size. This means that the efficiency (in terms of not incurring too much overhead) of $p_{\max} = \infty$ and the protection against a few stations dominating the line of $p_{\max} = 1$ can be simultaneously obtained by setting $1 < p_{\max} < \infty$. Table I shows that $p_{\max} = 3$ is almost as efficient as $p_{\max} = \infty$.

The approximation for the mean delay of a packet is less than 1/2 ms even when $R = 0.9$ and $p_{\max} = 1$.

V. THE EFFECTS OF BURSTY TRAFFIC

In this section we return to the exhaustive service model and replace the assumption that packets arrive according to a Poisson process with the assumption that packets arrive according to a compound Poisson process. Fuchs and Jackson give statistical analyses of arrival times for terminal-to-computer calls.⁸ Two of their conclusions are as follows:

1. The exponential distribution is a reasonably good approximation of the times between bursts.

Table I—Comparison of simulations and analytic approximations

p_{\max}	$E(Q)$ Simulation	$E(\hat{Q})$ Analysis	$E(\hat{D})$	
$R = 0.8$	1	0.216	0.209	130 μs
	3	0.184	—	—
	∞	0.184	0.150	94 μs
$R = 0.9$	1	0.684	0.782	430 μs
	3	0.440	—	—
	∞	0.398	0.346	192 μs

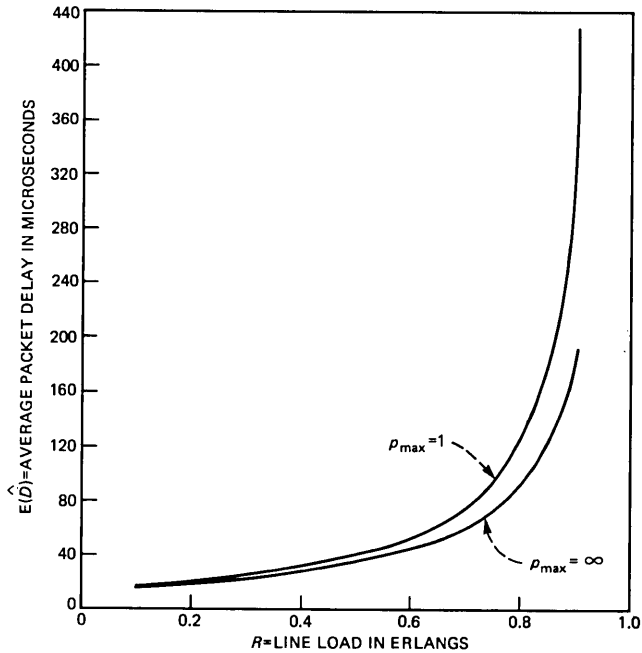


Fig. 2—Expected delay vs R for 1-kb packets, 50 stations, and 100-Mb/s line speed.

2. The size of a burst (measured in various ways) has a geometric distribution.

Recent analyses by Morgan of host-to-host file traffic indicate that the assumption of Poisson arrivals may not be justified.⁹

The purpose of this section is to find out how sensitive the average delay is to the assumption of Poisson arrivals. We will see that in the exhaustive service model, the average delay can be significantly greater with bursty arrivals than with Poisson arrivals with the same rate.

Specifically, we assume that the bursts arrive according to a Poisson process with rate λ_b and the burst sizes B_1, B_2, \dots are iid with

$$P\{B_1 = i\} = (1 - \xi)\xi^{i-1}, \quad i = 1, 2, \dots$$

This arrival process can be interpreted as one where messages arrive according to a Poisson process with rate λ_b , and the j th message consists of a random number of packets with a geometric distribution. One reason for choosing a geometric distribution is that it equates the average delay of a packet and the average delay of a message (see Halfin¹⁰). (The delay of a message is the delay of its last packet.) Another reason is that it uses only one parameter, and so we can

specify the mean (Mt , say) and variance (Vt , say) of the number of arrivals in an interval of length t and then solve for λ_b and ξ . Doing so yields

$$\lambda_b = \frac{2M^2}{M + V} \quad \text{and} \quad \xi = \frac{V - M}{V + M}.$$

Letting $z = V/M \geq 1$ yields

$$\lambda_b = \frac{2M}{1 + z} \quad \text{and} \quad \frac{z - 1}{z + 1}. \quad (20)$$

Equation (20) relates the parameters we might obtain from measurements, M and z , to the parameters of the model, λ_b and ξ .

We will now obtain the delay of an arbitrary packet in the steady state. The analysis is similar to the analysis in subsection 3.2; as before we assume that the stations have statistically identical arrival processes.

The analog of the Pollaczek-Khintchine formula for compound Poisson arrivals is given in Burke.¹¹ In our notation, the formula is

$$E(D) = \frac{\lambda_b \Delta^2 (1 + \xi)}{2(1 - \rho)} + \frac{\xi \Delta}{1 - \xi}, \quad (21)$$

where $\rho = \lambda_b \Delta / (1 - \xi) = M \Delta$.

To obtain the mean and variance of the vacation times, let X denote the number of packets at station 1 at the end of a vacation. From theorem 4.7 in Ref. 3, for $R < 1$

$$E(X) = \frac{\gamma M (1 - \rho)}{1 - R}, \quad (22a)$$

and

$$\text{Var}(X) = \frac{XV}{(1 - R)^2} [1 - (N + 1)\rho + (2N - 1)\rho^2]. \quad (22b)$$

Since X is the number of packets that arrive in an interval of length T ,

$$E(X) = ME(T), \quad (23a)$$

and

$$\begin{aligned} \text{Var}(X) &= E[\text{Var}(X | T)] + \text{Var}[E(X | T)] \\ &= E[VT] + \text{Var}[MT] \\ &= VE(T) + M^2 \text{Var}(T). \end{aligned} \quad (23b)$$

From eqs. (22) and (23) we obtain

$$\begin{aligned}\frac{E(T^2)}{E(T)} &= \frac{\text{Var}(X)}{ME(X)} - \frac{V}{M^2} + E(T) \\ &= \frac{(N-1)V\Delta^2 + \gamma(1-\rho)^2}{(1-\rho)(1-R)}.\end{aligned}\quad (24)$$

Substituting eqs. (21) and (24) into eq. (1) yields

$$E(D^*) = \frac{\lambda_b \Delta^2 (1 + \xi)}{2(1 - \rho)} + \frac{\xi \Delta}{1 - \xi} + \frac{(N - 1)V\Delta^2 + \gamma(1 - \rho)^2}{2(1 - \rho)(1 - R)}.$$

Using eq. (20) yields

$$E(D^*) = \frac{R\Delta z}{2(1 - R)} + \frac{\gamma(1 - \rho)}{2(1 - R)} + \frac{(z - 1)\Delta}{2} - \frac{\rho\Delta z(z - 1)}{2(1 - \rho)(1 + z)}.\quad (25)$$

To compare eqs. (6) and (25), let a subscript z denote batch arrivals with variance to mean ratio z . Then

$$E(D_z^*) - E(D^*) = \frac{\Delta(z - 1)}{2(1 - R)} - \frac{\rho\Delta z(z - 1)}{2(1 - \rho)(1 + z)}.$$

When N is large, so that ρ is much smaller than R , the first term dominates, especially in heavy traffic.

Table II shows the values of $E(D_z^*)$. The case $E(D_1^*)$ represents Poisson arrivals. The data are the same as in Section IV: $\Delta = \tau = 10 \mu\text{s}$, and $N = 50$.

Table II shows that bursty traffic can have much larger expected delays than Poisson traffic with the same arrival rate. A crude approximation of the increase is $E(D_z^*) = E(D_1^*)\sqrt{z - 1}$ for $2 \leq z \leq 10$. Even when $z = 10$ and $R = 0.9$, the mean delay is less than 1 ms.

VI. CONCLUSIONS

We have three conclusions. The first is that the approximations presented in Section III are sufficiently accurate for data transport performance studies of Fasnet. The second is that $p_{\max} = 3$ appears to be a good choice if the offered traffic is reasonably smooth (Poisson) and approximately equal to all stations. The third is that Fasnet should be able to provide 1-ms average-delay performance for bursty traffic.

Table II— $E(D_z^*)$ in μs for several values of z

	$E(D_1^*)$	$E(D_2^*)$	$E(D_3^*)$	$E(D_{10}^*)$
$R = 0.8$	94	119	193	318
$R = 0.9$	192	242	392	642

VII. ACKNOWLEDGMENTS

I would like to thank Lois E. Flamm for running the simulations, and John Limb and Jon Mark for their comments on a draft of this paper.

REFERENCES

1. J. O. Limb and C. Flores, "Description of Fasnet—A Unidirectional Local-Area Communications Network," *B.S.T.J.*, 61, No. 7, Part 1 (September 1982), pp. 1413-40.
2. M. Eisenberg, "Queues With Periodic Service and Changeover Times," *Oper. Res.*, 20, No. 2 (March-April 1972), pp. 440-51.
3. A. G. Konheim and B. Meister, "Waiting Lines and Times in a System with Polling," *J. Ass. Comput. Mach.*, 21, No. 3 (July 1974), pp. 470-90.
4. M. Eisenberg, "Two Queues with Alternating Service," *SIAM J. Appl. Math.*, 36, No. 2 (April 1979), pp. 287-303.
5. Y. Levy and U. Yechiali, "Utilization of Idle Time in an $M/G/1$ Queueing System," *Manage. Sci.*, 22, No. 2 (October 1975), pp. 202-11.
6. J. P. Lehoczky, L. Sha, and E. D. Jensen, "A Comparative Study of Variable TDM Schemes and CSMA Schemes," Technical Report No. 27, Department of Statistics, Carnegie-Mellon University (August 1981).
7. D. P. Heyman and M. J. Sobel, *Stochastic Models in Operations Research*, Vol. I, New York: McGraw-Hill, 1982.
8. E. Fuchs and P. E. Jackson, "Estimates of Distributions of Random Variables for Certain Communications Traffic Models," *Commun. ACM*, 13, No. 12 (December 1970), pp. 752-7.
9. S. P. Morgan, unpublished work.
10. S. Halfin, "Batch Delays Versus Customer Delays," *B.S.T.J.*, 62, No. 7, Part 1 (September 1983), pp. 2011-15.
11. P. J. Burke, "Delays in Single-Server Queues with Batch Input," *Oper. Res.*, 23, No. 4 (July-August 1975), pp. 830-3.

AUTHOR

Daniel P. Heyman, B.Mgt.E. (Management Engineering), 1960, Rensselaer Polytechnic Institute; M.I.E. (Industrial Engineering), 1962, Syracuse University; Ph.D. (Operations Research), 1966, University of California, Berkeley; U.S. Air Force, 1960-1963; Bell Laboratories, 1966—. Mr. Heyman has worked on a variety of operations research problems at Bell Laboratories, including studies of queues, inventories, and financial markets. He was a visiting faculty member at Yale University for the 1976-1977 academic year. Member, Sigma Xi, Alpha Pi, Mu, Operations Research Society of America.

Forecasting With Adaptive Gradient Exponential Smoothing

By A. FEUER*

(Manuscript received December 20, 1982)

Exponential Smoothing (ES) as a forecasting technique has been extensively used since its introduction in the 1960s. It is simple, hence easy to implement, and in many cases performs surprisingly well. However, many phenomena require a more sophisticated forecasting technique. In this paper we introduce a new forecasting technique, Adaptive Gradient Exponential Smoothing (AGES). This technique extends the classical ES as used on simple data or on data with linear trend. For data with both linear trend and seasonal effects this extension results in a new and more general form of ES, which is presented in this paper. The new forecasting technique is tested on simulated data and some real data of the types mentioned above, and its performance in all these tests is clearly superior to ES. It is shown by analysis and by the experimentations that for certain types of data it does in fact converge to the optimal (in the mean square error sense) forecasts.

I. INTRODUCTION

The need for quick and reliable forecasts of various time series is often encountered in economic and business situations. In the Bell System, forecasting is used to help plan trunk and facilities for the telephone network,¹⁻³ as well as to project computer workload, to determine staffing levels for operators or service observers, and more.

Many forecasting techniques exist and different time series may require different techniques. In general, there is a clear trade-off between simplicity (resulting in cheaper implementation) and per-

* Bell Laboratories.

©Copyright 1983, American Telephone & Telegraph Company. Photo reproduction for noncommercial use is permitted without payment of royalty provided that each reproduction is done without alteration and that the Journal reference and copyright notice are included on the first page. The title and abstract, but no other portions, of this paper may be copied or distributed royalty free by computer-based and other information-service systems without further permission. Permission to reproduce or republish any other portion of this paper must be obtained from the Editor.

formance of the forecasting technique. One of the simplest forecasting techniques, Exponential Smoothing (ES), has surprisingly good performance. This technique was presented originally by Winters⁴ and Brown⁵ and is described briefly in Section II. In Ref. 6 the optimality properties of ES are studied and we expand on these studies and use the conclusions as the basis for a new technique we introduce here.

In fact, these studies revealed a relationship between the ES and the Autoregressive-Integrated Moving Average (ARIMA) model-fitting-based forecasting suggested by Box and Jenkins.⁷ This is further discussed in Section III.

The extensive use of ES clearly indicated that for time series with nonstationary discontinuities or changes in the generating parameters, ES performance is not satisfactory. This prompted a number of researchers to develop the Adaptive Exponential Smoothing (AES) idea. In these techniques the algorithm is supposedly evaluating its own performance and correcting its parameters to obtain improved performance. Recently, the existing AESs (see, for example, Refs. 8 through 11) were reviewed critically by Ekern.¹² One of the points raised in Ref. 12 was that none of the existing AESs is supported by analysis or general performance claims (e.g., optimality). In addition, it should be pointed out that only Roberts' and Reed's AES¹¹ can be used on data with both linear trend and seasonal effects, while the other AESs are limited to simpler data and have no natural generalization.

In this paper we present a new AES algorithm, which we call Adaptive Gradient Exponential Smoothing (AGES). This technique naturally generalizes to data with both linear trend and seasonal effect. In addition, analysis of AGES for simple data and extensive simulations, using simple as well as more general data, strongly suggests that this technique converges to optimal performance in the mean square error (MSE) sense.

Section II presents ES as commonly used. A new, more general form is developed with a discussion of its optimal properties. The new technique, AGES, is derived and presented in Section III, while the results of experiments with this technique on both real and simulated data are presented in Section IV.

II. EXPONENTIAL SMOOTHING AND ITS OPTIMAL PROPERTIES

First we consider ES as Winters⁴ did for three types of data: simple* (S), with linear trend (LT), and with both linear trend and multiplicative seasonal effects (LSM). Common to all the configurations is

*Simple data are of the form $a + n(t)$, where a is a fixed value and $n(t)$ is noise with zero mean.

the following: a time series $\{x(t)\}$ is measured every time interval T (e.g., hour, day, or week), and t is an integer representing the time tT . Then, one is interested in forecasting the value $x(t + 1)^*$ based on the data available up to and including t , namely $x(0), x(1), \dots, x(t)$.

If $\hat{x}(t + 1)$ denotes the forecast, carried out at time t for $x(t + 1)$, from Ref. 4 we have (using our own notation for consistency with the discussions in the sequel), for S data:

$$\hat{x}(t + 1) = \alpha x(t) + (1 - \alpha)\hat{x}(t) \quad (1a)$$

$$0 \leq \alpha \leq 1; \quad (1b)$$

for LT data:

$$\hat{x}(t + 1) = \hat{a}(t) + \hat{b}(t) \quad (2a)$$

$$\hat{a}(t) = \alpha x(t) + (1 - \alpha)[\hat{a}(t - 1) + \hat{b}(t - 1)] \quad (2b)$$

$$\hat{b}(t) = \beta[\hat{a}(t) - \hat{a}(t - 1)] + (1 - \beta)\hat{b}(t - 1) \quad (2c)$$

$$0 \leq \alpha, \beta \leq 1; \quad (2d)$$

and for LSM data:

$$\hat{x}(t + 1) = (\hat{a}(t) + \hat{b}(t))\hat{c}(t - L + 1) \quad (3a)$$

$$\hat{a}(t) = \alpha \frac{x(t)}{\hat{c}(t - L)} + (1 - \alpha)[\hat{a}(t - 1) + \hat{b}(t - 1)] \quad (3b)$$

$$\hat{b}(t) = \beta[\hat{a}(t) - \hat{a}(t - 1)] + (1 - \beta)\hat{b}(t - 1) \quad (3c)$$

$$\hat{c}(t) = \gamma \frac{x(t)}{\hat{a}(t)} + (1 - \gamma)\hat{c}(t - L) \quad (3d)$$

$$0 \leq \alpha, \beta, \gamma \leq 1, \quad (3e)$$

where L is the known periodicity of the season.

In all the equations above, the parameters α , β , and γ are called the "smoothing coefficients".

Our first step is to rewrite eq. (1) and, more importantly, eq. (2). This provides the basis for a new form of ES for LSM data, more general than (3). The new form, which is a natural extension of (1) and (2), suggests types of data for which the ES algorithm can result in optimal (in the MSE sense) performance.

Equation (1) can be readily rewritten as

$$\hat{x}(t + 1) = \hat{\theta}_1 \hat{x}(t) + (1 - \hat{\theta}_1)x(t), \quad (4a)$$

*Note that we restrict our discussions to one-interval-ahead forecasting with the understanding that it can be generalized to more time intervals ahead.

where clearly

$$\hat{\theta}_1 = 1 - \alpha. \quad (4b)$$

With some algebra one can show that eq. (2) is equivalent to

$$\begin{aligned} \hat{x}(t + 1) &= \hat{\theta}_1 \hat{x}(t) + \hat{\theta}_2 \hat{x}(t - 1) \\ &+ (2 - \hat{\theta}_1)x(t) - (1 + \hat{\theta}_2)x(t - 1), \end{aligned} \quad (5a)$$

where

$$\hat{\theta}_1 = 2 - \alpha(1 + \beta) \quad (5b)$$

$$\hat{\theta}_2 = \alpha - 1. \quad (5c)$$

The basic difference between (2) and (5) is that (5) reflects the assumption that the noise-free part of the data $x(t)$ is generated by the difference equation

$$y(t) - 2y(t - 1) + y(t - 2) = 0, \quad (6)$$

while (2) reflects the assumption that the solution of (6) is

$$y(t) = a + bt. \quad (7)$$

[Note that in (2) $\hat{a}(t)$ is the current estimate of 'a + bt' and $\hat{b}(t)$ is the current estimate of 'b.'

The ES as given in (3) for LSM data is clearly based on the assumption that the noise-free part of the data has the form

$$y(t) = (a + bt)c(t), \quad (8a)$$

where

$$c(t + L) = c(t). \quad (8b)$$

The difference equation satisfied by (8) is

$$y(t) - 2y(t - L) + y(t - 2L) = 0, \quad (9)$$

and the corresponding ES

$$\begin{aligned} \hat{x}(t + 1) &= \sum_{j=1}^M \hat{\theta}_j \hat{x}(t - j + 1) - \sum_{j=1}^M \hat{\theta}_j x(t - j + 1) \\ &+ 2x(t - L + 1) - x(t - 2L + 1). \end{aligned} \quad (10)$$

The parameters $\hat{\theta}_j$, $j = 1, \dots, M$ and the constraints they have to satisfy are discussed later. Also, the claimed correspondence between (9) and (10) will become more apparent in later discussion.

At this point, however, we emphasize that while (7) is the general solution of (6), and thus (2) and (5) are equivalent, (8) is only one of

many possible solutions of (9). Hence (10) represents an ES form that is more general than (3).

Similarly, data with linear trend and additive seasonal effects* (LSA) have the underlying difference equation

$$y(t) - y(t - 1) - y(t - L) + y(t - L - 1) = 0 \quad (11)$$

and the corresponding ES is

$$\begin{aligned} \hat{x}(t + 1) = & \sum_{j=1}^M \hat{\theta}_j \hat{x}(t - j + 1) - \sum_{j=1}^M \hat{\theta}_j x(t - j + 1) \\ & + x(t) + x(t - L + 1) - x(t - L). \end{aligned} \quad (12)$$

To unify and simplify the discussions ahead we introduce the following notation. Let D be a unit delay operator, namely $Dx(t) = x(t - 1)$, and let $A(D)$ be a polynomial in D such that

$$A(D) = \begin{cases} 1 & \text{for S data} \\ 2 - D & \text{for LT data} \\ 2D^{L-1} - D^{2L-1} & \text{for LSM data} \\ 1 + D^{L-1} - D^L & \text{for LSA data.} \end{cases} \quad (13)$$

With these definitions (4), (5), (10), and (12) can be unified as

$$\hat{x}(t + 1) = \sum_{j=1}^M \hat{\theta}_j D^{j-1} (\hat{x}(t) - x(t)) + A(D)x(t), \quad (14)$$

where $M = 1$ will result in (4) and $M = 2$ in (5).

It should also be pointed out that the ES as given by eq(s). (1) [(2) or (3)] has an implicit assumption in it. The assumption is that one (two or three) coefficient(s) can, in fact, smoothen the data. In other words, M in (14) is equal to one (two or three). However, its general form, (14), allows for a larger number of coefficients to get better approximations.

To observe the optimal properties of the ES forecasts we define the forecast error as

$$e(t) = x(t) - \hat{x}(t) \quad (15)$$

and use as our criteria for the forecast quality the mean square error (MSE), i.e., $E\{e^2(t)\}$. With this in mind, it is clear that optimal performance is achieved if the $e(t)$ becomes a white noise sequence (i.e., independent and identically distributed with zero mean). Namely, the ES technique, while assuming knowledge of the generating process for the noise-free component of the data, attempts to "whiten" the

*This type of data was not addressed in Ref. 4 and, as far as we know, no form of ES applicable to it was proposed before the one here.

noise component. This attempt implies an underlying assumption that the data are generated through, or at least approximated by, the process

$$[1 - DA(D)]x(t) = \left[1 - \sum_{j=1}^M \theta_j D^j\right] \epsilon(t), \quad (16)$$

where $\epsilon(t)$ is a white noise with variance σ^2 .

Substituting (14) and (16) into (15) results in

$$\left[1 - \sum_{j=1}^M \hat{\theta}_j D^j\right] e(t) = \left[1 - \sum_{j=1}^M \theta_j D^j\right] \epsilon(t). \quad (17)$$

This equation satisfied by $e(t)$ is the basis of our claims for correspondence between eqs. (9) and (10), and (11) and (12). Equation (17) immediately suggests the conditions for optimal forecasting. First, to get bounded MSE one must require:

Condition 1: All zeros of the polynomial $[1 - \sum_{j=1}^M \hat{\theta}_j \lambda^j]$ are outside the unit circle.

If, in addition, we also require:

Condition 2: $\hat{\theta}_j = \theta_j, j = 1, 2, \dots, M,$

then, clearly, from eq. (17), $e(t)$ will converge to $\epsilon(t)$ and optimal forecasting (in the MSE sense) is achieved.

Remark 1: As we discussed here, the sufficiency of Conditions 1 and 2 is quite obvious; however, they are also necessary. This is argued in Appendix A.

Remark 2: In Ref. 4 α and β for LT data are restricted to interval $[0, 1]$, which corresponds to the set S_2 in Fig. 1. The actual constraints follow from applying Condition 1 to the $M = 2$ case. This results in the set S_1 in Fig. 1, which clearly contains S_2 and is considerably larger. Allowing for a larger constraint set for $\hat{\theta}_1$ and $\hat{\theta}_2$ (or, correspondingly, α, β) will result in more cases for which ES could result in optimal performance.

III. ADAPTIVE GRADIENT EXPONENTIAL SMOOTHING

In the previous section we argued that for data that can be approximated by (16), forecasting with ES of the form (14) can result in optimal performance in the MSE sense. To achieve this, Conditions 1 and 2 must be satisfied. However, while Condition 1 can be satisfied by proper choice of $\hat{\theta}_j$, Condition 2 is, in general, hard to satisfy since the values of θ_j in eq. (16) are not known. Basically, the ARIMA

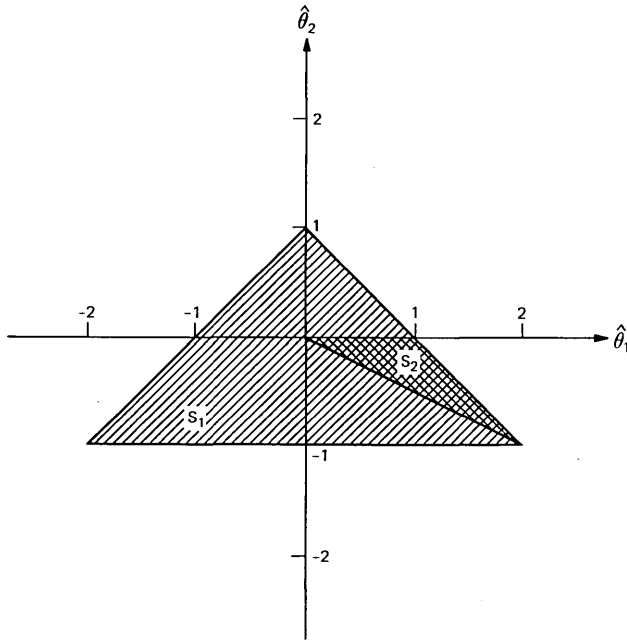


Fig. 1—The constraint sets:

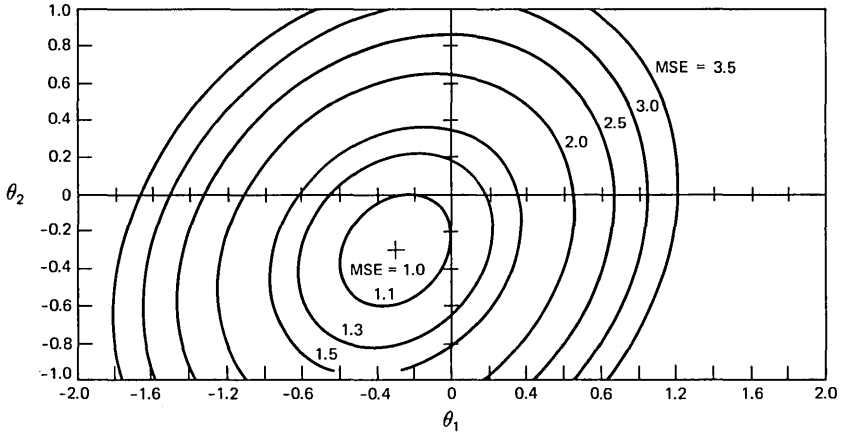
$$S_1 = \{(\hat{\theta}_1, \hat{\theta}_2): |\hat{\theta}_2| < 1, \hat{\theta}_2 + \hat{\theta}_1 < 1, \hat{\theta}_2 - \hat{\theta}_1 < 1\}$$

$$S_2 = \{(\hat{\theta}_1, \hat{\theta}_2): \hat{\theta}_1 = 2 - \alpha(1 + \beta), \hat{\theta}_2 = \alpha - 1, 0 < \alpha, \beta < 1\}.$$

model-fitting-based forecasting⁷ deals with exactly this type of problem. The θ_j 's of eq. (16) are estimated and these estimates are then used as the $\hat{\theta}_j$'s in eq. (14) in an attempt to satisfy Condition 2. In the ES algorithm no such attempt is made. In practice, the forecasters using ES choose some fixed values for the θ_j , which satisfy Condition 1 [or even more restrictively, e.g., eq. (2d)]. These values are based on intuition, experience, and familiarity with the data they forecast.

However, considerable differences between the underlying θ_j 's and the chosen $\hat{\theta}_j$'s can result in significant performance degradation. This is demonstrated in Fig. 2 for the case $M = 2$. The MSE for this case was computed in a closed form as a function of θ_1 and θ_2 for some fixed $\hat{\theta}_1$ and $\hat{\theta}_2$ and graphed in the figure. Together with phenomena like nonstationary discontinuity* and changes in the data-generating process (i.e., the θ_j change values), this resulted in unsatisfactory performance of the ES. The realization of what may cause this poor performance brought about the idea of using adaptive schemes where

*Step-like changes in the data.



MSE — MEAN SQUARED ERROR

Fig. 2—The mean squared error as a function of the data-generating parameters for $M = 2$. (The smoothing coefficients are fixed at $\theta_1 = -0.3$, $\theta_2 = -0.3$.)

the $\hat{\theta}_j$ are not fixed but are adjusted in an attempt to improve performance.

Compared to the existing Adaptive Exponential Smoothing (AES) techniques (see, e.g., Refs. 8 through 11), the new technique we introduce here is analytically more sound and there are strong indications that it converges to optimal performance in the MSE sense for the data approximated by (16).

This new technique is based on the gradient search for the minimum of the MSE. If the MSE would have been available as a function of the θ_j , then one could compute the gradient

$$\nabla = \frac{\partial E\{e^2(t)\}}{\partial \hat{\theta}}, \quad (18)$$

where $\hat{\theta} = [\hat{\theta}_1, \hat{\theta}_2, \dots, \hat{\theta}_M]^T$, and recursively update the $\hat{\theta}_j$ through

$$\hat{\theta}(t+1) = \hat{\theta}(t) - \mu \nabla, \quad (19)$$

where $\mu > 0$ is the adaptation constant. This is the gradient search technique, sometimes referred to as the steepest descent technique. In general, however, the MSE is not available as a function of the $\hat{\theta}_j$; hence, neither is the gradient. Instead, we use an instantaneous estimate of this gradient. To get this estimate we replace $E\{e^2(t)\}$ by $e^2(t)$ and the gradient by

$$\hat{\nabla} = \frac{\partial e^2(t)}{\partial \hat{\theta}} = 2e(t) \frac{\partial e(t)}{\partial \hat{\theta}}. \quad (20)$$

Let us denote

$$s(t) = \frac{\partial e(t)}{\partial \hat{\theta}}$$

as the “sensitivity vector,” since it gives an indication of how sensitive the error $e(t)$ is to the values of $\hat{\theta}_j$.

While $s(t)$ is not available we can use eq. (17) to develop a means for generating it. Let us take partial derivatives of both sides of this equation with respect to $\hat{\theta}$. Since the right-hand side does not depend explicitly on $\hat{\theta}$ we get:

$$\left(1 - \sum_{i=1}^M \hat{\theta}_i D^{i-1}\right) s_j(t) = D^{j-1} e(t) \quad j = 1, 2, \dots, M. \quad (21)$$

At this point we are ready to introduce the Adaptive Gradient Exponential Smoothing (AGES) technique. Combining eqs. (14), (19), (20), and (21) we get:

the *forecast*:

$$\hat{x}(t+1) = A(D)x(t) - \sum_{i=1}^M \hat{\theta}_i(t)e(t-i+1) \quad (22)$$

[see definition of $A(D)$ in eq. (13)],

the *sensitivity functions*:

$$s_j(t+1) = \sum_{i=1}^M \hat{\theta}_i(t)s_j(t-i+1) + e(t-j+1) \quad j = 1, 2, \dots, M, \quad (23)$$

and the *coefficient adjustments*:

$$\hat{\theta}_j(t+1) = \hat{\theta}_j(t) - 2\mu e(t)s_j(t) \quad j = 1, 2, \dots, M. \quad (24)$$

Recall that the error $e(t) = x(t) - \hat{x}(t)$.

Both our simulations and our experiments (as described in the next section) strongly indicate that AGES converges to optimal performance through convergence of $\hat{\theta}_j(t)$ to θ_j . Namely, the error $e(t)$ is adaptively whitened. Despite these indications, since the resulting equations are quite complex, a global proof of convergence of the AGES technique is beyond the scope of this paper. However, we conclude this section by treating the special case $M = 1$ and show local convergence properties for it.

Let $M = 1$; then eqs. (17), (23), and (24) become

$$e(t+1) = \hat{\theta}_1(t)e(t) + \epsilon(t+1) - \theta_1\epsilon(t)$$

$$s_1(t+1) = \hat{\theta}_1(t)s_1(t) + e(t),$$

and

$$\hat{\theta}(t+1) = \hat{\theta}_1(t) - 2\mu e(t)s_1(t).$$

Assuming $\hat{\theta}_j(t)$ is independent of $e(t)$ and $s_1(t)$ (similar assumptions are common in convergence proofs of adaptive filters) and observing that $E\{\epsilon(t) \cdot e(t)\} = \sigma^2$, $E\{\epsilon(t) \cdot \epsilon(t+1)\} = 0$, $E\{s(t) \cdot \epsilon(t)\} = 0$ we get

$$\begin{aligned} E\{e^2(t+1)\} &= E\{\hat{\theta}_1^2(t)\} \cdot E\{e^2(t)\} \\ &\quad + \sigma^2[1 + \theta_1^2 - 2\theta_1 E\{\hat{\theta}_1(t)\}] \\ E\{s_1(t+1) \cdot e(t+1)\} &= E\{\hat{\theta}_1^2(t)\} \cdot E\{s_1(t) \cdot e(t)\} \\ &\quad + E\{\hat{\theta}_1(t)\} \cdot E\{e^2(t)\} - \theta_1 \sigma^2 \\ E\{\hat{\theta}_1(t+1)\} &= E\{\hat{\theta}_1(t)\} - 2\mu E\{s_1(t)e(t)\}. \end{aligned} \quad (25)$$

If we assume in addition that $\hat{\theta}_1(t)$ has a small variance, namely $E\{\hat{\theta}_1^2(t)\} \approx [E\{\hat{\theta}_1(t)\}]^2$ (the simulation results tend to support this assumption), defining

$$\begin{aligned} \gamma_1(t) &= E\{e^2(t)\} - \sigma^2 \\ \gamma_2(t) &= E\{s_1(t) \cdot e(t)\} \\ \gamma_3(t) &= E\{\hat{\theta}_1(t)\} - \theta_1 \end{aligned} \quad (26)$$

and substituting in (25) results in

$$\begin{aligned} \gamma_1(t+1) &= [\gamma_3(t) + \theta_1]^2 \gamma_1(t) + \sigma^2 [\gamma_3(t)]^2 \\ \gamma_2(t+1) &= [\gamma_3(t) + \theta_1]^2 \gamma_2(t) + [\gamma_3(t) + \theta_1] \gamma_1(t) + \sigma^2 \gamma_3(t) \\ \gamma_3(t+1) &= \gamma_3(t) - 2\mu \gamma_2(t). \end{aligned} \quad (27)$$

Clearly, if we could prove that $\gamma_1(t)$, $\gamma_2(t)$, and $\gamma_3(t)$ converge to the origin globally (i.e., independent of the initial values), it would mean that [see eq. (26)] the MSE converges to the minimum σ^2 and $E\{\theta_1(t)\}$ converges to θ_1 . However, despite strong indications from our simulations that these variables do converge globally, we can prove only local convergence. In addition, the proof provides an indication as to how to choose the parameter μ .

Let us linearize eq. (27) around the origin to get

$$\begin{aligned} \gamma_1(t+1) &= \theta_1^2 \gamma_1(t) \\ \gamma_2(t+1) &= \theta_1^2 \gamma_2(t) + \theta_1 \gamma_1(t) + \sigma^2 \gamma_3(t) \\ \gamma_3(t+1) &= \gamma_3(t) - 2\mu \gamma_2(t). \end{aligned} \quad (28)$$

The coefficients matrix is

$$A = \begin{bmatrix} \theta_1^2 & 0 & 0 \\ \theta_1 & \theta_1^2 & \sigma^2 \\ 0 & -2\mu & 1 \end{bmatrix}$$

and to ensure convergence all eigenvalues of A must be within the unit circle. The eigenvalues of A are

$$\lambda_1 = \theta_1^2$$

$$\lambda_{2,3} = 1/2\{1 + \theta_1^2 \pm [(1 - \theta_1^2)^2 - 8\mu\sigma^2]^{1/2}\},$$

and it can be verified that choosing

$$\mu < \frac{1 - \theta_1^2}{2\sigma^2} \quad (29)$$

will guarantee the convergence of eq. (28).

Condition (29) implies that if $|\theta_1|$ is close to one, μ must be chosen very small and the convergence will be slow. Again, our simulation experiments verified this observation.

IV. SIMULATION RESULTS

We divide our experiments with AGES into two parts. In the first part we applied both ES and AGES on data generated by the computer

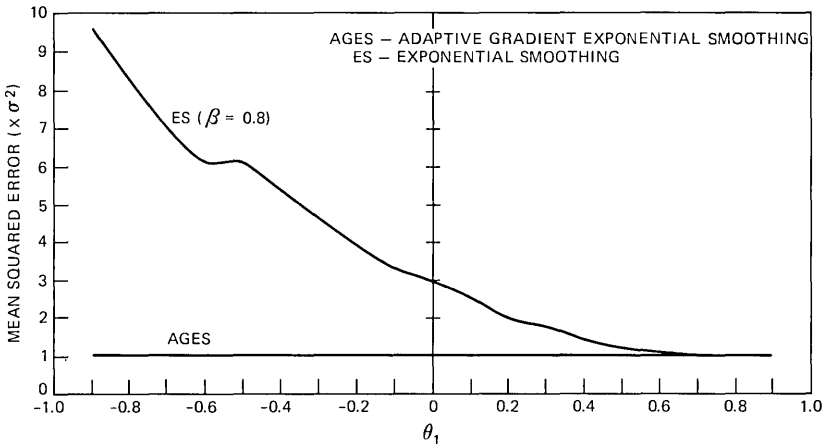


Fig. 3—Comparison of forecasting performance between Fig. ES ($\beta = 0.8$) and AGES.

and compared the results. In the second part we applied the AGES to real data that we took from Ref. 7.

Equation (16) was used to generate data of type S, LT, and LSM by the computer. The results of applying both ES and AGES on these data are presented in Figs. 3, 4, and 5 and in Table I. Each point on the curves of Fig. 3 corresponds to a complete run on a sequence of data generated with the particular choice of the θ_i . The resulting MSE for the ES and the AGES forecasts are presented and the comparison clearly indicates the superiority of the AGES algorithm. In addition, we observe that the AGES results, in almost all the runs, in a MSE very close to the minimum, σ^2 .

In Fig. 5, we followed the variation of the $\theta_i(t)$ with time in a number of runs. The results clearly show that the $\hat{\theta}_i(t)$ converge to the θ_i from a variety of initial values; this indicates global convergence properties. Similar results are observed in Table I for data with seasonal multiplicative effects and linear trend. The $\hat{\theta}_i(t)$ clearly converge to the θ_i 's, and the MSE, when AGES is applied, is again very close to the optimal

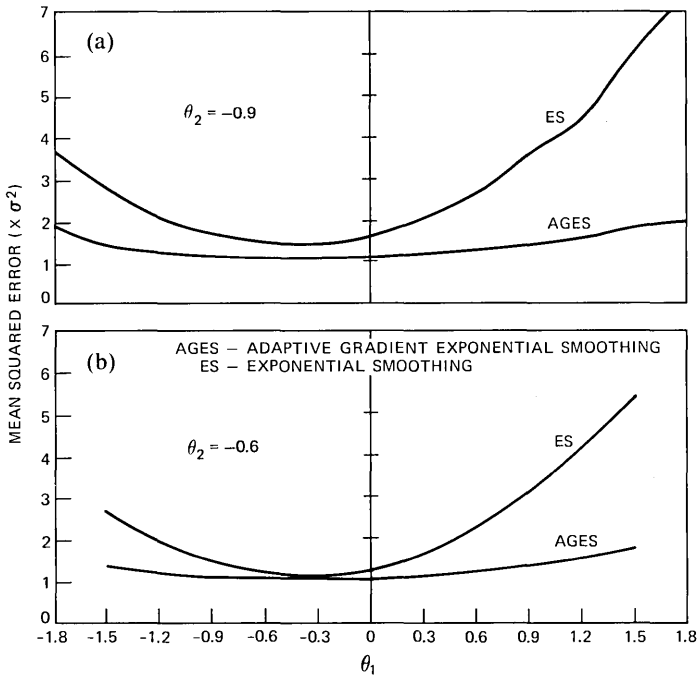


Fig. 4—Comparison of mean squared error in forecasting with ES ($\hat{\theta}_1 = \hat{\theta}_2 = -0.3$) and AGES as a function of the data-generating parameters θ_1 and θ_2 . (a) $\theta_2 = -0.9$. (b) $\theta_2 = -0.6$.

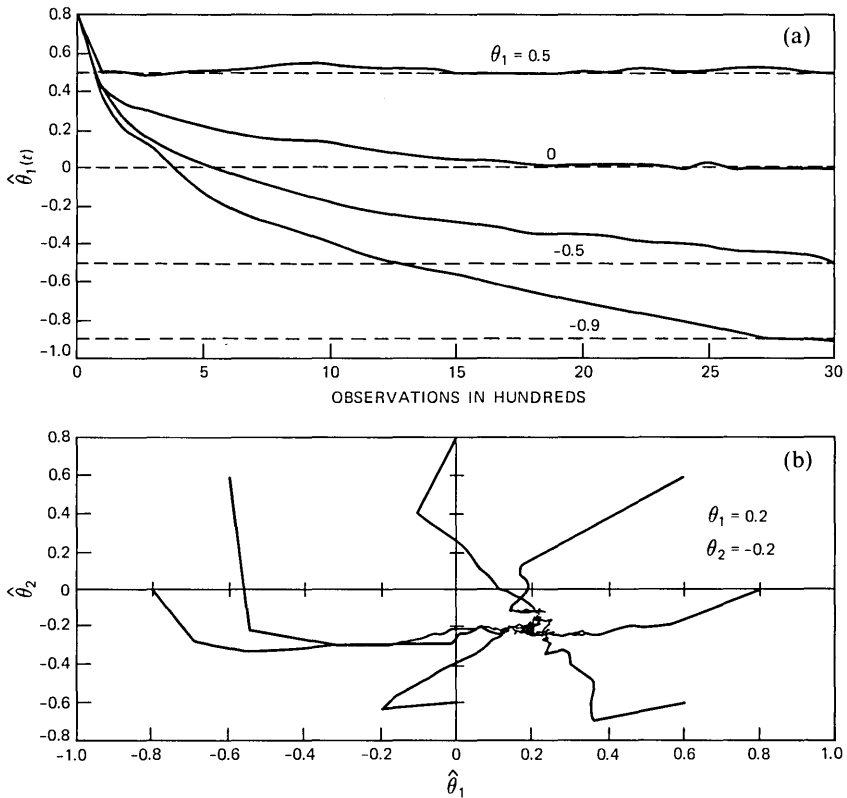


Fig. 5—Convergence of: (a) $\hat{\theta}_1(t)$ to the optimal value θ_1 in the AGES method. (b) $\hat{\theta}_1(t)$ and $\hat{\theta}_2(t)$ from various initial conditions to θ_1 and θ_2 , using AGES on data with linear trend.

value, σ^2 . From Ref. 7 we took data of the simple kind (no linear trend or seasonal effects): The IBM common stock closing prices, daily, from May 17, 1961 through November 2, 1962. On the data we applied both ES and AGES and the results are presented in Fig. 6. Each point on the curves corresponds to a run on the same data, each time with a different coefficient (for the ES) and different initial condition (for the AGES). The further the coefficient used in the ES is from θ_1 (which in this case is equal to -0.1 , as indicated in Ref. 7), the better the performance is for AGES.

Further experiments were conducted on monthly international airline passengers data.⁷ These data, as Fig. 7 indicates, are with linear trend and multiplicative seasonal effects. We applied the AGES algorithm (with $M = 3$) and the results are presented in Fig. 8. In Ref. 7 it is claimed that sometimes rather than work with the actual data it

Table I—Comparison of MSE in forecasting with ES ($\hat{\theta}_1 = -0.2$, $\hat{\theta}_2 = 0.5$, $\hat{\theta}_3 = 0.4$) and AGES

Data-Generating Coefficients (and Adaptive Coefficients)			MSE ($\times \sigma^2$)	
θ_1 ($\hat{\theta}_1$)*	θ_2 ($\hat{\theta}_2$)	θ_3 ($\hat{\theta}_3$)	AGES	ES
1.4 (1.39)	-1.3 (-1.29)	0.8 (0.75)	1.1972	11.7155
2.1 (1.97)	-1.95 (-1.79)	0.8 (0.68)	1.3831	20.5821
0.75 (0.69)	-0.6 (-0.56)	0.8 (0.78)	1.0749	5.1431
0.6 (0.6)	-0.75 (-0.76)	0.8 (0.77)	1.0600	5.0256
-0.75 (-0.73)	0.6 (0.6)	0.8 (0.79)	1.0663	1.3577
0.0 (-0.04)	0.0 (0.01)	0.0 (0.03)	1.0040	1.5737
1.0 (0.98)	-1.0 (-0.99)	1.0 (0.94)	1.2001	8.6414
-0.2 (-0.16)	0.5 (0.49)	0.4 (0.4)	1.0397	1.0137
-0.1 (-0.09)	0.25 (0.26)	0.4 (0.41)	0.9973	1.0839
1.2 (1.19)	-0.9 (-0.81)	0.4 (0.36)	1.1044	7.1069
1.8 (1.74)	-1.35 (-1.24)	0.4 (0.34)	1.2192	13.0215
0.3 (0.31)	-0.75 (-0.75)	0.4 (0.38)	1.0574	3.8630
1.0 (0.96)	-0.5 (-0.48)	0.0 (-0.04)	1.0605	4.2218
1.5 (1.42)	-0.75 (-0.66)	0.0 (-0.05)	1.1165	6.9455
0.75 (0.77)	0.0 (0.03)	0.0 (0.03)	1.0212	2.4687
0.0 (-0.03)	-0.75 (-0.74)	0.0 (0.02)	1.0314	3.5907
0.2 (0.19)	0.5 (0.53)	-0.4 (-0.43)	1.0186	1.7692
1.2 (1.19)	-0.15 (-0.14)	-0.4 (-0.39)	1.1115	4.0338
-1.8 (-1.7)	-1.35 (-1.22)	-0.4 (-0.36)	1.2077	13.8494
-0.3 (-0.3)	-0.75 (-0.76)	-0.4 (-0.39)	1.0438	4.6957
-0.75 (-0.79)	-0.3 (-0.28)	-0.4 (-0.38)	1.0062	3.9623
0.4 (0.43)	0.5 (0.49)	-0.8 (-0.78)	1.0461	2.6126
-0.7 (-0.73)	-0.65 (-0.62)	-0.8 (-0.8)	1.0670	6.1628
-0.6 (-0.61)	-0.75 (-0.75)	-0.8 (-0.79)	1.0815	6.8677
-0.75 (-0.74)	-0.6 (-0.56)	-0.8 (-0.74)	1.1065	7.0182
-0.5 (-0.52)	-0.4 (-0.38)	-0.8 (-0.81)	1.0759	5.1676

* The values to which $\hat{\theta}_i(t)$ converge are given in parentheses.

is more convenient to work with the logarithm of the data. As we argue in Appendix B, these logarithms, as data, have linear trend and additive seasonal effects (see Fig. 8). Hence, on the logarithms we applied AGES for linear trend and additive seasonal effects and the results are presented in Fig. 8a ($M = 3$). We used the same data (the logarithms) to see whether the performance improves with larger M . AGES was applied with $M = 13$ and the results, as presented in Fig. 8b, clearly indicate that for this data $M = 3$ was sufficient.

V. CONCLUSIONS

In this paper we have introduced a new forecasting technique, Adaptive Gradient Exponential Smoothing (AGES), which is based on Exponential Smoothing (ES). We have elaborated on the optimality properties in the MSE sense of the ES. For certain types of data, the ES can result in optimal performance provided some coefficients are known. In general, these coefficients are unavailable, and the AGES shows strong indications of converging to these unknown coefficients and providing optimal performance.

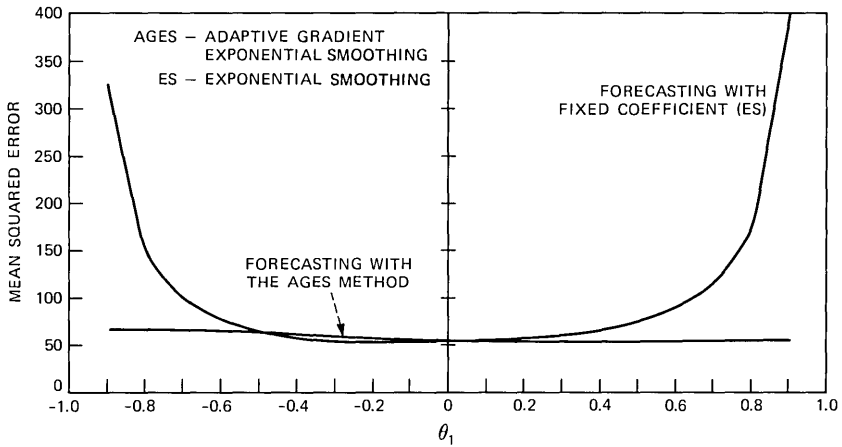


Fig. 6—Comparison of performance of forecasting with the ES (varying the coefficient in each run) and the AGES methods.

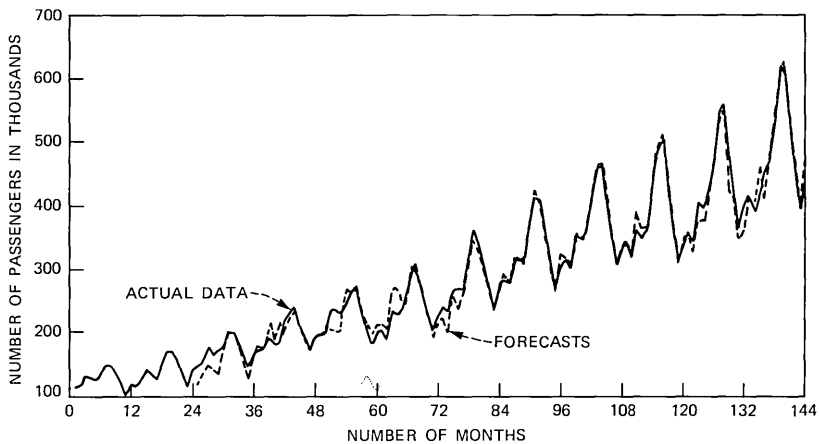


Fig. 7—Forecasting with AGES international airline passengers ($M = 3$). (Note that these data have linear trend and multiplicative seasonal effects.)

Clearly, more extensive experiments and practical use of the proposed forecasting technique, the AGES, are required. A user-friendly software package can be developed for implementation of this technique if sufficient interest is generated.

VI. ACKNOWLEDGMENT

The author wishes to thank the reviewers for their thoroughness. Their comments were very helpful in the revision of this paper.

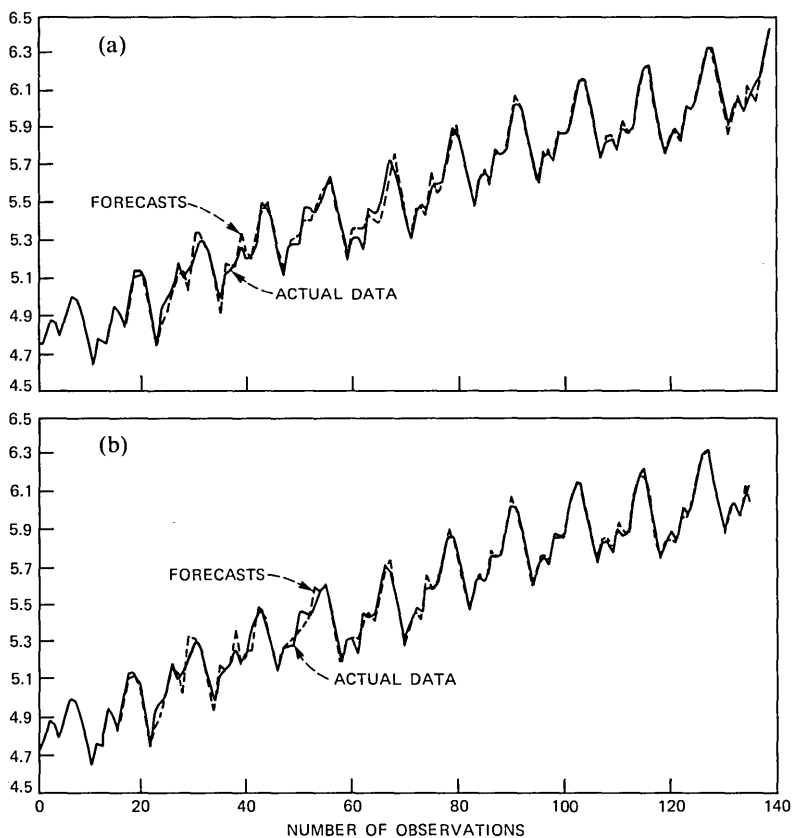


Fig. 8—Forecasting with AGES the logarithm of the data in Fig. 7 for: (a) $M = 3$. (b) $M = 13$. (Note that the logarithm of the data in Fig. 7 has the form of data with additive seasonal effects and linear trend.)

REFERENCES

1. C. D. Pack and B. A. Whitaker, "Kalman Filter Models for Network Forecasting," *B.S.T.J.*, 61, No. 1 (January 1982), pp. 1-14.
2. J. P. Moreland, "A Robust Sequential Projection for Traffic Load Forecasting," *B.S.T.J.*, 61, No. 1 (January 1982), pp. 15-38.
3. C. R. Szelag, "A Short-Term Forecasting Algorithm for Trunk Demand Servicing," *B.S.T.J.*, 61, No. 1 (January 1982), pp. 67-96.
4. P. R. Winters, "Forecasting Sales, by Exponentially Weighted Moving Averages," *Management Sciences*, 6, No. 3 (April 1960), pp. 324-42.
5. R. G. Brown, "Smoothing, Forecasting and Prediction of Discrete Time Series," Englewood Cliffs, NJ: Prentice-Hall, 1962.
6. J. F. Muth, "Optimal Properties of Exponentially Weighted Forecasts of Time Series With Permanent and Transitory Components," *J. Am. Statist. Assn.*, 55 (June 1960), pp. 299-306.
7. G. P. Box and G. M. Jenkins, "Time Series Analysis, Forecasting and Control," San Francisco, CA: Holden-Day, 1970.
8. W. M. Chow, "Adaptive Control of the Exponential Smoothing Constant," *J. Indust. Eng.*, 16, No. 5 (October 1965), pp. 314-7.

9. D. W. Trigg and A. G. Leach, "Exponential Smoothing With an Adaptive Response Rate," *Oper. Res. Quart.*, 18, No. 1 (March 1967), pp. 53-60.
10. D. C. Whybark, "A Comparison of Adaptive Forecasting Techniques," *Logist. Transport. Rev.*, 8 (1973), pp. 13-26.
11. S. D. Roberts and R. Reed, "The Development of a Self-Adaptive Forecasting Technique," *AIIE Trans.*, 1 (December 1969), pp. 314-22.
12. S. Ekern, "Adaptive Exponential Smoothing Revisited," *J. Oper. Res. Soc.*, 32, No. 9 (September 1981), pp. 775-82.

APPENDIX A

Necessity of Conditions 1 and 2 for the Convergence of $e(t)$ to $\epsilon(t)$ in Equation (17)

Condition 1 is clearly necessary (as well as sufficient) for the convergence of $E\{e^2(t)\}$ to a finite value. We want to show that Condition 2 is necessary for $E\{e^2(t)\}$ to converge to σ^2 .

Let

$$\gamma_{ee}(\tau) = E\{e(t) \cdot e(t - \tau)\} \quad (30)$$

and

$$\gamma_{ee}(\tau) = E\{e(t)\epsilon(t - \tau)\}. \quad (31)$$

Clearly,

$$\gamma_{ee}(\tau) = \gamma_{ee}(-\tau) \quad (32)$$

and, from eq. (17) and the definition of $\epsilon(t)$

$$\gamma_{e\epsilon}(-\tau) = 0. \quad (33)$$

With these definitions it follows from eq. (17), after transients die, that

$$\begin{aligned} \gamma_{ee}(0) &= \sigma^2 \\ \gamma_{ee}(1) - \hat{\theta}_1 \gamma_{ee}(0) &= -\theta_1 \sigma^2 \\ \gamma_{ee}(2) - \hat{\theta}_1 \gamma_{ee}(1) - \hat{\theta}_2 \gamma_{ee}(0) &= -\theta_2 \sigma^2 \\ &\vdots \\ \gamma_{ee}(M) - \hat{\theta}_1 \gamma_{ee}(M-1) - \dots - \hat{\theta}_M \gamma_{ee}(0) &= -\theta_M \sigma^2, \end{aligned}$$

or in matrix form

$$\begin{bmatrix} 1 & 0 & 0 & \dots & 0 \\ -\theta_1 & 1 & 0 & \dots & 0 \\ -\theta_2 & -\theta_1 & 1 & \dots & 0 \\ \cdot & \cdot & \cdot & \dots & \cdot \\ \cdot & \cdot & \cdot & \dots & \cdot \\ \cdot & \cdot & \cdot & \dots & \cdot \\ -\theta_M & -\theta_{M-1} & \cdot & \dots & 1 \end{bmatrix} \begin{bmatrix} \gamma_{ee}(0) \\ \gamma_{ee}(1) \\ \cdot \\ \cdot \\ \gamma_{ee}(M) \end{bmatrix} = -\sigma^2 \begin{bmatrix} -1 \\ \theta_1 \\ \theta_2 \\ \cdot \\ \cdot \\ \theta_M \end{bmatrix}. \quad (34)$$

Also,

$$\begin{aligned}
 & \gamma_{ee}(0) - \hat{\theta}_1 \gamma_{ee}(1) - \hat{\theta}_2 \gamma_{ee}(2) - \dots - \hat{\theta}_M \gamma_{ee}(M) \\
 & \quad = \gamma_{ee}(0) - \theta_1 \gamma_{ee}(1) - \dots - \theta_M \gamma_{ee}(M) \\
 & \gamma_{ee}(1) - \hat{\theta}_1 \gamma_{ee}(0) - \hat{\theta}_2 \gamma_{ee}(1) - \dots - \hat{\theta}_M \gamma_{ee}(M-1) \\
 & \quad = -\theta_1 \gamma_{ee}(0) - \dots - \theta_M \gamma_{ee}(M-1) \\
 & \gamma_{ee}(2) - \hat{\theta}_1 \gamma_{ee}(1) - \hat{\theta}_2 \gamma_{ee}(0) - \dots - \hat{\theta}_M \gamma_{ee}(M-2) \\
 & \quad = -\theta_2 \gamma_{ee}(0) - \dots - \theta_M \gamma_{ee}(M-2) \\
 & \quad \vdots \\
 & \gamma_{ee}(M) - \hat{\theta}_1 \gamma_{ee}(M-1) - \hat{\theta}_2 \gamma_{ee}(M-2) - \dots - \hat{\theta}_M \gamma_{ee}(0) \\
 & \quad = -\theta_M \gamma_{ee}(0)
 \end{aligned}$$

or again in a matrix form

$$\left\{ \begin{bmatrix} 1 & 0 & 0 & \dots & 0 \\ -\hat{\theta}_1 & 1 & 0 & & 0 \\ -\hat{\theta}_2 & -\hat{\theta}_1 & 1 & & 0 \\ \vdots & \vdots & & & \vdots \\ \vdots & \vdots & & & \vdots \\ -\hat{\theta}_M & -\hat{\theta}_{M-1} & \dots & & 1 \end{bmatrix} \right. - \left. \begin{bmatrix} 0 & \hat{\theta}_1 & \hat{\theta}_2 & \dots & \hat{\theta}_{M-2} & \hat{\theta}_{M-1} & \hat{\theta}_M \\ 0 & \hat{\theta}_2 & \hat{\theta}_3 & \dots & \hat{\theta}_{M-1} & \hat{\theta}_M & 0 \\ 0 & \hat{\theta}_3 & \hat{\theta}_4 & \dots & \hat{\theta}_M & 0 & 0 \\ \vdots & \vdots & \vdots & & \vdots & \vdots & \vdots \\ \vdots & \vdots & \vdots & & \vdots & \vdots & \vdots \\ 0 & \hat{\theta}_M & 0 & \dots & 0 & 0 & 0 \\ 0 & 0 & 0 & \dots & 0 & 0 & 0 \end{bmatrix} \right\} \begin{bmatrix} \gamma_{ee}(0) \\ \gamma_{ee}(1) \\ \gamma_{ee}(2) \\ \vdots \\ \vdots \\ \gamma_{ee}(M) \\ \gamma_{ee}(M) \end{bmatrix} \\
 = \begin{bmatrix} 1 & -\theta_1 & -\theta_2 & \dots & -\theta_M \\ -\theta_1 & -\theta_2 & -\theta_3 & & 0 \\ -\theta_2 & -\theta_3 & -\theta_4 & & 0 \\ \vdots & \vdots & \vdots & & \vdots \\ \vdots & \vdots & \vdots & & \vdots \\ \theta_M & 0 & 0 & & 0 \end{bmatrix} \begin{bmatrix} \gamma_{ee}(0) \\ \gamma_{ee}(1) \\ \gamma_{ee}(2) \\ \vdots \\ \vdots \\ \gamma_{ee}(3) \end{bmatrix} \quad (35)$$

Now, if we claim that $e(t)$ converges to $\epsilon(t)$, it means that

$$\gamma_{e\epsilon}(\tau) = \delta(\tau)\sigma^2 = \begin{cases} \sigma^2 & \text{for } \tau = 0 \\ 0 & \text{for } \tau \neq 0 \end{cases}$$

and

$$\gamma_{ee}(\tau) = \delta(\tau)\sigma^2.$$

Then, substituting this in (34) or (35) results in

$$\hat{\theta}_j = \theta_j \quad \text{for } j = 1, 2, \dots, M,$$

which is Condition 2. Hence this condition is necessary as claimed.

APPENDIX B

Possible Transformation of Multiplicative Seasonal Effects Into Additive Seasonal Effects

Suppose we are given data of the noise-free form

$$\left. \begin{aligned} y(t) &= (a + bt)c(t) \\ c(t + L) &= c(t) \end{aligned} \right\} \quad (36)$$

which is with linear trend and multiplicative seasonal effects.

Let

$$z(t) = \text{Log}[y(t)]. \quad (37)$$

Then substitution of (36) gives (if we assume $bt \ll a$, which is true in most real data):

$$\begin{aligned} z(t) &= \log a + \log \left(1 + \frac{b}{a} t \right) + \log c(t) \\ &\approx \log a + \frac{b}{a} t + \log c(t) \\ &\approx \tilde{a} + \tilde{b}t + \tilde{c}(t), \end{aligned} \quad (38)$$

where

$$\tilde{a} = \log a$$

$$\tilde{b} = \frac{b}{a}$$

$$\tilde{c}(t) = \log c(t).$$

Hence $z(t)$ clearly has the form of data with linear trend and *additive* seasonal effects.

AUTHOR

Arie Feuer, B.Sc. (Mechanical Engineering), 1967, M.Sc. (Mechanical Engineering), 1973, Technion, Israel; Ph.D. (Control Systems Engineering), 1978, Yale University; Bell Laboratories, 1978—. Since joining Bell Laboratories Mr. Feuer has been involved in telephone network measurement planning and implementations. He is actively involved in research in control system theory, signal processing, and adaptive systems, and currently looks into their possible applications for network measurements and operations.

Application of the Minimum-Weight Spanning- Tree Algorithm to Assignment of Communication Facilities

By N. A. STRAKHOV*

(Manuscript received March 2, 1982)

COSMOS—the Computer System for Main Frame Operations—is an operational support system that inventories and assigns central office facilities to serve customer circuits. As part of this assignment responsibility, COSMOS must provide the central office personnel who will physically connect the circuit not only with information about the facilities to be connected, but also the order in which they will be connected (i.e., connection sequence or “connectivity”). Also, COSMOS must determine the circuit connectivity to permit automatic assignment of tie pairs—inter- and intra-frame cables that permit the connection of facilities that are widely separated physically. A new algorithm has been added to COSMOS to permit the determination of connectivity. This algorithm is based on the algorithm that determines the minimum-weight spanning tree of a connected graph. However, the algorithm is specialized for COSMOS by taking into account such factors as minimizing the maximum number of connections at any node and restricting certain nodes to a maximum number of connections.

I. INTRODUCTION

When a mechanized system assigns facilities to provide a telephone circuit (to fulfill a request for service, say), it must accomplish three things. It must

1. Determine which facility types are required to provide the service

* Bell Laboratories.

©Copyright 1983, American Telephone & Telegraph Company. Photo reproduction for noncommercial use is permitted without payment of royalty provided that each reproduction is done without alteration and that the Journal reference and copyright notice are included on the first page. The title and abstract, but no other portions, of this paper may be copied or distributed royalty free by computer-based and other information-service systems without further permission. Permission to reproduce or republish any other portion of this paper must be obtained from the Editor.

2. Select a particular unit which is available for each such facility type

3. Determine the circuit topology of the assigned facilities.

Steps 1 and 2 can be reduced to an algorithm using straightforward procedures. Step 3, however, has proved to be difficult and has been left for manual determination in all but the simplest cases. In this paper an algorithm is reported that has been successful in determining the circuit topology for most of the circuits encountered in telephony.

II. A PARTICULAR APPLICATION—COSMOS

COSMOS is the name of a minicomputer system (DEC PDP 11/70 and PDP 11/45) designed for use by telephone operating companies to assign and administer central office equipment.¹ A major impetus for its development and continued deployment is to increase the efficiency of central office personnel who must physically connect, rearrange, and disconnect facilities to provide service to customers. Accordingly, an important feature of COSMOS is its ability to produce a report (called the Frame Output Report or "FOR") for the central office personnel that clearly specifies what should be connected to what. Most circuits for which COSMOS must create a FOR are simple, i.e., only two facilities must be interconnected on the frame. Some circuits, however, can be quite complicated in that some facilities in the circuit must be interconnected in series while others must be connected in parallel. An example of such a case would be a circuit with a main line and an off-premises extension where the bridge point is in the central office. This example becomes more complex if signal conditioning equipment must be placed in series with each line.

Such an example is illustrated in Fig. 1. This circuit includes a main line (cable pair 4-980) and three off-premises extensions (cable pairs 4-981, 4-982, and 4-983). Each cable pair must be connected to the line equipment through a bridge lifter (BL 49, 50, 51, and 52). Since the bridge lifters are located on a different frame from the line equipment and the cable pairs, tie pairs (TP 107, 304, 305, 306, and 307) must be used to interconnect all the components of this circuit.

Since the FOR must unambiguously state how the connections are to be made, either the person establishing the order for service in COSMOS must provide the connection sequence ("connectivity"), or COSMOS itself has to be capable of determining the connectivity. All initial versions of COSMOS had to be connected manually. Starting about 1977 logic was added so COSMOS could automatically determine connectivity in certain situations. The current generic of COSMOS (generic 9.0) is being developed to incorporate connectivity determination in all cases but still allow the user to manually override the automatic connectivity logic if necessary. This paper presents the

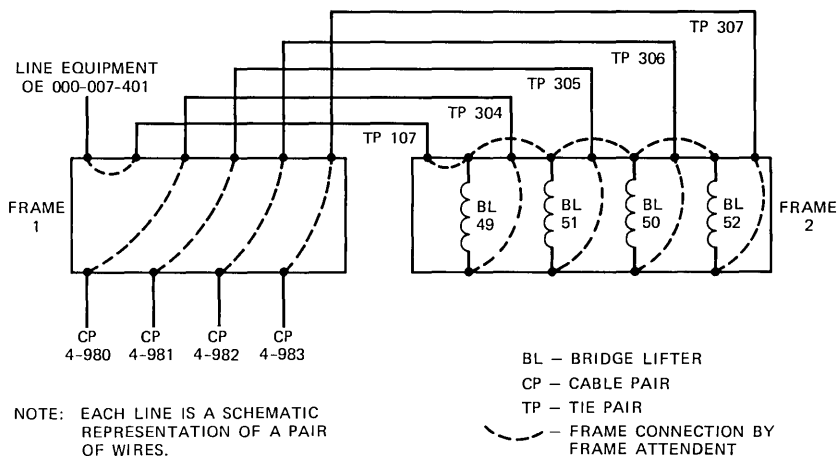


Fig. 1—Example of a main line with three off-premises extensions.

algorithm developed to achieve this capability and illustrates how it benefits the COSMOS user.

III. REVIEW OF COSMOS CAPABILITIES

As we already mentioned, COSMOS accepts a service order as input and creates the FOR as output. The service order is input to COSMOS by a clerk in the Loop Assignment Center (LAC). Certain information must be entered by the clerk so the order can be processed by COSMOS, while other information is optional, depending on the particular order. The required information is the order number and the order due date. If a switching equipment connection is to be assigned to the customer, then the switching equipment features and the customer class of service must be specified also. Specific facilities to be assigned to the customer can either be specified when entered or automatically assigned by COSMOS. Actually, the automatic assignment takes place in two levels, depending on the facilities: 1) COSMOS determines the need for the facility and then selects a particular facility for the circuit, or 2) the LAC clerk specifies the need for a facility on input and COSMOS selects a particular facility for the circuit. Table I lists the facilities administered by COSMOS and how they are selected for a particular circuit by COSMOS—i.e., manual specification of the particular facility, manual specification of the need for the facility, or complete automatic selection by COSMOS. Table I also specifies that some facilities are terminated on a Main Distributing Frame (MDF), while others are not. The facilities that are not terminated on an MDF either have no physical termination (for

Table 1—COSMOS administered facilities

Facility	MDF Frame Ter- mination	Manual	Assignment Mode	
			Need Specified	Full Auto
Telephone Number (TN)	No	Yes	Yes	No
Extra Number (XN)	No	Yes	No	No
Group (GP)	No	Yes	No	No
Terminal (TER)	No	Yes	No	No
Relay (RLY)	No	Yes	Yes	Yes
Message Register (MR)	No	Yes	Yes	Yes
Private Line Number (PL)	No	Yes	No	No
Special Equipment (SE)	No	Yes	No	No
Special Equipment (SE)	Yes	Yes	No	No
Cable Pair (CP)	Yes	Yes	No	No
Line Equipment (OE)	Yes	Yes	Yes	No
Concentrator (CON)	Yes	Yes	No	No
Tie Pair (TP)	Yes	Yes	Yes	Yes
Bridge Lifter (BL)	Yes	Yes	Yes	Yes
Trunk (TK)	Yes	Yes	No	No

example, telephone numbers, groups, and terminals on an electronic switching system are software variables) while others are terminated on an intermediate distributing frame [such as relays and message registers on a No. 5 crossbar switching system (5XB)].

Appendix A describes an overview of the input language for the Service Order Establishment (SOE) transaction. An appreciation of the language is helpful in understanding the example presented in Appendix B, which shows the effect of the connectivity algorithm on the user input. The example in this appendix shows the service order input, as well as excerpts from the FOR to connect the circuit shown in Fig. 1. The detailed functioning of the connectivity algorithm for a particular example is described in Appendix C.

So far, only orders resulting from customer requests for service have been described as input to COSMOS. Another major source of input to COSMOS are work orders; i.e., orders initiated by the telephone company personnel to change out defective equipment or to rearrange circuits to accommodate growth. These transactions also use the connectivity algorithm.

IV. THE CONNECTIVITY ALGORITHM

The connectivity algorithm, which was first proposed by H. L. York,² is based on the concept of a minimum-weight spanning tree of a connected graph. For each circuit whose connectivity is to be determined, a graph whose nodes correspond to each of the elements of the circuit is constructed. The edges of this graph are assigned weights such that the smaller the weight the more likely the two circuit elements (nodes) are to be connected directly to each other. The final connections between the circuit elements is determined by finding a

spanning tree whose edges have a total weight less than or equal to all other spanning trees for this graph. Well-known methods are available for finding the minimum-weight spanning tree of a connected graph. One very straightforward algorithm is given by E. Horowitz and S. Sahni³ (see especially Section 6.2). An apparently more efficient algorithm plus other extensions of the spanning-tree concept is given by R. C. Prim.⁴ As this paper describes later, none of these algorithms could be applied directly to the COSMOS problem because of additional side-constraints that had to be imposed on real circuits. These in turn led to a more efficient algorithm than can be obtained for the general case. The problem of determining circuit connectivity is now reduced to obtaining pair-wise connection weights for all facility combinations and to specifying the particular algorithm for calculating the minimum-weight spanning tree. These will each be discussed in turn.

4.1 Determination of connective weights

In Table I, two types of special equipment (SE) are noted: those with a frame location and those without. Even among SE terminated on the frame there are subgroupings that must be treated differently by the connectivity algorithm. These will now be described.

The SE file in COSMOS contains "miscellaneous" equipment that is not explicitly recorded in any of the other COSMOS equipment files. The name of the SE is created during the order input and a record for the SE is allocated at that time. When an order to disconnect the circuit is established and completed, the record allocated to this SE is released to a list of free records. During input of the name of the SE, the frame location (if one exists) is input also. The SE receives special treatment by the connectivity algorithm, depending on the SE name and the presence or absence of a frame location. The various subcategories of SE are shown in Table II.

With these subdivisions of the equipment that can be represented in the SE field, plus the other facilities that have frame terminations as listed in Table I, the user can construct a complete list of facility

Table II—Subcategories of special equipment

Input	Action
If no frame location is input	Ignore SE for connectivity determination
First two characters are RE	Treat as a REG (repeater with gain)
First two characters are DL	Treat as a DLL (dial Long Lines) unit
First two characters are VR	Treat as a VR (voice repeater)—an example would be an E6 repeater
First four characters are DPP- or character string begins with " "	Treat as a trunk
Anything else	Treat as an SE

types that must be processed by the connectivity algorithm. The next step is to construct a matrix whose rows and columns represent each of these facilities and whose elements are the numerical weights associated with how likely the two facilities are to be connected directly to one another. This will be referred to as the generalized weight table. When the algorithm is presented an actual list of elements that must be connected together, the weights for the graph constructed for this circuit will be obtained from the generalized weight table.

The generalized weight table is constructed as follows:

1. All possible facility types are classified in four broad categories: switching equipment, conditioning equipment, metallic facilities, and tie pairs. In general, any circuit must be connected in the order: switching equipment–conditioning equipment–metallic facilities. Tie pairs are assigned as needed to facilitate these connections.

2. Table III shows this classification of facilities. When assigning weights, the user should note that some conditioning equipment is likely to be connected directly to another conditioning equipment of the same type while other types would be unlikely to be connected directly to each other. For example, if several bridge lifters (BLs) were in the same circuit, they would likely all be connected together. Facilities of this type are noted as “bunching” on Table III.

The range of weights is arbitrarily chosen to lie between zero and one hundred. With the considerations just described plus a review of many likely circuits, the generalized weight table shown in Table IV was developed.

As mentioned earlier, for a particular circuit a graph is established and the weights for the edges are taken from the generalized weight table. After that step the weights are further modified if any of the following additional information applies to the circuit.

1. If tie pairs are already present in the circuit (i.e., an existing circuit is being modified), then the two facilities connected by the tie pair are recorded in the tie pair record. The weight between these two facilities and the tie pair is reduced to a small value.

Table III—Grouping of facilities

I Switching equipment	Line equipment
II Conditioning equipment	Bridge lifter (bunching)
	Special equipment (RE)
	Special equipment (DL)
	Special equipment (VR)
	Special equipment (bunching)
III Metallic facilities	Cable pair
	Trunk
	Concentrator
	Special equipment (DPP-)
	Special equipment (.)

Table IV—Generalized weight table

	OE	BL	SE: DL	SE: RE	SE: VR	SE	CP	TK	SE: .	SE: DPP-	CO	TP
OE	90											
BL	35	5										
SE:DL	40	50	90									
SE:RE	45	55	90	90								
SE:VR	45	55	7	90	90							
SE	45	55	10	15	10	10						
CP	65	60	30	30	6	30	70					
TK	65	60	25	25	5	25	75	70				
SE:.	65	60	25	25	5	25	75	70	70			
SE:DPP-	65	60	25	25	5	25	75	70	70	70		
CO	65	60	70	70	73	70	75	75	75	75	90	
TP	90	90	90	90	90	90	90	90	90	90	90	90

2. If a party circuit is being processed, then the facilities associated with each party are identified by a party number. Those facilities that do not belong to the same party have their weights increased to a maximum value.

3. If a circuit with one or more off-premises extensions is being processed, then those facilities belonging to the same "leg" will have a Different Premise Address (DPA) value assigned to them. Consequently, the weights are increased to a maximum value for those edges connecting facilities in different "legs".

4. If the circuit contains tie pairs, then the weights between facilities terminated on different frames will be increased somewhat. This is done to avoid assigning tie pairs unnecessarily.

4.2 Fundamental considerations

There are two special conditions that apply to determining circuits for central office facilities that do not apply to circuit connectivity in general. Not only do these conditions enable COSMOS to determine the correct configuration, but their use speeds up the algorithm as well since some nodes can be eliminated from consideration after a certain point in the algorithm has been reached. These special conditions are:

1. When a user is choosing among several Minimum-Weight Spanning Trees (MWSTs) (they need not be unique for a given graph), the tree with the minimum number of branches at the node with the most branches is preferred. An example of this is shown in Fig. 2. The algorithm does not actually calculate all possible MWSTs and then choose the one with the minimum number of branches at the node with the maximum number of branches. Instead, several strategies are employed, depending on the circuit being processed. If the circuit contains office equipment (OE), then most nodes have a maximum number of connections to them which is calculated before the MWST processing begins (as described in item 2 of this listing). The only

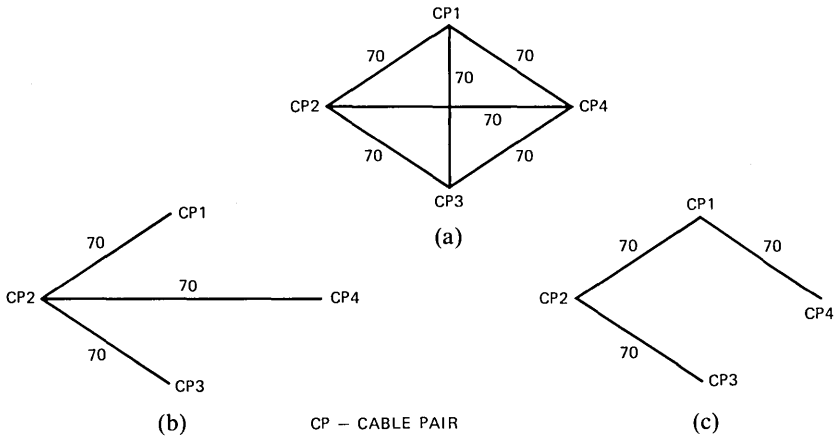


Fig. 2—The minimum-weight spanning tree showing (a) the graph; (b) a maximum of three branches; (c) a maximum of two branches. In this case (c) is the preferred tree.

exceptions are nodes that represent BLs. To prevent all BLs from connecting to one BL, the edge weights of all BL edges not yet selected for the MWST terminating on a BL just connected are incremented. For a circuit that contains no OE, the edge weights of all edges not yet selected for the MWST terminating on a node that has been selected for the MWST are incremented. These strategies direct the algorithm towards selecting the MWST with the required branch minimization. This requirement relates to how circuits are actually wired on the frame. If too many connections must be made at one terminal, the craftsperson may physically run out of room on the terminal and thus be unable to complete all the connections. Also, if an order is subsequently received to disconnect one of the legs of the circuit, proper “housekeeping” might require dismantling all connections at a terminal and then reconnecting the remaining legs. This process is much simplified if the number of connections at a terminal is minimized.

2. When an OE is present in the circuit, each facility is allowed a maximum number of “outward connections.” An outward connection is defined as a connection away from the OE. When an OE is present, it will be the root of the tree and therefore a direction away from the OE (root) is always defined. The maximum number of outward connections is determined by the following rules:

- (a) Metallic facilities (see Table III) have zero outward connections since they must always be at the outermost “tips” of the branches.
- (b) Conditioning equipment (see Table III) is allowed one outward connection. In determining outward connections, a connection

between two BLs is not counted. This is because a BL will usually be at a branch point and therefore will have additional outward connections.

- (c) If no BLs are present in the circuit, the number of outward connections from the OE equals the number of metallic facilities. If BLs are present, the number of outward connections from the OE equals the number of metallic facilities minus the number of BLs plus one. This formula reflects the actual way in which such circuits are wired: If BLs are present, they are the bridge point instead of the OE. In fact, BLs are often hard-wired in parallel in anticipation of their use as bridge points.

This set of rules (a through c) constitutes the principal reason for a speed-up of this algorithm over the general case, since once the maximum number of outward connections is achieved, a particular node no longer needs to be considered.

3. When an edge is chosen for the MWST, its weight is increased to the maximum value (100). This was chosen as the most efficient method to signal the algorithm not to consider this edge for the MWST again.

4.3 Detailed description

This section describes determining the list of facilities to be connected, the actual algorithm, and how the output list of facilities in connectivity order is assembled from the internal tables populated by the connectivity algorithm. This breakdown parallels the construction of the actual software.

4.3.1 The list of facilities to be connected

Connectivity processing is initiated when another COSMOS module determines that connectivity must be established. If this is the case, the connectivity module is invoked and a list of facilities is presented to it. Before this list can be passed along to the connectivity algorithm, certain facilities must be "weeded out".

There are two types of facilities that must be excluded from connectivity considerations. The first type includes facilities that have no mainframe terminations. These facilities are telephone numbers (TNs), No. 1XB coded terminals (XNs), No. 5XB relays, electronic switching system groups and terminals (GP and TER), and special equipment (SEs) for which no frame termination has been entered.

The second type of facility that must be excluded is frame-terminated facilities that will not be in the circuit at the time that the order being processed will be worked. This situation can arise because COSMOS allows multiple orders to be established on the same circuit if they are logically consistent with one another. Thus order number

1 with due date X may be removing facilities from an established circuit while order number 2 (the one being processed, say) with due date Y is adding facilities to the same circuit. If due date X precedes due date Y , then in processing order 2 the facilities being removed by order 1 should not be considered. However, if due date X is later than due date Y , then all facilities must be considered in processing order 2.

With these two considerations, a list of facilities is prepared for processing by the connectivity algorithm. After connectivity is determined for these facilities, those facilities that were excluded are added to the end of the list of facilities that were placed in connectivity order.

4.3.2 The algorithm itself

The first step performed by the algorithm is to identify the equipment types that have been presented to it. It then proceeds to calculate the connection weights for all the edges of the graph describing the circuit using the considerations outlined in Section 4.1. These weights are stored in a weight table. Next the actual MWST processing begins. This is facilitated by updating a "working" table. Each row of the table contains the following information: facility, count of connections to the facility, available outward connections, lowest connection cost, and the facility connected by the "lowest connection cost" edge. Also, as the algorithm proceeds, a third table, the connection list, is created. The connection list table maintains a list of the edges selected for the MWST.

The "working" table is populated as follows: each input facility is placed into the table. Initially, the count of all connections to the facility is set to zero for each facility. The available outward connections for each facility are determined based on the considerations described in item 2 of Section 4.2. The lowest cost connection and the corresponding facility are determined by scanning the weight table for each facility. In case of a tie the first edge encountered in the weight table is chosen for inclusion in the working table.

Now the first facility to be placed in the circuit must be chosen. If there is an OE in the working table, it is chosen as the first facility; otherwise the first facility in the working table is chosen. The first facility and the facility it is connected to in the working table are placed in the connection list.

In the following, the first facility is taken as a facility appearing in the connection list. While there are still facilities that have not been connected to the circuit, the following instructions are repeated:

1. Choosing among the facilities already in the circuit (i.e., in the connection list), find the facility in the working table with the lowest cost connection. In case of a tie take the facility that appears first in

the working table. The facility connected by the lowest cost connection edge will be referred to as the “new facility”; the original facility will be called the “old facility”.

2. If the number of connections to the new facility is not zero, this edge cannot be part of the MWST or else a cycle would be formed. Skip to instruction 8 below.

3. Add this connection to the connection list.

4. Increment the number of connections for the two facilities.

5. If the circuit contains an OE, decrement the number of available outward connections for the old facility unless both facilities are BLs. If both facilities are BLs, add one to the cost of all edges in the weight table that emanate from the old BL. This will reduce the maximum number of connections made at one bridge point, as explained in Section 4.2.

6. If the circuit contains an OE, and if either the old or the new facility (or both) have zero outward connections available, change the costs in the weight table for all edges emanating from such a node to a maximum value.

7. If the circuit does not contain an OE, and the old facility has two or more connections, add one to the cost of all edges in the weight table that emanate from the old facility node.

8. Change the cost of the edge in the weight table that connects the old and the new facility to a maximum value.

9. Reestablish the working table based on the new weight table costs.

We may now assume that all facilities have been placed in the connection list. (Note that if there are N facilities to be connected, there will be $N-1$ entries in the connection list so that the end of the algorithm is readily detected.) Now the connection list must be converted to a linear list. A tree will be described by a linear list that enumerates each branch, one after another. The beginning of a new branch is detected by the repetition of a facility that already appears higher up on the list (the branch point).

The algorithm for creating the linear list makes use of the working table left over from the MWST algorithm and the connection list. The algorithm

1. Searches the working table (in reverse order) until a facility is found with only one connection. This facility is one end of a branch. It places the facility in the linear list.

2. Searches the connection list (in reverse order) for the facility just placed in the linear list. It places the facility connected to it in the linear list.

3. Decrements the connection count for both the old and the new facilities. It removes their connection from the connection list.

4. If the connection count for the new facility is greater than zero, it repeats Steps 2 and 3. If the connection count for the new facility is zero, the end of the current branch has been reached. It will then go to the next step.

5. For each facility already on the linear list, it determines the number of remaining connections in the working table. If all connections are zero, the linear list is complete. Otherwise, it selects the first facility encountered with a nonzero connection count.

6. Enters this facility in the linear list and proceeds to Step 2.

Note that the lists in Steps 1 and 2 are searched in reverse order so that the frame instructions are in a more "pleasing" sequence: line equipment first, then the first "leg", then the second "leg", etc.

The connectivity algorithm is now complete. The facilities that were excluded from consideration at the start of the algorithm can be added to the end of the list.

The steps just described are applied to a particular example in Appendix C.

V. ACKNOWLEDGMENTS

As we mentioned earlier, the basic idea of applying the MWST algorithm to the problem of determining circuit connectivity in COSMOS is due to H. L. York, who also programmed the original version. The additional modifications for circuits containing an OE were conceived of and designed by J. B. Sharpless. The algorithm was rewritten by E. W. Merrill, who worked under Sharpless' direction.⁵ The current "owner" of the program is D. P. Bates.

REFERENCES

1. B. Bittner, "Computer System For Main Frame Operations (COSMOS)," Proc. IEEE Int. Conf. Commun., 1 (1976), pp 13-20.
2. H. L. York, unpublished work.
3. E. Horowitz and S. Sahni, "Fundamentals of Data Structures," Woodland Hills, CA: Computer Science Press, Inc., 1976.
4. R. C. Prim, "Shortest Connection Networks and Some Generalization," B.S.T.J., 36, No. 6 (November 1957), pp. 1389-1401.
5. J. B. Sharpless and E. W. Merrill, unpublished work.

APPENDIX A

COSMOS Service Order Language

When COSMOS is ready to accept a command, it will print a prompt (%). Immediately preceding the prompt character two alphanumeric characters are printed. These two characters represent the wire center with whose facilities the user wishes to work. The wire center is identified by the user at log-in time.

After the prompt letters have been printed the user can enter the

transaction name. All service orders are initiated in COSMOS through the transaction SOE (Service Order Establishment). Particular inputs to SOE are established on separate lines, as many as are needed to specify the order.

The first character of the first input line must be an H (standing for header). The remainder of the line contains general data pertaining to the order. Typical data items that appear on this line are the order number (identified by the prefix ORD), the order type (OT), and the due date (DD). The prefix-data groupings are separated by a vergule (/). This applies to all line types, not just to the H line.

If all the data do not fit on the first H line, they may be continued on subsequent H lines. Once all the header data have been entered, facilities to be connected on the order are entered on a line (or lines) whose first character is I (standing for "in"). Facilities to be disconnected by the order are entered on a line (or lines) whose first character is O (standing for "out"). Typical data items that appear on I or O lines are Cable Pair (CP), Telephone Number (TN), Office Equipment (OE), Universal Service Order Code (US), features (FEA), Telephone Number Exchange code (NNX), and Resistance Zone (RZ).

In the case of facilities that are automatically assigned by COSMOS, the facility prefix may be followed by a question mark (?). This is a signal to COSMOS to assign the facility automatically. For example, if COSMOS is to select a telephone number somewhere on the I line the construction

I /TN ?/

should appear. However, some wire centers contain several different switching entities. To distinguish among them the user is instead required to specify the exchange code. In this case automatic telephone number selection is triggered by the input.

I /NNX 351/

When all I and/or O lines have been input the user types a "." on a single line. At this point processing of the order commences. It should also be noted that as each line is entered, rudimentary checks are performed. When this processing is completed COSMOS prints an underscore (_) as a prompt to indicate that the next line can be processed.

APPENDIX B

An Example of Automatic Connectivity Determination

In this case COSMOS will be asked to process order number NAS0789. This is a new connect order (OT NC) and has a due date of August 1, 1981. The exchange code is 111 and COSMOS is to assign

the line equipment with a Universal Service Order Code (US) of 1FR and features (FEA) consisting of *Touch-Tone** service (T), nonsleeve lead (N), nonessential (N), and loop start (L). Four cable pairs are to be assigned to the order—pairs 980, 981, 982, and 983 in cable 4. The resistance zones of these pairs are 22, 11, 12, and 13, respectively. A parameter is maintained in the database to indicate whether bridge lifters are needed. If any one of these resistance zones exceeds this parameter, then all pairs will be assigned bridge lifters. In this case the parameter is set to 18, a value exceeded by the resistance zone of the first pair.

The input and the SOE response is as follows:

```
90% SOE
H ORD NAS0789/OT NC/DD 8-1-81
_I NNX 111/OE ?/US 1FR/FEA TNNL
_I CP 4-980/RZ 22
_I CP 4-981/RZ 11
_I CP 4-982/RZ 12
_I CP 4-982/RZ 13
```

```
—
SO000122
ORD NAS0789
IN: CP 4-0980
IN: CP 4-0981
IN: CP 4-0982
IN: CP 4-0983
IN: OE 000-007-401
IN: TN 111-1096
IN: BL 49
IN: BL 51
IN: BL 50
IN: BL 52
IN: TP CM11-0107
IN: TP CM11-0304
IN: TP CM11-0305
IN: TP CM11-0306
IN: TP CM11-0307
```

**TRANSACTION COMPLETED

90%

The string “SO000122” immediately following the period is the record number in the service order file selected by COSMOS to hold information about the order. This record number is useful in the event

* Registered service mark of AT&T.

the order is not established properly and manual corrective action is required.

The rest of the SOEs output are COSMOS assignments. First the four cable pairs are echoed back. These are followed by eleven automatically assigned facilities: an office equipment, a telephone number, four bridge lifters, and five tie pairs. (The tie pairs are needed to interconnect the bridge lifters and the office equipment and cable pairs since the bridge lifters are terminated on a different frame.) The facilities are listed by SOE in the order in which they are assigned. This is not the connectivity order.

To show the connectivity order the frame output report must be executed. This is the report used by telephone company personnel to actually wire the circuit in the central office. The report itself is in a lengthy format for ease of reading. Instead of reproducing the entire report here, only excerpts that show connectivity are listed below:

```

      :
LINE EQP IN      : 000-007-401
      :
TIE PAIR IN     : CM11-0107
      :
MISC EQP IN     : BL 49
      :
TIE PAIR IN     : CM11-0304
      :
CABLE PR IN     : 4-0980
      :
*MISC EQP IN    : BL 49
      :
MISC EQP IN     : BL 51
      :
TIE PAIR IN     : CM11-0305
      :
CABLE PR IN     : 4-0981
      :
*MISC EQP IN    : BL 51
      :
MISC EQP IN     : BL 50
      :
TIE PAIR IN     : CM11-0306
      :
CABLE PR IN     : 4-0982
      :
*MISC EQP IN    : BL 50
      :
```

```

MISC EQP IN      BL 52
                  :
TIE PAIR IN      CM11-0307
                  :
CABLE PR IN      4-0983
                  :

```

Note the first leg of the circuit—extending from OE 000-007-401 to CP 4-0980. The beginning of the next leg is indicated by the asterisk (*) and the repetition of the facility BL 49. This is the first bridge point. This leg extends down to CP 4-0981. Now BL 51 is shown as the next bridge point. Notice that BL 49 is not the bridge point for all legs. This is the effect of the algorithm described in Section 4.2 to minimize the maximum number of legs emanating from a single bridge point. The remaining two legs extend from BL 51 to CP 4-0982 and BL 50 to CP 4-0983.

APPENDIX C

An Example of the Algorithm's Execution

The algorithm described in Section 4.3.2 will be followed in detail for a particular set of facilities: two bridge lifters (BL1 and BL2), two cable pairs (CP1 and CP2), and one line equipment (OE). The first step is to determine the connection weights for all the edges of the graph. These weights are determined from Table IV. Note that the diagonal terms are given a weight of 100, since a facility cannot be connected to itself.

Step 1—Weight table

	BL1	BL2	CP1	CP2	OE
BL1	100	5	60	60	35
BL2	5	100	60	60	35
CP1	60	60	100	70	65
CP2	60	60	70	100	65
OE	35	35	65	65	100

In this particular case CP1 and BL1 have been assigned a DPA value of “ ” (i.e., a blank) and CP2 and BL2 have been assigned a DPA value of “999” by a previously invoked load module of SOE. Thus those edges connecting facilities in different “legs” (i.e., BL1-CP2 and BL2-CP1) have their weights changed to a maximum value. (In the next and in all following tables entries that have changed from the previous table are enclosed in parentheses.)

Step 2—Weight table

	BL1	BL2	CP1	CP2	OE
BL1	100	5	60	(100)	35
BL2	5	100	(100)	60	35
CP1	60	(100)	100	70	65
CP2	(100)	60	70	100	65
OE	35	35	65	65	100

Now the working table is constructed. Each facility has an entry and the connection count is initially set to zero. The Available Outward Connections (AOC) equal zero for the two metallic facilities (CP1 and CP2), equals one for the two conditioning facilities (BL1 and BL2), and equals one for the OE based on the formula:

$$\begin{aligned} \text{AOC} &= \# \text{ metallic facilities} - \# \text{ BL's} + 1 \\ &= 2 - 2 + 1 = 1 \end{aligned}$$

The lowest connection cost and corresponding facility are obtained from the weight table.

Step 3—Working table

Facility	Connection Count	Available Outward Connections	Lowest Connection Cost	Corresponding Facility
BL1	0	1	5	BL2
BL2	0	1	5	BL1
CP1	0	0	60	BL1
CP2	0	0	60	BL2
OE	0	1	35	BL1

Since the circuit contains an OE, this facility is chosen first and placed on the connection list.

Step 4—Connection list

OE-BL1

The number of connections to the OE and BL1 are incremented (Step 6, working table). The number of AOC to the old facility (the OE) is decremented (Step 6, working table). The old facility now has zero AOC so the weight of all edges emanating from it is changed to a maximum value (Step 5, weight table). Finally, the working table is modified due to changes in the weight table.

Step 5—Weight table

	BL1	BL2	CP1	CP2	OE
BL1	100	5	60	100	(100)
BL2	5	100	100	60	(100)
CP1	60	100	100	70	(100)
CP2	100	60	70	100	(100)
OE	(100)	(100)	(100)	(100)	100

Step 6—Working table

Facility	Connection Count	Available Outward Connections	Lowest Connection Cost	Corresponding Facility
BL1	(1)	1	5	BL2
BL2	0	1	5	BL1
CP1	0	0	60	BL1
CP2	0	0	60	BL2
OE	(1)	(0)	(100)	BL1

If we choose among the facilities already in the connection list (OE and BL1), the one with the lowest connection cost in the weight table is the first entry. The edge BL1-BL2 is added to the connection list.

Step 7—Connection list

OE-BL1
BL1-BL2

Since the connection count to BL2 is zero, this is an acceptable choice. The number of connections to BL1 and BL2 are incremented (Step 9, working table). However, the number of AOC to the old facility (BL1) is not decremented, since both facilities are BLs. Instead, one is added to the cost of all edges that emanate from BL1 (Step 8, weight table). Since neither the old nor the new facility has zero AOC, the edges emanating from these nodes do not have their weights set to 100. However, the BL1-BL2 weights are set to the maximum value (Step 8, weight table). Finally, the working table is modified according to changes in the weight table.

Step 8—Weight table

	BL1	BL2	CP1	CP2	OE
BL1	(101)	(100)	(61)	(101)	(101)
BL2	(100)	100	100	60	100
CP1	(61)	100	100	70	100
CP2	(101)	60	70	100	100
OE	(101)	100	100	100	100

Step 9—Working table

Facility	Connection Count	Available Outward Connections	Lowest Connection Cost	Corresponding Facility
BL1	(2)	1	(61)	(CP1)
BL2	(1)	1	(60)	(CP2)
CP1	0	0	(61)	BL1
CP2	0	0	60	BL2
OE	1	0	100	(BL2)

If we choose among the facilities already on the connection list (OE, BL1, and BL2), the one with the lowest connection cost in the weight table is the BL2 entry. Therefore, BL2-CP2 is added to the connection list.

Step 10—Connection list

OE-BL1
BL1-BL2
BL2-CP2

Since the connection count to CP2 is zero, this is an acceptable choice. The number of connections to BL2 and CP2 are incremented (Step 12, working table). The number of AOC to the old facility (BL2) is decremented (Step 12, working table). Since both BL2 and CP2 now have zero AOC, the weights for all edges emanating from BL2 and CP2 are set to the maximum value (Step 11, weight table). Finally, the working table is modified according to changes in the weight table.

Step 11—Weight table

	BL1	BL2	CP1	CP2	OE
BL1	101	100	61	101	101
BL2	100	100	100	(100)	100
CP1	61	100	100	(100)	100
CP2	101	(100)	(100)	100	100
OE	101	100	100	100	100

Step 12—Working table

Facility	Connection Count	Available Outward Connections	Lowest Connection Cost	Corresponding Facility
BL1	2	1	61	CP1
BL2	(2)	(0)	(100)	(BL1)
CP1	0	0	61	BL1
CP2	(1)	0	(100)	BL2
OE	1	0	100	BL2

If we choose among the facilities already on the connection list (OE, BL1, BL2, CP2), the one with the lowest connection cost in the weight table is the BL1 entry. Therefore, BL1-CP1 is added to the connection list.

Step 13—Connection list

OE-BL1
BL1-BL2
BL2-CP2
BL1-CP1

Since the connection count to CP1 is zero, this is an acceptable choice. The number of connections to BL1 and CP1 are incremented (Step 15, working table). The number of AOC to the old facility (BL1) is decremented (Step 15, working table). Since both BL1 and CP1 now have zero AOC, the weight of all edges emanating from BL1 and CP1 are set to the maximum value (Step 14, weight table). Finally, the working table is modified according to changes in the weight table.

Step 14—Weight table

	BL1	BL2	CP1	CP2	OE
BL1	101	100	(100)	101	101
BL2	100	100	100	100	100
CP1	(100)	100	100	100	100
CP2	101	100	100	100	100
OE	101	100	100	100	100

Step 15—Working table

Facility	Connection Count	Available Outward Connections	Lowest Connection Cost	Corresponding Facility
BL1	(3)	(0)	(100)	(BL2)
BL2	2	0	100	BL1
CP1	(1)	0	(100)	BL1
CP2	1	0	100	BL2
OE	1	0	100	BL2

The algorithm is completed when the connection list contains $N-1$ entries, where N equals the number of facilities. In this case $N-1 = 4$ and so all connections have been obtained. The remainder of the algorithm transforms the connection list to a linear list.

Initially, the connection count for each facility, the connection list, and the linear list are as shown in Step 16. Search the connection count (from the bottom) to find a facility with a connection count of one. In this case the facility found is the OE. Next, search the

connection list (from the bottom) to find a corresponding facility. In this case the facility is BL1. Place these two facilities on the linear list and decrement the connection count for each.

Step 16—Linear list

Facility	Connection Count	Connection List	Linear List
BL1	3	OE-BL1	
BL2	2	BL1-BL2	
CP1	1	BL2-CP2	
CP2	1	BL1-CP1	
OE	1		

Applying this algorithm results in the table shown in Step 17. Since the connection count for BL1 is greater than zero, search the connection list (from the bottom) to find another entry for BL1. The connection BL1-CP1 is found, so CP1 is added to the linear list, and the connection count for both BL1 and CP1 are decremented.

Step 17—Linear list

Facility	Connection Count	Connection List	Linear List
BL1	2	-----	OE
BL2	2	BL1-BL2	BL1
CP1	1	BL2-CP2	
CP2	1	BL1-CP1	
OE	0		

The table now changes to what is shown in Step 18. Since the connection count for CP1 is zero, the connection count list is again searched (from the bottom) but only for facilities on the linear list (i.e., OE, BL1, CP1) for an entry with a nonzero connection count. The entry found is BL1. Searching the connection list for a corresponding facility results in the addition of the BL1-BL2 connection to the linear list. The connection count of each of these facilities is therefore decremented.

Step 18—Linear list

Facility	Connection Count	Connection List	Linear List
BL1	1	-----	OE
BL2	2	BL1-BL2	BL1
CP1	0	BL2-CP2	CP1
CP2	1	-----	
OE	0		

The table now changes to what is shown in Step 19. Since the connection count for BL2 is greater than zero, search the connection list to find another entry for BL2. The connection BL2-CP2 is found so CP2 is added to the linear list and the connection count for both BL2 and CP2 are decremented.

Step 19—Linear list

Facility	Connection Count	Connection List	Linear List
BL1	0	-----	OE
BL2	1	-----	BL1
CP1	0	BL2-CP2	CP1
CP2	1	-----	BL1
OE	0		BL2

The table now changes as shown in Step 20. Since all connection counts are zero, the algorithm terminates.

Step 20—Linear list

Facility	Connection Count	Connection List	Linear List
BL1	0	-----	OE
BL2	0	-----	BL1
CP1	0	-----	CP1
CP2	0	-----	BL1
OE	0	-----	BL2
			CP2

AUTHOR

Nicholas A. Strakhov, BSME, 1959, Massachusetts Institute of Technology; MEE, 1961, New York University; Ph.D., 1967, New York University; Georgia Institute of Technology, 1972-1974; Bell Laboratories, 1959—. At the Georgia Institute of Technology Mr. Strakhov was a part-time lecturer. He presently supervises a group developing software for COSMOS—an Operational Support System used by the telephone companies to administer facilities assigned to customers.

Note on the Properties of a Vector Quantizer for LPC Coefficients

By L. R. RABINER,* M. M. SONDHI,* and S. E. LEVINSON*

(Manuscript received March 15, 1983)

Vector quantization has been used in coding applications for several years. Recently, quantization of linear predictive coding (LPC) vectors has been used for speech coding and recognition. In these latter applications, the only method that has been used for deriving the vector quantizer code book from a set of training vectors is the one described by Linde, Buzo, and Gray. In this paper, we compare this algorithm to several alternative algorithms and also study the properties of the resulting code books. Our conclusion is that the various algorithms that we tried gave essentially identical code books.

I. INTRODUCTION

The technique of vector quantization for LPC voice coding has been in use for several years, and has been shown to be of great utility for LPC analysis/synthesis systems.¹⁻⁴ Recently, vector quantization of LPC vectors has been applied to speech-recognition systems both in direct applications^{5,6} and in conjunction with work on the application of hidden Markov models (HMMs) to recognition.^{7,8}

The main idea of vector quantization is summarized as follows: assume that a training set $\{T\}$ of I LPC vectors is given. It is desired to find a code book of M^* LPC vectors such that the average distance of a vector in $\{T\}$ from the closest code book entry is minimized. Thus we wish to find a set $\{R\}$ of reference vectors that minimizes the

* Bell Laboratories.

©Copyright 1983, American Telephone & Telegraph Company. Photo reproduction for noncommercial use is permitted without payment of royalty provided that each reproduction is done without alteration and that the Journal reference and copyright notice are included on the first page. The title and abstract, but no other portions, of this paper may be copied or distributed royalty free by computer-based and other information-service systems without further permission. Permission to reproduce or republish any other portion of this paper must be obtained from the Editor.

average distance $\bar{D}_I(M^*)$ given by

$$\bar{D}_I(M^*) = \min_{\{R\}} \left[\frac{1}{I} \sum_{i=1}^I \min_{1 \leq m \leq M^*} [d(T_i, R_m)] \right], \quad (1)$$

where $d(T_i, R_m)$ is the LPC distance between training vector T_i and code book entry R_m .

The optimum code book is generated by a method similar to the K -means algorithm. Starting with an initial guess of M^* entries, each vector of the training set is assigned to the closest entry. The centroids of the M^* subsets (clusters) obtained in this manner are used as new trial entries in the code book, and the iteration is continued until some stopping criterion is satisfied.

For large M^* , the choice of initial guesses can be quite important, and it is unlikely that a randomly chosen initial guess is a good one. For this reason the splitting algorithm was devised in Ref. 1. In this algorithm a code book of $M = 2$ entries is optimized, as described above, starting with a random initial guess. Next, each optimum code book entry for $M = 2$ is split into 2 and used as an initial guess for a code book of size $2M$. This process is used until $M = M^*$. To distinguish this algorithm from others considered later, we call it the *binary-split* algorithm.

To the best of our knowledge, all speech-related applications of vector quantization so far have used this binary-split algorithm. However, a priori, the requirement that every code word be split appears to be too restrictive. For example, after optimizing an $M = 2$ code book, if one cluster contains almost all the training set and the other contains just a few elements, it might be argued that only the larger cluster should be split. Thus it is of interest to consider "single-split" algorithms in which a single cluster is split at each iteration.

For very large M^* (e.g., 1024 or 2048) single-split algorithms might require prohibitive amounts of computation. However, M^* on the order of 64 or 128 can be quite useful in certain applications.⁸ In these cases a single-split algorithm is quite feasible. In any case, it is of interest to know whether or not a single-split algorithm yields a better code book than the binary-split algorithm.

There are at least three reasonable ways of implementing the splitting rule of a single-split algorithm for training the vector quantizer. To describe these three splitting rules we need some definitions. Let

$\{\hat{T}_M(m)\}$ = The set of training vectors represented by the m th code book entry (cluster) in a size M vector quantizer

$C_M(m)$ = The number of training vectors in $\hat{T}_M(m)$

$d_M(m)$ = The average distance (distortion) of the $C_M(m)$ vectors from the m th code-book entry

$D_M(m)$ = The total distance (distortion) of the $C_M(m)$ vectors.

We then have the relationships

$$I = \sum_{m=1}^M C_M(m) \quad (2)$$

$$d_M(m) = \frac{1}{C_M(m)} \sum_{q=1}^{C_M(m)} d(\hat{T}_M(m)_q, R_m) \quad (3)$$

$$D_M(m) = C_M(m) \cdot d_M(m). \quad (4)$$

Using eqs. (2) through (4) we can write the average distortion of eq. (1) as

$$\bar{D}_I(m) = \min_{\{R\}} \left[\frac{\sum_{m=1}^M D_M(m)}{\sum_{m=1}^M C_M(m)} \right] \quad (5a)$$

$$= \min_{\{R\}} \left[\frac{\sum_{m=1}^M d_M(m) C_M(m)}{\sum_{m=1}^M C_M(m)} \right]. \quad (5b)$$

Based on the above definitions, the three splitting rules we have considered are:

Rule 1: Split the cluster, m , with the largest number of vectors, $C_M(m)$. We denote the resulting (vector quantizer) VQ code-word set as R_c .

Rule 2: Split the cluster, m , with the largest average distortion, $d_M(m)$. We denote the resulting VQ code-word set as R_d .

Rule 3: Split the cluster, m , with the largest total distortion, $D_M(m)$. We denote the resulting VQ code-word set as R_D .

The key issue is how do the different splitting rules affect the properties of the resulting vector quantizer—in particular the average distortion [eq. (1)] and the coverage of the LPC space.

We have run a series of experimental evaluations of the single-split and binary-split algorithms for training the VQ. We have found that each of the different splitting criteria leads to a different reference prototype set (VQ code book); however, all the VQ sets had essentially the *same average distortion*. We were also able to show that the coverage of the LPC space for all VQ sets was identical, and that the

average distance of any one VQ set from another VQ set was smaller than the average distortion of the training set. Hence, the different implementations of the training algorithm for the VQ lead to equivalent VQ reference sets. Thus for any practical application the simple binary-split algorithm is effective for deriving the VQ code book entries.

The outline of this paper is as follows. In Section II we review the Linde et al.¹ implementation of the binary-split VQ training algorithm and show how we modified it to handle the single-split case. In Section III we discuss the results of several experiments on testing the different implementations of the training algorithm. In Section IV we provide a discussion and summary of the results.

II. IMPLEMENTATION OF THE VQ TRAINING ALGORITHM

The implementation of the VQ training algorithm is essentially the one proposed by Linde et al.¹ A flow diagram of this procedure for the binary-split case is given in Fig. 1a and for the single-split case in Fig. 1b. Given M code words, each vector of the training set T is assigned to the code word closest to it. The average distortion $\bar{D}_I(M)$ is computed for this assignment of the I training vectors to M clusters. M new code words are obtained as centroids (i.e., averaged normalized autocorrelations) of each cluster, and the distortion $\bar{D}_I(M)$ computed again. This process is iterated until it converges, i.e., until the percent change in distortion is less than a preset value ϵ (chosen to be 1 percent in our simulations). Once convergence is achieved, M is doubled by splitting each code word into two. The entire process is repeated until $M = M^*$. The iteration is initialized by choosing two arbitrary code words.

In our implementation, we made one modification to the VQ training algorithm of Fig. 1. We inserted a check after the classification of the training set vectors to see if any cluster is empty (i.e., contains none of the training set vectors). In such a case the "largest" cluster is split into two clusters, and the convergence test is bypassed (to ensure a reclassification in which each cluster is nonempty). However, for the data used in this experiment, an empty cluster never occurred. In subsequent tests with larger M^* we did encounter such cases.

For the single-split algorithm (Fig. 1b), only one modification is required. After convergence, only the "largest cluster" is split. Here largest can refer to the cluster with the largest average distortion, total distortion, or count.

For a convergence criterion of $\epsilon = 1$ percent, typically it takes three to six iterations of the classification loop to obtain a convergent set of clusters and centroids. We also found that the algorithms of Fig. 1a and 1b work extremely reliably over a broad range of types of training

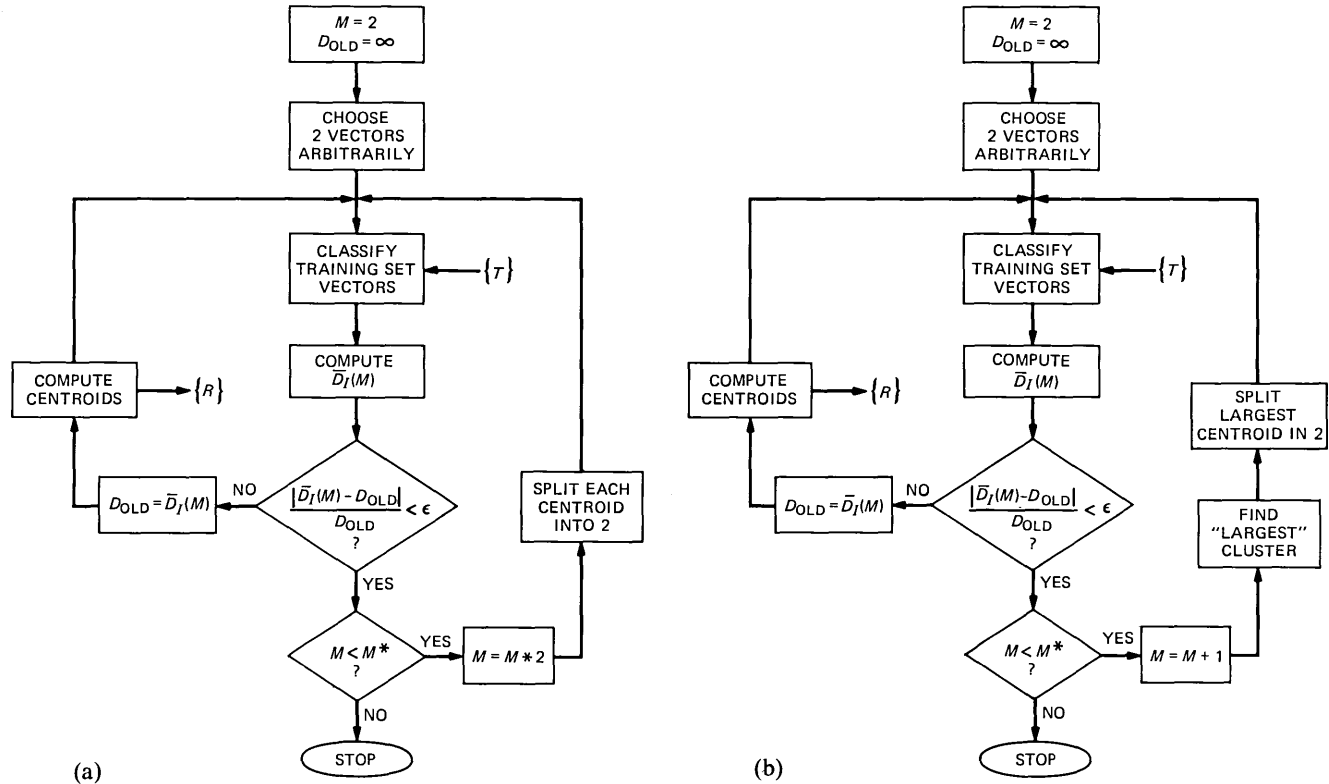


Fig. 1—Flow charts of the vector quantizer training algorithms. (a) The binary-split algorithm. (b) The single-split algorithm.

data (e.g., collected from a single talker, collected from many talkers, collected from a corpus of isolated words, collected from sentence-length material, etc.).

III. COMPARISON OF THE BINARY- AND SINGLE-SPLIT ALGORITHMS

To compare the performances of the binary- and single-split VQ training algorithms of Fig. 1, several tests were run. The database consisted of a set of 39,708 LPC vectors. The LPC analysis used a 6.67-kHz sampling rate and an eighth-order analysis of 300 sample (45 ms) frames of speech. The sample frames had been preemphasized with a simple, first-order digital network (preemphasis factor of 0.95) and windowed by a 300-sample Hamming window. Frames were taken 100 samples apart across the duration of each word of a series of 1000 isolated words (digits) spoken by 100 talkers (50 male, 50 female). All recordings were made over dialed-up telephone lines through a local PBX connection. All silence outside the spoken words was eliminated by a word endpoint detector;⁹ hence, all LPC training frames were from within word boundaries.

Several aspects of the binary- and single-split training algorithms were studied. The first question considered was whether the two training procedures yielded identical results (i.e., whether the resulting LPC code words and the clusters from which they were derived were identical). Figure 2 shows plots of the cluster splitting for an $M^* = 8$ solution for the binary-split algorithm (Fig. 2a) and the single-split algorithm based on average distance splitting (Fig. 2b). It can be seen that the resulting eight clusters in the single-split case come from very different splits than those for the binary-split case. For example, in

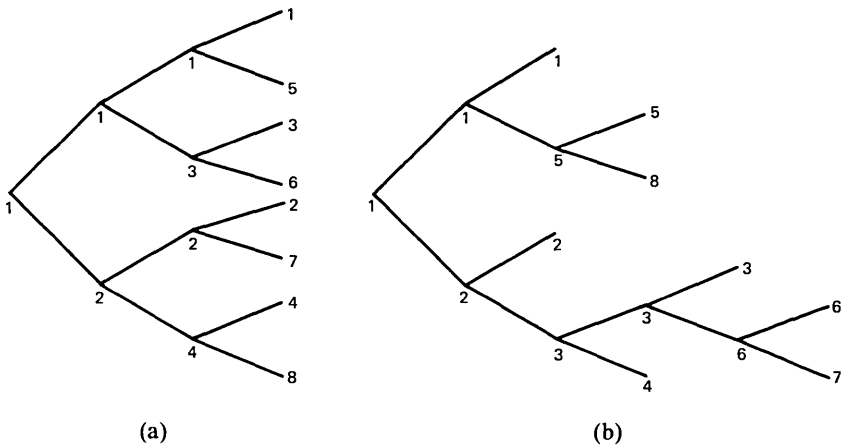


Fig. 2—Splitting charts for an $M^* = 8$ vector quantizer with splits based on average distortion. (a) The binary-split training algorithm. (b) The single-split algorithm.

the single-split case, final clusters 6 and 7 come from four splits of the original cluster 2, whereas final clusters 1 and 2 come from single splits of original clusters 1 and 2. In the binary-split case all final clusters come from two splits of original clusters 1 and 2. Similarly, the actual clusters were grossly different for the three different criteria for the single-split algorithm.

The next question we considered was how the different training procedures differed in performance. Figures 3 through 5 show a series of plots of statistics comparing some of the details of the individual training procedures. For each of these plots, Parts (a) through (d) show results for the binary-split case, the single-split case based on count, the single-split case based on average distortion, and the single-

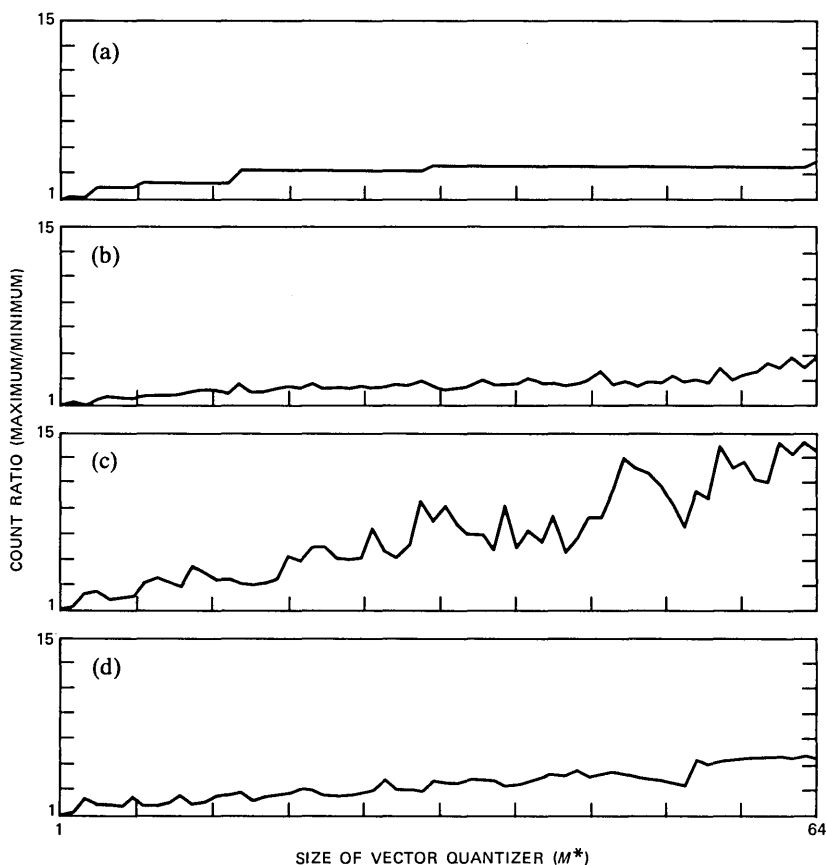


Fig. 3—Plots of count ratio (maximum cluster count divided by minimum cluster count) as a function of the size of the vector quantizer. (a) Binary-split training. (b) Single-split training based on count. (c) Single-split training based on average distortion. (d) Single-split training based on total distortion.

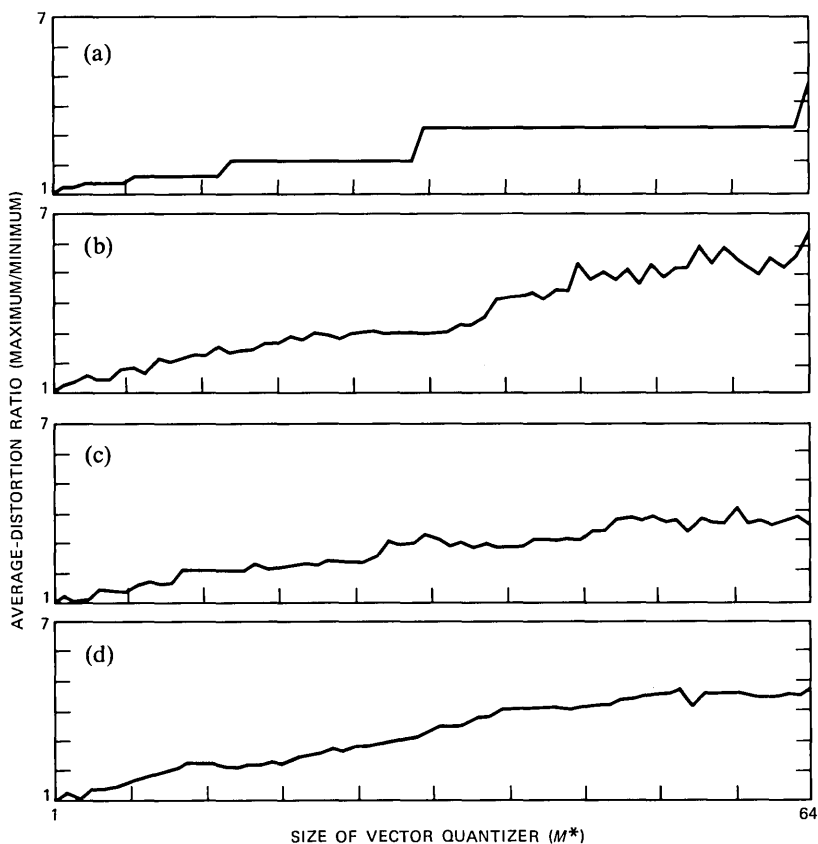


Fig. 4—Plots of average distortion ratio as a function of the size of the vector quantizer. (a) Binary-split training. (b) Single-split training based on count. (c) Single-split training based on average distortion. (d) Single-split training based on total distortion.

split case based on total distortion. The statistics plotted are ratio of maximum to minimum cluster count (Fig. 3), ratio of maximum to minimum average distortion (Fig. 4), and ratio of maximum to minimum total distortion (Fig. 5) versus size of the vector quantizer. These statistics were chosen because each of them should ideally approach 1.0 for clusters that are of equal size according to the corresponding splitting criterion. For example, we would expect the count ratio to approach 1.0 for the split on count criterion but not necessarily for the other splitting criteria.

Examination of Figs. 3 through 5 shows several interesting things. As seen in Fig. 3, the count ratio for the binary-split case for $M^* = 64$ (4.1) is actually smaller than the count ratio for the single split on count case for $M^* = 64$ (4.8). The count ratios for the other two split

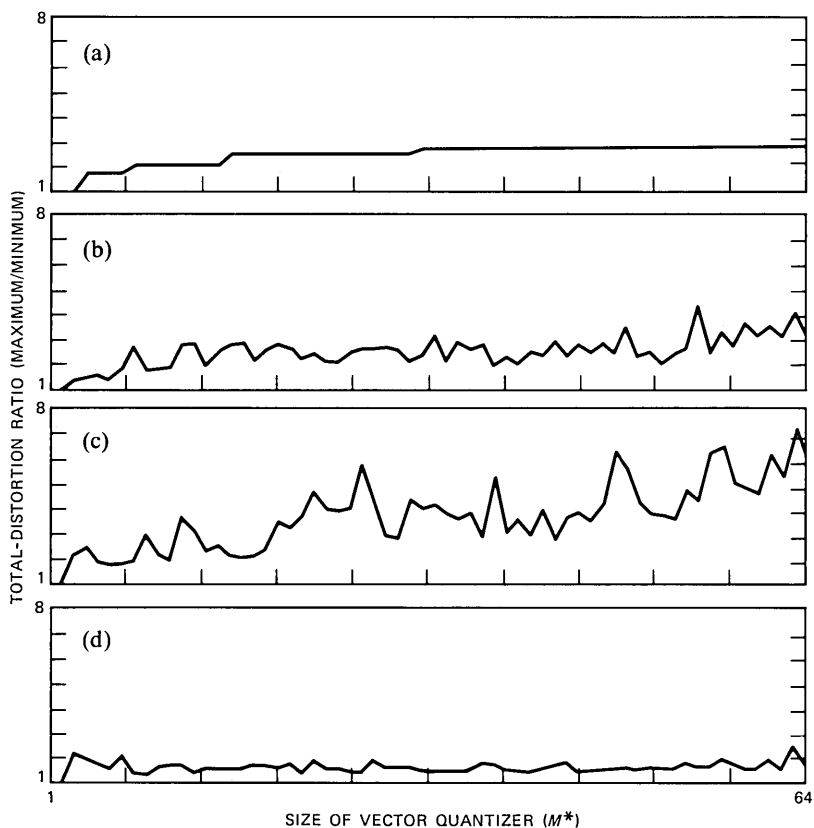


Fig. 5—Plots of total-distortion ratio as a function of the size of the vector quantizer. (a) Binary-split training. (b) Single-split training based on count. (c) Single-split training based on average distortion. (d) Single-split training based on total distortion.

criteria are indeed larger than for the split on count, as expected. Figure 4 shows that the average-distortion ratio is smallest (4.1) at $M^* = 64$ for the single split on average-distortion case; however, the distortion ratios for the binary case (4.4) and the single split on total-distortion (4.7) cases are only slightly larger. Finally, Fig. 5 shows a similar set of results on the total-distortion-ratio statistic in which the results for $M^* = 64$ for the binary-split case (2.7) are only slightly worse than for the single split on total-distortion case (2.6).

The results of Figs. 3 through 5 indicate that the binary-split case seems to yield cluster training statistics that are almost as good as the best statistics for any of the single-split cases in terms of count ratio, average-distortion ratio, and total-distortion ratio. Hence, from the point of view of cluster statistics, the binary-split cases appear to give the best overall performance.

Two gross performance checks were made on the training algorithms. In the first test, the average distance between vector quantizer sets obtained from the different training procedures was calculated as a function of M^* . The results of this test are given in Table I. It can

Table I—Average distance between code book entries of vector quantizers designed on the basis of count (R_c), average distortion (R_d), total distortion (R_D), and binary splitting (R_B)

M^*	$\bar{d}(R_c, R_d)$	$\bar{d}(R_c, R_D)$	$\bar{d}(R_c, R_B)$	$\bar{d}(R_d, R_D)$	$\bar{d}_T(M^*)^\dagger$
4	0.384	0.019	0.047	0.270	0.707
8	0.125	0.138	0.157	0.101	0.426
16	0.148	0.143	0.160	0.065	0.326
32	0.191	0.108	0.175	0.132	0.255
64	0.216	0.131	0.148	0.131	0.203

† Average distance between the training vectors and the code words representing them.

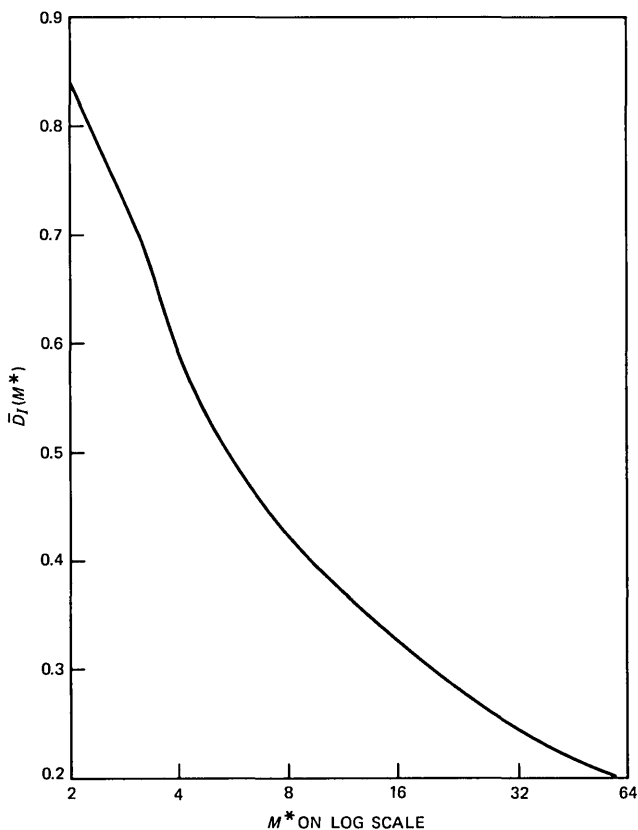


Fig. 6—Plot of average training set distortion $\bar{D}_T(M^*)$ as a function of the size of the vector quantizer.

be seen that the average distance between vector quantizer sets is as small or smaller than the average distance of the training vectors to the code book sets. Hence, the code book sets derived from the different training algorithms are, on average, quite close to each other.

The second test we performed was to measure the average distortion, $\bar{D}_1(M^*)$ versus M^* for the different training algorithms for values of M^* from 2 to 64. The results of this test are plotted in Fig. 6. On the

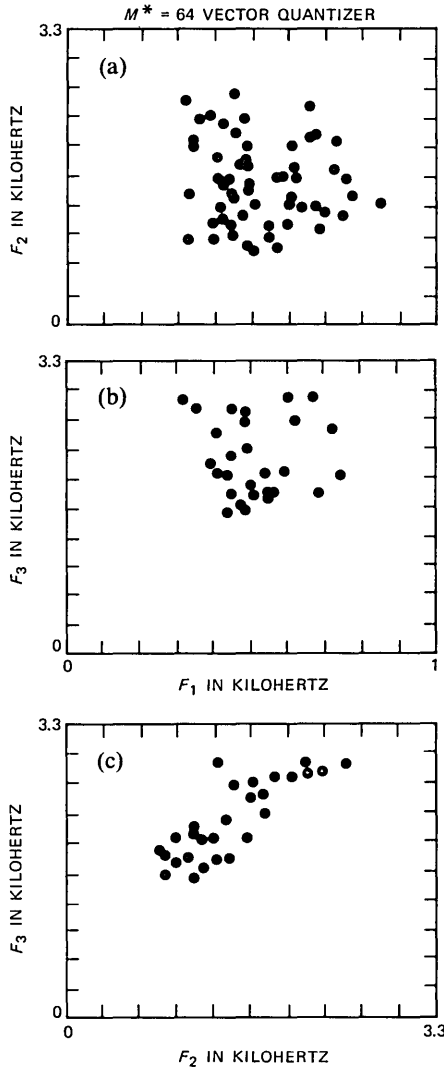


Fig. 7—Plots of code-word coverage in the F_1 - F_2 , F_1 - F_3 , and F_2 - F_3 planes for an $M^* = 64$ vector quantizer.

scale of this plot, the differences in average distortion are *indistinguishable* among the different vector quantizers.

The third and final question we considered concerns the coverage of the space of speech sounds by the optimum code books. A good way of displaying this coverage is to look at the code books in the space of formant frequencies. The formant frequencies (and bandwidths) for each entry of the code book are given by the zeroes of the trigonometric polynomial associated with it. Thus each code book may be displayed

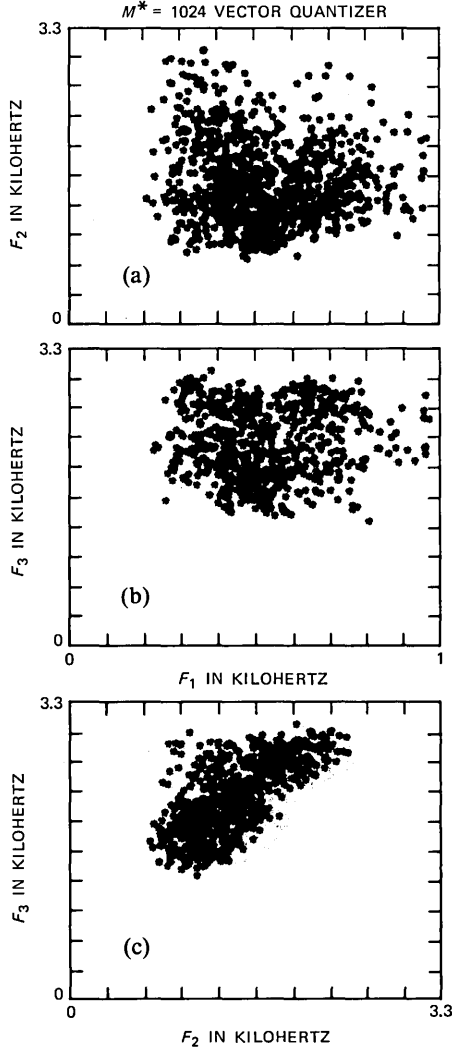


Fig. 8—Plots of code-word coverage in the F_1 - F_2 , F_1 - F_3 , and F_2 - F_3 planes for an $M^* = 1024$ vector quantizer.

as a scatter plot in F_1 - F_2 - F_3 space. Projections of this scatter diagram on the F_1 - F_2 , F_1 - F_3 , and F_2 - F_3 planes are shown for a typical code book in Figs. 7 and 8 for the code books obtained from the binary-split training algorithm for $M^* = 64$ (Fig. 7) and $M^* = 1024$ (Fig. 8). It is seen that the code words cover the expected regions in the formant frequency planes fairly uniformly. The major difference between the coverage of the $M^* = 1024$ and the $M^* = 64$ code books is the density of coverage of the areas in the respective formant frequency planes. The coverage of the single-split algorithms for $M^* = 64$ was essentially identical to that of the binary-split algorithm.

IV. DISCUSSION

Our overall conclusion from the tests that compared the fine and gross differences in clustering LPC vectors via a VQ training algorithm is that all the variations in the training procedure that we studied (i.e., different splitting procedures, different convergence criteria, etc.) lead to essentially indistinguishable differences in the set of VQ code book entries. Since the binary-split algorithm, as discussed by Linde et al.¹ requires the least amount of computation, it is the best of the algorithms considered.

In this paper we present the results of a series of experiments on a training set of 39,708 vectors. More recently we have experimented with the binary-split VQ training procedure on a number of different training sets whose size varied from 10,000 to 600,000 vectors. We found that the training procedure always rapidly and reliably converged to a set of code book vectors whose properties were similar to those described in this paper. We are currently using the VQ code book sets in work related to speech recognition and speech coding.

V. ACKNOWLEDGMENTS

The authors gratefully acknowledge several fruitful discussions with Fred Juang of Bell Laboratories concerning the characteristic properties of the VQ clusters. Juang's insight into the training procedure and the resulting properties of the code book vectors coincided with the results we found in this study.

REFERENCES

1. Y. Linde, A. Buzo, and R. M. Gray, "An Algorithm for Vector Quantization," *IEEE Trans. Commun.*, COM-28, No. 1 (January 1980), pp. 84-95.
2. B. Juang, D. Wong, and A. H. Gray, Jr., "Distortion Performance of Vector Quantization for LPC Voice Coding," *IEEE Trans. on Acoust., Speech, and Signal Proc.*, ASSP-30, No. 2 (April 1982), pp. 294-303.
3. A. Buzo, et al., "Speech Coding Based Upon Vector Quantization," *IEEE Trans. on Acoust., Speech, and Signal Proc.*, ASSP-28, No. 5 (October 1980), pp. 562-74.
4. D. Wong, B. Juang, and A. H. Gray, Jr., "An 800 Bit/S Vector Quantization LPC Vocoder," *IEEE Trans. on Acoust., Speech, and Signal Proc.*, ASSP-30, No. 5 (October 1982), pp. 770-80.

5. A. Buzo, H. Martinez, and C. Rivera, "Discrete Utterance Recognition Based Upon Source Coding Techniques," Proc. ICASSP-82 (May 1982), pp. 539-42.
6. J. E. Shore and D. Burton, "Discrete Utterance Speech Recognition Without Time Normalization," Proc. ICASSP-82 (May 1982), pp. 907-10.
7. R. Billi, "Vector Quantization and Markov Source Models Applied to Speech Recognition," Proc. ICASSP-82 (May 1982), pp. 574-7.
8. L. R. Rabiner, S. E. Levinson, and M. M. Sondhi, "On the Application of Vector Quantization and Hidden Markov Models to Speaker Independent, Isolated Word Recognition," B.S.T.J., 62, No. 4 (April 1983), pp. 1075-105.
9. L. F. Lamel, et al. "An Improved Endpoint Detector for Isolated Word Recognition," IEEE Trans. on Acoust., Speech, and Signal Proc., ASSP-29, No. 4 (August 1981), pp. 777-85.

AUTHORS

Stephen E. Levinson, B. A. (Engineering Sciences), 1966, Harvard; M.S. and Ph.D. (Electrical Engineering), University of Rhode Island, Kingston, 1972 and 1974, respectively; General Dynamics, 1966-1969; Yale University, 1974-1976; Bell Laboratories, 1976—. From 1966 to 1969, Mr. Levinson was a design engineer at Electric Boat Division of General Dynamics in Groton, Connecticut. From 1974 to 1976, he held a J. Willard Gibbs Instructorship in Computer Science at Yale University. In 1976, he joined the technical staff at Bell Laboratories, where he is pursuing research in the areas of speech recognition and cybernetics. Member, Association for Computing Machinery; Fellow, Acoustical Society of America; Senior Member, IEEE, editorial board of Speech Technology; Associate Editor, IEEE Transactions on Acoustics, Speech and Signal Processing.

Lawrence R. Rabiner, S.B. and S. M., 1964, Ph.D. (Electrical Engineering), The Massachusetts Institute of Technology; Bell Laboratories, 1962—. From 1962 through 1964, Mr. Rabiner participated in the cooperative plan in electrical engineering at Bell Laboratories. He worked on digital circuitry, military communications problems, and problems in binaural hearing. Presently, he is engaged in research on speech communications and digital signal processing techniques. He is coauthor of *Theory and Application of Digital Signal Processing* (Prentice-Hall, 1975), *Digital Processing of Speech Signals* (Prentice-Hall, 1978), and *Multirate Digital Signal Processing* (Prentice-Hall, 1983). Former President, IEEE, ASSP Society; former Associate Editor, ASSP Transactions; former member, Technical Committee on Speech Communication of the Acoustical Society, ASSP Technical Committee on Speech Communication; Member, IEEE Proceedings Editorial Board, Eta Kappa Nu, Sigma Xi, Tau Beta Pi. Fellow, Acoustical Society of America, IEEE.

Man Mohan Sondhi, B.Sc. (Physics), Honours degree, 1950, Delhi University, Delhi, India; D.I.I.Sc. (Communications Engineering), 1953, Indian Institute of Science, Bangalore, India; M.S., 1955; Ph.D. (Electrical Engineering), 1957, University of Wisconsin, Madison, Wisconsin; Bell Laboratories, 1962—. Before joining Bell Laboratories, Mr. Sondhi worked for a year at the Central Electronics Engineering Research Institute, Pilani, India and taught for a year at the University of Toronto. At Bell Laboratories his research has included work on speech signal processing, echo cancellation, adaptive filtering, modelling of auditory and visual processes, and acoustical inverse problems. From 1971 to 1972 Mr. Sondhi was a guest scientist at the Royal Institute of Technology, Stockholm, Sweden.

Upper Bounds on the Minimum Distance of Trellis Codes

By A. R. CALDERBANK,* J. E. MAZO,* and H. M. SHAPIRO†

(Manuscript received March 16, 1983)

A trellis code is a "sliding window" method of encoding a binary data stream into a sequence of real numbers that are input to a noisy transmission channel. When a trellis code is used to encode data at the rate of k bits/channel symbol, each channel input will depend not only on the most recent block of k data bits to enter the encoder but will also depend on, say, the ν bits preceding this block. The ν bits determine the state of the encoder and the most recent block of k bits generates the channel symbol conditional on the encoder state. The performance of trellis codes, like that of block codes, depends on a suitably defined minimum-distance property of the code. In this paper we obtain upper bounds on this minimum distance that are simple functions of k and ν . These results also provide a lower bound on the number of states required to achieve a specific coding gain.

I. INTRODUCTION

In this paper we are concerned with transmission of digital data using trellis codes to gain some noise immunity over standard uncoded methods. We assume pulse amplitude modulation whereby the values of the transmitted data are estimated from a sequence of samples r^j generated by a receiver. These output samples are often modeled as

$$r^j = x^j + n^j, \quad (1)$$

where x^j is a real number sequence determined by the source sequence of binary data and n^j is an independent zero-mean white Gaussian

* Bell Laboratories. † Swarthmore College, Swarthmore, Pennsylvania.

©Copyright 1983, American Telephone & Telegraph Company. Photo reproduction for noncommercial use is permitted without payment of royalty provided that each reproduction is done without alteration and that the Journal reference and copyright notice are included on the first page. The title and abstract, but no other portions, of this paper may be copied or distributed royalty free by computer-based and other information-service systems without further permission. Permission to reproduce or republish any other portion of this paper must be obtained from the Editor.

noise sequence of variance σ^2 . For uncoded transmission at rate k bits/symbol, x^j takes on one of 2^k fixed values. Error performance may be improved using coding, but if we insist on transmitting at rate k bits/symbol then we must increase the number of possible values taken by the x^j . We can choose either a block or tree (trellis) structure for the code. In this paper we consider only trellis codes. The performance of trellis codes, like that of block codes, depends on a suitably defined minimum-distance property of the code. We obtain upper bounds on this minimum distance, d_{\min} . The analogous problem for block codes is well studied, but little work has been done on distance properties of trellis codes.^{1,2}

We assume the following model for encoding the binary data (i.e., choosing the x^j) prior to transmission over the Gaussian channel. Regard the incoming binary digits as partitioned into blocks of k consecutive bits. The real number x^j is to be a time-independent function of the most recent k -bit block and also of the ν bits preceding this block. Thus if $\{a_i\}$ is the binary data sequence, we assume

$$x^j = x(a_{jk}, a_{jk-1}, \dots, a_{j(k-\nu)+1}, a_{(j-1)k}, \dots, a_{(j-1)k-(\nu-1)}). \quad (2)$$

This is an example of a k -bit/symbol trellis code. We regard the ν "old" bits as determining the state of the encoder (there are 2^ν possible states) and the k "new" bits as generating the channel symbol (there are 2^k possible symbols) conditional on the encoder state. The trellis structure is made evident by drawing an example. Fig. 1 shows the case $k = 1, \nu = 2$.

If, in this example, the encoder is in state (00) at time j , and the next bit (block of $k = 1$ bits) to be transmitted is a 1, then we transmit the symbol $x(100)$ and move to state (10).

Other trellis codes exist. For example, we could define a code with just three trellis states or the symbols x^j could also depend on the time index j . However, we shall only consider trellis codes determined by (2). The trellis structure of (2) is identical to that of linear algebraic

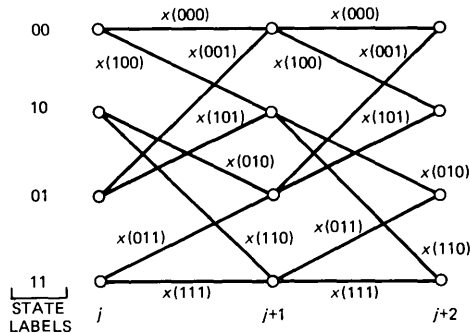


Fig. 1—Diagram of a trellis code.

convolutional codes. We use the term sliding window trellis codes for trellis codes determined by (2).

To simplify the discussion in the text we shall assume that k divides ν . The general case is treated in Appendix B.

The problem we consider involves certain distance properties of trellis codes. To motivate it, consider the decoding problem. Optimum decoding involves finding the most likely path through the trellis, given the observed sequence (1).³ Typically, the path chosen will not coincide with the correct path for all time but will occasionally diverge from it and remerge at a later time. This is called an error event, and we generically denote it by the letter E . For example, with the trellis in Fig. 1, $x(000)$ may have been sent several times in succession, resulting in the straight path shown in Fig. 2, but noise may have caused the decoder to choose an alternate path. In Fig. 2 the decoder chose the symbols $x(100)$, $x(010)$, $x(001)$ instead of $x(000)$, $x(000)$, $x(000)$.

An error event E of length L lasts from time i to time $i + L$, the decoder having decided upon the symbol sequence $\hat{x}^{i+1}, \dots, \hat{x}^{i+L}$ instead of the correct sequence x^{i+1}, \dots, x^{i+L} . The (squared) Euclidean distance $d^2 (= d^2(E))$ between the two paths of E is given by

$$d^2 = \sum_{j=i+1}^{i+L} (x^j - \hat{x}^j)^2 \quad (3)$$

and is crucial to determining the probability $P(E)$ of an error event E . With the white noise assumption made in (1), $P(E)$ is easy to calculate and, when $d^2 \gg \sigma^2$, it is approximately given by

$$P(E) \approx \exp\left(-\frac{d^2}{8\sigma^2}\right). \quad (4)$$

Equation (4) leads us to expect that, for small noise, symbol error probabilities will be determined by error events having the smallest minimum distance between their two paths and it becomes of interest to design codes that have good minimum-distance properties in this sense. Such designs have recently been considered by Ungerboeck, who obtained on the order of 3-dB performance improvements (factor

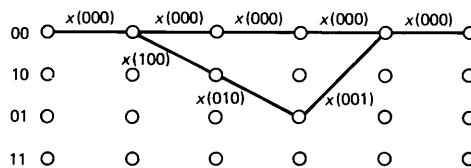


Fig. 2—Example of an error event.

of 2 in minimum distance) over the uncoded case for $k = 1, 2$, and four or eight states in the trellis.⁴

Ungerboeck based his designs on a computer search of binary convolutional codes with 2^ν states, rate $k/(k + 1)$, and a particular mapping of the output binary $(k + 1)$ tuples to 2^{k+1} equally spaced channel symbols ($\pm 1, \pm 3$, etc.). His use of convolutional codes thus conforms to the general scheme of (2), which implies the same trellis structure as described herein. However, his a priori choice of only 2^{k+1} equally spaced channel symbols is certainly restrictive in principle. In this paper we consider the natural question of how large d_{\min}^2/P can be made if these restrictions are removed. Here, d_{\min} is the minimum distance between all pairs of paths associated with error events in the trellis, and P is the average transmitted power.

Section II gives a detailed description of the trellis structure and of error events. If S is a finite set of error events, then

$$\min_{E \in S} \{d^2(E)\} \leq \frac{1}{|S|} \sum_{E \in S} d^2(E), \quad (5)$$

since the minimum of a set of real numbers is bounded above by their average. This observation is the basis of our first two bounds. The first and simplest bound is

$$\frac{d_{\min}^2}{P} \leq 4 \left(1 + \frac{\nu}{k}\right), \quad (6)$$

which is obtained in Section III. A more detailed analysis in Section IV gives

$$\frac{d_{\min}^2}{P} \leq \frac{2^{k+1}}{2^k - 1} \left(1 + \frac{\nu}{k}\right), \quad (7)$$

which is stronger than (6) provided $k > 1$. Let T be another finite set of error events and let $r_1, r_2 \geq 0$ be real numbers satisfying $r_1 + r_2 = 1$. Then,

$$\min_{E \in S \cup T} \{d^2(E)\} \leq r_1 \left(\frac{1}{|S|} \sum_{E \in S} d^2(E)\right) + r_2 \left(\frac{1}{|T|} \sum_{E \in T} d^2(E)\right), \quad (8)$$

since the minimum of a set of real numbers is bounded above by any weighted average of those numbers. In Section V, by choosing S, T, r_1 , and r_2 , appropriately, we prove

$$\frac{d_{\min}^2}{P} \leq \left(\frac{2^{2k+1}}{2^{2k} - 1}\right) \left(2 + \frac{\nu}{k}\right). \quad (9)$$

This bound is stronger than (7) provided $\nu > k(2^k - 1)$. Combining (7)

and (9) we have

$$\frac{d_{\min}^2}{P} \leq \min \left[\frac{2^{k+1}}{2^k - 1} \left(1 + \frac{\nu}{k} \right), \frac{2^{2k+1}}{2^{2k} - 1} \left(2 + \frac{\nu}{k} \right) \right]. \quad (10)$$

Extensions of bounds (6), (7), and (9) to the case when k does not divide ν are given in Appendix B.

II. A GROUP ACTION ON THE TRELIS

In later sections we obtain upper bounds on d_{\min}^2/P by considering sets of error events that are fixed by a group of symmetries of the trellis. In this section we describe the group.

We consider trellis codes with 2^ν states transmitting k bits/channel symbol and for simplicity we assume that k divides ν . States are labelled with binary ν tuples, and edges of the trellis are labelled with binary $\nu + k$ tuples. We identify the binary r tuple (b_0, \dots, b_{r-1}) with the integer

$$b_0 2^0 + b_1 2^1 + \dots + b_{r-1} 2^{r-1}.$$

The states are labelled with binary ν tuples $00 \dots 0, 10 \dots 0, 010 \dots 0, 110 \dots 0, \dots, 11 \dots 1$, in increasing order, from top to bottom as in Fig. 1. The edges are labelled with binary $\nu + k$ tuples $x_0 = x(0 \dots 0), x_1 = x(10 \dots 0), x_2 = x(010 \dots 0), x_3 = x(110 \dots 0), \dots, x_{2^{r+k}-1} = x(11 \dots 1)$, also in increasing order, from top to bottom as in Fig. 1. Set $N = (\nu + k)/k$. If we write an edge label as $x(s_0, \dots, s_{N-1})$, then it will be understood that each s_j is a binary k tuple. A "+" appearing in the argument of a label means bit-by-bit modulo 2 addition. A similar notation will be used for states.

We define a group of symmetries of the trellis. These symmetries will map error events of length L to error events of length L . For each binary $\nu + k$ tuple t , we define a permutation g_t of the edge labels $x(s)$ by the rule

$$g_t(x(s)) = x(s + t). \quad (11)$$

For example, when $k = 1, \nu = 2$, and $t = (010)$,

$$\underline{x} = \begin{bmatrix} x(000) \\ x(100) \\ x(010) \\ x(110) \\ x(001) \\ x(101) \\ x(011) \\ x(111) \end{bmatrix} \mapsto g_{010}(\underline{x}) = \begin{bmatrix} x(010) \\ x(110) \\ x(000) \\ x(100) \\ x(011) \\ x(111) \\ x(001) \\ x(101) \end{bmatrix} \quad (12)$$

Similarly, the permutation g_{t^1} permutes encoder states at time 1 and encoder states at time 2. If we want to map error events to error events, then the action of g_{t^1} on encoder states at time 1 must be given by (16). Choose $t^1 = 001$, $t^2 = 100$, $t^3 = 010$, $t^4 = 001, \dots$. The action of g_{t^0} , g_{t^1} , and g_{t^2} on components 0, 1, and 2 is shown in Fig. 4. Thus the sequence $(g_{t^0}, g_{t^1}, g_{t^2}, \dots)$ transforms the error event shown in Fig. 2 to the error event shown in Fig. 5.

For general k and ν , let $t = t^0 = (t_0, \dots, t_{N-1})$ where $N = (k + \nu)/k$ and t_0, \dots, t_{N-1} are binary k tuples. Let $t^1 = (t_{N-1}, t_0, \dots, t_{N-2})$ be the vector obtained from t^0 by cycling the blocks of k bits to the right and moving the last block, t_{N-1} , to the front. Repeat this operation i times to obtain $t^i = (t_{N-i}, \dots, t_{N-1}, t_0, \dots, t_{N-i-1})$. For $i \geq N$ we view i as an integer modulo N . Thus $t^N = t^0 = t$, $t^{N+1} = t^1, \dots$. The action of g_{t^i} on encoder states at time i coincides with that of $g_{t^{i-1}}$ being given by the rule

$$s \mapsto (t_{N-i+1}, \dots, t_{N-1}, t_0, \dots, t_{N-i-1}) + s. \quad (17)$$

If $\mathbf{G}_{k,\nu}^* = \{(g_{t^0}, g_{t^1}, \dots) | t^0 \text{ is a binary } k \text{ tuple}\}$, then $\mathbf{G}_{k,\nu}^*$ is a group of $2^{\nu+k}$ symmetries of the trellis. The group $\mathbf{G}_{k,\nu}^*$ is abelian, and every element has order 2. We denote $(g_{t^0}, g_{t^1}, \dots)$ by $g_{t^0}^*$, since it is determined by t^0 .

Lemma 2: If $i \geq 0$ and if $x(s)$, $x(t)$ are any pair of edge labels in component i , then there is a unique element of $\mathbf{G}_{k,\nu}^*$ that interchanges $x(s)$ and $x(t)$.

Proof: This follows from Lemma 1, since the restriction of $\mathbf{G}_{k,\nu}^*$ to the edges in component i is just $\mathbf{G}_{k,\nu}$. \square

A set S of error events is said to be *fixed* by $\mathbf{G}_{k,\nu}^*$ if for all $g \in \mathbf{G}_{k,\nu}^*$ and all $E \in S$ we have $g(E) \in S$.

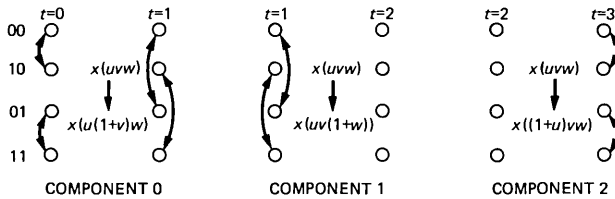


Fig. 4—Action of g_{t^0} , g_{t^1} , and g_{t^2} .

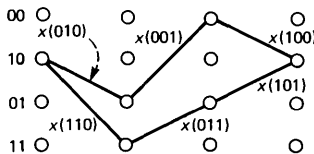


Fig. 5—The symmetry $(g_{t^0}, g_{t^1}, g_{t^2}, \dots)$ applied to an error event.

Lemma 3: Let $i \geq 0$ and let S be a set of error events of the same length that is fixed by $G_{k,\nu}^$. If $m_i(x(a))$ is the total number of times the edge label $x(a)$ occurs in component i of the error events of S , then*

$$m_i(x(a)) = \frac{2|S|}{2^{k+\nu}} \quad \text{for all } \nu + k \text{ tuples } a.$$

Proof: Let s, t be binary $\nu + k$ tuples. By Lemma 2 there is an element of $G_{k,\nu}^*$ interchanging error events involving $x(s)$ in component i with error events involving $x(t)$ in component i . Hence $m_i(x(s)) = m_i(x(t))$. Since the total number of edges in component i is $2|S|$, we have $m_i(x(a)) = 2|S|/2^{k+\nu}$ for all $\nu + k$ tuples a .

An orbit S of the group $G_{k,\nu}^*$ is a set of error events satisfying

1. if $E \in S$ and $g \in G_{k,\nu}^*$ then $g(E) \in S$, and
2. if $E_1, E_2 \in S$ then there exists $g \in G_{k,\nu}^*$ such that $g(E_1) = E_2$.

Fig. 6 shows an orbit of $G_{1,2}^*$. Observe that $m_i(x(a)) = 1$ for all i and for all a .

III. THE FIRST BOUND

In this section we derive the upper bound

$$\frac{d_{\min}^2}{P} \leq 4 \left(1 + \frac{\nu}{k} \right).$$

This bound will be strengthened in later sections but it seems worth presenting the simpler argument here.

Observe that the average transmitted signal power is simply the average of the transmitted channel symbols, namely

$$P = \frac{1}{2^{\nu+k}} \sum_{i=0}^{2^{\nu+k}-1} x_i^2. \quad (18)$$

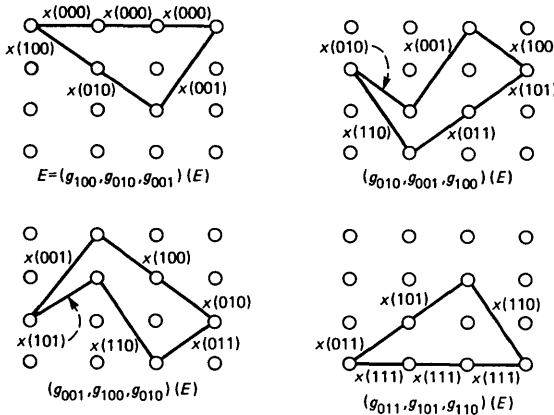


Fig. 6—An orbit of $G_{1,2}^*$.

(Recall that the channel symbol $x(a_0 \cdots a_{\nu+k-1})$ is also denoted x_i where $i = a_0 + a_1 2^1 + \cdots + a_{\nu+k-1} 2^{\nu+k-1}$.) The Euclidean distance between the paths of the error event E shown in Fig. 2 is

$$d^2(E) = (x_0 - x_1)^2 + (x_0 - x_3)^2 + (x_0 - x_5)^2,$$

which is a quadratic form in the variables x_i . In general we define

$$\underline{x}^T = (x_0, x_1, \cdots, x_{2^{\nu+k}-1}), \quad (19)$$

where the superscript T denotes matrix transpose. Then the Euclidean distance $d^2(E)$ between the paths of an error event E is given by

$$d^2(E) = \underline{x}^T A(E) \underline{x}, \quad (20)$$

where $A(E)$ is a symmetric, positive semi-definite matrix which we call the *distance matrix* of E . The distance matrix $A(E)$ has two properties that we wish to note:

Property I. The i th diagonal element of $A(E)$ counts the number of times the symbol x_i occurs in the error event.

Property II. The rows of $A(E)$ sum to zero.

By (18) and (20),

$$\frac{d_{\min}^2}{P} = \min_E \frac{\underline{x}^T A(E) \underline{x}}{P} = 2^{\nu+k} \min_E \frac{\underline{x}^T A(E) \underline{x}}{\underline{x}^T \underline{x}}, \quad (21)$$

where we minimize over all error events E .

Although we will make no use of the fact in this work, we note that in (21) only a finite number of error events need be considered, for no error event need be considered that has a repeated pair of states. Thus, if the pair of states u and w occur at time i and also at a later time j , all components between i and j may be eliminated and the remainder of the error event after time j may be placed after time i . Since components cannot make a negative contribution to $d^2(E)$ the new error event has distance no greater than the original one. By (21) the best normalized minimum distance that can be achieved for any choice of channel symbols is

$$2^{\nu+k} \max_x \min_E \frac{\underline{x}^T A(E) \underline{x}}{\underline{x}^T \underline{x}}. \quad (22)$$

Consider an error event E with initial state (time $t = 0$) $a = (a_1, \cdots, a_{N-1})$ and final state $z = (z_1, \cdots, z_{N-1})$. If k tuples b_1, b_1^* are input at time 0, then at time 1 the two paths occupy states $(b_1, a_1, \cdots, a_{N-2})$ and $(b_1^*, a_1, \cdots, a_{N-2})$. There must be at least $N - 1$ further inputs before the paths can remerge. To remerge at z , the k tuples $z_{N-1}, z_{N-2}, \cdots, z_1$ must be input in that order to both paths. We denote this error event by $E(a, z; b_1, b_1^*)$. Thus, the minimal length

of an error event is $N = (k + \nu)/k$. Fig. 2 shows the error event $E(00, 00; 0, 1)$ which has minimal length 3.

Given an arbitrary set S of error events, define

$$Q(S) = \frac{1}{|S|} \sum_{E \in S} A(E). \quad (23)$$

Let S^N be the set of all error events of length N . Note that S^N is fixed by the group $\mathbf{G}_{k,\nu}^*$.

Theorem 1: If k divides ν then the normalized minimum distance of any sliding window trellis code with 2^ν states and rate k bits/channel symbol satisfies

$$\frac{d_{\min}^2}{P} \leq 4 \left(1 + \frac{\nu}{k} \right).$$

Proof: By (22),

$$\begin{aligned} \frac{d_{\min}^2}{P} &\leq 2^{\nu+k} \max_{\underline{x}} \min_E \frac{\underline{x}^T A(E) \underline{x}}{\underline{x}^T \underline{x}} \\ &\leq 2^{\nu+k} \max_{\underline{x}} \min_{E \in S^N} \frac{\underline{x}^T A(E) \underline{x}}{\underline{x}^T \underline{x}} \\ &\leq \frac{2^{\nu+k}}{|S^N|} \max_{\underline{x}} \frac{\underline{x}^T \left(\sum_{E \in S^N} A(E) \right) \underline{x}}{\underline{x}^T \underline{x}}. \end{aligned}$$

The last inequality simply states that the minimum is not more than the average. Setting $A_N = \sum_{E \in S^N} A(E)$, we have

$$\frac{2^{\nu+k}}{|S^N|} \max_{\underline{x}} \frac{\underline{x}^T A_N \underline{x}}{\underline{x}^T \underline{x}} = \frac{2^{\nu+k}}{|S^N|} \lambda_1(A_N),$$

where $\lambda_1(A_N)$ denotes the largest eigenvalue of A_N . By Property I, the i th diagonal entry of A_N counts the total number of times the edge x_i appears in some component of the error events of length N . By Lemma 3 all diagonal entries are equal to $2N|S^N|/2^{\nu+k}$. Property II implies that all row sums of A_N are zero. By the Gersgorin Circle Theorem⁵

$$\lambda_1(A_N) \leq 2(\text{diagonal entry}) = 2 \left(\frac{2N|S^N|}{2^{\nu+k}} \right),$$

and so

$$\frac{d_{\min}^2}{P} \leq 4N = 4 \left(1 + \frac{\nu}{k} \right). \quad \square$$

Remarks: In Section IV we derive a formula for $Q(S^N)$, and, by computing $\lambda_1(A_N)$, we prove

$$\frac{d_{\min}^2}{P} \leq \frac{2^{k+1}}{2^k - 1} \left(1 + \frac{\nu}{k} \right).$$

In Appendix B we prove that if $\nu = (N - 1)k + l$, where $0 \leq l < k$, then

$$\frac{d_{\min}^2}{P} \leq 4 \left(1 + \left\lfloor \frac{\nu}{k} \right\rfloor \right),$$

where $\lfloor y \rfloor$ denotes the integer part of y .

IV. A FORMULA FOR $Q(S^N)$ AND A SHARPER BOUND

In this section we derive a formula for $Q(S^N)$, the matrix obtained by averaging the distance matrices of all error events of minimal length $N = (k + \nu)/k$. We require a matrix representation of the group $G_{k,\nu}$.

If A is an $m \times n$ matrix and B is an $m_1 \times n_1$ matrix, then the tensor product $A \otimes B$ (also called the Kronecker product) is the $mm_1 \times nn_1$ matrix

$$A \otimes B = \begin{bmatrix} a_{11}B & a_{12}B & \cdots & a_{1n}B \\ a_{21}B & a_{22}B & \cdots & a_{2n}B \\ \cdot & \cdot & \cdots & \cdot \\ a_{m1}B & a_{m2}B & \cdots & a_{mn}B \end{bmatrix}.$$

Tensor products are discussed in Ref. 5, where they are called direct products. For appropriately sized matrices, A , B , C , and D , we have $(A \otimes B)(C \otimes D) = (AC) \otimes (BD)$. If λ is an eigenvalue of A with associated eigenvector v , and μ is an eigenvalue of B with associated eigenvector w , then $\lambda\mu$ is an eigenvalue of $A \otimes B$ with eigenvector $v \otimes w$.

We denote the $n \times n$ identity matrix by I_n and we abbreviate I_2 to I . Set

$$A = \begin{bmatrix} 0 & 1 \\ 1 & 0 \end{bmatrix}. \tag{24}$$

matrices $M(t)$ in $\mathbf{G}_{k,\nu}$. To calculate $\lambda_1(Q(S^N))$ we need to work with eigenvectors and eigenvalues of the matrices $M(t)$.

The matrices $M(t)$ are symmetric and they all commute; hence, they can be simultaneously diagonalized. Let H be the tensor product of $\nu + k$ copies of

$$\frac{1}{\sqrt{2}} \begin{bmatrix} 1 & 1 \\ 1 & -1 \end{bmatrix}.$$

Observe that $H^{-1} = H^T$. Since $(1, 1)^T$ and $(1, -1)^T$ are eigenvectors of A , the columns of H are eigenvectors of $M(t)$ for all $\nu + k$ tuples t . Thus, $H^T M(t) H$ is diagonal for every matrix $M(t)$ in $\mathbf{G}_{k,\nu}$. If $p = (p_0, \dots, p_{\nu+k-1})$ is a binary $\nu + k$ tuple, define

$$w(p) = w_{\nu+k-1} \otimes \dots \otimes w_1 \otimes w_0,$$

where

$$w_j = \begin{cases} (1, 1)^T, & \text{if } p_j = 0 \\ (1, -1)^T, & \text{if } p_j = 1. \end{cases} \quad (29)$$

The vectors $w(p)$ are the columns of H . Note that $w(p)$ is formed by reversing the vector p . We have $A(1, 1)^T = (1, 1)^T$ and $A(1, -1)^T = -(1, -1)^T$. If $t = (t_0, \dots, t_{\nu+k-1})$ then by (27) and (29)

$$\begin{aligned} M(t)w(p) &= \bigotimes_{j=0}^{\nu+k-1} M_j w_j = \left(\prod_{j=0}^{\nu+k-1} (-1)^{t_j p_j} \right) w(p) \\ &= (-1)^{p \cdot t} w(p), \end{aligned} \quad (30)$$

where $p \cdot t$ is the dot product of the vectors p and t .

Lemma 5: Suppose R is a diagonalizable matrix that commutes with every matrix $M(t)$ in $\mathbf{G}_{k,\nu}$. Then R is a linear combination of the matrices $M(t)$ in $\mathbf{G}_{k,\nu}$.

Proof: If s, t are different $\nu + k$ tuples, then by Lemma 1, $g_s(x_0) \neq g_t(x_0)$. The permutation matrices $M(t)$ are therefore linearly independent because the 1's in row 0 are in different positions. Thus we have $2^{\nu+k}$ linearly independent diagonal matrices $H^{-1}M(t)H$. Since R commutes with every matrix $M(t)$, $H^{-1}RH$ commutes with every matrix $H^{-1}M(t)H$, and therefore $H^{-1}RH$ is diagonal. The matrices $H^{-1}M(t)H$ span the set of diagonal matrices so $H^{-1}RH$ is a linear combination of matrices $H^{-1}M(t)H$ and the lemma follows. \square

Lemma 6: If S is a set of error events fixed by $\mathbf{G}_{k,\nu}^*$, then $(\sum_{E \in S} A(E))$ is a linear combination of the matrices $M(t)$ in $\mathbf{G}_{k,\nu}$.

Proof: The distance matrix $A(E)$ of an error event is the sum of contributions from each component:

$$A(E) = \sum_c A_c(E), \quad (31)$$

where we sum over the components c of E . The restriction of $\mathbf{G}_{k,\nu}^*$ to the edges in any component c is just the group $\mathbf{G}_{k,\nu}$. If edges $x(s), x(\hat{s})$ appear in component c of error event E , then edges $g_t(x(s)), g_t(x(\hat{s}))$ appear in component c of error event $E' = g_t(E)$. We have

$$A_c(E') = M(t)^T A_c(E) M(t). \quad (32)$$

Since $M(t)$ is a permutation matrix and $M(t)^2 = I$, we have $M(t)^T = M(t)^{-1}$. Now g_t merely permutes the error events in S , so that by (32),

$$\begin{aligned} \sum_{E \in S} A_c(E) &= \sum_{E \in S} A_c(g_t(E)) = \sum_{E \in S} M(t)^{-1} A_c(E) M(t) \\ &= M(t)^{-1} \left(\sum_{E \in S} A_c(E) \right) M(t) \end{aligned} \quad (33)$$

for all matrices $M(t)$ and for all components c . Summing (33) over all components c finishes the proof. \square

Example: If S is the orbit of error events shown in Fig. 6 then

$$\begin{aligned} \sum_{E \in S} A(E) &= \begin{array}{|cccc|} \hline 3 & -1 & -1 & -1 \\ -1 & 3 & & -1 \\ \hline -1 & & 3 & -1 \\ & -1 & -1 & 3 \\ \hline -1 & & & 3 & -1 & -1 \\ & -1 & & -1 & 3 & -1 \\ \hline & & -1 & -1 & & 3 & -1 \\ & & & -1 & -1 & -1 & 3 \\ \hline \end{array} \\ &= 3I \otimes I \otimes I - (I \otimes I \otimes A + I \otimes A \otimes I + A \otimes I \otimes I). \end{aligned} \quad (34)$$

Consider S^N , the set of all error events $E(a, z; b_1, b_1^*)$ of minimal length $N = (k + \nu)/k$. Recall that $a = (a_1, \dots, a_{N-1})$ is the initial state, $z = (z_1, \dots, z_{N-1})$ is the final state, and b_1, b_1^* are the first pair of inputs. We have $|S^N| = \binom{2^k}{2} 2^\nu \cdot 2^\nu$.

Lemma 7:

(1) Let $t = (t_0, \dots, t_{N-1})$ and let $t' = (t_1, \dots, t_{N-1})$ where $t_i, i = 0, 1, \dots, N-1$, is a binary k tuple. If $g_t^* = (g_t^0, g_t^1, \dots, g_t^{N-1}) \in \mathbf{G}_{k,\nu}^*$, then

$$g_t^*(E(a, z; b_1, b_1^*)) = E(a + t', z + t', b_1 + t_0, b_1^* + t_0). \quad (35)$$

(2) The group $\mathbf{G}_{k,\nu}^*$ partitions the set S^N of error events of length N into $2^\nu(2^k - 1)$ orbits each of size $2^{\nu+k-1}$.

Proof: Part (1) follows from the definition of g_t^* given in (17). To verify part (2) we note that $E(a, z; b_1, b_1^*)$ is fixed only by the symmetry g_b^* , where $b = (b_1 + b_1^*, 0, 0, \dots, 0)$. Hence, each orbit consists of

$2^{\nu+k-1}$ distinct error events. Since the total number of error events in S^N is $(2^\nu \cdot 2^\nu (2^k - 1))/2$, we see that there are $2^\nu (2^k - 1)$ orbits. \square

The orbit containing the error event $E(a, z; b_1, b_1^*)$ is determined by $a + z$ and $b_1 + b_1^*$. Setting $f = b_1 + b_1^*$, we denote this orbit by $S(a + z; f)$. This orbit contains $E(a, z; 0, f)$; note that $f \neq 0$ because $b_1 \neq b_1^*$. Recall that if f is a k tuple, then the $\nu + k$ tuple $(f0 \dots 0)^i$ equals $(y_0, y_1, \dots, y_{N-1})$ where $y_i = f$ and $y_j = 0$ for $j \neq i$.

Lemma 8: Let S^N be the set of all error events of length N and let $S(a + z; f)$ be the orbit of $\mathbf{G}_{k,\nu}^*$ containing the error event $E(a, z; 0, f)$. Then

$$(1) \quad 2^{\nu+k} Q(S(a + z; f)) = 2NI_{2^{\nu+k}} - 2 \sum_{i=0}^{N-1} M((f0 \dots 0)^i) \quad (36)$$

$$(2) \quad 2^{\nu+k} (2^k - 1) Q(S^N) = 2(2^k - 1) NI_{2^{\nu+k}} - 2 \sum_{f \neq 0} \sum_{i=0}^{N-1} M((f0 \dots 0)^i). \quad (37)$$

Proof: We calculate the contribution to $Q(S(a + z; f))$ made by pairs of edges in component 0. Since the restriction of $\mathbf{G}_{k,\nu}^*$ to the edges in any component is just the group $\mathbf{G}_{k,\nu}$, this distance contribution is

$$\begin{aligned} & \frac{1}{2^{\nu+k}} \sum_t [g_t(x(0a_1 \dots a_{N-1})) - g_t(x(fa_1 \dots a_{N-1}))]^2 \\ &= \frac{1}{2^{\nu+k}} \sum_t [x(t + (0a_1 \dots a_{N-1})) - x(t + (fa_1 \dots a_{N-1}))]^2 \\ &= \frac{1}{2^{\nu+k}} \left[2 \sum_t x(t)^2 - 2 \sum_t x(t)x(t + (f0 \dots 0)) \right] \\ &= \frac{1}{2^{\nu+k}} \underline{x}^T [2I_{2^{\nu+k}} - 2M(f0 \dots 0)] \underline{x}. \end{aligned}$$

In general, the distance contribution made by edges in component i is

$$\begin{aligned} & \frac{1}{2^{\nu+k}} \sum_t [g_t(x(z_{N-i} \dots z_{N-1} 0a_1 \dots a_{N-i-1})) \\ & \quad - g_t(x(z_{N-i} \dots z_{N-1} fa_1 \dots a_{N-i-1}))]^2 \\ &= \frac{1}{2^{\nu+k}} \sum_t [x(t + (z_{N-i} \dots z_{N-1} 0a_1 \dots a_{N-i-1})) \\ & \quad - x(t + (z_{N-i} \dots z_{N-1} fa_1 \dots a_{N-i-1}))]^2 \\ &= \frac{1}{2^{\nu+k}} \underline{x}^T [2I_{2^{\nu+k}} - 2M((f0 \dots 0)^i)] \underline{x}. \quad (38) \end{aligned}$$

Summing (38) over all components i , we obtain (36). Since (36) is independent of $a + z$, we obtain the formula for $Q(S^N)$ by summing (36) over all nonzero k tuples f . \square

Remark: When $k = 1$, there is only one choice for f , namely $f = 1$, and so every form $Q(S(a + z; f))$ is equal to $Q(S^N)$. For $k = 1, \nu = 2$, we have

$$\begin{aligned} Q(S(00; 1)) &= Q(S(10; 1)) = Q(S(01; 1)) = Q(S(11; 1)) = Q(S^3) \\ &= 1/4[3I_8 - (I \otimes I \otimes A + I \otimes A \otimes I + A \otimes I \otimes I)] \end{aligned}$$

[see the matrix given as (34)]. However, for $k > 1$, the form $Q(S(a + z; f))$ will change with f . Thus, for $k = 2, \nu = 4$, we have

$$\begin{aligned} Q(S(a + z; 11)) &= 1/32[3I_{64} - (I_4 \otimes I_4 \otimes (A \otimes A) \\ &\quad + I_4 \otimes (A \otimes A) \otimes I_4 + (A \otimes A) \otimes I_4 \otimes I_4)], \end{aligned}$$

while

$$\begin{aligned} Q(S(a + z; 10)) &= 1/32[3I_{64} - (I_4 \otimes I_4 \otimes (I \otimes A) \\ &\quad + I_4 \otimes (I \otimes A) \otimes I_4 + (I \otimes A) \otimes I_4 \otimes I_4)]. \end{aligned}$$

Theorem 2: If k divides ν , then the normalized minimum distance of any sliding window trellis code with 2^ν states and rate k bits/channel symbol satisfies

$$\frac{d_{\min}^2}{P} \leq \frac{2^{k+1}}{2^k - 1} \left(1 + \frac{\nu}{k} \right).$$

Proof: From the proof of Theorem 1, we have

$$\begin{aligned} \frac{d_{\min}^2}{P} &\leq 2^{\nu+k} \lambda_1[Q(S^N)] \\ &= \frac{1}{2^k - 1} \lambda_1(Q_N), \end{aligned} \tag{39}$$

where $Q_N = (2^k - 1)2^{\nu+k}Q(S^N)$. Let $c = (c_0, \dots, c_{N-1})$ be a binary $\nu + k$ tuple and let γ be the number of nonzero k tuples c_i . Then by (30), the eigenvalue of Q_N associated with $w(c)$ is

$$\begin{aligned} &2(2^k - 1)N - 2 \sum_{f \neq 0} \sum_{i=0}^{N-1} (-1)^{c_i \cdot f} \\ &= 2(2^k - 1)N - 2 \sum_{i=0}^{N-1} \sum_{f \neq 0} (-1)^{c_i \cdot f}, \end{aligned} \tag{40}$$

where we sum over all nonzero k tuples f . Since

$$\sum_{f \neq 0} (-1)^{c_i f} = \begin{cases} 2^k - 1, & \text{if } c_i = 0 \\ -1, & \text{if } c_i \neq 0, \end{cases}$$

eq. (40) becomes

$$2(2^k - 1)N - 2[(2^k - 1)(N - \gamma) - \gamma] = 2^{k+1}\gamma. \quad (41)$$

The largest eigenvalue of Q_N is obtained when $\gamma = N = (1 + (\nu/k))$. The theorem now follows from (39). \square

Remarks: Observe that the largest eigenvalue of $Q(S^N)$ is associated with $w(c)$, where c_0, c_1, \dots, c_{N-1} are all nonzero. For example, with $k = 1$, the largest eigenvalue, $4(1 + (\nu/k))$ has multiplicity one and is associated with the eigenvector $(1, -1)^T \otimes (1, -1)^T \otimes \dots \otimes (1, -1)^T$. When $k > 1$, there will be several linearly independent eigenvectors associated with $\lambda_1(Q(S^N))$ because there are several choices for c with all $c_i \neq 0$. Also, note that Theorem 2 gives the same bound as Theorem 1 when $k = 1$. For $k \geq 2$, the bound of Theorem 2 is an improvement.

In Appendix B we prove that if $\nu = (N - 1)k + l$ where $0 \leq l < k$, then

$$\frac{d_{\min}^2}{P} \leq \frac{2^{k-l+1}}{2^{k-l} - 1} \left(1 + \left\lfloor \frac{\nu}{k} \right\rfloor \right),$$

where $\lfloor y \rfloor$ denotes the integer part of y .

V. A FINAL BOUND OBTAINED FROM A WEIGHTED AVERAGE

Let S^{N+1} be the set of all error events of length $N + 1 = 2 + (\nu/k)$. Let $Q(S^{N+1})$ be the matrix obtained by averaging the distance matrices of all error events of length $N + 1$. In this section we derive a formula for $Q(S^{N+1})$ and we prove

$$\frac{d_{\min}^2}{P} \leq \frac{2^{2k+1}}{2^{2k} - 1} \left(2 + \frac{\nu}{k} \right)$$

using a weighted average of $Q(S^N)$ and $Q(S^{N+1})$.

An error event E of length $N + 1$ is determined by the initial state $a = (a_1, \dots, a_{N-1})$, the final state $z = (z_1, \dots, z_{N-1})$, the inputs b_1, b_1^* at time 0, and the inputs b_2, b_2^* at time 1. Since the two paths diverge at time 0, we must have $b_1 \neq b_1^*$. To remerge at z the last $N - 1$ inputs must be the k tuples $z_{N-1}, z_{N-2}, \dots, z_1$ in that order. After N inputs the two paths occupy states $z_2 \dots z_{N-1}b_2$ and $z_2 \dots z_{N-1}b_2^*$. At this stage the two paths must be disjoint so $b_2 \neq b_2^*$. We denote this error event E by $E(a, z; b_1, b_1^*; b_2, b_2^*)$ [equivalently $E(a, z; b_1^*, b_1; b_2^*, b_2)$].

The group $G_{k,\nu}^*$ maps error events of length $N + 1$ to error events of

length $N + 1$. To be specific, let $t = (t_0, \dots, t_{N-1})$ be a $\nu + k$ tuple and set $t' = (t_1, \dots, t_{N-1})$, $t'' = (t_0, \dots, t_{N-2})$. If $g_t^* = (g_t, g_{t^1}, \dots, g_{t^{N-1}}, g_t)$ then it follows from the definition of g_t^* given in (7) that

$$g_t^*(E(a, z; b_1, b_1^*, b_2, b_2^*)) \\ = E(a + t', z + t''; b_1 + t_0, b_1^* + t_0; b_2 + t_{N-1}, b_2^* + t_{N-1}). \quad (42)$$

This group action does not preserve $a + z$ but it does preserve $b_1 + b_1^*$ and $b_2 + b_2^*$. Set $g = b_1 + b_1^*$ and $f = b_2 + b_2^*$. We denote the orbit of $\mathbf{G}_{k,\nu}^*$ containing the error event $E(a', z'; 0, g; 0, f)$ by $S(a', z'; g, f)$ (in the discussion above, $a' = (a_1, \dots, a_{N-2}, a_{N-1} + b_2)$ and $z' = (z_1 + b_1, z_2, \dots, z_{N-1})$). Note that $f, g \neq 0$.

If f, g are k tuples, then the $\nu + k$ tuple $(fg0 \dots 0)^0 = (fg0 \dots 0)$ and $(fg0 \dots 0)^i$ is obtained from $(fg0 \dots 0)^{i-1}$ by cycling the blocks of k bits to the right and moving the last block to the front. Thus $(fg0 \dots 0)^{N-2} = (0 \dots 0fg)$. Define matrices $M_i(fg0 \dots 0)$, $i = 0, \dots, N$ in $\mathbf{G}_{k,\nu}$ as follows:

$$M_0(fg0 \dots 0) = M(g0 \dots 0) \\ M_i(fg0 \dots 0) = M((fg0 \dots 0)^{i-1}) \quad i = 1, \dots, N - 1, \\ M_N(fg0 \dots 0) = M(0 \dots 0f). \quad (43)$$

Example: For $k = 1, \nu = 2$, the orbit $S(00, 00; 1, 1)$ is shown in Fig. 7. The quadratic form $Q(S(00, 00; 1, 1))$ is given by

$$Q(S(00, 00; 1, 1)) = \frac{1}{8} \begin{array}{|c|c|c|c|c|c|} \hline 8 & -2 & & -2 & -2 & -2 \\ -2 & 8 & -2 & & -2 & -2 \\ \hline & -2 & 8 & -2 & -2 & -2 \\ -2 & & -2 & 8 & -2 & -2 \\ \hline & -2 & & -2 & 8 & -2 \\ -2 & & -2 & -2 & 8 & -2 \\ \hline & -2 & & -2 & -2 & 8 \\ -2 & & -2 & -2 & -2 & 8 \\ \hline \end{array} \\ = \frac{1}{8} (8I_8 - 2(I \otimes I \otimes A + I \otimes A \otimes A + A \otimes A \otimes I \\ + A \otimes I \otimes I)) \\ = \frac{1}{8} \left(8I_8 - 2 \sum_{i=0}^3 M_i(110) \right). \quad (44)$$

Lemma 9: Let S^{N+1} be the set of all error events of length $N + 1$ and let $S(a, z; g, f)$ be the orbit of $\mathbf{G}_{k,\nu}^*$ containing the error event $E(a, z; 0, g; 0, f)$. Then,

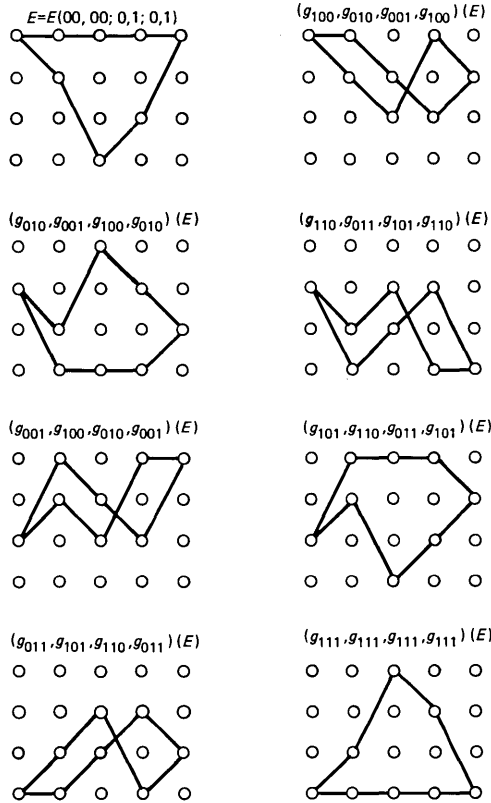


Fig. 7—The orbit $S(00, 00; 1, 1)$.

$$(1) \quad 2^{\nu+k} Q(S(a, z; g, f)) = 2(N+1)I_{2^{\nu+k}} - 2 \sum_{i=0}^N M_i(fg0 \dots 0). \quad (45)$$

$$(2) \quad 2^{\nu+k}(2^k - 1)^2 Q(S^{N+1}) = 2(2^k - 1)^2(N+1)I_{2^{\nu+k}} \\ - 2 \sum_{f, g \neq 0} \sum_{i=0}^N M_i(fg0 \dots 0). \quad (46)$$

Proof: We calculate the contribution to $Q(S(a, z; g, f))$ made by pairs of edges in component 0. This distance contribution is

$$\frac{1}{2^{\nu+k}} \sum_t [x(t + (0a_1 \dots a_{N-1})) - x(t + (ga_1 \dots a_{N-1}))]^2 \\ = \frac{1}{2^{\nu+k}} x^T [2I_{2^{\nu+k}} - 2M(g0 \dots 0)]x$$

as found in the proof of Lemma 8. Similarly, the contribution made

by pairs of edges in component N (the last component of the error events) is

$$\begin{aligned} & \frac{1}{2^{\nu+k}} \sum_t [x(t + (z_1 \cdots z_{N-1}0)) - x(t + (z_1 \cdots z_{N-1}f))]^2 \\ &= \frac{1}{2^{\nu+k}} \underline{x}^T [2I_{2^{\nu+k}} - 2M(0 \cdots 0f)] \underline{x}. \end{aligned}$$

For $i = 1, \dots, N - 1$, the contribution made by pairs of edges in component i is

$$\begin{aligned} & \frac{1}{2^{\nu+k}} \sum_t [x(t + (z_{N-i+1} \cdots z_{N-1}00a_1 \cdots a_{N-i-1})) \\ & \quad - x(t + (z_{N-i+1} \cdots z_{N-1}fga_1 \cdots a_{N-i-1}))]^2 \\ &= \frac{1}{2^{\nu+k}} \left[2 \sum_t x(t)^2 - 2 \sum_t x(t)x(t + (fg0 \cdots 0)^{i-1}) \right] \\ &= \frac{1}{2^{\nu+k}} \underline{x}^T [2I_{2^{\nu+k}} - 2M((fg0 \cdots 0)^{i-1})] \underline{x}. \end{aligned}$$

The sum of the contributions from all $N + 1$ components is

$$Q(S(a, z; g, f)) = \frac{1}{2^{\nu+k}} \underline{x}^T \left[2(N + 1)I_{2^{\nu+k}} - 2 \sum_{i=0}^N M_i(fg0 \cdots 0) \right] \underline{x}.$$

This proves part (1). Observe that (45) is independent of a and z . We obtain $Q(S^{N+1})$ by summing (45) over all pairs g, f of nonzero k tuples. Since there are $(2^k - 1)^2$ such pairs,

$$\begin{aligned} & (2^k - 1)^2 2^{\nu+k} Q(S^{N+1}) \\ &= 2(2^k - 1)^2 (N + 1) I_{2^{\nu+k}} - 2 \sum_{f,g \neq 0} \sum_{i=0}^N M_i(fg0 \cdots 0) \end{aligned}$$

as required. \square

Remarks: When $k = 1$, we must have $f = g = 1$ and so every form $Q(S(a, z; g, f))$ is equal to $Q(S^{N+1})$. In this case, $N = 1 + \nu$ and

$$Q(S^{N+1}) = \frac{1}{2^{\nu+1}} \left[2(2 + \nu) I_{2^{\nu+1}} - 2 \sum_{i=0}^{1+\nu} M_i(110 \cdots 0) \right]$$

[see the matrix given as (44)]. For $k > 1$, there are several choices for f and g . Thus, for $k = 2, \nu = 4$, we have, with $g = (1, 1)$ and $f = (0, 1)$,

$$\begin{aligned} Q(S(a, z; 11, 01)) &= 1/64 [8I_{64} - 2(I_4 \otimes I_4 \otimes (A \otimes A) \\ & \quad + I_4 \otimes (A \otimes A) \otimes (A \otimes I) \\ & \quad + (A \otimes A) \otimes (A \otimes I) \otimes I_4 \\ & \quad + (A \otimes I) \otimes I_4 \otimes I_4], \end{aligned}$$

while with $g = (01)$ and $f = (10)$ we get

$$\begin{aligned} Q(S(a, z; 01; 10)) = & 1/64[8I_{64} - 2(I_4 \otimes I_4 \otimes (A \otimes I) \\ & + I_4 \otimes (A \otimes I) \otimes (I \otimes A) \\ & + (A \otimes I) \otimes (I \otimes A) \otimes I_4 \\ & + (I \otimes A) \otimes I_4 \otimes I_4)]. \end{aligned}$$

Theorem 3: If k divides ν then the normalized minimum distance of any convolutionally derived trellis code with 2^ν states and rate k bits/channel symbol satisfies

$$\frac{d_{\min}^2}{P} \leq \frac{2^{2k+1}}{2^{2k} - 1} \left(2 + \frac{\nu}{k} \right).$$

Proof: If \bar{Q} is any weighted average of $Q(S^N)$ and $Q(S^{N+1})$, then by (8) we have

$$\frac{d_{\min}^2}{P} \leq 2^{\nu+k} \lambda_1(\bar{Q}). \quad (47)$$

Let $\delta = 1/(2^{2k} - 1)$. Then $2(2^k - 1)\delta + (2^k - 1)^2\delta = 1$. Define \bar{Q} to be the following weighted average of $Q(S^N)$ and $Q(S^{N+1})$:

$$\bar{Q} = 2(2^k - 1)\delta Q(S^N) + (2^k - 1)^2\delta Q(S^{N+1}).$$

Set

$$Q_N = 2^{\nu+k}(2^k - 1)Q(S^N)$$

and

$$Q_{N+1} = 2^{\nu+k}(2^k - 1)^2Q(S^{N+1}).$$

Then by (47)

$$\frac{d_{\min}^2}{P} \leq \delta \lambda_1(2Q_N + Q_{N+1}). \quad (48)$$

The eigenvectors, $w(c)$, of Q_N and Q_{N+1} are in 1-1 correspondence with binary vectors $c = (c_1, \dots, c_N)$, where c_i , $i = 1, \dots, N$ are k tuples. By (41)

$$Q_N w(c) = 2^{k+1} \gamma(c) w(c), \quad (49)$$

where $\gamma(c)$ is the number of nonzero k tuples c_i . Introduce k tuples $c_0 = c_{N+1} = 0$ and define

$$\alpha(c) = |\{i | c_i = 0, c_{i+1} \neq 0 \text{ or } c_i \neq 0, c_{i+1} = 0\}|$$

and

$$\beta(c) = |\{i | c_i \neq 0 \text{ and } c_{i+1} \neq 0\}|. \quad (50)$$

There are $(N + 1) - \alpha(c) - \beta(c)$ indices i , $0 \leq i \leq N$, for which $c_i = c_{i+1} = 0$. By (30) the eigenvalue of Q_{N+1} associated with $w(c)$ is

$$\begin{aligned} & 2(2^k - 1)^2(N + 1) - 2 \sum_{f,g \neq 0} \sum_{i=0}^N (-1)^{c_i \cdot f + c_{i+1} \cdot g} \\ &= 2(2^k - 1)^2(N + 1) - 2 \sum_{i=0}^N \left(\sum_{f \neq 0} (-1)^{c_i \cdot f} \right) \left(\sum_{g \neq 0} (-1)^{c_{i+1} \cdot g} \right). \end{aligned} \quad (51)$$

Recall that the sum $\sum_{f \neq 0} (-1)^{c_i \cdot f}$ is $(2^k - 1)$ when $c_i = 0$, but equal to -1 whenever $c_i \neq 0$. Hence (50) is equal to

$$\begin{aligned} & 2(2^k - 1)^2(N + 1) - 2[(N + 1) - \alpha(c) - \beta(c)](2^k - 1)^2 \\ & \quad - \alpha(c)(2^k - 1) + \beta(c)] \\ &= 2(2^k - 1)^2(\alpha(c) + \beta(c)) + 2(2^k - 1)\alpha(c) - 2\beta(c) \\ &= 2^{k+1}(2^k(\alpha(c) + \beta(c)) - 2(\alpha(c) + \beta(c)) + \alpha(c)) \\ &= 2^{k+1}[2^k(\alpha(c) + \beta(c)) - (\alpha(c) + 2\beta(c))]. \end{aligned} \quad (52)$$

Now, $\gamma(c)$ is the number of nonzero c_i 's. Since each nonzero c_i appears in two pairs, (c_{i-1}, c_i) and (c_i, c_{i+1}) , we have

$$\alpha(c) + 2\beta(c) = 2\gamma(c). \quad (53)$$

Substitution in (52) shows that the eigenvalue in (51), of Q_{N+1} associated with $w(c)$ is

$$2^{k+1}[2^k(2\gamma(c) - \beta(c)) - 2\gamma(c)]. \quad (54)$$

By (49) and (54) we have

$$\begin{aligned} & (2Q_N + Q_{N+1})w(c) \\ &= 2^{k+1}(2\gamma(c) + 2^k(2\gamma(c) - \beta(c)) - 2\gamma(c))w(c) \\ &= 2^{2k+1}(2\gamma(c) - \beta(c))w(c). \end{aligned} \quad (55)$$

There are $N - \gamma(c)$ indices i , $1 \leq i \leq N$, for which $c_i = 0$. Since every c_j , $1 \leq j \leq N$, appears in the two pairs (c_{j-1}, c_j) and (c_j, c_{j+1}) , there are at most $2 + 2(N - \gamma(c))$ indices i , $0 \leq i \leq N$, for which $c_i = 0$ or $c_{i+1} = 0$. Hence

$$\beta(c) \geq (N + 1) - 2 - 2(N - \gamma(c)) = 2\gamma(c) - N - 1$$

and

$$2(\gamma(c)) - \beta(c) \leq N + 1. \quad (56)$$

Now (48), (55), and (56) imply

$$\frac{d_{\min}^2}{P} \leq \frac{2^{2k+1}}{2^{2k} - 1} (N + 1) = \frac{2^{2k+1}}{2^{2k} - 1} \left(2 + \frac{\nu}{k} \right). \quad \square$$

Remarks: Equality can hold in (56). If N is odd, set $c_0 = c_2 = \dots = c_{N+1} = 0$ and $c_1, c_3, \dots, c_N \neq 0$. Then $\gamma(c) = (N + 1)/2$ and $\beta(c) = 0$. (Observe that for $k = 1, \nu = 2$, the largest eigenvalue of the form $2Q_N + Q_{N+1}$ is associated with eigenvector $(1, -1)^T \otimes (1, 1)^T \otimes (1, -1)^T$.) If N is even, set $c_0 = c_3 = c_5 = c_7 = \dots = c_{N+1} = 0$ and $c_1, c_2, c_4, c_6, \dots, c_N \neq 0$ to get $\gamma(c) = (N + 2)/2$ and $\beta(c) = 1$. Setting

$$\frac{2^{k+1}}{2^k - 1} \left(1 + \frac{\nu}{k} \right) = \frac{2^{2k+1}}{2^{2k} - 1} \left(2 + \frac{\nu}{k} \right)$$

yields $\nu = k(2^k - 1)$. If $\nu < k(2^k - 1)$, then Theorem 2 gives the stronger bound; if $\nu > k(2^k - 1)$ then Theorem 3 gives the stronger bound. In particular, for $k = 1$, Theorem 3 gives a stronger bound for any $\nu > 1$.

The bound given by Theorem 3 is obtained from the largest eigenvalue of a particular weighted average of $Q(S^N)$ and $Q(S^{N+1})$. In Appendix A we use the duality theorem of linear programming to prove that no other weighted average of $Q(S^N)$ and $Q(S^{N+1})$ gives a stronger bound.

In Appendix B we prove that if $\nu = (N - 1)k + l$, where $0 \leq l < k$, then

$$\frac{d_{\min}^2}{P} \leq \frac{2^{2(k-l)+1}}{2^{2(k-l)} - 1} \left(2 + \left\lfloor \frac{\nu}{k} \right\rfloor \right),$$

where $\lfloor y \rfloor$ denotes the integer part of y .

VI. CONCLUSIONS

Three upper bounds on the normalized minimum distance, (d_{\min}^2/P) , have been given for trellis codes. The bound

$$\frac{d_{\min}^2}{P} \leq 4 \left(1 + \frac{\nu}{k} \right)$$

given in Theorem 1 is typical. This certainly provides nontrivial information. For example, is it possible to gain 10 dB in minimum distance using $2^6 = 64$ states at rate 1 bit/symbol? The answer is no. Theorem 1 bounds the gain at 8.4 dB; Theorem 3 bounds the gain at 7.3 dB. Nevertheless, there still remain the questions of how tight these bounds are and if they exhibit the "right" dependence on the

Table I—Possible gains at rate
1 bit/symbol

ν	Lower Bound (Ungerboeck)	Upper Bounds	
		Theorems 1 and 2	Theorem 3
2	2.5 db	4.7 db	4.3 db
3	3	6.0	5.2
4	3.4	7.0	6.0
5	4.2	7.8	6.7
6	4.5	8.4	7.3
7	5.1	9.0	7.8
8	5.3	9.5	8.2
9	5.6	10.0	8.6
10	5.8	10.4	9.0
11	6	10.7	9.4

parameters ν and k . For example, consider the normalized minimum distance for block codes of length n , having 2^{nk} code words (k bits/symbol). In that case, known upper bounds behave, for large n , like $d^2/P \lesssim 2n/4^k$. Thus the linear dependence on ν , a quantity analogous to block length, appears correct. However, the true dependence on k may be different from our bound. Table I gives upper and lower bounds on the gain (in dB) that is possible at rate 1 bit/channel symbol. The lower bounds arise from codes constructed by Ungerboeck.⁴

Also minimum distance is by no means the complete story with regard to error rate. The heuristics leading to the claim that terms involving d_{\min} would dominate an upper bound on the error rate make the assumption that the infinite series determining the upper bound converges. Even if a code with a good d_{\min} were found, an upper bound on error rate should still be computed for that particular code. As an example of a catastrophe that may occur, consider the assignment of edge labels $\underline{x}^T = (1, -1, -1, 1, -1, 1, 1, -1)$ to the trellis of Fig. 1. One observes that a pair of edges leaving a node always contributes $(1 - (-1))^2 = 4$ to the distance and similarly for a pair of edges merging into a node. One immediately concludes that no error event has distance less than 8 for this edge assignment. Since $P = 1$, this is a 3 dB gain over the uncoded ± 1 situation. How could this happen with only ± 1 symbols? One answer is that we forgot to include unmerged events, events which go on forever. We had implicitly assigned infinity to their distance, but now some have distance 4. However, this could be rectified by perturbing the ± 1 edge labels by small amounts. A more serious trouble with this code is that an infinite number of error events have (essentially) the minimum distance and so a coefficient that we did not explicitly consider turns out to be infinite for this particular code.

REFERENCES

1. A. D. Wyner, "On Coding and Information Theory," *SIAM Review*, 11, No. 3 (July 1969), pp. 317-46.
2. F. J. MacWilliams and N. J. A. Sloane, *The Theory of Error-Correcting-Codes*, Amsterdam: North-Holland and New York: Elsevier/North-Holland, 1977.
3. G. D. Forney, "The Viterbi Algorithm," *Proc. IEEE*, 61, No. 3 (March 1973), pp. 268-78.
4. G. Ungerboeck, "Channel Coding with Multilevel/Phase Signals," *IEEE Trans. Inform. Theory*, IT-28, No. 1 (January, 1982), pp. 55-67.
5. Peter Lancaster, *Theory of Matrices*, New York: Academic Press, 1969.

APPENDIX A

The upper bound of Theorem 3 is obtained from the largest eigenvalue of a particular weighted average of the quadratic forms $Q(S^N)$ and $Q(S^{N+1})$. In this appendix we prove that no other weighted average gives a stronger bound. We shall assume throughout that $\nu \geq k(2^k - 1)$ since the bound given in Theorem 3 improves upon that given in Theorem 2 only for ν in this range.

If $r_1, r_2 \geq 0$ and $r_1 + r_2 = 1$, then

$$\frac{d_{\min}^2}{P} \leq 2^{\nu+k} \lambda_1(r_1 Q(S^N) + r_2 Q(S^{N+1})).$$

Recall from (29) that the eigenvectors $w(c)$ of $Q(S^N)$ and $Q(S^{N+1})$ are 1:1 correspondence with binary $\nu + k$ tuples c . Let $c = (c_1, \dots, c_N)$, where $c_i, i = 1, \dots, N$ is a binary k tuple and let $c_0 = c_{N+1} = 0$. Recall that

$$\alpha(c) = |\{i | c_i = 0, c_{i+1} \neq 0 \text{ or } c_i \neq 0, c_{i+1} = 0\}|,$$

$$\beta(c) = |\{i | c_i \neq 0 \text{ and } c_{i+1} \neq 0\}|,$$

and

$$\gamma(c) = |\{i | c_i \neq 0\}|.$$

Define $\phi_N(c)$ and $\phi_{N+1}(c)$ by $2^{\nu+k}(2^k - 1)Q(S^N)w(c) = \phi_N(c)w(c)$ and $2^{\nu+k}(2^k - 1)^2Q(S^{N+1})w(c) = \phi_{N+1}(c)w(c)$. Then by (49) and (54)

$$\phi_N(c) = 2^{k+1}\gamma(c) \tag{57}$$

and

$$\phi_{N+1}(c) = 2^{k+1}[2^k(2\gamma(c) - \beta(c)) - 2\gamma(c)]. \tag{58}$$

To find the optimal weighted average we have to solve the following linear programming problem.

Choose real variables $r_1, r_2, r \geq 0$ so as to minimize r subject to the inequalities

$$-(r_1 + r_2) \leq -1 \tag{59}$$

and

$$r_1 \frac{\phi_N(c)}{2^k - 1} + r_2 \frac{\phi_{N+1}(c)}{(2^k - 1)^2} - r \leq 0, \quad \text{for all } \nu + k \text{ tuples } c.$$

In Theorem 3 we proved that a feasible solution to (43) is

$$r_1 = \frac{2}{2^k + 1}, \quad r_2 = \frac{2^k - 1}{2^k + 1}, \quad r = \frac{2^{2k+1}}{2^{2k} - 1} \left(2 + \frac{\nu}{k} \right). \quad (60)$$

The linear program (59) is the dual of the primal linear program given below.

Choose real variables $a_c, a \geq 0$, where the index c runs through all binary $\nu + k$ tuples, so as to maximize a subject to the inequalities

$$\begin{aligned} \frac{1}{2^k - 1} \left(\sum_c \phi_N(c) a_c \right) - a &\geq 0 \\ \frac{1}{(2^k - 1)^2} \left(\sum_c \phi_{N+1}(c) a_c \right) - a &\geq 0 \\ - \left(\sum_c a_c \right) &\geq -1. \end{aligned} \quad (61)$$

If we can find a feasible solution to (61) with

$$a = \frac{2^{2k+1}}{2^{2k} - 1} \left(2 + \frac{\nu}{k} \right),$$

then by the duality theorem of linear programming,² (60) is an optimal solution to (59). We consider two cases.

Case 1. N odd

Pick $f = (f_1, \dots, f_N)$, where $f_i, i = 1, \dots, N$ is a binary k tuple and every f_i is nonzero. Pick $g = (g_1, \dots, g_N)$, where $g_i, i = 1, \dots, N$ is a binary k tuple and $g_i \neq 0$ if and only if i is odd. Then $\gamma(f) = N, \beta(f) = N - 1$ and $\gamma(g) = (N + 1)/2, \beta(g) = 0$. By (57) and (58), $\phi_N(f), \phi_N(g), \phi_{N+1}(f)$, and $\phi_{N+1}(g)$ are as follows:

	f	g
ϕ_N	$2^{k+1}N$	$2^k(N + 1)$
ϕ_{N+1}	$2^{k+1}[2^k(N + 1) - 2N]$	$2^{k+1}[(2^k - 1)(N + 1)]$

Set

$$a_c = \begin{cases} \left(\frac{2^k - 1}{2^k + 1} \right) \left(\frac{N + 1}{N - 1} \right), & \text{if } c = f \\ 1 - a_f = \frac{2(N - 2^k)}{(2^k + 1)(N - 1)}, & \text{if } c = g \\ 0, & \text{otherwise,} \end{cases}$$

$$a = \frac{2^{2k+1}}{2^{2k} - 1} \left(2 + \frac{\nu}{k} \right). \quad (62)$$

Direct calculation shows that (62) is a feasible solution to (61). (Since $\nu \geq k(2^k - 1)$, the variables a_c are all nonnegative.)

Case 2. N even

Pick $h = (h_1, \dots, h_N)$, where $h_i, i = 1, \dots, N$, is a binary k tuple, $h_2 = h_5 = h_7 = h_9 = \dots = h_{N-1} = 0$, and $h_1, h_3, h_4, h_6, h_8, \dots, h_N$ are nonzero. Then $\gamma(h) = (N + 2)/2$, $\beta(h) = 1$ and, by (57) and (58),

$$\phi_N(h) = 2^k(N + 2) \quad \text{and} \quad \phi_{N+1}(h) = 2^{k+1}[(2^k - 1)(N + 2) - 2^k].$$

Set

$$a_c = \begin{cases} \frac{(2^k - 1)N - 2}{(2^k + 1)(N - 2)}, & \text{if } c = f \\ 1 - a_f = \frac{2(N - 2^k)}{(2^k + 1)(N - 2)}, & \text{if } c = g \\ 0, & \text{otherwise,} \end{cases}$$

$$a = \frac{2^{2k+1}}{2^{2k} - 1} \left(2 + \frac{\nu}{k} \right). \quad (63)$$

Direct calculation shows that (63) is a feasible solution to (61). (Again since $\nu \geq k(2^k - 1)$, the variables a_c are all nonnegative.)

We have now shown that (60) is an optimal solution to (59).

APPENDIX B

In this appendix we extend Theorems 1, 2, and 3 to the case when k does not divide ν . Setting $\nu = (N - 1)k + l$, where $0 \leq l < k$, we have $N = \lfloor (\nu + k)/k \rfloor$ where $\lfloor y \rfloor$ denotes the integer part of y .

Encoder states are labelled with binary ν tuples in the way described in Section II. Edges of the trellis are labelled with real numbers $x(s)$, where s is a binary $\nu + k$ tuple. The group $G_{k,\nu}$ is defined in the way

described in Section II; for each binary $\nu + k$ tuple t , we define a permutation of the edge labels $x(s)$ by the rule

$$g_t(x(s)) = x(s + t).$$

The symmetry g_t^* is the sequence

$$g_t^* = (g_{t^0}, g_{t^1}, g_{t^2}, \dots),$$

where $t^0 = t$ and t^i is obtained from t^{i-1} by cycling the entries k bits to the right and moving the last k bits to the front. When $k = 2$ and $\nu = 3$,

$$g_{11001}^* = (g_{11001}, g_{01110}, g_{10011}, g_{11100}, g_{00111}, g_{11001}, \dots).$$

In general, $t^i = t^{d+i}$ where $d = (k + \nu)/\text{gcd}(k, k + \nu)$. Given any component of the trellis and any pair of edges $x(s)$, $x(t)$ in that component there is a unique element of $G_{k,\nu}^*$ interchanging $x(s)$ and $x(t)$. The proof of Theorem 1 goes through without change and we have

$$\frac{d_{\min}^2}{P} \leq 4N_0, \quad (64)$$

where N_0 is the minimal length of an error event.

To see that $N_0 = N$, consider an error event E with initial state (time $t = 0$) $a = (a_1 \dots a_{N-1} a_N)$, where a_1, \dots, a_{N-1} , are k tuples and a_N is an l tuple. If k tuples b_1, b_1^* are input at time 0 then at time 1 the two paths occupy states $(b_1, a_1, \dots, a_{N-2}, \tilde{a}_{N-1})$ and $(b_1^*, a_1, \dots, a_{N-2}, \tilde{a}_{N-1})$, where \tilde{s} denotes the l tuple $(s_1 \dots s_l)$ obtained from the k tuple $(s_1 \dots s_k)$ by deleting the last $k - l$ bits. At time 1 the k -tuple z_{NC} is input to both paths, where c is a fixed but arbitrary $k - l$ tuple. At time 2 the two paths occupy states $(z_{NC}, b_1, a_1, \dots, a_{N-3}, \tilde{a}_{N-2})$ and $(z_{NC}, b_1^*, a_1, \dots, a_{N-3}, \tilde{a}_{N-2})$. At time N , after inputs z_{N-1}, \dots, z_2 , the two paths occupy states $(z_2, z_3, \dots, z_{N-1}, z_{NC}, \tilde{b}_1)$ and $(z_2, z_3, \dots, z_{N-1}, z_{NC}, \tilde{b}_1^*)$. If $\tilde{b}_1 = \tilde{b}_1^*$ then the two paths remerge at time N in state $z = (z_2, z_3, \dots, z_{N-1}, z_{NC}, \tilde{b}_1)$. We denote this error event by $E(a, z; b_1, b_1^*)$. Thus by (64)

$$\frac{d_{\min}^2}{P} \leq 4 \left(1 + \left\lfloor \frac{\nu}{k} \right\rfloor \right) \quad (65)$$

for general k and ν .

Let $S(a, z; b_1, b_1^*)$ be the orbit of $G_{k,\nu}^*$ containing the error event $E(a, z; b_1, b_1^*)$. We calculate the contribution to $Q(S(a, z; b_1, b_1^*))$ made by pairs of edges in component 0 in the same way as Lemma 8. Setting

$f = b_1 + b_1^*$ this distance contribution is

$$\begin{aligned} & \frac{1}{2^{\nu+k}} \sum_t [g_t(x(b_1 a_1 \dots a_{N-1} a_N)) - g_t(x(b_1^* a_1 \dots a_{N-1} a_N))]^2 \\ &= \frac{1}{2^{\nu+k}} \underline{x}^T [2I_{2^{\nu+k}} - 2M(f_0 \dots 0)] \underline{x}. \end{aligned}$$

Similarly, the distance contribution made by pairs of edges in component $N - 1$ is

$$\frac{1}{2^{\nu+k}} \underline{x}^T [2I_{2^{\nu+k}} - 2M((f_0 \dots 0)^{N-1})] \underline{x}.$$

Note that the first l bits of f are zero and that the last l bits of $(f_0 \dots 0)^i$ are zero for $0 \leq i \leq N - 1$. Arguing as in Lemma 8 we obtain

$$2^{\nu+k} Q(S(a, z; b_1, b_1^*)) = 2NI_{2^{\nu+k}} - 2 \sum_{i=0}^{N-1} M((f_0 \dots 0)^i).$$

There are $(2^{k-l} - 1)k$ tuples f for which $f \neq 0$ and $\tilde{f} = 0$. Hence

$$2^{\nu+k}(2^{k-l} - 1)Q(S^N) = 2(2^{k-l} - 1)NI_{2^{\nu+k}} - 2 \sum_{\substack{\tilde{f} \neq 0 \\ \tilde{f}=0}} \sum_{i=0}^{N-1} M((f_0 \dots 0)^i).$$

Setting $Q = 2^{\nu+k}(2^{k-l} - 1)Q(S^N)$ we obtain

$$\frac{d_{\min}^2}{P} \leq \frac{1}{2^{k-l} - 1} \lambda_1(Q), \quad (66)$$

which reduces to (39) when $l = 0$. The proof of Theorem 2 goes through (change " $c_i = 0 (\neq 0)$ " to "the last $k - l$ digits of c_i are zero (nonzero)")

$$\lambda_1(Q) = 2^{k-l+1}N. \quad (67)$$

By (66) and (67)

$$\frac{d_{\min}^2}{P} \leq \frac{2^{k-l+1}}{2^{k-l} - 1} \left(1 + \left\lfloor \frac{\nu}{k} \right\rfloor \right) \quad (68)$$

for general k and ν .

Finally we consider the set S' of all error events of length $N + 1$ for which the k tuples b_1, b_1^* input at time 0 satisfy $\tilde{b}_1 = \tilde{b}_1^* = 0$ and for which the k tuples b_2, b_2^* input at time 1 satisfy $\tilde{b}_2 = \tilde{b}_2^* = 0$. Let $E \in S'$ with initial state $a = (a_1, \dots, a_{N-1}, a_N)$ and final state $z = (z_1, \dots, z_{N-1}, z_N)$, where $a_i, z_i, i = 1 \dots, N - 1$ are k tuples and a_N, z_N are l tuples. At time 2 the two paths occupy states $((z_N 0 \dots 0) + b_2,$

$b_1, a_1, \dots, a_{N-3}, \tilde{a}_{N-2}$) and $((z_N 0 \dots 0) + b_2^*, b_1^*, a_1, \dots, a_{N-3}, \tilde{a}_{N-2})$. At time N the two paths occupy states $(z_2, z_3, \dots, z_{N-1}, (z_N 0 \dots 0) + b_2, \tilde{b}_1)$ and $(z_2, z_3, \dots, z_{N-1}, (z_N 0 \dots 0) + b_2^*, b_1^*)$. Set $f = b_2 + b_2^*$ and $g = b_1 + b_1^*$ and define $M_i(fg) i = 0, \dots, N$ as in (43). Arguing as in Lemma 9 we obtain

$$2^{\nu+k}(2^{k-l})(2^{k-l} - 1)Q(S')$$

$$= 2(2^{k-l} - 1)(2^{k-l} - 1)(N + 1)I_{2^{\nu+k}} - 2 \sum_{\substack{f \neq 0 \\ \tilde{f} = 0}} \sum_{\substack{g \neq 0 \\ \tilde{g} = 0}} \sum_{i=0}^N M_i(fg 0 \dots 0).$$

Let $\delta = 1/(2^{2(k-l)} - 1)$ and let $\bar{Q} = 2(2^{k-l} - 1)\delta Q(S^N) + (2^{k-l} - 1)^2\delta Q(S')$. Then $2(2^{k-l} - 1)\delta + (2^{k-l} - 1)^2\delta = 1$ and so

$$\frac{d_{\min}^2}{P} \leq 2^{\nu+k}\lambda_1(\bar{Q}).$$

The proof of Theorem 3 goes through [change “ $c_i = 0$ ($\neq 0$)” to “the last $k - l$ digits of c_i are zero (nonzero)”] and we obtain

$$\frac{d_{\min}^2}{P} \leq \frac{2^{2(k-l)+1}}{2^{2(k-l)} - 1} \left(2 + \left\lfloor \frac{\nu}{k} \right\rfloor \right), \quad (69)$$

for general k and ν .

AUTHORS

Helene Shapiro, B.A. (Mathematics), 1975, Kenyon College; Ph.D. (Mathematics), 1979, California Institute of Technology; Assistant Professor of Mathematics, University of Wisconsin-Madison, 1979–80; Assistant Professor of Mathematics, Swarthmore College, 1980—. Ms. Shapiro’s research has been in matrix theory and deals with generalized commutativity problems.

Robert Calderbank, B.Sc. (Mathematics), 1975, University of Warwick; M.Sc. (Mathematics), 1976, University of Oxford; Ph.D. (Mathematics), 1980, California Institute of Technology; Bell Laboratories, 1980—. Mr. Calderbank is presently employed in the Mathematics and Statistics Research Center.

James E. Mazo, B.S. (Physics), 1958, Massachusetts Institute of Technology; M.S. (Physics), 1960, and Ph.D. (Physics), 1963, Syracuse University; Research Associate, Department of Physics, University of Indiana, 1963–1964; Bell Laboratories, 1964—. At the University of Indiana, Mr. Mazo worked on studies of scattering theory. At Bell Laboratories, he has been concerned with problems in data transmission and is now working in the Mathematics and Statistics Research Center. Member, IEEE.

PAPERS BY BELL LABORATORIES AUTHORS

COMPUTING/MATHEMATICS

- Benes V., Karatzas I., **On the Relation of Zakai Equations and Mortensen Equations.** *Siam J Con* 21(3):472-489, 1983.
- Bos A., Conway J. H., Sloane N. J. A., **Further Lattice Packings in High Dimensions.** *Mathematika* 29(58):171-180, 1982.
- Bremner A. et al., **Two-Weight Ternary Codes and the Equation $Y^2 = 4 \times 3^A + 13$.** *J Number Th* 16(2):212-234, 1983.
- Burman D. Y., Smith D. R., **A Light-Traffic Theorem for Multi-Server Queues.** *Math Oper R* 8(1):15-25, 1983.
- Chung F. R. K. **On a Ramsey-Type Problem.** *J Graph Th* 7(1):79-83, 1983.
- Chung F. R. K. et al., **A Survey of Bounds for Classical Ramsey Numbers.** *J Graph Th* 7(1):25-37, 1983.
- Chung F. R. K., Graham R. L., **On Universal Graphs for Spanning-Trees.** *J Lond Math* 27(Apr):203-211, 1983.
- Cleveland W. S., McGill R., **A Color-Caused Optical Illusion on a Statistical Graph.** *Am Statistn* 37(2):101-105, 1983.
- Coffman E. G., Garey M. R., Johnson D. S., **Dynamic Bin Packing.** *Siam J Comp* 12(2):227-258, 1983.
- Cunningham W. H., Klinecicz J. G., **On Cycling in the Network Simplex-Method.** *Math Progr* 26(2):182-189, 1983.
- Dalal S. R., Phadia E. G., **Nonparametric Bayes Inference for Concordance in Bivariate Distributions.** *Comm St-The* 12(8):947-963, 1983.
- Graham R. L., **Euclidean Ramsey Theorems on the N -Sphere.** *J Graph Th* 7(1):105-114, 1983.
- Halfin S., **The Sphere Method and the Robustness of the Ellipsoid Algorithm.** *Math Progr* 26(1):109-116, 1983.
- Derosa F., **Commodore Pet Computer Used as a Programmable Gated Integrator.** *Rev Sci Ins* 54(5):630-632, 1983.
- Haddon R., Lamola A., **The Organic Computer—Can Microchips be Built by Bacteria?.** *Science* 23(3):40-44, 1983.
- Hennessy J. L. et al., **Complex Versus Reduced Instruction Set Computers.** *ISSCC Diges* 26:218-219, 1983.
- Johnson D. S., Niemi K. A., **On Knapsacks, Partitions, and a New Dynamic-Programming Technique for Trees.** *Math Oper R* 8(1):1-14, 1983.
- Kruskal J. B., **An Overview of Sequence Comparison—Time Warps, String Edits, and Macromolecules.** *Siam Rev* 25(2):201-237, 1983.
- Kruskal J. B., Landwehr J. M., **Icicle Plots—Better Displays for Hierarchical-Clustering.** *Am Statistn* 37(2):162-168, 1983.
- Lagarias J. C., Odlyzko A. M., Shearer J. B., **On the Density of Sequences of Integers the Sum of No Two of Which is a Square. 2. General Sequences.** *J Comb Th A* 34(2):123-139, 1983.
- Lagarias J. C., Aminzade F., **Multistage Planning and the Extended Linear-Quadratic-Gaussian Control Problem.** *Math Oper R* 8(1):42-63, 1983.
- Leon R. V., Lynch J., **Preservation of Life Distribution Classes Under Reliability Operations.** *Math Oper R* 8(2):159-169, 1983.
- Reilly T. M., **The Extended Classroom.** *Datamation* 29(4):199-200, 1983.
- Riffelmacher D., **Multiplicative Complexity and Algebraic Structure.** *J Comput Sy* 26(1):92-106, 1983.
- Sandberg I. W., **Volterra-Like Expansions for Solutions of Non-Linear Integral-Equations and Non-Linear Differential-Equations.** *IEEE Circ S* 30(2):68-77, 1983.
- Stuck B. W., **Calculating the Maximum Mean Data Rate in Local Area Networks.** *Computer* 16(5):72-76, 1983.

Witsenhausen H. S., **Team Guessing With Lacunary Information.** *Math Oper R* 8(1):110-121, 1983.

Yu Y. K., Banerji R. B., **Periodicity of Sprague-Grundy Function in Graphs With Decomposable Nodes.** *Cybern Syst* 13(4):299-310, 1982.

ELECTRICAL ENGINEERING

Alavi K., Pearsall T. P., Forrest S. R., Cho A. Y., **Ga_{0.47}In_{0.53}As/Al_{0.48}In_{0.52} Multiquantum-Well LEDs Emitting at 1.6 μm .** *Electr Lett* 19(6):227-229, 1983.

Allara D. L., Nuzzo R. G., **The Application of Reflection Infrared and Surface Enhanced Raman-Spectroscopy to the Characterization of Chemisorbed Organic Disulfides on Au.** *J Elec Spec* 30(Feb):11, 1983.

Antler M., Ratliff E. T., **Sliding Wear of Inlay Clad Metals and Electrodeposited Cobalt-Gold.** *IEEE Compon* 6(1):3-7, 1983.

Auston D. H., **Impulse-Response of Photoconductors in Transmission-Lines.** *IEEE J Q El* 19(4):639-648, 1983.

Arnold H. W., Bodtmann W. F., **A Hybrid Multichannel Hardware Simulator for Frequency-Selective Mobile Radio Paths.** *IEEE Commun* 31(3):370-377, 1983.

Banu M., Tsvividis Y., **Fully-Integrated Active RC-Filters in MOS Technology.** *ISSCC Diges* 26:244+, 1983.

Bergmann E. E., **Polarization Independent Beam Splitter.** *Rev Sci Ins* 54(5):579-581, 1983.

Blum E. B., Siemann R. H., Auston D. H., Freeman R. R., **Bunch Length Measurements in CeSr Using an X-Ray Sensitive Photoconducting Detector.** *Nucl Instru* 207(3):321-324, 1983.

Bobek A. H., **Citation Classic—Properties and Device Applications of Magnetic Domains in Ortho-Ferrites.** *CC/Eng Tech* 1983(20):24, 1983.

Boll H. J. et al., **Practical Versus Theoretical Limits of VLSI (Discussion).** *ISSCC Diges* 26:212-216, 1983.

Chu T. S., **A Semi-Empirical Formula for Microwave Depolarization Versus Rain Attenuation on Earth-Space Paths (Letter).** *IEEE Commun* 30(12):2550-2554, 1982.

Coffey B. J., Lax M., Elliott C. J., **Three-Dimensional Propagation in Free-Electron Laser-Amplifiers.** *IEEE J Q El* 19(2):297-305, 1983.

Dorros I., **Telephone Nets Go Digital.** *IEEE Spectr* 20(4):48-53, 1983.

Ducorps A. M., Yashinovitz C. J., **CAMAC Controller for a Conventional and Pseudo-Random Time-of-Flight System.** *Rev Sci Ins* 54(4):444-453, 1983.

Dutta N. K., Deimel P. P., **Optical-Properties of a GaAlAs Superluminescent Diode.** *IEEE J Q El* 19(4):496-498, 1983.

Ericson T., Korner J., **Successive Encoding of Correlated Sources.** *IEEE Info T* 29(3):390-395, 1983.

Feldman M., White A. D., White D. L., **Application of Zone Plates to Alignment in X-Ray-Lithography.** *Opt Eng* 22(2):203-207, 1983.

Fork R. L., Shank C. V., Yen R., Hirlmann C. A., **Femtosecond Optical Pulses.** *IEEE J Q El* 19(4):500-506, 1983.

Foschini G. J., Gopinath B., **Sharing Memory Optimally.** *IEEE Commun* 31(3):352-360, 1983.

Fraser D. L., Williams G. F., Jindal R. P., Kushner R. A., Owen B., **A Single-Chip NMOS Pre-Amplifier for Optical Fiber Receivers.** *ISSCC Diges* 26:80-81, 1983.

Friesem A. A. et al., **Parallel Transmission of Images Through Single Optical Fibers.** *P IEEE* 71(2):208-221, 1983.

Fuls E. N., **X-Ray-Lithography Applied to the Fabrication of One Micrometer N-Channel Metal-Oxide Semiconductor Circuits.** *Opt Eng* 22(2):199-202, 1983.

Guancial E., Kohl R. W., Dunbar J. J., Milton J. L., Dasgupta S., **Qualification of Connectors Manufactured With Diffused Gold RI56 Inlay Contacts.** *IEEE Compon* 6(1):100-107, 1983.

Haque C. A., Drozdowicz M. H., Frank R. A., Hanlon J. T., **Extraneous Metal Deposits From Production Processes on Contact Materials.** *IEEE Compon* 6(1):55-60, 1983.

- Hartman D. H., **Multiple Reflection Noise on Transmission-Systems With Periodic or Quasi-Periodic Impedance Disturbances—A Frequency-Domain Approach.** *IEEE Circ S* 30(4):242–246, 1983.
- Hatamian M., Anderson D. J., **Design Considerations for a Real-Time Ocular Counterroll Instrument.** *IEEE Biomed* 30(5):278–288, 1983.
- Johnson P. D., Perlman M. L., **Slit Width Calibration With a Radioactive Photon Source.** *Nucl Instru* 206(3):593–594, 1983.
- Kadota T. T., **Piecewise Linear Random-Paths on a Plane and a Central Limit-Theorem.** *IEEE Info T* 29(2):241–245, 1983.
- Kadota T. T., Seery J. B., **Detection of Weak Secondary Signals With the Aid of Already Detected Strong Primary Signals.** *IEEE Acoust* 31(2):426–437, 1983.
- Kaminow I. P., Eisenstein G., Stulz L. W., **Measurement of the Modal Reflectivity of an Anti-Reflection Coating on a Superluminescent Diode.** *IEEE J Q El* 19(4):493–495, 1983.
- Macrander A., Barr D., Wagner A., **Resist Possibilities in Ion-Beam Lithography.** *Opt Eng* 22(2):215–219, 1983.
- O'Connor K. J., Kushner R. A., **A Five ns 4K × 1 NMOS Static RAM.** *ISSCC Diges* 26:104+, 1983.
- Prabhu K. A., Netravali A. N., **Motion Compensated Component Color Coding.** *IEEE Commun* 30(12):2519–2527, 1982.
- Prabhu K. A., Netravali A. N., **Motion Compensated Composite Color Coding.** *IEEE Commun* 31(2):216–223, 1983.
- Prabhu V. K., **Error Rate Bounds for Differential PSK (Letter).** *IEEE Commun* 30(12):2547–2550, 1982.
- Saari V. R., **Low-Power High-Drive CMOS Operational-Amplifiers.** *IEEE J Soli* 18(1):121–127, 1983.
- Sandberg I. W., **On Volterra Expansions for Time-Varying Non-Linear Systems.** *IEEE Circ S* 30(2):61–67, 1983.
- Sharma S. P., Hines L. L., **Oxidation of Ruthenium.** *IEEE Compon* 6(1):89–92, 1983.
- Sloane N. J. A., Thompson J. G., **Cyclic Self-Dual Codes.** *IEEE Info T* 29(3):364–366, 1983.
- Stone J., Chraplyvy A. R., **Spontaneous Brillouin Noise in Long-Distance High-Bandwidth Optical-Fibre Transmission.** *Electr Lett* 19(8):275–277, 1983.
- Swanson E. J., Starke R. J., Cross G. F., Olson K. H., Waldron C. J., Copeland R. A., Surek S. A., Ribble R. J., Vera A. J., **A Fully Adaptive Transversal Canceller and Equalizer Chip.** *ISSCC Diges* 26:20+, 1983.
- Tucker R. S., Pope D. J., **Microwave Circuit Models of Semiconductor Injection-Lasers.** *IEEE Micr T* 31(3):289–294, 1983.
- Uman M. A., Master M. J., Krider E. P., **A Comparison of Lightning Electromagnetic-Fields With the Nuclear Electromagnetic Pulse in the Frequency-Range 104–107 Hz.** *IEEE Elmag* 24(4):410–416, 1982.
- Winters J. H., **Switched Diversity With Feedback for DPSK Mobile Radio Systems.** *IEEE Veh T* 32(1):134–150, 1983.
- Wittmer N. C., Michejda J. A., Gannett J. W., Bechtold P. F., Taylor G. W., Lifshitz N., Dennis D. C., Bayruns R. J., **A NMOS LSI 16 × 16 Multiplier.** *ISSCC Diges* 26:32–33, 1983.
- Wong W. C., Steele R., Glance B., Horn D., **Time Diversity With Adaptive Error-Detection to Combat Rayleigh Fading in Digital Mobile Radio.** *IEEE Commun* 31(3):378–387, 1983.
- Wu F. F., Tsai Y. K., **Probabilistic Dynamic Security Assessment of Power-Systems. 1. Basic Model.** *IEEE Circ S* 30(3):148–159, 1983.
- Yue O. C., **Spread Spectrum Mobile Radio, 1977–1982.** *IEEE Veh T* 32(1):98–105, 1983.

MANAGEMENT/ECONOMICS

- Porter R. H., **On The Rationality of Buying From a Price Predator.** *Econ Lett* 11(4):385–389, 1983.

Whitt W., **Untold Horrors of the Waiting Room—What the Equilibrium Distribution Will Never Tell About the Queue-Length Process.** *Manag Sci* 29(4):395-408, 1983.

PHYSICAL SCIENCES

Abrahams S. C., et al., **Dielectric and Thermal-Properties, Expansion, and High-Temperature Plastic-Deformation of $\text{Cd}_4\text{Na}(\text{VO}_4)_3$.** *J Appl Cryst* 16(FEB):133-135, 1983.

Adams A. C., **Plasma Deposition of Inorganic Films.** *Sol St Tech* 26(4):135-139, 1983.

Anderson P. W., **Localization Redux.** *Physica B&C* 117(MAR):30-36, 1983.

Antonio M. R., Teo B. K., Cleland W. E., Averill B. A., **Iron and Molybdenum Extended X-Ray Absorption Fine-Structure Studies of Double-Cubane Clusters Containing MoFe_3S_4 .** *J Am Chem S* 105(11):3477-3484, 1983.

Aspnes D. E., **Surface Transition Regions and Visible-Near UV Optical-Properties of Some Semiconductors.** *Physica B&C* 117(MAR):359-361, 1983.

Azbel M. Y., **Impurities in Semimetals.** *Sol St Comm* 46(2):113-115, 1983.

Bates F. S., Baker G. L., **Soluble Polyacetylene Graft Co-Polymers (Letter).** *Macromolec* 16(4):704-707, 1983.

Belanger R. M. et al., **Determination of the Group-Velocity of Magnetic Polaritons in FeF_2 .** *J Magn Magn* 31-4(FEB):681-682, 1983.

Benbow R. L., Smith N. V., **Photoemission Spectra and Band Structures of D-Band Metals. 10. Relativistic Momentum Matrix-Elements.** *Phys Rev B* 27(6):3144-3151, 1983.

Bertz S. H., Jelinski L. W., Dabbagh G., **Conjugate Addition of Lithium Isopropyl Dithioisobutyrate to 4-Acetoxy cyclopent-2-enone. Assignment of Stereochemistry in Flexible 5-Membered Rings.** *J Chem S* CH1983(7):388-390, 1983.

Bethea C. G., Chen C. Y., Cho A. Y., Garbinski P. A., Levine B. F., **Picosecond $\text{Al}_x\text{Ga}_{1-x}\text{As}$ Modulation-Doped Optical Field-Effect Transistor Sampling Gate.** *Appl Phys L* 42(8):682-684, 1983.

Blumenfeld K. S., Kozlowski S., Breslauer K. J., **Salt-Dependent Conformational Transitions in the Self-Complementary Deoxydodecanucleotide d(CGCAATTCGCG)-Evidence for Hairpin Formation.** *Biopolymers* 22(4):1247-1257, 1983.

Bokor J., Bucksbaum P. H., Freeman R. R., **Generation of 35.5-nm Coherent Radiation.** *Optics Lett* 8(4):217-219, 1983.

Bondyby V. E., Milton S. V., English J. H., Rentzepis P. M., **Spectroscopic and Picosecond Time-Resolved Studies of Vibrational-Relaxation in Naphthazarine in Solid Neon.** *Chem P Lett* 97(2):130-134, 1983.

Bondyby V. E., English J. H., Miller T. A., **Spectroscopic and Dynamical Studies of Vibrationally Unrelaxed Fluorescence From Halobenzene Cations in a Neon Matrix.** *J Phys Chem* 87(8):1300-1305, 1983.

Bondyby V. E., Heaven M., Miller T. A., **Laser Vaporization of Tin—Spectra and Ground-State Molecular-Parameters of Sn_2 .** *J Chem Phys* 78(6):3593-3598, 1983.

Bosch M. A., Good E., Lemons R. A., **Electrically Amplified Optical-Recording in Polymer-Films.** *Appl Phys L* 42(6):484-486, 1983.

Bovey F. A., Cais R. E., Jelinski L. W., Schilling F. C., Starnes W. H., Tonelli A. E., **Structural and Dynamic Characterization of Polymers by C-13 and F-19 NMR (Review).** *Adv Chem SE* 1983(203):421-439, 1983.

Bowden M. J., Keith H. D., **A Comment on Crystallinity in Poly(olefin Sulfones).** *Eur Polym J* 19(3):259-261, 1983.

Bowden M. J., Novembre T., **Initiation Considerations and Kinetics of Formation of Poly(2-Methyl-1-Pentene Sulfone) (Review).** *ACS Symp S* 1983(212):125-136, 1983.

Bowmer T. N., Hellman M. Y., Vocom W. I., **Radiation Crosslinking of Polyvinyl-Chloride With Trimethylolpropanetrimethacrylate. 2. Dependence on Radiation-Dose and Blend Composition.** *J Appl Poly* 28(6):2083-2092, 1983.

Brand H., Swift J., **Macroscopic Dynamics in Nematics Near the Uniaxial-Biaxial Phase-Transition.** *J Phys Lett* 44(9):L333-L337, 1983.

- Bruinsma R., Aeppli G., **One-Dimensional Ising-Model in a Random Field.** *Phys Rev L* 50(19):1494-1497, 1983.
- Capizzi M., Frova A., Martelli F., Modesti S., Quagliano L. G., Staehli J. L., Guzzi M., Logan R. A., Chiaretti G., **The E-H Plasma in Direct-Gap GaAlAs Under Three-D Confinement.** *Physica B&C* 117(Mar):333-335, 1983.
- Chabal Y. J., Chaban E. E., Christman S. B., **High-Resolution Infrared Study of Hydrogen Chemisorbed on Si(100).** *J Elec Spec* 29(Jan):35-40, 1983.
- Chandler D., Weeks J. D., Andersen H. C., **Vanderwaals Picture of Liquids, Solids, and Phase-Transformations.** *Science* 220(4599):787-794, 1983.
- Chandross E. A., Reichmanis E., Wilkins C. W., Hartless R. L., **New Photoresists for Deep Ultraviolet (Less-Than 300 nm) Exposure.** *Can J Chem* 61(5):817-823, 1983.
- Chang C. C., Sheng T. T., Shankoff T. A., **Phosphorus Depth Profiles in Thermally Oxidized P-Doped Polysilicon.** *J Elchem So* 130(5):1168-1171, 1983.
- Chemla D. S., Damen T. C., Miller D. A. B., Gossard A. C., Wiegmann W., **Electro-Absorption by Stark-Effect on Room-Temperature Excitons in GaAs-GaAlAs Multiple Quantum Well Structures.** *Appl Phys L* 42(10):864-866, 1983.
- Chemla D. S., Heritage J. P., Liao P. F., Isaacs E. D., **Enhanced Four-Wave Mixing From Silver Particles.** *Phys Rev B* 27(8):4553-4558, 1983.
- Chen C. H., Fleming R. M., Petroff P. M., **Time-Dependent Strandlike Domains in the Charge-Density-Wave States of NbSe₃—an Effect Not Induced by Electric-Field.** *Phys Rev B* 27(7):4459-4462, 1983.
- Chen H. S., Aust K. T., Waseda Y., **Effect of Low-Temperature Annealing on the Structure of Cu₅₇Zr₄₃ Glass.** *J Mat Sci L* 2(4):153-157, 1983.
- Chin A. K., **A Simple, High Collection Efficiency Cathodoluminescence Imaging Technique—Application to GaSb and CdTe.** *Scan Elec M1982(P3):1069-1075, 1982.*
- Chin, A. K., Camlibel I., Dutt B. V., Swaminathan. V., Bonner W. A., Ballman A. A., **Extremely Rapid Outdiffusion of N-Type Impurities in InP.** *Appl Phys L* 42(10):901-903, 1983.
- Cho A. Y., **Growth of III-V Semiconductors by Molecular-Beam Epitaxy and Their Properties.** *Thin Sol Fi* 100(4):291-317, 1983.
- Citrin P. H., Hamann D. R., Mattheiss L. F., Rowe J. E., **Comment on the Geometry and Electronic-Structure of Cl on Cu(100) and Ag(001)—Reply (Letter).** *Phys Rev L* 50(22):1824, 1983.
- Citrin P. H., Rowe J. E., Eisenberger P., Comin F., **SEXAFS Studies of Adsorbate Structure on Si and Ge Surfaces.** *Physica B&C* 117(Mar):786-788, 1983.
- Citrin P. H., Wertheim G. K., **Photoemission From Surface-Atom Core Levels, Surface Densities of States, and Metal-Atom Clusters—A Unified Picture (Review).** *Phys Rev B* 27(6):3176-3200, 1983.
- Citrin P. H., Wertheim G. K., Baer Y., **Surface-Atom X-Ray Photoemission From Clean Metals—Cu, Ag, and Au.** *Phys Rev B* 27(6):3160-3175, 1983.
- Copeland J. A., **Fluctuations in Semiconductor-Laser Emissions.** *J Appl Phys* 54(5):2813-1819, 1983.
- Cottam M. G., So V., Lockwood D. J., Katiyar R. S., Guggenheim H. J., **Raman-Scattering From Magnon Pair Excitations in FeF₂.** *J Phys C* 16(9):1741-1755, 1983.
- Cottrell P. T., Frankenthal R. P., Kammlott, G. W., Siconolfi D. J., Draper C. W., **Effect of Laser Surface Melting on Some Corrosion Characteristics of an Iron-Chromium Alloy.** *J Elchem So* 130(5):998-1001, 1983.
- Danner D. A., Flamm D. L., Mucha J. A., **Downstream Atomic Monitoring for Absolute Etch Rate Determinations.** *J Elchem So* 130(4):905-907, 1983.
- Defreez R. K. et al., **High-Output Room-Temperature Pulsed Operation for Broad Contact InP/In_{0.53}Ga_{0.47}As/InP Lasers Grown By Molecular-Beam Epitaxy.** *J Appl Phys* 54(5):2177-2182, 1983.
- Denbroeder F. J. A., Nakahara S., **Diffusion Induced Grain-Boundary Migration and Recrystallization in the Cu-Ni System.** *Scrip Metal* 17(3):399-404, 1983.
- Dillon J. F., **Magneto-Optics and Its Uses.** *J Magn Magn* 31-4(Feb):1-9, 1983.
- Dimauro L. F., Wood D. E., Lloyd R. V., **Polarized Emission From Doublet State Organic Free-Radicals.** *J Chem Phys* 78(10):5920-5925, 1983.

- Donovan E. P., Spaepen F., Turnbull D., Poate J. M., Jacobson D. C., **Heat of Crystallization and Melting-Point of Amorphous-Silicon.** Appl Phys L 42(8):698-700, 1983.
- Dubois L. H., Schwartz G. P., **High-Resolution EELS Studies of Clean and Oxide Covered Semiconductor Surfaces.** J Elec Spec 29(Jan):175-180, 1983.
- Dudderar T. D. et al., **Achieving Stability in Remote Holography Using Flexible Multimode Image Bundles.** Appl Optics 22(7):1000-1005, 1983.
- Edelson D., **Sensitivity Analysis of Proposed Mechanisms for the Briggs-Rauscher Oscillating Reaction.** J Phys Chem 67(7):1204-1208, 1983.
- Eisenberger P., Okamura M. Y., Feher G., **The Electronic-Structure of Fe-2+ in Reaction Centers From Rhodospseudomonas-Sphaeroides. 2. Extended X-Ray Fine-Structure Studies.** Biophys J 37(2):523-538, 1982.
- Englert T., Maan J. C., Tsui D. C., Gossard A. C., **A Study of Intersubband Scattering in GaAs-Al_{1-x}Ga_{1-x}As Heterostructures by Means of a Parallel Magnetic-Field.** Sol St Comm 45(11):989-991, 1983.
- Englert T., Maan J. C., Uihlein C., Tsui D. C., Gossard A. C., **Oscillations of the Cyclotron-Resonance Linewidth With Landau-Level Filling Factor in GaAs/AlGaAs Heterostructures.** Physica B&C 117(Mar):631-633, 1983.
- Englert T., Maan J. C., Uihlein C., Tsui D. C., Gossard A. C., **Observation of Oscillatory Linewidth in the Cyclotron-Resonance of GaAs-Al_{1-x}Ga_{1-x}As Heterostructures.** Sol St Comm 46(7):545-548, 1983.
- Fisher D. S., **Threshold Behavior of Charge-Density Waves Pinned by Impurities.** Phys Rev L 50(19):1486-1489, 1983.
- Fisher D. S., Weeks J. D., **Shape of Crystals at Low-Temperatures—Absence of Quantum Roughening.** Phys Rev L 50(14):1077-1080, 1983.
- Flamm D. L., Ibbotson D. E., Mucha J. A., Donnelly V. M., XeF₂ and F-Atom Reactions with Si—Their Significance for Plasma-Etching. Sol St Tech 26(4):117-121, 1983.
- Flamm D. L., **Plasma Processing (Editorial).** Sol St Tech 26(4):115, 1983.
- Frankenthal R. P., Siconolfi D. J., **The Equilibrium Surface-Composition of Some Indium Lead and Indium Tin Alloys.** Surf Sci 125(2):595-603, 1983.
- Fulton T. A., Dolan G. J., **New Approach to Electron-Beam Lithography.** Appl Phys L 42(8):752-754, 1983.
- Gibson J. M., Chen C. H., McDonald M. L., **Ultrahigh-Resolution Electron-Microscopy of Charge-Density Waves in 2H-TaSe₂ Below 100-K.** Phys Rev L 50(18):1403-1406, 1983.
- Glarum S. H., Marshall J. H., **An Admittance Study of the Tin Electrode.** J Elchem So 130(5):1088-1096, 1983.
- Graebner J. E., Allen L. C., Golding B., Kane A. B., **Acoustic Saturation in a Glass at Low-Temperatures.** Phys Rev B 27(6):3697-3708, 1983.
- Greywall D. S., **Specific Heat of Normal Liquid ³He.** Phys Rev B 27(5):2747-2766, 1983.
- Georgy E. M., McWhan D. B., Dillon J. F., Walker L. R., Waszczak J. V., Musser D. P., Willens R. H., **Structural and Magnetic-Properties of Compositionally Modulated Cu-Ni Films.** J Magn Magn31-4(Feb):915-919, 1983.
- Haavasoja T., Narayanamurti V., Chin M. A., **Propagation of Near-Zone-Boundary, Acoustic Phonons in Solid ⁴He With the Use of Superconducting Tunnel-Junctions.** Phys Rev B 27(5):2767-2769, 1983.
- Hall P. M., **Solder Attachment of Leadless Ceramic Chip Carriers.** Sol St Tech 26(3):103-107, 1983.
- Hamann D. R., **Computers in Physics—An Overview (Review).** Phys Today 36(5):24-33, 1983.
- Haque C. A., **Durability of Solid Fluoropolymer Thin-Films on Metal-Surfaces for Silicone Oil Creep.** Appl Surf S 15(1-4):293-306, 1983.
- Harley R. T., Lyons K. B., Fleury P. A., Smith S. R. P., **Fluctuation Dynamics at the Cooperative Jahn-Teller Phase Transition in TbVO₄.** J Phys C 16(8):1407-1422, 1983.
- Hasegawa A., **Recent Topics in Physics of Hot Plasmas in Space Environment.** Phys Scr T2(NSI):223-227, 1982.

- Hauser J. J., **Effect of Crystal Structure on the Magnetic-Properties of Semiconducting $\text{Cd}_{0.5}\text{Mn}_{0.5}\text{Te}$** . *Phys Rev B* 27(6):3460-3464, 1983.
- Hebard A. F., Fiory A. T., **Critical-Exponent Measurements of a Two-Dimensional Superconductor**. *Phys Rev L* 50(20):1603-1606, 1983.
- Helfand E., **Brownian Dynamics Simulation of Systems With Transitions. Particularly Conformational Transitions in Chain Molecules**. *Physica A*, 118(1-3):123-135, 1983.
- Hemmerle W. J., Carey M. B., **Some Properties of Generalized Ridge Estimators**. *Comm St-Sim* 12(3):239-256, 1983.
- Hilinski E. F., Milton S. V., Ramana C., Rentzepis, P. M., **On the Chemistry of Metastable Species**. *Can J Chem* 61(5):999-1006, 1983.
- Hilinski E. F., Rentzepis P. M., **Biological Applications of Picosecond Spectroscopy (Review)**. *Nature* 302(5908):481-487, 1983.
- Hong M. et al., **Superconducting Properties of a Liquid-Infiltration Nb-Nb₃Sn Composite Formed During a Low-Temperature Reaction**. *Appl Phys L* 42(7):621-623, 1983.
- Hopfel R. A., Gornik E., Gossard A. C., Wiegmann W., **Plasmon Excitation by Coulomb Scattering of Electrons in Two-D-Systems**. *Physica B&C* 117(MAR):646-648, 1983.
- Hu E. L., Howard R. E., Grabbe P., Tennant D. M., **Ion-Beam Processing Using Metal on Polymer Masks**. *J Elchem So* 130(5):1171-1173, 1983.
- Jackel J. L., Rice C. E., Veselka J. J., **Composition Control in Proton-Exchanged LiNbO_3** . *Electr Lett* 19(10):387-388, 1983.
- Jelinski L. W., Dumais J. J., Engel A. K., **Motions About 3 Bonds in Polymers—Solid-State Deuterium NMR-Studies (Letter)**. *Macromolec* 16(3):492-496, 1983.
- Jelinski L. W., Dumais J. J., Engel A. K., **Multitechnique Solid-State NMR Approach to Assessing Molecular-Motion—Poly(Butylene Terephthalate) and Poly(Butylene Terephthalate)-Containing Segmented Co-Polymers. 4**. *Macromolec* 16(3):403-409, 1983.
- Jelinski L. W., Dumais J. J., Watnick P. I., Engel A. K., Sefcik M. D., **NMR Relaxation in Poly(Butylene Terephthalate) and Poly(Butylene Terephthalate)-Containing Segmented Co-Polymers. 5**. *Macromolec* 16(3):409-415, 1983.
- Johnson D. W. et al., **Use of Mn-Based and Mg-Based Ferrites for Negative-Temperature-Coefficient Thermistors**. *Am Ceram S* 62(5):597-600, 1983.
- Johnson L. F., Ingersoll K. A., **Ion Polishing With the Aid of a Planarizing Film**. *Appl Optics* 22(8):1165-1167, 1983.
- Jopson R. M., Darack S., Freeman R. R., Bokor J., **Laser-Plasma-Induced Extreme-Ultraviolet Radiation From Liquid Mercury**. *Optics Lett* 8(5):265-267, 1983.
- Kamgar A., Johnston R. L., **Delay Times in Si MOSFETs in the 4.2-400 K Temperature-Range**. *Sol St Elec* 26(4):291-294, 1983.
- Kang K. S., Shay J. L., **Blue Sputtered Iridium Oxide-Films (Blue SIROFS)**. *J Elchem So* 130(4):766-769, 1983.
- Kelley D. F., Milton S. V., Huppert D., Rentzepis P. M., **Formation Kinetics and Spectra of Aromatic Radicals in Solution (Letter)**. *J Phys Chem* 87(11):1842-1843, 1983.
- Kelley D. F., Rentzepis P. M., **Picosecond Emission-Spectroscopy of Two Predisociative Isomeric Methylenepyrazolines and Product Trimethylenemethane**. *J Am Chem S* 105(7):1820-1824, 1983.
- Kelso S. M., Aspnes D. E., Olson C. G., Lynch D. W., **Optical Determination of Exciton Sizes in Semiconductors**. *Physica B&C* 117(MAR):362-364, 1983.
- Kinsbron E. et al., **Crystallization of Amorphous-Silicon Films During Low-Pressure Chemical Vapor-Deposition**. *Appl Phys L* 42(9):835-837, 1983.
- Klauder J. R., Ezawa H., **Remarks on a Stochastic Quantization of Scalar Fields**. *Prog T Phys* 69(2):664-673, 1983.
- Kodama Y., Hasegawa A., **Amplification and Reshaping of Optical Solitons in Glass-Fiber. 3. Amplifiers With Random Gain**. *Optics Lett* 8(6):342-344, 1983.
- Kolodner P., Katzir A., Hartsough N., **Non-Contact Surface-Temperature Measurement During Reactive-Ion Etching Using Fluorescent Polymer-Films**. *Appl Phys L* 42(8):749-751, 1983.

- Kurkjian C. R., Krause J. T., Paek U. C., **Tensile-Strength Characteristics of Perfect Silica Fibers.** *J Physique* 43(NC-9):585-586, 1982.
- Levine B. F., Bethea C. G., Tsang W. T., Capasso F., Thornber K. K., Fulton R. C., Kleinman D. A., **Measurement of High Electron-Drift Velocity in a Sub-Micron, Heavily Doped Graded GaP $Al_xGa_{1-x}As$ Layer.** *Appl Phys L* 42(9):769-771, 1983.
- Levinson M., Benton J. L., Kimerling L. C., **Electronically Controlled Metastable Defect Reaction in InP.** *Phys Rev B* 27(10):6216-6221, 1983.
- Levinson M., Temkin H., **Defect States in Electron-Irradiated InGaAsP.** *Appl Phys L* 42(7):605-607, 1983.
- Lewis J. A., **Thermal-Convection and Equilibrium Liquid-Phase Epitaxial-Growth.** *Ann NY Acad* 404(MAY):301, 1983.
- Lin C., **Non-Linear Optics in Fibers and Near-Infrared Frequency-Conversion.** *P Soc Photo* 355:17-26, 1982.
- Lin P. S. D., Leamy H. J., **Tunneling Current Microscopy.** *Appl Phys L* 42(8):717-719, 1983.
- Lines M. E., **Topical Review—Computer Modeling of Amorphous Magnetic-Materials (Review).** *J Magn Magn* 36(1-2):1-25, 1983.
- Lines M. E., Eibschutz M., **Influence of Isomer-Shift Distribution on Mossbauer Quadrupole Spectra in Amorphous Magnetic Insulators.** *Phys Rev B* 27(9):5308-5312, 1983.
- Lovinger A. J., **Ferroelectric Polymers.** *Science* 220(4602):1115-1121, 1983.
- Lum R., Wilkins C. W., Robbins M., Lyons A. M., Jones R. P., **Thermal-Analysis of Graphite and Carbon Phenolic Composites by Pyrolysis-Mass Spectrometry.** *Carbon* 21(2):111-116, 1983.
- Lynn J. W., Erwin R. W., Chen H. S., Rhyne J. J., **Evolution From Ferromagnetism to Spin-Glass Behavior.** *Sol St Comm* 46(4):317-320, 1983.
- Lynn J. W., Erwin R. W., Rhyne J. J., Chen H. S., **Ferromagnetic and Spin-Glass Behavior Near the Critical Concentration in Amorphous $(Fe_xNi_{1-x})_{75}G1_{25}$.** *J Magn Magn* 31-4(FEB):1397-1398, 1983.
- MacDonald J. R., Davies J. A., Jackman T. E., Feldman L. C., **How Well Does 4He Backscattering From Low-Z Nuclei Obey the Rutherford Formula?** *J Appl Phys* 54(4):1800-1803, 1983.
- Marcus M., Dynes R. C., Griffiths J. E., McWhan D., **Effect of Ion-Beam Damage on X-Ray-Diffraction and Raman-Spectra of Amorphous $GeSe_2$.** *J Appl Phys* 54(4):1792-1794, 1983.
- Marcus M. A., Tsai C. L., Giessen B. C., **Interstitial Site of Cu in Ca.** *Sol St Comm* 46(6):455-456, 1983.
- Mccroryjoy C., Joy D. C., **Chemical and Instrumental Analysis of Ferrites (Review).** *Talanta* 30(5):299-315, 1983.
- McShera C., Colleran P. J., Glynn T. J., Imbusch G. F., Remeika J. P., **Luminescence Study of $LiGa_5-xFe_xO_8$.** *J Luminesc* 28(1):41-52, 1983.
- Miller B. et al., **Applications of Hydrodynamic Modulation at Rotating-Disk Electrodes to Semiconductor Electrochemistry.** *Ann NY Acad* 404(MAY):473-474, 1983.
- Miller R. C., Gossard A. C., Tsang W. T., **Extrinsic Photo-Luminescence From GaAs Quantum Wells.** *Physica B&C* 117(MAR):714-716, 1983.
- Mollenauer L. F., Stolen R. H., Gordon J. P., Tomlinson W. J., **Extreme Picosecond Pulse Narrowing by Means of Soliton Effect in Single-Mode Optical Fibers.** *Optics Lett* 8(5):289-291, 1983.
- Mollenauer L. F., Vieira N. D., Szeto L., **Optical-Properties of the $T1^0(1)$ Center in KCl.** *Phys Rev B* 27(9):5332-5346, 1983.
- Mucha J. A., Hess D. W., **Plasma-Etching (Review).** *ACS Symp S* 1983(219):215-285, 1983.
- Munch R. et al. **High-Pressure and Extended X-Ray-Absorption Fine-Structure Study of Cr-Rich Cr-Ge Alloys.** *Phys Rev L* 50(20):1619-1622, 1983.
- Murarka S. P., Retajczyk T. F., **Effect of Phosphorus Doping on Stress in Silicon and Polycrystalline Silicon.** *J Appl Phys* 54(4):2069-2072, 1983.
- Murnick D. E., **Intense Polarized 3He Source for Use in Fusion Reactors.** *Appl Phys L* 42(6):544-545, 1983.
- Murray C. A., **Using Surface Enhanced Raman-Scattering to Study Vibrations**

- of Adsorbates on Thin Metallic Overlayers on Silver.** *J Elec Spec* 29(JAN):371-382, 1983.
- Nakahara S., **Diffusion-Induced Grain-Boundary Migration in Heated Cu-Ni Alloy Targets During Sputtering.** *Scrip Metal* 17(5):607-610, 1983.
- Nakahara S., Okinaka Y., **Microstructure and Ductility of Electroless Copper-Deposits.** *Act Metall* 31(5):713-724, 1983.
- Nassau K., Chadwick D. L., **Multicomponent Glasses of GeO₂ and Sb₂O₃ With Bi₂O₃, Ti₂O, and/or PbO.** *J Am Ceram* 66(5):332-337, 1983.
- Nazarathy M., Hardy A., Shamir J., **Generalized-Mode Theory of Conventional and Phase-Conjugate Resonators.** *J Opt Soc* 73(5):576-586, 1983.
- Nazarathy M., Shamir J., Hardy A., **Nonideal Phase-Conjugate Resonators—A Canonical Operator Analysis.** *J Opt Soc* 73(5):587-593, 1983.
- Nelson D. F., Abraham D. L., Cooper J. A., **Measurement of Cube-Root Broadening of Charge Packets in Metal-Oxide-Semiconductor Structures.** *Appl Phys L* 42(9):815-817, 1983.
- Nicholas R. J., Brummell M. A., Portal J. C., Cheng K. Y., Cho A. Y., Pearsall T. P., **An Experimental-Determination of Enhanced Electron g-Factors in GaInAs-AllnAs Heterojunctions.** *Sol St Comm* 45(10):911-914, 1983.
- Nicholas R. J., Brummell M. A., Portal J. C., Cho A. Y., Cheng K. Y., Pearsall T. P., **Quantum Transport in GaInAs-AllnAs Heterojunctions.** *Lect N Phys* 177:110-113, 1983.
- Nicholas R. J., Brummell M. A., Portal J. C., Razeghi M., Poisson M. A., **Magneto-transport in GaInAs-InP Heterojunctions and Super-Lattices.** *Lect N Phys* 177:98-109, 1983.
- Niklasson G. A., Craighead H. G., **Optical-Properties of Codeposited Aluminum-Silicon Composite Films.** *Appl Optics* 22(8):1237-1240, 1983.
- Nitzan A., Tully J. C., **Stochastic Classical Trajectory Approach to Relaxation Phenomena. III. Comparison of Trajectory Results to Quantum-Mechanical Perturbation-Theory.** *J Chem Phys* 78(6):3959-3963, 1983.
- Nordblad P. et al., **Critical Behavior of Induced Linear Birefringence in Isotropic Anti-Ferromagnets.** *J Magn Magn* 31-4(FEB):1093-1094, 1983.
- Olego D., Pinczuk A., Ballman A. A., **Resonant Inelastic Light-Scattering by Free-Electrons in InP.** *Sol St Comm* 45(11):941-944, 1983.
- Patterson G. D., Carroll P. J., Pearson D. S., **Rayleigh-Brillouin Spectroscopy of Normal-Tetracosane—Are There Transitions in the Melt?** *J Chem S F2* 79(P5):677-685, 1983.
- Patterson G. D., Carroll P. J., Stevens J. R., **Photon-Correlation Spectroscopy of Poly(Methyl Methacrylate) Near the Glass-Transition.** *J Pol Sc Pp* 21(4):613-623, 1983.
- Patterson G. D., Carroll P. J., Stevens J. R., **Photon-Correlation Spectroscopy of Polystyrene as a Function of Temperature and Pressure.** *J Pol Sc Pp* 21(4):605-611, 1983.
- Pfeiffer L., Kovacs T., Celler G. K., Gibson J. M., Lines M. E., **Mössbauer-Effect of ⁷³Ge in Laser-Processed Si and Ge Crystals.** *Phys Rev B* 27(7):4018-4026, 1983.
- Phillips J. C., **Separable Spectral Model of the Metal-Insulator Transition in Si:P.** *Phil Mag B* 47(4):407-418, 1983.
- Pinczuk A., Worlock J. M., **Light-Scattering by Two-Dimensional Electron-Systems.** *Physica B&C* 117(MAR):637-642, 1983.
- Rabinovich E. M., **On the Structural Role of Fluorine in Silicate-Glasses (Letter).** *Phys C Glas* 24(2):54-56, 1983.
- Raghavachari K., **Theoretical-Study of Conformational Processes in Sulfur Diimides.** *J Phys Chem* 87(8):1308-1312, 1983.
- Raghavachari K., Haddon R. C., Roth H. D., **Theoretical Studies in the Norbornadiene Quadricyclane System.** *J Am Chem S* 105(10):3110-3114, 1983.
- Raghavan P., Raghavan R. S., **Nuclear g Factors of the 17⁻/2 and 21⁺/2 Isomeric States of ⁹¹Mo.** *Phys Rev C* 27(4):1532-1535, 1983.
- Reichmanis E., Gooden R., Wilkins C. W., Schonhorn H., **A Study of the Photochemical Response of Ortho-Nitrobenzyl Cholate Derivatives in P(MMA-MAA) Matrices.** *J Pol Sc Pc* 21(4):1075-1083, 1983.

- Reimer J. A., Duncan T. M., **Local Bonding Configuration of Phosphorus in Doped and Compensated Amorphous Hydrogenated Silicon.** Phys Rev B 27(8):4895-4901, 1983.
- Robinson I. K., **Direct Determination of the Au(110) Reconstructed Surface by X-Ray-Diffraction.** Phys Rev L 50(15):1145-1148, 1983.
- Rosamilia J. M., Miller B., **Amplitude Enhancement and Automatic Scanning in Electroanalysis With Hydrodynamically Modulated Rotating-Disk Electrodes (Review).** Analyst Chem 55(7):1142-1145, 1983.
- Roth H.D., Schilling M. L., **Radical Cations of Strained Ring Hydrocarbons-Cyclopropane Derivatives.** Can J Chem 61(5):1027-1035, 1983.
- Rowe J. E., Pearsall T. P., Logan R. A., **A Study of the Valence Band-Structure of Ga_{0.47}In_{0.53}As by Angle Resolved Photoemission.** Physica B&C 117(MAR):347-349, 1983.
- Scalco E., Moore W. F., **A New Radiolytically Crosslinkable Polyvinyl-Chloride Insulation For Telecommunications Wire.** Radiat Ph C 21(4):389-396, 1983.
- Schilling F. C., Bovey F. A., Tseng S., Woodward A. E., **C13NMR of Partially Epoxidized 1,4-Trans-Polybutadiene Crystals.** Macromolec 16(5):808-816, 1983.
- Schwenk H., Andres K., Wudl F., Aharon-Shalom E., **Direct Observation of a Large London Penetration Depth in an Organic Superconductor.** Sol St Comm 45(8):767-769, 1983.
- Shockley W., **Do Dislocations Hold Technological Promise?** Sol St Tech 26(1):75-78, 1983.
- Simpson J. R., Mac Chesney J. B., **Optical Fibers with an Al₂O₃-Doped Silicate Core Composition.** Electr Lett 19(7):261-262, 1983.
- Skocpol W. J., Jackel L. D., Howard R. E., Hu E. L., Fetter L. A., **Non-Metallic Localization and Interaction in One-Dimensional (0.1- μ m) Si MOS-FETs.** Physica B&C 117(MAR):667-669, 1983.
- Solomon P. M., Stark A. A., Sanders D. B., **CO Emission in the Outer Galaxy Between Longitudes 50 Degrees and 72 Degrees.** Astrophys J 267(1):L29-L35, 1983.
- Soto L., Franey J. P., Graedel T. E., Kammlott G. W., **On the Corrosion-Resistance of Certain Ancient Chinese Bronze Artifacts.** Corros Sci 23(3):241-250, 1983.
- Spalink J. D. et al., **Bathorhodopsin Intermediates From 11-CIS-Rhodopsin and 9-CIS-Rhodopsin.** P Nas Biol 80(7):1887-1891, 1983.
- Starnes W. H., Schilling F. C., Plitz I. M., Cais R. E., Freed D. J., Hartless R. L., Bovey F. A., **Branch Structures in Polyvinyl-Chloride and the Mechanism of Chain Transfer to Monomer During Vinyl-Chloride Polymerization.** Macromolec 16(5):790-807, 1983.
- Stillinger F. H., **Variational Model for Micelle Structure.** J Chem Phys 78(7):4654-4661, 1983.
- Stillinger F. H., Weber T. A., **Two-Dimensional Gaussian Core Model at High-Temperature.** Phys Rev A 27(5):2642-2648, 1983.
- Stormer H. L., Chang A., Tsui D. C., Hwang J. C. M., Gossard A. C., Wiegmann W., **Fractional Quantization of the Hall-Effect.** Phys Rev L 50(24):1953-1956, 1983.
- Stormer H. L., Tsui D. C., Gossard A. C., Hwang J. C. M., **Observation of Quantized Hall-Effect and Vanishing Resistance at Fractional Landau-Level Occupation.** Physica B&C 117(MAR):688-690, 1983.
- Stormer H. L., Tsui, D. C., **The Quantized Hall-Effect.** Science 220(4603):1241-1246, 1983.
- Svensson C. et al., **Structural Temperature-Dependence in Alpha-Lithium Iodate—Neutron and X-Ray Study Between 20-K and 500-K.** J Chem Phys 78(12):7343-7352, 1983.
- Swaminathan V., Anthony P. J., Pawlik J. R., Tsang W. T., **Temperature and Excitation Dependences of Active Layer Photo-Luminescence in (Al, Ga)As Laser Heterostructures.** J Appl Phys 54(5):2623-2629, 1983.
- Tan S. L., Anderson P. W., **Long-Range Vanderwaals Forces Between Restricted-Dimensional Metals.** Chem P Lett 97(1):23-25, 1983.
- Taniuti T., Hasegawa A., **Non-Linear Drift Waves.** Phys Scr T2(NSI):529-533, 1982.
- Temkin H., Alavi K., Wagner W. R., Pearsall T. P., Cho A. Y., **1.5-1.6- μ m**

- Ga_{0.47}In_{0.53}As/Al_{0.48}In_{0.52}As Multiquantum Well Lasers Grown by Molecular-Beam Epitaxy.** Appl Phys L 42(10):845-847, 1983.
- Thomas G. A., **Experimental Tests of Localization in Semiconductors.** Physica B&C 117(Mar):81-83, 1983.
- Thompson L. F., **Advances in Microlithography (Editorial).** Sol St Tech 26(5):85, 1983.
- Thompson L. F., **An Introduction to Lithography (Review).** ACS Symp S 1983(219):1-13, 1983.
- Thompson L. F., Bowden M. J., **Resist Processing (Review).** ACS Symp S 1983(219):161-214, 1983.
- Thompson L. F., Bowden M. J., **The Lithographic Process—The Physics (Review).** ACS Symp S 1983(219):15-85, 1983.
- Tonelli A. E., **Stereosequence-Dependent C-13 NMR Chemical-Shifts in Polystyrene.** Macromolec 16(4):604-607, 1983.
- Tonelli A. E., Schilling F. C., Cais R. E., **C-13-NMR and F-19-NMR Chemical-Shifts and the Microstructures of Fluoropolymers (Review).** Adv Chem SE 1983(203):441-454, 1983.
- Tsang W. T., Hartman R. L., **cw Electro-Optical Characteristics of Graded-Index Wave-Guide Separate-Confinement Heterostructure Lasers With Proton-Delineated Stripe.** Appl Phys L 42(7):551-553, 1983.
- Tsang W. T., Olsson N. A., **New Large Optical Cavity Laser With Distributed Active Layers.** Appl Phys L 42(10):850-852, 1983.
- Tsang W. T., Olsson N. A., Logan R. A., **High-Speed Direct Single-Frequency Modulation With Large Tuning Rate and Frequency Excursion in Cleaved-Coupled-Cavity Semiconductor-Lasers.** Appl Phys L 42(8):650-652, 1983.
- Tsang W. T., Olsson N. A., Logan R. A., Linke R. A., **Demonstration of Multilevel Multichannel Optical Frequency-Shift Keying (FSK) With Cleaved-Coupled-Cavity (C³) Semiconductor-Lasers.** Electr Lett 19(9):341-343, 1983.
- Tsuda T., Yasuoka H., Kitaoka Y., DiSalvo F. J., **⁵¹V NMR-Study of the Phase-Transition in 1T-VS₂.** J Magn Magn 31-4(Feb):1101-1102, 1983.
- Tung R. T., Gibson J. M., Poate J. M., **Growth of Single-Crystal Epitaxial Silicides on Silicon by the Use of Template Layers.** Appl Phys L 42(10):888-890, 1983.
- Vansaarloos W., **Use of the Star-Triangle Transformation for the Application of Differential Real-Space Renormalization-Group Theory.** Phys Rev B 27(9):5678-5685, 1983.
- Van Uitert L. G., **Chelate Compound Stability Constant Calculations on Metal Diketonate Complexes.** Polyhedron 2(4):285-289, 1983.
- Van Uitert L. G., **Relations Between Normal Boiling-Point and Melting-Point for Simple Halides and Oxides.** J Am Ceram 66(5):380-382, 1983.
- Wagner A., **Applications of Focused Ion-Beams to Microlithography.** Sol St Tech 26(5):97-103, 1983.
- Walker L. R., Walstedt R. E., **Computer Studies of RKKY Spin-Glasses.** J Magn Magn 31-4(Feb):1289-1292, 1983.
- Walsh W. M., **Magnetic-Resonance Studies of Itinerant Antiferromagnetism in Organic Superconductors.** J Magn Magn 31-4(Feb):1273-1276, 1983.
- Warren W. W., Schönherr G., Hensel F., **Intervalence Excitations of a Mixed-Valence Salt: NMR and Optical Absorption in Molten InCl₂.** Chem P Lett 96(4):505-508, 1983.
- Warren W. W., Sotier S., Brennert G. F., **Resolution of the Conductivity Dilemma in Liquid Solutions of Alkali-Metals in Alkali-Halides.** Phys Rev L 50(19):1505-1508, 1983.
- Weeks J. D. et al., **Vanderwaals Theory of Melting in Two-Dimensions and Three-Dimensions.** J Chem Phys 78(6):4197-4205, 1983.
- Wiesenfeld J. M., Stone J., **Chirp in Picosecond Film Lasers and Pulse-Compression by Linear Dispersion in Optical Fibers.** Optics Lett 8(5):262-264, 1983.
- Wilson B. A., Hu P., Harbison J. P., Jedju T. M., **Subnanosecond Total-Light Decay and Spectra in α -Si:H.** Phys Rev L 50(19):1490-1493, 1983.
- Wilson R. J., Hahn E. L., **Local-Field-Induced Multiple-Pulse Free-Induction Decay.** Phys Rev B 27(7):4129-4134, 1983.

- Wilson R. J., Mills A. P., **Positron and Positronium Emission From Tungsten (111)**. *Phys Rev B* 27(7):3949-3954, 1983.
- Worlock J. M., Maciel A. C., Perry C. H., Tien Z. J., Aggarwal R. L., Gossard A. C., Wiegmann W., **Inelastic Light-Scattering by Two-Dimensional Electron-Systems in High Magnetic-Fields**. *Lect N Phys* 177:186-193, 1983.
- Wright C. E., Meyer D. E., **Conditions for a Linear Speed-Accuracy Trade-Off in Aimed Movements**. *Q J Exp P-A* 35(May):279-296, 1983.
- Wu C. C., Leventhal M., Sarazin C. L., Gull T. R., **High-Velocity Iron-Absorption Lines in Super-Nova Remnant-1006 (Letter)**. *Astrophys J* 269(1):L 5-L 9, 1983.
- Yoshioka D., **Hall Conductivity of Two-Dimensional Electrons in a Periodic Potential**. *Phys Rev B* 27(6):3637-3645, 1983.
- Yoshioka D., Halperin B. I., Lee P. A., **Ground-State of Two-Dimensional Electrons in Strong Magnetic-Fields and 1/3 Quantized Hall-Effect**. *Phys Rev L* 50(16):1219-1222, 1983.
- Yoshioka D., Lee P. A., **Ground-State Energy of a Two-Dimensional Charge-Density-Wave State in a Strong Magnetic-Field**. *Phys Rev B* 27(8):4986-4996, 1983.
- Yurke B., Denker J. S., Johnson B. R., Bigelow N., Levy L. P., Lee D. M., Freed J. H., **NMR-Induced Recombination of Spin-Polarized Hydrogen**. *Phys Rev L* 50(15):1137-1140, 1983.

SOCIAL/LIFE SCIENCES

- Culligan N., Gelperin A., **One-Trial Associative Learning by an Isolated Molluscan CNS—Use of Different Chemoreceptors for Training and Testing**. *Brain Res* 266(2):319-327, 1983.
- Hoch S. J., Tschirgi J. E., **Cue Redundancy and Extra Logical Inferences in a Deductive Reasoning Task**. *Mem Cognit* 11(2):200-209, 1983.
- Julesz B., **Textons, Rapid Focal Attention Shifts, and Iconic Memory**. *Behav Brain* 6(1):25-27, 1983.
- Lamola A. A., Flores J., Blumberg W. E., **Binding of Photobilirubin to Human-Serum Albumin—Estimate of the Affinity Constant**. *Eur J Bioch* 132(1):165-169, 1983.
- Lund A. M. et al., **Frequency Judgment Accuracy as a Function of Age and School-Achievement (Learning-Disabled Versus Non-Learning-Disabled) Patterns**. *J Exp C Psy* 35(2):236-247, 1983.
- Miller J., **Can Response Preparation Begin Before Stimulus-Recognition Finishes**. *J Exp Psy P* 9(2):161-182, 1983.
- Ondrias M. R., Friedman J. M., Rousseau D. L., **Metastable Species of Hemoglobin—Room-Temperature Transients and Cryogenically Trapped Intermediates**. *Science* 220(4597):615-617, 1983.
- Ondrias M. R., Rousseau D. L., Simon S. R., **Resonance Raman-Spectra of Photodissociated Carbonmonoxy Hemoglobin and Deoxy Hemoglobin at 10-K**. *J Biol Chem* 258(9):5638-5642, 1983.
- Patel D. J., Ikuta S., Kozlowski S., Itakura K., **Sequence Dependence of Hydrogen-Exchange Kinetics in DNA Duplexes at the Individual Base Pair Level in Solution**. *P Nas Biol* 80(8):2184-2188, 1983.
- Patel D. J., Kozlowski S. A., Ikuta S., Itakura K., Bhatt R., Hare D. R., **NMR-Studies of DNA Conformation and Dynamics in Solution**. *Cold S Harb* 47(P1):197-206, 1982.
- Pattipati K. R., Kleinman D. L., Ephrath A. R., **A Dynamic Decision-Model of Human Task Selection Performance**. *IEEE Syst M* 13(2):145-166, 1983.
- Radin D. I., **Experimental Attempts to Influence Pseudo-Random Number Sequences**. *J Am S Psyc* 76(4):359-374, 1982.
- Shaw M. L., **Two-State Versus Continuous State Stimulus Representations—A Test Based on Attentional Constraints**. *Perc Psych* 33(4):338-354, 1983.

SPEECH/ACOUSTICS

- Allen J. et al., **Speech Recognition (Discussion)**. *ISSCC Diges* 26:214-215, 1983.

- Cordell R. R., Phase Intermodulation Distortion Instrumentation and Measurements.** J Aud Eng S 31(3):114-124, 1983.
- Cox R. V., Crochiere R. E., Johnston J. D., Real-Time Implementation of Time Domain Harmonic Scaling of Speech for Rate Modification and Coding.** IEEE J Sol I 18(1):10-24, 1983.
- Cox R. V., Crochiere R. E., Johnston J. D., Real-Time Implementation of Time Domain Harmonic Scaling of Speech for Rate Modification and Coding.** IEEE Acoust 31(1):258-272, 1983.
- Streeter L. A., MacDonald N. H., Apple W., Krauss R. M., Galotti K. M., Acoustic and Perceptual Indicators of Emotional Stress.** J Acoust So 73(4):1354-1360, 1983.

CONTENTS, NOVEMBER 1983

Calculation of Modes in an Optical Fiber Using the Finite Element Method and EISPACK

T. A. Lenahan

Measurements of 800-MHz Radio Transmission Into Buildings With Metallic Walls

D. C. Cox, R. R. Murray, and A. W. Norris

Penetration of Radio Signals Into Buildings in the Cellular Radio Environment

E. H. Walker

Transmission Errors and Forward Error Correction in Embedded Differential Pulse Code Modulation

D. J. Goodman and C.-E. Sundberg

CCITT Compatible Coding of Multilevel Pictures

H. Gharavi and A. N. Netravali

The Queueing Network Analyzer

W. Whitt

Performance of the Queueing Network Analyzer

W. Whitt

THE BELL SYSTEM TECHNICAL JOURNAL is abstracted or indexed by *Abstract Journal in Earthquake Engineering, Applied Mechanics Review, Applied Science & Technology Index, Chemical Abstracts, Computer Abstracts, Current Contents/Engineering, Technology & Applied Sciences, Current Index to Statistics, Current Papers in Electrical & Electronic Engineering, Current Papers on Computers & Control, Electronics & Communications Abstracts Journal, The Engineering Index, International Aerospace Abstracts, Journal of Current Laser Abstracts, Language and Language Behavior Abstracts, Mathematical Reviews, Science Abstracts (Series A, Physics Abstracts; Series B, Electrical and Electronic Abstracts; and Series C, Computer & Control Abstracts), Science Citation Index, Sociological Abstracts, Social Welfare, Social Planning and Social Development, and Solid State Abstracts Journal*. Reproductions of the Journal by years are available in microform from University Microfilms, 300 N. Zeeb Road, Ann Arbor, Michigan 48106.



Bell System